uOttawa

L'Université canadienne
Canada's university

FACULTÉ DES ÉTUDES SUPÉRIEURES ET POSTOCTORALES

u Ottawa

L'Université canadienne
Canada's university

FACULTY OF GRADUATE AND POSDOCTORAL STUDIES

Robin Hughes
AUTEUR DE LA THÈSE / AUTHOR OF THESIS

Ph.D. (Chemical Engineering)
GRADE / DEGREE

Department of Chemical and Biological Engineering
FACULTÉ, ÉCOLE, DÉPARTEMENT / FACULTY, SCHOOL, DEPARTMENT

Fluidized bed Combustion with Integrated Carbon Dioxide Capture
TITRE DE LA THÈSE / TITLE OF THESIS

Arturo Macchi
DIRECTEUR (DIRECTRICE) DE LA THÈSE / THESIS SUPERVISOR

Edward John Anthony
CO-DIRECTEUR (CO-DIRECTRICE) DE LA THÈSE / THESIS CO-SUPERVISOR

Xudong Cao

Christopher Lan

Poupak Mehrani

John Denis (University of Cambridge)

Gary W. Slater
Le Doyen de la Faculté des études supérieures et postdoctorales / Dean of the Faculty of Graduate and Postdoctoral Studies

Fluidized Bed Combustion with Integrated Carbon Dioxide Capture

By

Robin Hughes

Thesis submitted to the Faculty of Graduate and Postdoctoral Studies
In partial fulfillment of the requirements for Doctorate of Philosophy in
Chemical Engineering

Department of Chemical and Biochemical Engineering University of Ottawa

September 2009

Your file Votre référence
ISBN: 978-0-494-65997-7
Our file Notre référence
ISBN: 978-0-494-65997-7

Statement of Contribution of Collaborators

The technologies and facilities designed, constructed and investigated within this work require a multidisciplinary team approach to successfully develop. Therefore, some of the publications that form the chapters of this thesis have been partially authored by collaborators.

Sorbent Development

In Chapter 2, Improved Long-term Capacity of Limestone Sorbents for *In Situ* Capture of CO_2 in a Fluidized Bed Combustor, I modified a commercial thermogravimetric analyzer to operate over multiple cycles with varying temperature, flow rates and gas compositions including steam. I performed all experimental work and authored the paper.

In Chapter 3, Sintering and Reactivity of $CaCO_3$-based Sorbents for *In Situ* CO_2 Capture in Fluidized Beds under Realistic Calcination Conditions I performed a portion of the experimental work and worked with Dr. Lu in analyzing and interpreting the results.

In Chapter 4, Hydration and Pelletization of $CaCO_3$ Derived Sorbents for *In-Situ* CO_2 Capture I developed the facilities and methods for preparing the sorbent pellets. I performed a portion of the experimental work and worked with Dr. Lu in analyzing and interpreting the results. Dr Lu and I worked together to author the paper.

Process Simulation

I was the sole author of Chapter 5, Design, Process Simulation, and Construction of an Atmospheric Dual Fluidized Bed Combustion System for *In Situ* CO_2 Capture using High-temperature Sorbents. I developed the process simulations and basic engineering packages for the facility.

Design and Construct a Pilot Plant for Proof of Technology

In Chapter 6, Oxy-Fuel Combustion of Coal in a Circulating Fluidized Bed Combustor, I developed the test plan, operated the facility with technologists (and Dr. Lu), analyzed the data and authored the paper. I was responsible for process and instrumentation diagrams, mechanical systems including 3D vessel and piping drawings, and controls systems, procurement of materials, construction, and commissioning of the facility.

In Chapter 7, Ca-Based Sorbent Looping Combustion for CO_2 Capture in Pilot-Scale Dual Fluidized Beds, I developed the test plan, while Dr. Lu and I operated the test facility and analyzed the data together. I was responsible for process and instrumentation diagrams, mechanical systems including 3D vessel and piping drawings, and controls systems, procurement of materials, construction, and commissioning of the facility.

Evaluate Sorbent Characteristics and Performance at Pilot Scale

In Chapter 8, I was responsible for experimental work and authoring the section of the paper regarding attrition during multi-cycle carbonation / calcination cycles.

In Chapter 9, I was responsible for the test plan, analysis, and authoring of the paper. Dr. Lu and I operated the test facility together.

I am the sole author of Chapter 10.

Signature:_____ Date:_____

Abstract

The connection between increasing atmospheric CO_2 concentrations and climate change is now recognized by a number of international organizations including the United Nations Framework Convention on Climate Change (UNFCCC), the Intergovernmental Panel on Climate Change (White et al, 2003), and the European Union FP6 Framework. The research described in this thesis brings two carbon dioxide capture technologies from concept through to bench scale testing, simulation, and demonstration at pilot scale.

Facilities for demonstrating and investigating oxy-fuel circulating fluidized bed combustion with recycled flue gas and and calcium-based sorbent looping cycles are developed and described. The facilities were commissioned with coal and biomass.

It is shown that high CO_2 concentration in the calciner is highly detrimental to the performance of the sorbent. Hydration of the sorbent can greatly improve the capacity of the sorbent when relatively low CO_2 concentrations are present, however, when CO_2 concentration is high there is little difference between untreated and hydrated sorbent capacity after 20 cycles. Steam hydration together with pelletization of limestone was used to improve sorbent utilization for *in-situ* CO_2 capture under operating conditions typical of fluidized bed combustion. The pelletized particles in general showed good performance, comparable to or better than hydrated samples.

Attrition of the sorbents has been greater than expected for some of the limestones. The results suggest that multiple carbonation/calcination cycles result in severe attrition during the first one or two calcination periods. Afterwards, the particles attrite at rates similar to what would be expected from a bed of particles continuously subjected to similar forces over an extended period of time. In limestones where material loss is a problem, however, it is clear that partial sulphation can dramatically reduce this loss, albeit with the risk of reduction of CO_2 carrying capacity or $CaO\text{-}CaCO_3$ looping cycle reversibility.

Sorbent capacity was significantly lower than expected based on previous thermogravimetric analyses. A thin, non-porous shell was formed around the sorbent particles under some of the

test conditions at the pilot scale. The causes for the formation of this shell must be verified prior to investing substantially in this technology as the shell greatly reduces the capacity of the sorbent. The fact that the shell was not formed in all tests provides hope that a suitable set of conditions can be found for operation where the shell does not hinder sorbent performance.

The calcium-based sorbent looping cycle process has been demonstrated using the CANMET 75 kW_{th} pilot-scale dual fluidized bed facility and more than 50 hrs operating experience in total has been accumulated. Havelock limestone from eastern Canada was used as the CO_2 sorbent, while a synthesis gas mixture of air and CO_2 (15%) was employed to simulate combustion flue gas. A high CO_2 capture efficiency (> 95%) was achieved for the first several cycles, which decreased to a lower level (> 72%) after more than 25 cycles. Oxy-fuel combustion of biomass and coal was employed in the sorbent regeneration step, in which pure O_2 was mixed with recycled flue gas and this, along with the excellent heat transfer characteristics of CFBs, allowed the use of an O_2 concentration of 40 vol% in the combustion gas.

Sommaire

Le lien entre l'augmentation des concentrations de CO_2 dans l'atmosphère et le changement climatique est maintenant reconnu par un certain nombre d'organismes internationaux dont la Convention-Cadre des Nations Unies sur le Changement Climatique (UNFCCC en anglais), le Panneau Intergouvernemental sur le Changement Climatique et le Cadre de l'Union Européenne FP6 (White et al., 2003). La recherche décrite dans cette thèse apporte deux technologies de capture du dioxide de carbone de la phase concept à travers à les phases: essai en laboratoire, simulation, et démonstration à l'échelle pilote.

Des équipements pour démontrer et investiguer la combustion oxy-carburant en lit fluidisé circulant avec recyclage des gaz d'échappement et les cycles calcination/carbonation avec des sorbants à base de calcium (i.e. calcaires) sont développés et décrits. Les équipements ont été commissionnés avec du charbon et la de biomasse come carburant.

Il a été démontré qu'une concentration élevée en CO_2 lors de la calcination (régénération du sorbant) est fortement nuisible à la performance du sorbant. L'hydratation du sorbant peut considérablement améliorer la capacité du sorbant lorsque les concentrations en CO_2 sont relativement basses, cependant, quand la concentration en CO_2 est élevée, il y a peu de différence entre la capacité d'un sorbant non-traitée et hydratée après 20 cycles de calcination/carbonation. L'hydratation à la vapeur ainsi que la pelletisation des calcaires ont été employées pour améliorer l'utilisation du sorbant pour la capture in-situ du CO_2 dans des conditions d'opérations typiques de la combustion en lit fluidisé. En général, les particules pelletisées ont montré une bonne performance, comparable ou meilleure que les échantillons hydratés.

L'usure par attrition des sorbants a été plus grande que prévue pour certains des calcaires. Les résultats suggèrent que les multiples cycles de carbonation/calcination aient comme conséquence une sévère fragmentation des calcaires au cours des une ou deux premières périodes de calcination. Après, les calcaires s'usent à des taux similaires que dans un lit de particules continuellement soumis à des forces semblables sur une période prolongée. Cependant, pour les calcaires où la perte matérielle est un problème, il est clair qu'une

sulphation partielle peux nettement réduire cette perte, quoiqu'avec le risque de réduction de capacité de capture du CO_2 ou de la réversibilité du cycle $CaO\text{-}CaCO_3$.

La capacité du sorbant était sensiblement inférieure à celle prévue basé sur des analyses thermogravimétriques antérieures. Une coquille mince et non poreuse a été formée autour des particules de sorbant dans certaines des conditions d'essai à l'échelle pilote. Les causes pour la formation de cette coquille doivent être vérifiées avant d'investir sensiblement dans cette technologie puisque la coquille réduit considérablement la capacité du sorbant. Le fait que la coquille n'a pas été formée dans tous les essais fournit l'espoir qu'un ensemble de conditions opérationnelles appropriées peut être trouvé où la coquille ne diminue pas la performance du sorbant.

Le procédé cyclique de calcination/carbonation avec des sorbants à base de calcium a été démontré utilisant les lits fluidisés à échelle pilote de 75 kWth de CANMET et plus de 50 heures d'expérience d'opération a été accumulées au total. Le calcaire provenant de Havelock dans l'est du Canada a été employée comme sorbant de CO_2, alors qu'un mélange d'air et de CO_2 (15% vol.) était utilisé pour simuler les gaz de combustion. Une efficacité élevée de capture de CO_2 (> 95%) a été réalisé pour les plusieurs premiers cycles, et qui a diminuée à un niveau inferieur (> 72%) après plus de 25 cycles. La combustion oxy-carburant de la biomasse et du charbon a été utilisée dans l'étape de calcination, dans laquelle l'O_2 pur a été mélangé avec les gaz d'échappement recyclés et ceci, avec les excellentes caractéristiques de transfert de chaleur des lits fluidisés circulants, a permis l'utilisation d'une concentration en O_2 de 40% vol. dans le gaz de combustion.

Acknowledgement

I would like to acknowledge the ongoing support and assistance of Dr. Arturo Macchi, my acedemic supervisor and thesis advisor. I also wish to thank my co-supervisor Dr. E. J. 'Ben' Anthony, and my colleague and friend Dr. Dennis Lu, who have supported my research throughout the period it has taken me to concieve, develop, and write this thesis. In addition, Mr. Jeffery Slater and Mr. Ryan Burchat were integral to the completion of my research through their dedication and good humor.

Table of Contents

List of Figures

List of Tables

Chapter 1 Introduction

1.1 Energy Production and Climate Change

Fossil fuels currently supply 90% of the world's energy requirements (Gupta, 2003). Fossil fuels are normally combusted to yield the energy contained within them in a useful state, releasing carbon dioxide. The increasing concentration of carbon dioxide, on a global scale, is raising concerns about the possibility of global warming. Atmospheric concentrations of CO_2 have increased 30% since the pre-industrial era from 280 ppm to the current level of 360 ppm today.

The connection between increasing atmospheric CO_2 concentrations and climate change is now recognized by a number of international organizations including the United Nations Framework Convention on Climate Change (UNFCCC), the Intergovernmental Panel on Climate Change (White et al, 2003), and the European Union FP6 Framework. It is recognized that three major methods must all be utilized to stabilize atmospheric carbon dioxide concentrations:

- Increase energy efficiency
- Use less carbon intensive energy sources
- Sequester carbon dioxide in geological formations

1.1.1 Need for Carbon Dioxide Capture Technologies

Geological sequestration of carbon dioxide has been defined as 'the capture of CO_2 directly from anthropogenic sources and disposing of it deep into the ground for geologically significant periods of time' (Bachu, 2002). The CO_2 stream can be sequestered profitably in a number of ways including enhanced oil recovery (EOR) and enhanced coal bed methane (ECBM) operations. Geologic formations where CO_2 storage may be practical include deep saline aquifers, depleted CO_2 domes, salt domes, salt formations, hydrocarbon-containing shales, and depleted natural gas formations.

The first step in sequestering carbon dioxide is capture. Technologies for CO_2 capture have existed for decades in the natural gas processing and chemical processing industries. However,

when these technologies are applied to fossil fuel based electrical power generating plants, representing approximately 1/3 of anthropogenic CO_2 emissions (Herzog et al., 1991), the resulting cost of electricity is significantly higher than current levels. In order to avoid excessive economic disadvantage to nations adopting CO_2 sequestration more cost effective means of capturing carbon dioxide must be developed. An overview of carbon dioxide capture technologies and capture costs is given by the International Energy Agency (2004). Salem (2006) has prioritized research needs in the area of carbon dioxide capture technology for the coal powered electricity industry.

1.2 State-of-the-Art in Carbon Dioxide Capture Technologies

Carbon dioxide capture technologies associated with large combustion systems are generally classified into three categories: pre-combustion, combustion, and post-combustion (Berger, 2004).

1.2.1 Pre-Combustion

Pre-combustion carbon dioxide capture systems remove carbon from the fuel prior to final combustion. The major representatives of this category are the various gasification technologies in which solid or liquid fuels are gasified to create syngas composed primarily of H_2 and CO. The syngas is then further reacted to provide a low-carbon fuel gas, such as hydrogen, that is combusted.

These systems can be built at the commercial scale. The facilities will have high operating and capital costs. An example of this type of technology is the EPCOR 500 MW IGCC facility currently at the front-end engineering design stage. This facility is to be designed to capture 90% of the carbon from the coal fed to the facility with sequestration in geological formations in the Leduc area of central Alberta.

Huang et al. (2008) provide an overview and costs for CO_2 capture from pre-combustion facilities.

1.2.2 Combustion (Oxy-Fuel Combustion)

Carbon dioxide capture within the combustion system typically refers to power plants that supply a high purity oxygen stream along with a diluent – recycled flue gas or steam to moderate combustion temperature. Oxy-fuel combustion is currently being considered for both Pulverized Coal Combustors (PCC) and Circulating Fluidized Bed Combustors (CFBC). CFBC has the advantages of increased heat flux inside the combustor and the capability of transferring large quantities of solids through the combustor, which is a useful means of transferring heat from the combustor. The capability of a CFBC to remove large quantities of heat from the reactor greatly reduces the required flow of the diluent gas stream, reducing the costs associated with operation.

These systems are not yet commercially available at sizes relevant to large electrical power plants and are currently under development. CANMET is currently commissioning a 1 MWth CFBC combustor of this type. Foster Wheeler has announced plans for a 50 MWe demonstration plant to showcase this technology (Hack et al., 2007).

Buhre et al. (2005) provide an overview of oxy-fuel combustion technology for power generation.

1.2.3 Post-Combustion

Post-combustion carbon dioxide capture systems include a number of separation technologies including chemical and physical solvents, membranes, and adsorption onto solids such as activated carbon.

When used in large power plants these systems are generally characterized by low net efficiency for electrical power production, high capital costs, and/or high operating costs due to poor heat integration and the requirement to process large flue gas flows as a result of the high nitrogen content of air blown combustion processes.

Rao and Rubin (2002) provide a technical and economic assessment of post combustion CO_2 capture technology.

1.2.4 CaO-$CaCO_3$ Looping Combustion

A low cost option for carbon dioxide capture may be a hybrid of the combustion and post-combustion categories. CaO-$CaCO_3$ looping combustion uses high temperature sorbents for post-combustion capture of the CO_2. Regeneration can be performed via oxy-fuel combustion in a fluidized bed. An economic evaluation of this type of process has been completed by Abanades et al. (2004) and proves quite promising.

DuMotay and Marechal first patented the idea of using lime in reaction 1.1 for CO_2 separation in 1867 to aid in the gasification of carbon by steam (Squires, 1967). The reaction was again used in the Acceptor Gasification Process (Curran et al, 1967).

$$CaO\ (s) + CO_2\ (g) \Leftrightarrow CaCO_3\ (s) \qquad 1.1$$

Combustion, CO_2 segregation, and nearly complete sulphur removal could occur in twin-fluidized beds operating at atmospheric or elevated pressures. (Shimizu et al., 1999; Abanades et al., 2003b; Epple and Strohle, 2008; Fennel, 2008; Masek et al., 2008; Romeo et al., Schuster, 2008). In operation, the process would provide a relatively pure stream of CO_2 for sale or sequestration. Deactivated limestone or lime could be used in the construction industries resulting in reduced CO_2 emissions from lime kilns.

Figure 1.1 provides a block flow diagram of the CaO-$CaCO_3$ looping process. Flue gases from a conventional air-blown combustor are directed to a fluidized bed carbonator where reaction 1.1 occurs resulting in carbon dioxide being removed from the flue gas. Reaction 1.1 is exothermic resulting in heat being released into the fluid bed. This heat is used for generating high quality steam for the power cycle. The hot flue gases exiting the carbonator pass through a series of heat exchangers where additional steam is produced.

The $CaCO_3$ formed in the carbonator flows to an oxygen-fired circulating fluidized bed combustor (calciner). The calciner is operated at a sufficiently high temperature (850-950°C) for the carbon dioxide to be released into the gas phase thus regenerating the sorbent. The reverse of reaction 1.1 is endothermic and so heat must be supplied for it to proceed. Combustion of a fossil fuel supplies the necessary heat. In order to avoid diluting the generated carbon dioxide

gas purified oxygen is used as the oxidant rather than air. Recycled flue gas, primarily composed of carbon dioxide and water, is mixed with the oxygen to provide sufficient fluidizing gas and in order to avoid hot spots in the calciner. The hot flue gases exiting the calciner are passed through heat exchangers to produce steam for the power cycle. The gases undergo limited tail gas treatment before being compressed for sequestration.

In this process carbon dioxide capture and sorbent regeneration occur at elevated temperatures that are suitable for producing high quality steam. This is in contrast with the carbon dioxide separation steps in most pre-combustion (ex. Rectisol, Selexol) and post-combustion (ex. amine scrubbing, chilled ammonia) technologies in which large quantities of low quality heat must be supplied to regenerate the CO_2 absorbent. This difference is the reason CaO-$CaCO_3$ looping technology is expected to have a much lower efficiency penalty than the more conventional pre-combustion and post-combustion technologies. Oxy-fuel combustion requires the production of large quantities of purified oxygen resulting in large efficiency penalties. CaO-$CaCO_3$ looping technology requires approximately 1/3 of the purified oxygen that an equivalently sized oxy-fuel combustor does and therefore has a much smaller energy penalty for the production of oxygen.

An advantage of this approach is that CO_2 removal conditions result in a Ca:S molar ratio on the order of 20-30, yielding SO_2 emissions levels in the area of a few parts per million (Abanades, 2003) via:

$$CaO\ (s) + 1/2O_2 + SO_2 \Rightarrow CaSO_4 \qquad 1.2$$

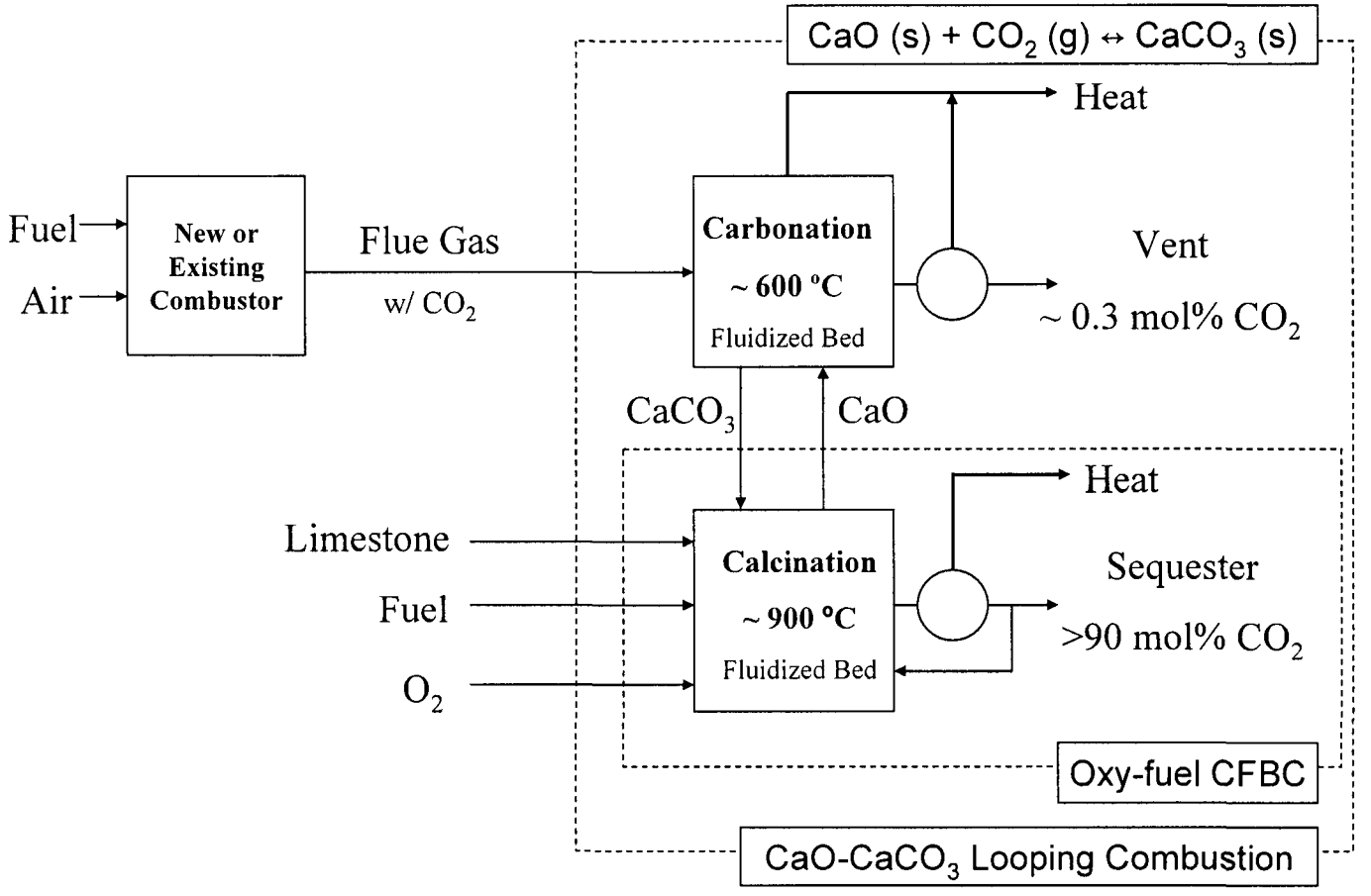

Figure 1.1: Processes for CO_2 capture; CaO-$CaCO_3$ looping and Oxy-fuel CFBC

1.3 Research Objectives

Table 1-1: Research Objectives

	Development Step	Objectives
1.0	Sorbent Development	1.1 Extend the lifetime of the sorbent providing a conversion of CaO to $CaCO_3$ of at least 0.4 after 20 calcination-carbonation cycles.
2.0	Process Simulation	2.1 Provide plant sizing and equipment selection information for both pilot scale and commercial scale fluidized bed carbon dioxide capture technologies. 2.2 Provide a platform for process and economic optimization studies.
3.0	Design and Construct a Pilot Plant for Proof of Technology	3.1 Prove the capabilities of each of the configurations. 3.2 Determine acceptable operating conditions and practical operational limitations for each of the configurations. 3.3 Determine practical start-up and shut-down routines for each of the configurations. 3.4 Allow the validation of process modeling and scale-up activities.
4.0	Evaluate Sorbent Characteristics and Performance at Pilot Scale	4.1 Evaluate sorbent attrition to determine variation and extent of material loss from the looping system. 4.2 Evaluate changes in sorbent morphology and localized sorbent composition to provide a basis for particle reaction modeling.

1.4 Techniques for Obtaining and Analyzing Data

A variety of bench-scale and pilot-scale equipment has been used for obtaining the data for this thesis. The equipment used is described within each chapter of the thesis since in many cases the same test facility was configured differently to meet the needs of the various research objectives. The primary piece of equipment utilized was a dual fluidized bed combustion facility that was

constructed as part of this work. Each of the two beds has an inner diameter of 0.1 m and can operate in fixed bed, bubbling bed or fast fluidized bed fluidization regimes. The beds are arranged in order to allow fluidization of the sorbent with varying concentrations of gases including oxygen, recycled flue gas, steam, air, and CO_2. The facility is equipped with data logging and control equipment allowing automatic monitoring and operation.

Bench-scale and analytical equipment was used to determine individual characteristics of the sorbents and sorbent precursors in a more 'controlled' manner since it is often difficult to independently vary parameters in pilot facilities. Thermogravimetric analysis was used to determine changes in weight of the sorbent, and thereby extent of reaction, under various gas atmospheres and temperatures. A rotating drum friabilator was used to determine relative resistance to attrition. Optical microscopy with a digital counting algorithm was used to determine particle sphericity and size distribution. Scanning electron microscopy with energy dispersive x-ray diffraction was used to determine sorbent morphology while providing semi-quantitative elemental composition. Unless otherwise noted, composition was determined using ASTM methods.

Nitrogen porosymmetry was used to determine sorbent surface area and pore size distribution. When considering the results one should understand that surface area is indicative of the rate of carbonation during the rapid reaction phase while the pore volume at pore radii of less than about 200 nm is indicative of the capture capacity of the CaO during the rapid reaction phase (Bhatia and Perlmutter, 1983; Abanades et al., 2003a; Fennel et al., 2007). It should be noted that the paper by Bhatia and Perlmutter provides a useful reference for determining the kinetics of carbonation.

Example calculations are provided in appendices for the determination of single point surface area (Appendix 1), pore size distribution by the BJH method (Appendix 2), and the conversion of CaO to $CaCO_3$ and CaO to $CaSO_4$ (Appendix 3). Dimensioned drawings of some portions of the dual fluidized bed pilot facility are provided in Appendix 4. Selected initial 'as-built' process and instrumentation diagrams (P&ID) for the dual fluidized bed pilot facility system are provided in Appendix 5 showing the oxy-fuel CFBC and recycle flue gas system.

1.5 Research Outline

This research began with a series of bench scale studies (Chapters 2 through 4) directed toward evaluating and improving the performance of limestone derived sorbents for CO_2 capture. In Chapter 2, Improved Long-term Capacity of Limestone Sorbents for *In Situ* Capture of CO_2 in a Fluidized Bed Combustor, surface mapping methods based on thermogravimetric analysis of the sorbent are described that were used to determine the optimal operating temperatures for carbonation and calcination in order to maximize the conversion of CaO to $CaCO_3$ over multiple cycles. A sorbent pre-treatment method, hydration, was used to increase the performance of the sorbents for CO_2 capture to the point where conversion would appear to be sufficient to make CaO-$CaCO_3$ looping competitive with conventional CO_2 capture technologies. Porosymmetry methods were used in order to determine the textural changes that occur over multiple calcination/carbonation cycles.

The studies described in Chapter 2 do not include gas species that would be present in commercial CO_2 capture facilities that are known to degrade the performance of the sorbent. In Chapter 3, Sintering and Reactivity of $CaCO_3$-based Sorbents for *In Situ* CO_2 Capture in Fluidized Beds under Realistic Calcination Conditions, further bench scale studies are described in which carbon dioxide and sulphur dioxide are present in the calcining environment used in the thermogravimetric analysis. These studies include both untreated and hydrated sorbents. In this work it is recommended that sulphur capture be performed prior to carbon dioxide capture since the formation of $CaSO_4$ occurs preferentially near the surface of the sorbent particles resulting in rapid reduction in CO_2 capture capacity. It is determined that realistic CO_2 concentrations, i.e. >90 vol.%, greatly reduce the performance of the sorbents over multiple cycles, though the hydrated sorbents do perform better than the untreated sorbents.

Unfortunately, hydrated sorbents are quite friable and are expected to attrite rapidly under fluidized bed conditions. Hence, the final bench scale studies involved pelletization of the sorbent with various binders to produce more highly reactive and attrition recent sorbent pellets. These studies are described in Chapter 4, Hydration and Pelletization of $CaCO_3$ Derived Sorbents for *In-Situ* CO_2 Capture. Here, pelletized limestone derived sorbents are compared to untreated crushed limestone for carbonation conversion over multiple cycles both with and without SO_2 addition. A portion of

the pellet recipes investigated resulted in sorbents with much superior performance compared with untreated crushed limestone sorbents. These pellet recipes showed carbonation conversions well within the commercially viable envelope.

While performing the bench scale studies I had obtained funding for constructing pilot-scale facilities to demonstrate and investigate the technologies. In order to design the pilot-scale facilities I created process simulations in ASPEN Plus for both oxy-fuel circulating fluidized bed combustion and CaO-$CaCO_3$ looping technologies. The results of the bench scale studies described in Chapters 2 through 4 were used to set the parameters for the process simulations. The simulations provided equipment selection and sizing information for the pilot plant and are suitable for performing process and economic studies. A description of the facilities and some selected results from process studies are provided in Chapter 5, Design, Process Simulation, and Construction of an Atmospheric Dual Fluidized Bed Combustion System for *In Situ* CO_2 Capture using High-temperature Sorbents.

Construction of the pilot facility began with the oxy-fuel circulating fluidized bed combustor since I felt that development of this portion of the CaO-$CaCO_3$ looping technology was the most critical to demonstrate as it involved the most severe conditions and this portion of the process had the greatest effect on degrading the sorbent. In Chapter 6, Oxy-Fuel Combustion of Coal in a Circulating Fluidized Bed Combustor, the first commissioning runs of the oxy-fuel CFBC are described. In these tests coal and blends of coal with biomass were burned with oxygen combined with recycled flue gas. Air-blown and oxy-fuel tests performed as part of commissioning are compared. During these commissioning runs information was gathered that allowed me to develop practical start-up and shut-down routines (both network diagram and stepwise procedures) and verify acceptable operating conditions and operational limitations for the pilot facility that I had initially determined by process simulation.

After the oxy-fuel CFBC was deemed to be operating in a safe and dependable fashion the balance of the dual fluidized bed facility was constructed and commissioned. Chapter 7, Ca-Based Sorbent Looping Combustion for CO_2 Capture in Pilot-Scale Dual Fluidized Beds describes some of the early testing performed on the dual fluidized bed facility. In these tests oxy-fuel combustion of coal or oxy-fuel combustion of blends of coal and biomass were used for calcining the sorbent. Synthetic

flue gas was passed through the carbonator where CO_2 was captured by the sorbent to equilibrium levels. The sorbent was pneumatically conveyed between reactors in a semi-continuous fashion with solids flow rates controlled by rapid acting solenoid valves. Operating routines and operational limitations were verified for the CaO-$CaCO_3$ looping facility.

During these tests it was found that sorbent attrition was more extensive than expected. In Chapter 8, Attrition of Calcining Limestones in Circulating Fluidized-Bed Systems, studies evaluating sorbent attrition are presented for several limestones. The studies include testing in the pilot scale equipment with analysis using an optical counting technique. It was found that limestone attrition was highly variable from stone to stone and could be reduced somewhat with low levels of sulphation.

In the early CaO-$CaCO_3$ looping studies (Chapters 7 to 8) the calciner had a problem with air in-leakage that resulted in CO_2 concentrations being lower than would be expected in a commercially operating facility. After the air in-leakage problem had been mitigated and carbon dioxide concentrations had increased within the calciner it was found that conversion of CaO to $CaCO_3$ was greatly reduced. At the same time, in order to provide sufficient temperature to calcine the sorbent while maintaining the desired fluidization velocities, the oxygen concentration in the fluidizing gas was increased. In order to understand what changes had occurred in the sorbent a series of tests were initiated in which low-ash, low-sulphur fuels were burned for supplying the heat of calcination. These studies are presented in Chapter 9, Changes in Limestone Sorbent Morphology During CaO-$CaCO_3$ Looping at Pilot Scale.

1.6 References

Abanades, J.C., Alvarez, D., (2003a). 'Conversion Limits in the Reaction of CO_2 with Lime', Energy and Fuels 17(2), 308-315.

Abanades, J. C.; Alvarez, D.; Anthony, E. J.; Lu, D. (2003b). '*In-situ* Capture of CO_2 in a Fluidized Bed Combustor'. Proceedings of the 17th FBC Conference, Jacksonville, Florida.

Abanades, J.C., Rubin, E.S., Anthony, E.J., (2004). 'Sorbent Cost and Performance in CO_2 capture Systems', Ind. Eng. Chem. Res. 43(13), 3462-3466.

Bachu, S., (2002). 'Sequestration of CO_2 in Geological Media in Response to Climate Change: Road Map for Site Selection using the Transform of the Geological Space into the CO_2 Phase Space', Energy Convers. Mgmt. 43(1), 87-102.

Berger, R. (2004). 'Calcium Cycle for Efficient and Low Cost CO_2 Capture in Fluidized Bed Systems', European Union Specified Targeted Research Project, University of Stuttgart, Germany.

Bhatia, S.K., Perlmutter, D.D. (1983). 'Effect of the Product Layer on the Kinetics of the CO_2-Lime Reaction', AIChE J. 29(1) 79.

Buhre B.J.P., Elliot, L.K., Sheng, C.D., Gupta, R.P., Wall, T.F., (2005). 'Oxy-fuel Combustion Technology for Coal-Fired Power Generation', Progress in Energy and Combustion Science 31, 283-307.

Curran, F.P, Fink, C.E., Gorin, E., (1967). 'Carbon Dioxide Acceptor Gasification: Process Studies of Acceptor Properties', Adv. Chem. Ser. 69, 141.

Epple, B., Strohle, J., (2008). 'Feasibility Study on Carbonate Looping Process for Post Combustion CO_2-Capture from Coal Fired Power Plants' 4th International Workshop on *In-Situ* CO_2 Removal, London.

Fennel, P., (2008). 4th International Workshop on *In-Situ* CO_2 Removal, London.

Gupta, M., Coyle, I., Thambimuthu, K., (2003). 'CO_2 Capture Technologies and Opportunities in Canada', 1st Canadian CC&S Technology Roadmap Workshop, Alberta, Canada.

Hack, H., Seltzer, A., Stanko, G., (2007). 'Design Considerations for Advanced Materials in Oxygen-Fired Supercritical and Ultra-Supercritical Pulverized Coal Boilers', 5th Int. conf. on Advanced Materials technology for Fossil Power Plants, Forida.

Herzog, H., Golomb, D., Zemba, S., (1991). 'Feasibility, Modelling and Economics of Sequestering Power Plant CO_2 Emissions in the Deep Ocean', Envir. Prog. 10(1), 64-74.

Huang, Y., Rezvani, S., McIlveen-Wright, D., Minchener, A., Hewitt, N., (2008). 'Techno-economic Study of CO_2 Capture and Storage in Coal Fired Oxygen Fed Entrained Flow IGCC Power Plants', Fuel Proc. Tech. 89, 916-925.

International Energy Agency, (2004). 'Prospects for CO_2 Capture and Storage', OECD/IEA, France.

Masek, O., Bosoaga, A., Oakey, J., (2008). 'Progress in Ca-based CO_2 capture research at Cranfield University', 4th International Workshop on *In-Situ* CO_2 Removal, London.

Rao, A., Rubin, E., (2002). 'A Technical, Economic, and Environmental Assessment of Amine-Based CO_2 Capture Technology for Power Plant Greenhouse Gas Control', Env. Sci. Tech. 36(20), 4467-4475.

Romeo, L., Lisbona, P., Martinez, A., Lara, Y., (2008). 'Test Facility for the Hydrodynamic Characterization of Two CFBs for Ca Looping Systems', 4th International Workshop on *In-Situ* CO_2 Removal, London.

Salem, G., (2006). 'Carbon Dioxide Capture Technology for the Coal Powered Electricity Industry: A Systematic Prioritization of Research Needs', MSc Thesis, Massachusetts Institute of Technology, USA.

Schuster, A., (2008). 'Calcium Looping Activities at IVD', 4th International Workshop on *In-Situ* CO_2 Removal, London.

Shimuzu, T., Hirama, T., Hosoda, H., Kitano, K., Inagaki, M., (1999). 'A Twin Fluid-bed Reactor for Removal of CO_2 from Combustion Processes', Chem. Eng. Res. Des. 77(1), 62-68.

Squires, A. M. , (1967). 'Cyclic Use of Calcined Dolomite to Desulfurize Fuels Undergoing Gasification'. Adv. Chem. Ser., 69, 205-229.

White, C.M., Strazisar, B.R., Granite, E.J., Hoffman, J.S., Pennline, H.W., (2003). 'Separation and Capture of CO_2 from Large Stationary Sources and Sequestration in Geological Formations – Coalbeds and Deep Saline Aquifers', J Air Waste Manag Assoc 53(6), 645-715.

Chapter 2 Improved Long-term Capacity of Limestone Derived Sorbents For In Situ Capture of CO_2 in a Fluidized Bed Combustor

Published in Industrial & Engineering Chemistry Research

Hughes, R.W.[1], Lu, D.[1], Anthony, E.J.[1], Wu, Y.[1], 'Improved Long-term Capacity of a Limestone Derived Sorbent for In Situ Capture of CO_2 in a Fluidized Bed Combustor', Ind. Eng. Chem. Res. 43, 2004, 5529-5539.

[1]Natural Resources Canada, CETC-O, 1 Haanel Drive, Ottawa, Canada K1A 1M1

2.1 Abstract

Cyclic carbonation and calcination reactions are investigated for capturing CO_2 from combustion and gasification processes. Sorbent particles in the size range 600-1400 μm were subjected to multiple capture cycles at atmospheric pressure to obtain a surface mapping of conversion based on calcination and carbonation temperatures. Steam hydration of CaO was utilized to increase both pore area and pore volume to improve long-term conversion to $CaCO_3$ over multiple cycles. The steam hydration improved the long-term performance of the sorbent resulting in directly measured conversions as high as 52% and estimated conversions as high as 59% after up to 20 cycles. It is estimated that the increase in conversion has improved the economics of the proposed process to the point where commercialization is attractive. It has been shown that, when carbonating in the temperature range from 700°C to 740°C, calcination temperatures from 700°C to 900°C can be used without seriously reducing the capacity of CaO for CO_2 capture over multiple cycles. Processes based on this approach are expected to be able to reduce CO_2 emissions from coal- and petroleum coke-fired fluidized bed combustors by up to 85%, while avoiding excessive sorbent replacement.

Keywords: carbon dioxide capture, separation, calcium oxide, fluidized bed

2.2 Introduction

The need to reduce CO_2 emissions along with pollutants such as SO_2 and NO_x is now generally accepted (Harrison, 1992). At the same time there is a growing need for increased electricity generation. If both sets of requirements are to be met without excessive economic disadvantage to the world economy, then new electrical generation methods with low or zero CO_2 emissions must be developed. Typically, processes supplying high capacity, low value products, such as electricity, are most economical when the feedstock is of low cost and commonly available, the processes are simple and have high dependability, when the capital costs are low, and when by-products are of a value-added form. Economics and risk analysis will often preclude the use of processes utilizing multiple steps, unproven technologies, and exotic materials either for construction or as integral components of a new technology (*e.g.*, palladium for H_2 storage).

The reversible carbonation of lime (reaction 2.1) has the potential to form the basis of a clean, economically feasible combustion process using currently available technologies under moderate conditions for generation of electricity.

$$CaO\ (s) + CO_2\ (g) \Leftrightarrow CaCO_3\ (s) \qquad 2.1$$

The feed stocks for such a process would include limestone and inexpensive fuels such as coal and petroleum coke. Combustion, CO_2 segregation, and nearly complete sulphur removal could occur in twin-fluidized beds operating at atmospheric or elevated pressure. Circulating fluidized bed combustors (CFBCs) are intrinsically low producers of NO and are amenable to NH_3 injection if very low emissions of NO are desired (Grace et al., 1997). N_2O emissions can be minimized by operating at temperatures around 900°C or by producing high-temperature windows in the cyclone (Gustavsson, 1995). In operation, the process would provide a relatively pure stream of CO_2 for sale or sequestration. Deactivated limestone or lime could be used in the construction industries.

An advantage of this approach is that CO_2 removal conditions result in a Ca:S molar ratio on the order of 20-30, meaning that SO_2 emissions levels will be of the order of a few parts per million (Abanades, 2003). This has two advantages. First, excess lime does not have to be used for sulphur

removal itself, which means that lime use for sulphur removal can be regarded as effectively quantitative, *i.e.*, it is necessary to replace lime for the actual amount of sulphur removed but no extra lime need be used for the goal of sulphur removal itself. Second, polishing the gas stream for CO_2 removal with amine scrubbing, which involves reducing SO_2 levels to below 10 ppm (Couturier, 1986), would involve no extra treatment step. Polishing would allow such a process to achieve any desired level of CO_2 removal, whereas the basic process itself could be used to remove 80-85% of the CO_2.

DuMotay and Marechal first patented the idea of using lime in reaction for CO_2 separation in 1867 to aid in the gasification of carbon by steam (Squires, 1967). The reaction was again used in the Acceptor Gasification Process (Curran et al., 1967). In both cases reaction 2.1 was used to improve the equilibrium conditions by the removal of CO_2 from the gas phase, which shifts the equilibrium of the water gas shift reaction 2.2 to the right, increasing hydrogen production following the Law of Mass Action.

$$H_2O + CO \Leftrightarrow CO_2 + H_2 \qquad 2.2$$

However, the primary goal was not to segregate carbon dioxide. Recently, there have been a number of investigations focused on CO_2 separation from process and flue gases accommodated by the carbonation reaction. Such a process, producing a high purity CO_2 stream, was developed by Silaban and Harrison (1995) as it related to work on the simultaneous shift reaction and carbon dioxide separation for direct production of hydrogen in a fixed bed. Shimizu et al. (1999) proposed a combustion process for carbon dioxide removal from a flue gas using twin fluid bed reactors with a CaO-$CaCO_3$ looping cycle. Shimizu et al. claimed that the proposed process had a higher overall efficiency including O_2 production and CO_2 liquefaction (95% pure, dry basis) than competing O_2/CO_2 combustion processes. Abanades et al. (2003) proposed a similar process using fluidized bed combustion operating at elevated pressures and temperatures in order to improve steam cycle efficiency and allow the combustion of a variety of fuels with *in situ* CO_2 removal.

For any fluidized bed combustion process, the use of CaO as a sorbent will have a number of limitations. The limitation that most directly affects the steam cycle is the thermal equilibrium of the carbonation reaction. The equilibrium vapour pressure of CO_2 over CaO is given by Baker (1962):

$$\log_{10} P_{eq}[atm] = 7.079 - \frac{8308}{T[K]} \qquad 2.3$$

At combustion temperatures conducive to high steam cycle efficiency, the equilibrium of the reaction is unfavourable at atmospheric pressure. In addition, at temperatures allowing efficient combustion of most fuels excluding biomass (> 800°C, 101 kPa), the reaction equilibrium is unfavourable.

Figure 2.1 shows CO_2 concentration at equilibrium for reaction 2.1 at atmospheric pressure over the temperature range 600 to 900°C. The approximate maximum CO_2 concentration for petroleum coke in an air-blown combustor is plotted at $[CO_2]$ = 15 mol%. It is apparent that at atmospheric pressure, no carbon dioxide can be removed from such a system at temperatures above 778°C using the carbonation reaction. Clearly, combustion and carbonation must occur at differing temperatures in an atmospheric air-blown system. Carbonation and combustion could occur in separate vessels as proposed by Shimizu et al. (1999), or alternatively, in an integrated two-stage fluidized bed combustor as we have proposed (Abanades et al., 2003).

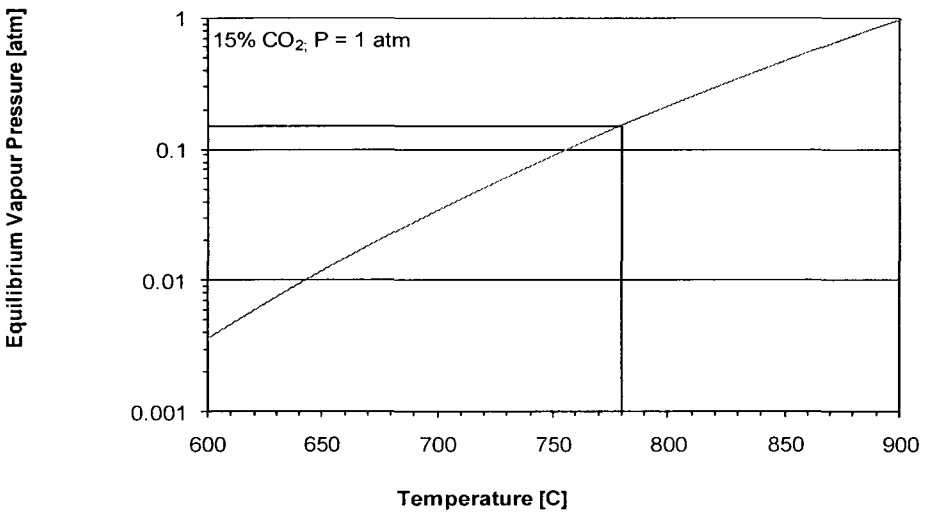

Figure 2.1: Equilibrium vapour pressure of CO_2 over CaO as predicted by Equation 2.3.

Figure 2.2 shows a process flow diagram of a twin fluid bed combustion system with CO_2 segregation operating at atmospheric pressure. A scheme such as this could burn low-grade fuels, such as petroleum coke, while producing a relatively pure CO_2 stream (~95%+, dry basis) suitable for liquefaction and emitting less than 5 mol% CO_2, a few parts per million of SO_2, and at most a few hundred parts per million of NO to the atmosphere (Grace *et al.*, 1997). Combustion occurs in the first stage of the carbonating combustor (R-101) at an optimum temperature for combustion (850°C-950°C) and carbonation occurs in the second stage at an optimum temperature for CO_2 capture, which will be determined by the pressure of the carbonator. Calcination occurs in the second fluid bed (R-100).

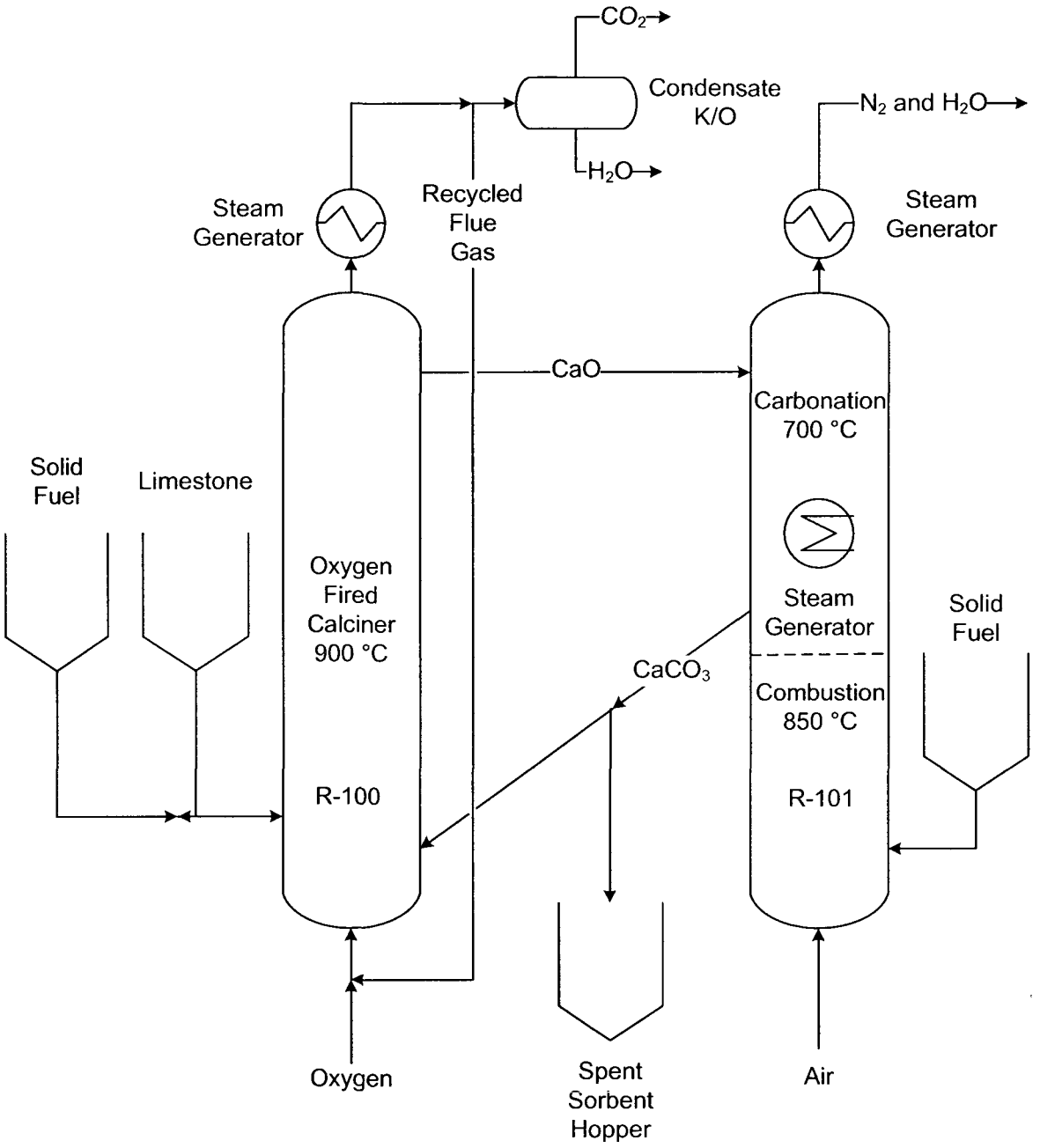

Figure 2.2: Process for CO_2 removal at atmospheric pressure

While this is a viable process, CaO is further limited as a sorbent. Carbon dioxide sorption onto CaO is rapidly reduced with each cycle of conversion. The capacity of untreated limestone decreases from cycle to cycle as seen by Curran et al. (1967), Baker (1962), Silaban and Harrison (1995), and Shimizu et al. (1999). The reduction in capacity for untreated limestone can be modeled using the equation proposed by Abanades and Alvarez (2003). This model predicts capacity using the concept of suitable porosity where there are a decreasing quantity of small pores and an increasing number of large pores. The available surface area is reduced as the number of calcination-carbonation cycles increases due to textural changes of the sorbent. The model results in the following equation for conversion based on cycle number:

$$X_N = f_m^N (1 - f_W) + f_W \qquad 2.4$$

where X_N is the carbonation conversion after N calcination-carbonation cycles.

Abanades and Alvarez (2003) indicate that values of $f_m = 0.77$ and $f_W = 0.17$ fit most experimental data quite well. This model predicts that as $N \rightarrow \infty$ carbonation conversion will approach a value of 0.17. For this process to be economical, it is estimated that the value of X_N after 20 cycles should increase to a minimum of approximately 0.45 (Abanades, 2004). The goal of this work is to increase X_N by sorbent modification (Salvador et al., 2003) to a value that would allow commercial implementation of this process at an industrial scale. Equation 2.4 is used in this work to compare the ultimate performance of sorbents under varying conditions.

A further goal of this work is to understand how any performed sorbent modifications have improved long-term carbonation conversion. The use of limestone for SO_2 removal from within fluidized beds has been under study for over 30 years (Anthony and Granatstein, 2001). The effective use of limestone for SO_2 capture has been shown to be dependent on a number of parameters including diffusional resistance as affected by the size, volume and configuration of the pore structure, surface area, and reaction kinetics (Gullet and Bruce, 1987). The same parameters affect the carbonation reaction and much of what has been learned from the sulphation reaction can be applied.

Previous investigators have shown that it is possible to modify the pore size distribution in CaO to improve capacity for the sulphation reaction. Gullet and Bruce (1987) showed that the optimum pore size for the sulphation reaction was in the range of 10 to 20 nm. This size range reduced pore plugging while not reducing surface area excessively. While the molar volume of $CaCO_3$ (36.9 cm^3/gmole) is somewhat less than that for $CaSO_4$ (46 cm^3/gmole), the optimum pore size range will likely be in the same region.

It is reasonable to assume that, in the initial fast reaction phase of the carbonation reaction, the rate of reaction is largely dependent on the surface area of the reacting particle. As the carbonation reaction proceeds, CO_2 diffusion resistance will become rate limiting due to pore filling at the outer portion of the lime particle. As the relatively slow second reaction phase begins, product layer diffusion becomes rate controlling. Reaction continues in the second phase at a relatively constant rate for a long period. Pre-screening investigations have shown that reaction continues for more than 24 hours. If it was possible to avoid product layer diffusion until higher conversion was achieved, then the reaction could proceed at a heightened rate for an extended period. One method of overcoming the diffusional resistance in solid particles is to introduce larger pores allowing rapid diffusion to the centre of the particle. This generally has the effect of reducing overall surface area, but if the reaction is severely diffusion limited, it may increase overall conversion for a given reaction time.

Upon hydration, cracks are formed in lime particles. These cracks can create channels extending towards the interior of the particle. This has the effect of modifying the pore structure to allow rapid diffusion of CO_2 through large pores to the particle interior followed by slower diffusion into the locally available high surface area pores. A scanning electron micrograph (SEM) of $CaO/CaSO_4$ bed ash particles in the size range 300 to 600 μm can be seen in Figure 2.3. The outer shell of the particle is composed of $CaSO_4$, while the interior is composed primarily of CaO. It is apparent that the particles are free of cracks and large diameter pores leading to the particle interior.

Figure 2.4 shows a bed ash particle in the same size range that has been hydrated in steam for 30 minutes at 150°C. It is apparent that both large cracks and larger diameter pores have been created. Pores of larger diameter will allow conversion to proceed further before the reaction becomes diffusion limited due to pore plugging. It should also be noted that some small particles have been created which will have a reduced residence time in a fluidized bed and this will limit conversion for these smaller particles.

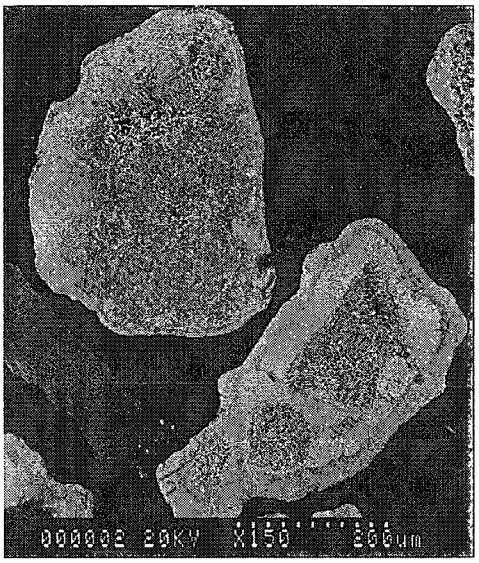

Figure 2.3: SEM photograph of un-hydrated bed ash, 300-600 μm

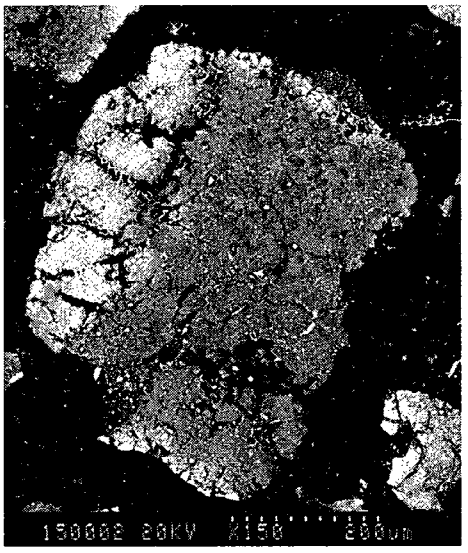

Figure 2.4: SEM Photograph of bed ash steam hydrated at 150°C for 30 minutes, 300-600 μm.

2.3 Experimental Method

The temperature ranges selected for the carbonation and calcination reactions are based on thermodynamic considerations as given by Equation 2.1. The carbonation temperature range is limited to less than 780°C for a stream containing 15 mol% CO_2 at atmospheric pressure. Preliminary runs indicated that multi-cycle performance was degraded at calcination temperatures in excess of 850 °C. Carbonation temperatures below 650°C were deemed too low for the combustion of most fuels and, therefore, too low for the *in situ* removal of CO_2 in a fluidized bed combustor.

In an effort to improve the multiple cycle conversion, a subset of the experimental runs was performed using pre-treated material. The pre-treatment consisted of calcination and hydration steps. The pre-treatment calcination was carried out in an oven at atmospheric pressure in air. The calcination during a cycle is with N_2 and the temperature range utilized is that given in Table 2-1. The pre-treatment calcination was varied independently of the multiple cycle calcination temperature to determine optimum conditions. The sample was weighed before and after

calcination to verify that complete calcination had occurred. The sample remained in the oven at the set temperature for 2 hours.

The hydration step was performed within a 2 L Parr 4522M-pressure reactor, which has been described elsewhere (Anthony et al., 2000). The sample was placed on a piece of filter paper in an aluminum sample dish within the vapour space of the pressure reactor. The vapour space consisted of saturated steam at 150°C and 475 kPa. Air was purged from the system after the temperature in the bomb exceeded 100°C. After hydration the sample was dried in a vacuum oven at 50°C for 2 hours.

Design of experiment software was used to select experimental conditions within the boundaries given in Table 2-1. Calcination and carbonation temperatures were selected using the central composite surface design method. The method utilizes a 2(k-p) design that is enhanced by centre and star points.

Table 2-1. Experimental conditions

Pre-treatment	730 to 884°C; 101 kPa; 100% Air
Calcination	730 to 884°C; 101 kPa; 100% N_2
Carbonation	630 to 771°C; 101 kPa; 15% CO_2, 85% N_2
Steam Hydration	150°C; 475 kPa; 100% H_2O; 2 hours

Four cycles were completed for each experimental run performed since capacity decay is nonlinear and effective curve fitting would require multiple cycles. The capacity of untreated limestone decreased from cycle to cycle following the decay process described by Abanades and Alvarez (2003).

The sample mass was monitored in multi-cycle calcination and carbonation runs using a Cahn Model C-1100 thermogravimetric analyzer (TGA). The sample was suspended in a 316 stainless steel hang-down tube on a platinum pan. Temperature was measured using a Type K thermocouple that was inserted axially into the hang-down tube below the sample pan. The temperature was controlled using a Lab-Temp tube furnace and Lab-Temp controller. The heating rate used was 20°C/min. The cooling rate was dependent on the operating temperature, but was typically in the area of 50°C/min.

N_2 and CO_2 feed rates were controlled using Matheson mass flow controllers. The gases flowed upwards within the hang-down tube of the Cahn Thermo Balance. Data were recorded at 5-second intervals using a Keithley 2700 data acquisition system connected to a personal computer running Keithley Xlinx Software. The experimental setup is described elsewhere (Anthony and Jia, 2003).

To help understand why a single hydration treatment can improve the long-term conversion of CaO to $CaCO_3$ over multiple cycles a number of adsorption and desorption experiments were performed. The experiments were performed using Cadomin and Kelly Rock limestones, both with and without hydration after the initial calcination step.

Two sets of conditions were used for carbonation and calcination (Table 2-2) prior to the adsorption experiments. The first set of conditions was chosen because previous experiments had indicated that this combination of calcination and carbonation temperatures often gave the highest conversion after 4 cycles. The second set of conditions was chosen to simulate the temperatures that might be employed in a potential design for the CO_2 separation process described earlier.

Table 2-2. Range of experimental conditions for pore structure analysis

Condition Set	Initial Calcination Temp. [°C]	Hydration Pre-Treatment Temp. [°C]	Carbonation Temp. [°C]	Calcination Temp. [°C]
1	820	150	750	750
2	820	150	700	915

Initial calcination was performed in an air atmosphere in an oven as described earlier. Hydration was performed in the Parr reactor as described above for the conversion maximization experiments. Due to the quantity of sample required to determine Brunauer-Emmett-Teller (BET) surface areas, cyclic carbonation-calcination could not be performed in the TGA, as was done for the earlier tests. Instead, a tube furnace was employed to produce the samples by operating at the appropriate temperatures and gas concentrations.

Adsorption and desorption isotherms were created for all samples. The isotherms were created for samples after one cycle and 10 cycles for hydrated and untreated samples with a constant temperature of 750°C for carbonation and calcination. The samples were to represent the sorbent as used in a partial pressure swing system.

Adsorption and desorption isotherms were also generated for a carbonation temperature of 700°C and a calcination temperature of 915°C for both hydrated and untreated limestones. These samples were used to represent the sorbent as used in a temperature swing system. However, multi-cycle tests were not completed for these samples.

2.4 Sorbent Properties

The complete set of experimental runs was performed using Kelly Rock and Cadomin limestones. Preliminary runs were also performed using Havelock limestone. Analytical data for the two limestones are shown in Table 2-3.

Table 2-3. Limestone composition (wt%) by X-ray flourescence

Comp.	Kelly Rock	Cadomin
Al_2O_3	1.54	0
BaO	0.18	0
CaO	51.74	55.12
Fe_2O_3	0.36	0
K_2O	0.36	0.21
MgO	0.58	2.25
MnO	0.16	-
Na_2O	0.07	0
NiO	-	0
P_2O_5	0	0
SiO_2	5.31	1.5
SO_3	0.98	0.32
SrO	0.04	0
TiO_2	0.08	0
V_2O_5	-	0
LOF	43.14	42.77
SUM	104.55	102.19

2.5 Results and Discussion

2.5.1 Thermogravimetric Analysis

A chart for a typical multi-cycle run for pre-hydrated Cadomin sorbent showing the decay of sorbent capacity is shown in Figure 2.5. For this experimental run the pre-calcination temperature was 800 °C, the carbonation temperature was 700 °C, and the calcination temperature was 730 °C. It is apparent that calcination is rapid and complete at these conditions. Carbonation appears to be split into two phases, as has been previously reported (Curran et al., 1967; Silaban and Harrison, 1995) - a rapid reaction phase followed by a slow reaction phase.

The experiments were carried out at various conditions in an attempt to find the maximum multiple cycle capacity. The resulting conversion ratios between cycle 1 and cycle 2 from these runs are given in Table 2-4 for Cadomin and Table 2-5 for Kelly Rock limestone at a reaction time of 20 minutes. Table entries in bold highlight the most successful conditions for carbonation and calcination. The average first cycle conversion for Kelly Rock (0.74) over all conditions is somewhat higher than for Cadomin (0.71). The average ratio of conversions between cycle 1 and cycle 2 for the two limestones is nearly identical.

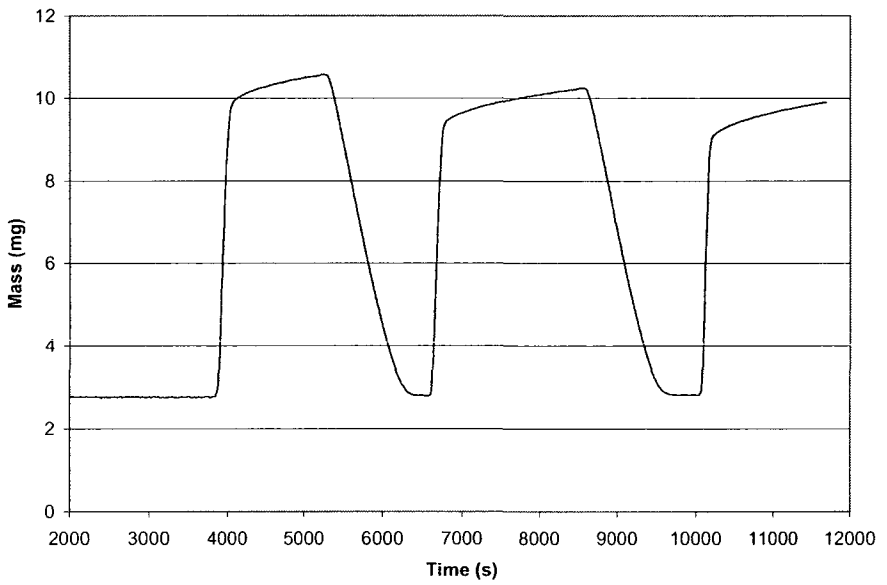

Figure 2.5: Typical multi-cycle weight of pre-hydrated Cadomin sorbent (Pre-calcined 800 °C, Carbonated 700 °C, Calcined 730 °C).

Table 2-4. Untreated and pre-treated Cadomin limestone conversion at 20 min.

		Untreated		Hydration Pre-treatment		
Calcination [° C]	Carbonation [°C]	X_1	X_2/X_1	X_1	Pre-Calc [°C]	X_2/X_1
740	**700**	0.69	0.83	**0.66**	**800**	**0.94**
750	650	--	--	0.74	750	0.85
		--	--	0.67	850	0.91
750	**750**	0.70	0.90	**0.73**	**750**	**0.93**
		--	--	0.71	850	0.99
800	630	0.66	0.79	0.75	800	0.78
800	700	0.71	0.86	0.46	730	0.85
		0.68	0.83	0.73	800	0.88
		--	--	0.69	800	0.88
		--	--	0.66	884	0.93
800	770	--	--	0.57	800	0.98
850	**650**	0.71	0.80	0.47	750	0.83
		--	--	**0.69**	**850**	**0.91**
850	**750**	0.72	0.84	**0.79**	**750**	**0.92**
		--	--	0.70	850	0.94
884	700	0.77	0.82	0.73	800	0.87

The ratios of conversions between cycles are similar in magnitude to those reported by Silaban and Harrison (1995) based on tests using reagent grade $CaCO_3$ at a cycle time of 40 min. They reported an X_2/X_1 ratio of approximately 0.87 at a calcination temperature of 750°C, carbonation temperature of 750°C, and atmospheric pressure with a 15% CO_2 in N_2 gas composition. Their results also indicated that the capacity maintenance ratio decreased slowly with increasing calcination temperature. They reported that, at a calcination temperature of 820°C, the capacity maintenance ratio was reduced to approximately 0.77.

Table 2-5 Untreated and pre-treated Kelly Rock limestone conversion at 20 min.

		Untreated		Hydrated		
Calcination [°C]	Carbonation [°C]	X_1	X_2/X_1	X_1	Pre-Calc [°C]	X_2/X_1
740	**700**	--	--	**0.73**	**800**	**0.96**
750	650	0.72	0.83	0.66	750	0.89
		--	--	0.67	850	0.89
750	**750**	0.78	0.87	**0.67**	**750**	**0.94**
		--	--	**0.75**	**850**	**0.94**
800	630	0.71	0.82	0.59	800	0.89
800	**700**	0.75	0.85	0.70	740	0.87
		0.75	0.84	**0.72**	**800**	**0.95**
		--	--	0.69	800	0.96
		--	--	**0.72**	**884**	**0.96**
800	770	0.76	0.86	0.65	800	0.95
850	650	0.71	0.82	0.52	750	0.88
		--	--	0.58	850	0.88
850	750	0.72	0.84	0.70	850	0.90
		--	--	0.57	750	0.94
884	700	0.75	0.84	0.67	800	0.95

The data for the untreated samples show that the conditions in the first cycle result in a variety of different conversions at the first cycle. Both calcination and carbonation temperature can change the first conversion from as low as 0.66 to as high as 0.78. Furthermore, various combinations of the two temperatures can result in a wide range of conversion levels. However, there is evidently a divergence in the way the two limestones behave when the relationship between X_1 and X_2/X_1 are considered. Plots of this relationship are shown in Figure 2.6 and Figure 2.7 for Cadomin and Kelly Rock limestones, respectively. Unlike Cadomin, Kelly Rock shows a direct correlation between X_1

and X_2/X_1. For Kelly Rock higher X_1 results in better maintenance of capacity and the reasons for this difference will be discussed in the section on pore analysis.

To aid in visualization of the results, contour plots have been utilized. The first cycle conversion for untreated Cadomin limestone is plotted in Figure 2.8, while first cycle conversion for untreated Kelly Rock is plotted in Figure 2.9.

The two limestones appear to be reacting similarly at calcination temperatures below 800°C with a slowly decreasing capacity as the calcination temperature increases. Above 800°C, the two limestones behave differently. Kelly Rock limestone continues to decrease in conversion as the calcination temperature increases, while conversion of Cadomin starts to increase as calcination temperature increases above 800°C. By contrast, Silaban and Harrison (1995) found that the first cycle conversion was nearly constant across this temperature range at a cycle time of 40 minutes; however, they also found that initial reactivity was reduced as the calcination temperature increased.

Surface mapping has been used to estimate CaO conversion over multiple cycles. Since the optimum conditions for maintaining carbonation capacity are not ideally suited for combustion or gasification processes, estimates of capacity are required for process modeling at a variety of conditions. The surface on the 3D maps has been plotted using a second order equation with interaction effects of the form:

$$X = AT_{Calc} + BT_{Calc}^{\ 2} + CT_{Carb} + DT_{Carb}^{\ 2} + ET_{Calc}T_{Carb} + F \qquad 2.5$$

Where T_{Calc} is the calcination temperature (°C) and T_{Carb} is the carbonation temperature (°C). Equation (2.5) can be used to estimate first cycle capture efficiency for a given set of calcination and carbonation temperatures within the range of temperatures investigated.

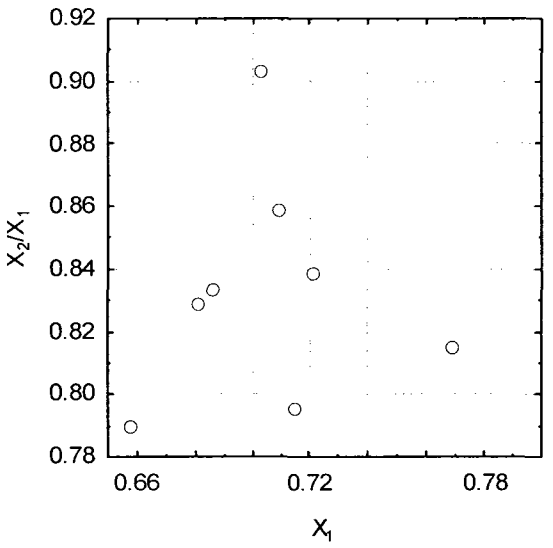

Figure 2.6: Relationship between X_1 and X_2/X_1 – Cadomin limestone – few impurities present

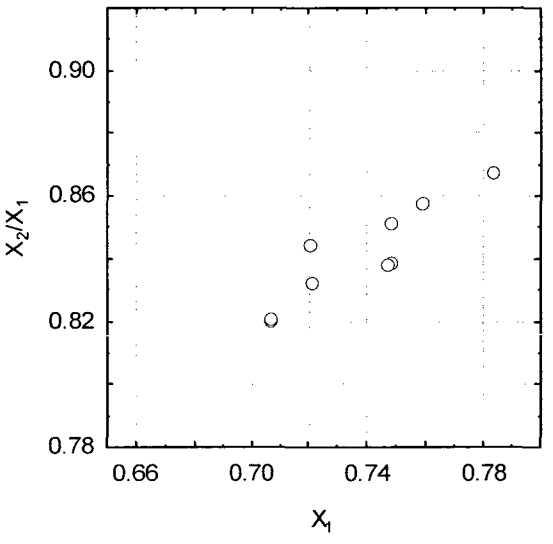

Figure 2.7: Relationship between X_1 and X_2/X_1 - Kelly Rock limestone – high impurities content

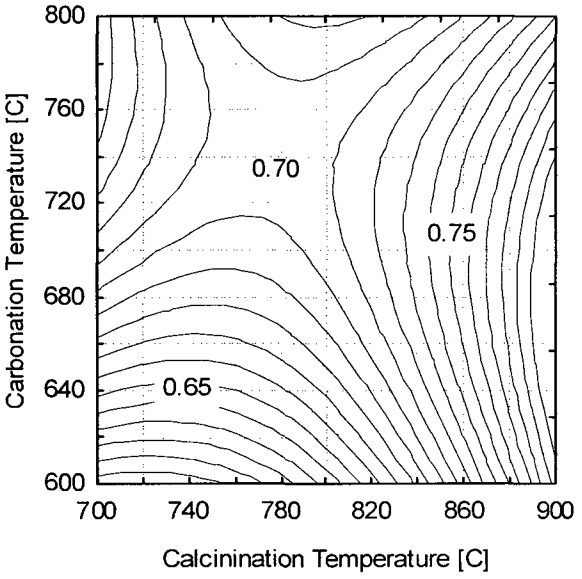

Figure 2.8: Cadomin limestone conversion at 20 min. - first cycle - no pre-treatment

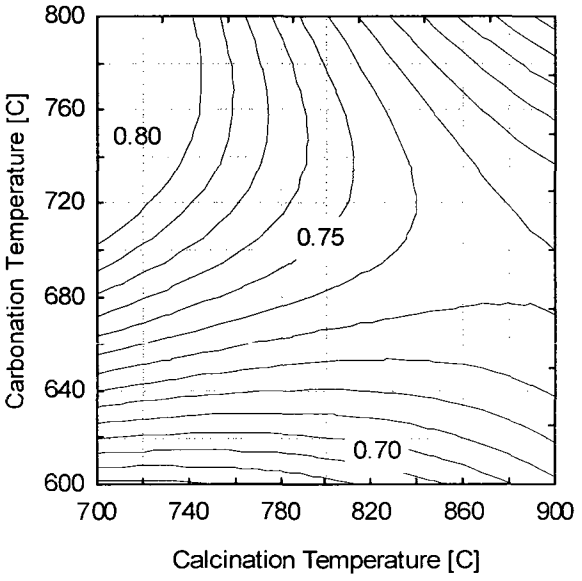

Figure 2.9: Kelly Rock limestone conversion at 20 min. - first cycle - no pre-treatment

For both Cadomin and Kelly Rock, the optimum temperature with respect to capacity maintenance is 750°C for both carbonation and calcination at a value in the area of X_2/X_1 = 0.87 to 0.90 as reported by Silaban (1993). The capacity maintenance for Kelly Rock limestone is not *strongly* affected by the temperature of calcination, and so we can surmise that the reduction in surface area available for reaction for this stone is not strongly dependent on thermal sintering. This assumption is also supported by the work of Gullet and Bruce (1987). It should be noted that separation using the optimum condition would require a constant temperature process where calcination would have to occur using either a reduced pressure or stripping method to provide CO_2 separation. Unfortunately, reduced pressures would not make economic sense if the CO_2 were to be later pressurized for downstream treatment. Similarly, a stripping method would require large quantities of stripping gas that would have to be easily separated from CO_2. Steam would be an obvious possibility; however, this would require extensive heat exchange equipment and would be an expensive option.

The maintenance of capacity of hydrated Cadomin limestone is shown in Figure 2.10 at a cycle time of 20 minutes for varying calcination and carbonation temperatures. The hydrated samples have improved cyclic performance compared with untreated samples. The conversion ratio for Cadomin, X_2/X_1, for the untreated limestone is 0.90 while that for the hydrated sample is 0.93 indicating an improvement in cyclic performance. At first, this would seem to be a small difference; however, the range of calcination temperatures at which the untreated sorbent maintains its capacity is limited. As the calcination temperature is increased to the point where calcination can proceed, in the presence of relatively large partial pressures of CO_2 the capacity maintenance is greatly reduced. For example, at a calcination temperature of 850°C, X_2/X_1 for untreated Cadomin limestone has been reduced to 0.84, while the pre-hydrated sample has maintained an X_2/X_1 of 0.94. The capacity maintenance of the pre-hydrated Cadomin is remarkably constant at higher calcination temperatures.

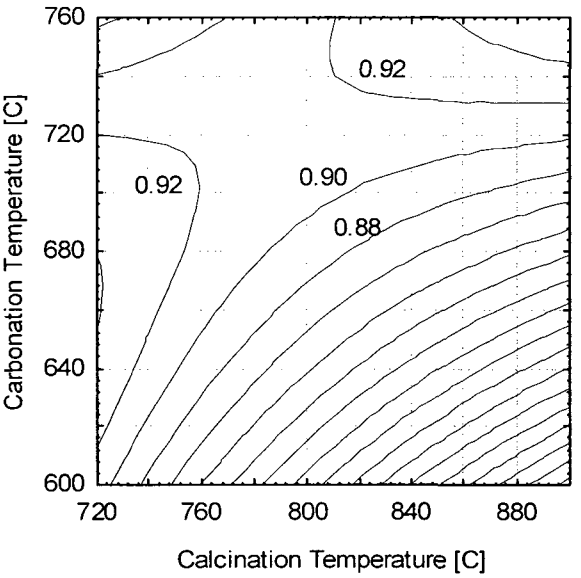

Figure 2.10: Hydrated Cadomin limestone - capacity maintenance X_2/X_1

The capacity maintenance of hydrated Kelly Rock limestone behaves in much the same manner as Cadomin as can be seen in Figure 2.11. The capacity is nearly constant for carbonation temperatures between ~700°C and 740°C across the whole range of calcination temperatures tested. The maintenance of capacity over this temperature range would allow the separation of CO_2 using temperature swing and/or pressure-temperature swing methods.

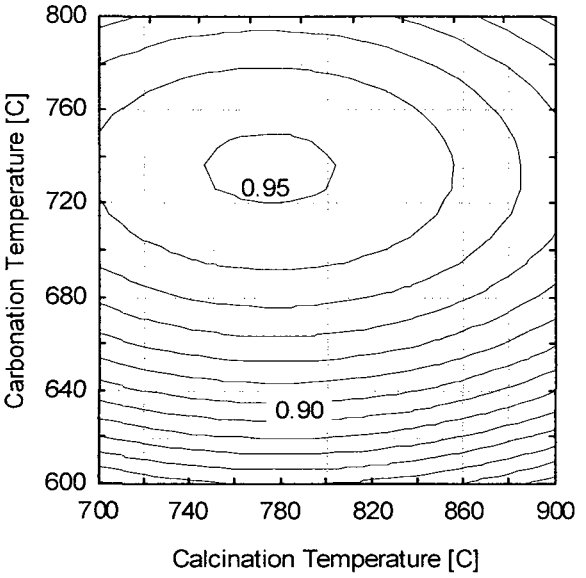

Figure 2.11: Hydrated Kelly Rock Limestone -- Capacity Maintenance X_2/X_1

The multiple cycle capacity for the hydrated samples has been estimated using equation 2.4. The best five conditions tested for each of Kelly Rock and Cadomin can be seen in Figure 2.12 and Figure 2.13. The capacity at 20 cycles has been confirmed through a multiple cycle TGA run and can be seen on Figure 2.12 for carbonation at 750°C and calcination at 750°C. The model fits the data reasonably well, though it will tend to under predict conversion at high cycle numbers. Steam hydration improved long-term performance of the sorbent resulting in conversions as high as 52% for Cadomin and estimated conversions as high as 59% for Kelly Rock.

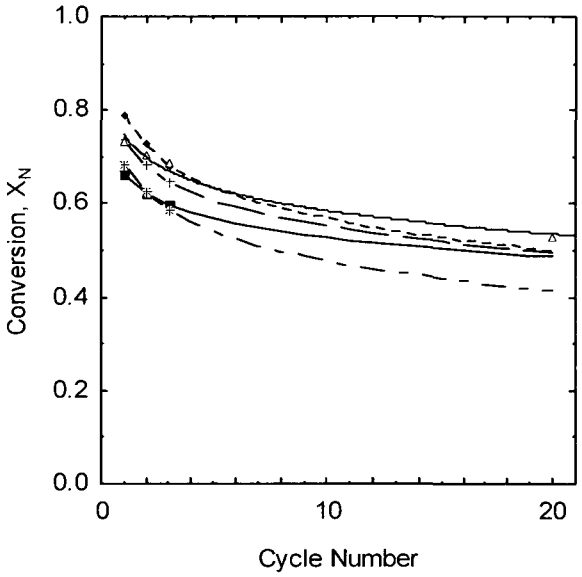

Figure 2.12: Extrapolated capacities for pre-hydrated Cadomin limestone

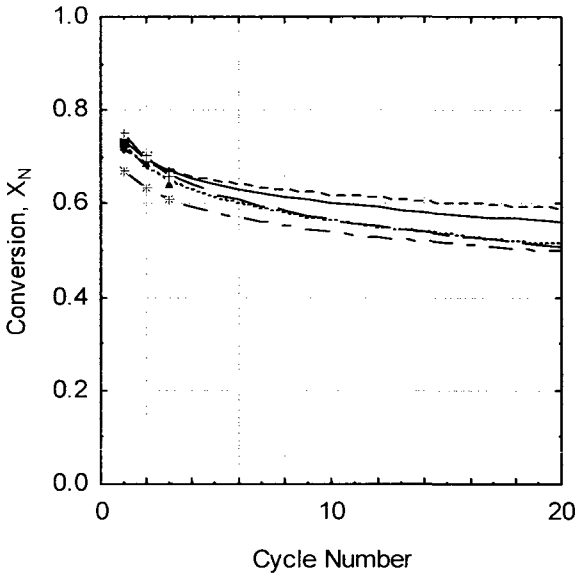

Figure 2.13: Extrapolated capacities for pre-hydrated Kelly Rock limestone

Figure 2.14 and Figure 2.15 show capacity maintenance based on pre-calcination temperature and the first cycle conversion. From these plots, it can be seen that both limestones have an X_2/X_1 local maxima at a pre-calcination temperature of approximately 800°C. However, the first cycle capacity is somewhat low in this region at a value of less than ~0.75. It appears that it is possible to enhance the first cycle capacity further while maintaining a very high X_2/X_1 by utilizing a high pre-calcination temperature, *i.e.*, greater than 850°C. It is proposed that calcination at high temperature (~850°C-900°C) followed by a hydration step maximizes the suitable porosity for the carbonation reaction over many cycles. The maximum X_2/X_1 achieved during this set of tests was 0.99 with an X_1 of 0.71. The conditions at this point were a pre-calcination temperature of 750°C, followed by carbonation and calcination at 750°C. However, this is a single point and may prove difficult to reproduce. A process operating at these conditions would require the use of a stripping gas in the calciner. It would be capable of reducing the CO_2 concentration to 9% representing a reduction in CO_2 emissions of 40% when burning coal and petroleum coke, but this process would have a very low sorbent decay rate. A suitable stripping gas that did not enhance sintering would need to be found.

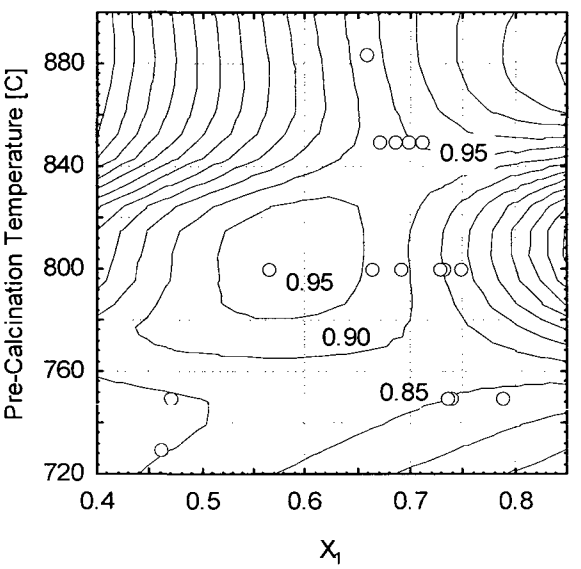

Figure 2.14: Contour plot indicating X_2/X_1 for a combination of X_1 and pre-calcination temperature – Cadomin limestone

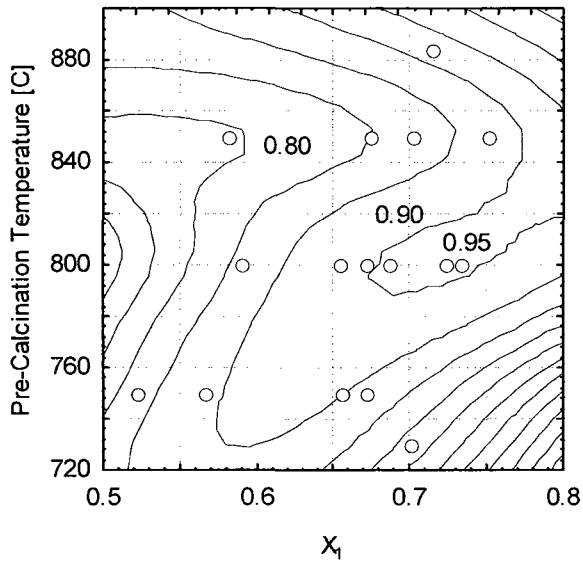

Figure 2.15: Contour Plot Indicating X_2/X_1 for a Combination of X_1 and Pre-calcination Temperature – Kelly Rock Limestone

Conditions for a process without stripping gas in the calciner would require operation at temperatures sufficiently high to cause calcination in a nearly pure CO_2 atmosphere. This would require calciner operation in the area of 900°C to 915°C. If we consider X_2/X_1 as it varies with carbonation and calcination temperature, as shown in Figure 2.14 and Figure 2.15, we can see that the capacity is maintained reasonably well for calcination temperatures up to at least 884°C when carbonating at a temperature of 725°C. We can estimate the capacity maintenance for an operation with Cadomin limestone at a pre-calcination temperature of 884°C, calcining at 900°C and carbonating at 725°C. This operation could result in CO_2 emissions as low as 6.2%, a reduction of 59%, with an X_2/X_1 as high as 0.92. Further improvements are expected as we more fully explore higher pre-calcination temperatures.

2.5.2 Pore Analysis

BET surface area and pore volume were calculated for each sample (Table 2-6). It can be seen that the hydration treatment has increased both the surface area and pore volume of all samples tested

relative to the untreated samples. The increase in both values simultaneously is the result of crack formation and particle expansion.

Based on the BET surface areas and pore volumes reported in Table 2-6 the capacity of the hydrated samples would be expected to be much greater than the untreated samples for the first carbonation cycle. The surface areas for the hydrated samples are 1.7 to 2.3 times greater than the equivalent untreated sample. However, the first cycle capacities are nearly identical for both the hydrated and untreated samples from the TGA, so we may surmise that much of the additional pore volume is not necessary during the first cycle.

Table 2-6. BET surface area and pore volume (BJH) for untreated and hydrated samples

Limestone	Carbonation	Calcination	Hydrated	Cycles	SA_{BET}	V_M
	[°C]	[°C]		#	m^2/g	cm^3/g
Kelly Rock	750	750	Y	1	5.61	1.30
Kelly Rock	750	750	N	1	2.40	0.55
Kelly Rock	750	750	Y	10	4.41	1.01
Kelly Rock	750	750	N	10	2.39	0.55
Kelly Rock	700	915	Y	1	3.13	0.72
Kelly Rock	700	915	N	1	1.82	0.42
Cadomin	750	750	Y	1	5.52	1.21
Cadomin	750	750	N	1	3.27	0.75
Cadomin	750	750	Y	10	3.55	0.81
Cadomin	750	750	N	10	2.11	0.49
Cadomin	700	915	Y	1	3.77	0.87
Cadomin	700	915	N	1	2.20	0.50

In both Kelly Rock and Cadomin limestones, the surface area and pore volume for the hydrated samples that have undergone 10 cycles are greater than the untreated samples at their first cycle. However, the capacity of the hydrated limestones after 10 cycles is less than the untreated limestone after one cycle. This again indicates that much of the volume created upon hydration is not available for reaction and this suggests that active sites are lost regardless of actual pore volume size or surface area.

Pore size distributions were calculated for each of the samples using ASAP 2010 software to help understand the effect of hydration on the carbonation reaction. The pore area distributions for Kelly Rock and Cadomin can be seen in Figure 2.16 and Figure 2.17, respectively, while the pore volume distributions for these two limestones are shown in Figure 2.18 and Figure 2.19, respectively. These figures show that hydration increases both pore volume and surface area over the entire pore size range measured.

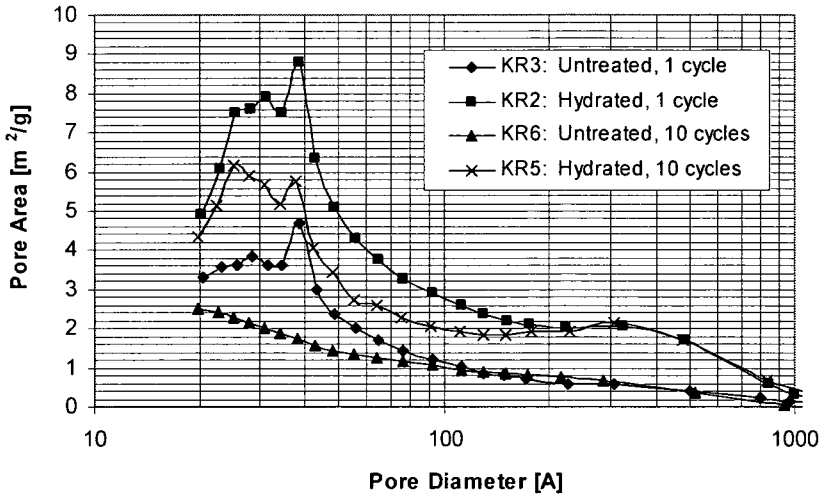

Figure 2.16: Pore area distribution (BJH) - Kelly Rock limestone (Carbonation 750 °C, Calcination 750 °C)

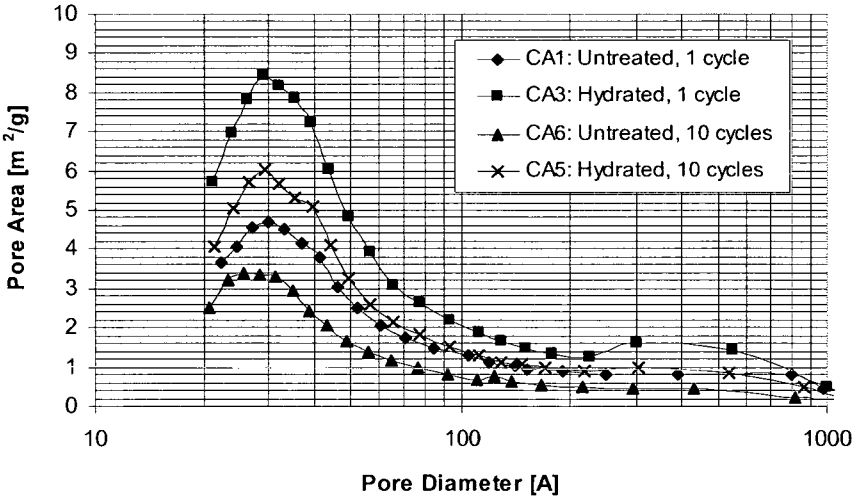

Figure 2.17: Pore area distribution (BJH) - Cadomin limestone (Carboantion 750 °C, Calcination 750 °C)

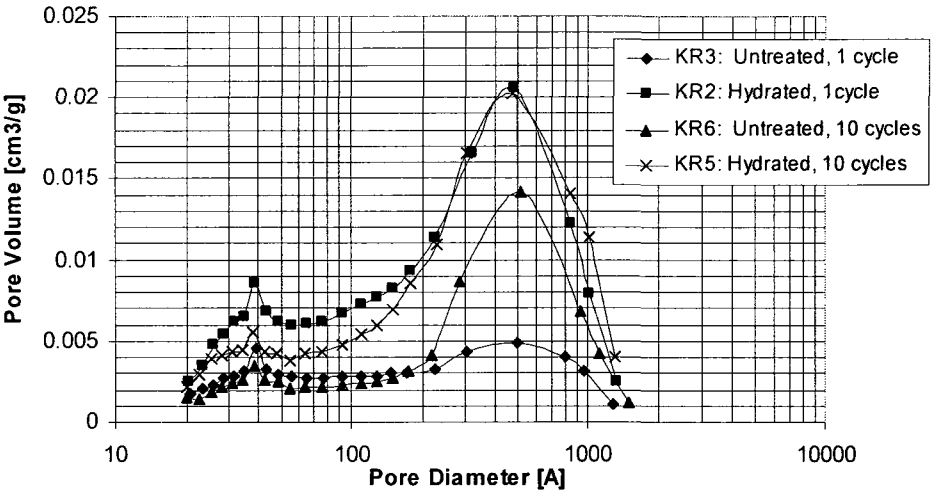

Figure 2.18: Pore volume distribution (BJH) - Kelly Rock limestone (Carboantion 750 °C, Calcination 750 °C)

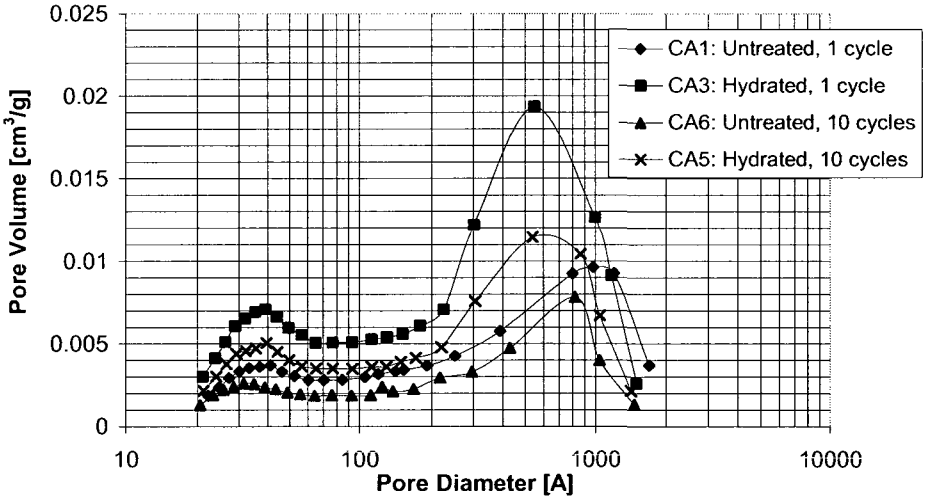

Figure 2.19: Pore Volume Distribution (BJH) – Cadomin Limestone (Carboantion 750 °C, Calcination 750 °C)

Interestingly, in Figure 2.16 it can be seen that the pore area found for pores of size greater than approximately 10 nm is not significantly reduced after 10 cycles for Kelly Rock limestone. It may be that these pores allow relatively large diffusion rates as the conversion proceeds. It is worth noting that the overall pore area of pores in the 10-100 nm range represents 40% of the total pore area and may help to maintain the limestone capacity over many cycles. What is clear is that there is little or no change in pore area in this size range over the entire 10 cycles studied, and one may speculate that the impurities found in Kelly Rock are responsible for this behaviour by providing imperfections in the crystal structure which prevent crystallization and significant reductions in pore area and volume (German, 1996). By contrast, the maintenance of pore area in this size range is clearly less for Cadomin. However, even with the reduction in pore area the hydrated sample after 10 cycles has more pore area, over all pore sizes, than the untreated sample at the first cycle.

In a similar fashion the hydrated Kelly Rock limestone appears to maintain more pore volume in the pore size range of 10-100 nm from cycle 1 to cycle 10. The untreated Kelly Rock shows a significant reduction in pore volume indicating a collapse in the pores that are responsible for rapid diffusion of CO_2 into the particle interior over multiple cycles. The hydrated Cadomin limestone does not maintain pore volume to the same extent as that of Kelly Rock, but at cycle 10 still has significantly more pore volume in the pore range 10-100 nm than the untreated Cadomin at cycle 10.

2.6 Conclusions

Pore area and pore volume were increased *via* steam hydration at 150°C to allow improved conversion of limestone particles over multiple cycles. Steam hydration improved long-term performance of the sorbent resulting in repeatable confirmed conversions as high as 52% and estimated conversions as high as 59%. It is estimated that the increase in conversion has improved the economics of the proposed process to an economic state. This work also provides evidence that the presence of impurities in the limestone is beneficial in maintaining the treated sorbent's pore size and volume over multiple cycles.

Surface mapping techniques have been used to estimate CaO conversion over multiple cycles for both hydrated and untreated CaO at a variety of operating conditions at atmospheric pressure. It

has been shown that when carbonating in the temperature range from 700°C to 740°C various calcination temperatures from 700°C to 900°C can be used without seriously reducing the multiple cycle capacity of CaO for CO_2 capture.

The proposed process conditions appear to fall in the scope of what would generally be considered a reliable and economic process: moderate operating conditions, low cost, widely available feedstocks, simplicity and proven technology.

2.7 Acknowledgement

The authors thank Lufei Jia for operating the N_2 adsorption apparatus used for pore distribution analysis.

2.8 Nomenclature

f_m	Parameter for estimating conversion at N cycles
f_w	Parameter for estimating conversion at N cycles
N	Cycle Number
P_{eq}	Equilibrium pressure
SA_{BET}	Bet surface area
T	Temperature
V_M	Monolayer volume
X	Conversion of CaO to $CaCO_3$
X_N	Conversion of CaO to $CaCO_3$ at the Nth cycle

2.9 References

Abanades, J.C., (2003). Private Communication, CSIS, Spain.

Abanades, J.C.; Alvarez, D.; Anthony, E.J.; Lu, D., (2003). '*In-situ* Capture of CO_2 in a Fluidized Bed Combustor', Proceedings of the 17th FBC Conference, Jacksonville, Florida.

Abanades, J.C.; Alvarez. D., (2003). 'The Conversion Limits in the Reaction of CO_2 with Lime', Energy & Fuels 18, 308.

Anthony, E.J.; Jia, L., Woods, J.; Roque, W.; Burwell, S., (2000). 'Pacification of High Calcic Residues Using Carbon Dioxide', Waste Management 20, 1.

Anthony, E.J.; Granatstein, D.L., (2001). 'Sulfation Phenomena in Fluidized Bed Combustion Systems', Progress in Energy and Combustion Science 27, 215.

Anthony, E.J.; Jia, L., (2003). 'CaS Oxidation by Reaction with CO_2 and H_2O', Energy and Fuels 17, 363.

Baker, E.H., (1962). 'The calcium oxide-carbon dioxide system in the pressure range 1-300 atmospheres', J. Chem. Soc., 464.

Couturier, M.F., (1986). 'Sulphur Dioxide Removal in Fluidized Bed Combustors', Technical Report FBC.TR.86.1.

Curran, G.P.; Fink, C.E.; Gorin, E., (1967). 'Carbon dioxide acceptor gasification process–studies of acceptor properties', Adv. Chem. Ser. 69, 141.

German, R.M., (1996). 'Sintering Theory and Practise', John Wiley: New York.

Grace, J.R.; Avidan, A.A.; and Knowlton, T.M. (eds.), (1997). 'Circulating Fluidized Beds', Blackie Academic and Professional.

Gullet, B.K.; Bruce, K.R., (1987). 'Pore Distribution Changes of Calcium Based Sorbents Reacting with Sulfur Dioxide', AIChE J. 33, 1719.

Gustavsson, L., (1995). 'Reduction of N_2O in Fluidized Bed Combustion by Afterburning', PhD Thesis. Chalmers University, Sweden.

Harrison, R.M. (ed.), (1992). 'Understanding our Environment: An Introduction to Environmental Chemistry and Pollution', Royal Society of Chemistry.

Salvador, C.; Lu, D.; Anthony, E.J.; Abanades, J.C., (2003). 'Enhancement of CaO for CO_2 Capture in an FBC Environment', Chemical Engineering Journal 96, 187.

Shimizu, T.; Hirama, T.; Hosoda, H.; Kitano, K.; Inagaki, M.; Tejima, K., (1999). 'A Twin Fluid-bed Reactor for Removal of CO_2 from Combustion Processes', Trans IchemE 77, 62.

Silaban, A., (1993). 'High-Temperature High-Pressure CO_2 Removal From Coal', Gas PhD Dissertation, Louisiana State University.

Silaban, A.; Harrison, D.P., (1995). 'High temperature capture of carbon dioxide: characteristics of the reversible reaction between CaO(s) and CO_2(g)', Chem. Eng. Comm. 137, 177

Squires, A. M., (1967). 'Cyclic use of calcined dolomite to desulfurize fuels undergoing gasification', Adv. Chem. Ser 69, 205.

Chapter 3 Sintering and Reactivity of $CaCO_3$-based Sorbents for *In-situ* CO_2 Capture in Fluidized Beds under Realistic Calcination Conditions

Accepted for Publication in a Special Issue of the Journal of Environmental Engineering

Lu, D.[1], **Hughes, R.W.**[1], Anthony, E.J.[1], Manovic, V.[1], (2009). 'Sintering and Reactivity of $CaCO_3$-based Sorbents for In-situ CO_2 Capture in Fluidized Beds under Reaslistic Calcination Conditions', J. Env. Eng. 35(6), p 404-410.

[1]Natural Resources Canada, CETC-O, 1 Haanel Drive, Ottawa, Canada K1A 1M1

3.1 Abstract

Sintering during multiple calcination /carbonation cycles may introduce substantial economic penalties for a CaO-$CaCO_3$ looping cycle using limestone/dolomite-derived sorbents. Here, cyclic carbonation and calcination reactions were investigated for CO_2 capture under fluidized bed combustion conditions. The cyclic carbonation characteristics of $CaCO_3$-derived sorbents were compared at various calcination temperatures (700-925°C) and different gas stream compositions: pure N_2 and a realistic calciner environment where high concentrations of CO_2 between to 80-90% (and the presence of SO_2) are expected. The conditions during carbonation employed here were 700°C and 15% CO_2 in N_2 and 0.18% or 0.50% SO_2 in selected tests, i.e., typically expected for a carbonator. Up to twenty calcination/carbonation cycles were conducted using a thermogravimetric analyzer (TGA) apparatus. Three Canadian limestones were tested: Kelly Rock, Havelock and Cadomin, using a pre-screened particle size range of 400-650 μm. In addition, calcined Kelly Rock and Cadomin samples were hydrated by steam and examined. Sorbent reactivity was reduced whenever SO_2 was introduced to either the calcining or carbonation streams. The multicyclic capture capacity of CaO for CO_2 was substantially reduced at high concentrations of CO_2 during the sorbent regeneration process and carbonation conversion of the Kelly Rock sample obtained after 20 cycles was only 10.5%. Hydrated sorbents performed better for CO_2 capture, but also showed significant deterioration following calcination in high-CO_2 gas streams. This indicates that high CO_2 and SO_2 levels in the gas stream lead to lower CO_2 conversion because of enhanced sintering and irreversible formation of $CaSO_4$. Such effects can be reduced by separating sulphation and carbonation and by introducing steam to avoid extremely high CO_2 atmospheres, albeit at higher cost and/or increased engineering complexity.

3.2 Introduction

The reversible reaction (3.1) between CaO and CO_2 may find application in high-temperature processes to control CO_2 emissions from advanced power generation facilities in a CaO-$CaCO_3$ looping cycle (Abanades and Alvarez, 2003; Abanades *et al.*, 2004; Gupta and Fan, 2002). Circulating fluidized bed (CFB) systems are suitable for looping cycle technology because they excel in transferring large amounts of solids between reactors and, hence, from one chemical environment to another. Good reaction between solids and gas streams is also greatly enhanced by the excellent solid mixing in CFBs, which in turn maximizes mass and heat transfer and, hence, reaction rates (Abanades *et al.*, 2004; Shimizu *et al.*, 1999; Salvador *et al.*, 2003). CFBs using limestone or dolomite sorbent can have another advantage—simultaneous sulphur removal *via* the sulphation reaction (3.2) when burning sulphur-containing solid fossil fuels.

$$CaO\ (s) + CO_2\ (g) \Leftrightarrow CaCO_3\ (s) \qquad 3.1$$

$$CaO\ (s) + 1/2O_2 + SO_2 \Rightarrow CaSO_4 \qquad 3.2$$

However, CaO-derived sorbents from natural sources fail to achieve complete reconversion to $CaCO_3$ and instead show a rapid fall-off in reversibility for reaction 3.1 (Salvador *et al.*, 2003; Hughes *et al.*, 2004; Fennell *et al.*, 2007). A decrease in the microporosity of the sorbents appears to be the major factor causing the decay of sorbent activity and conversion, *i.e.*, pore sintering associated with the calcination process, which depends on final calcination temperature, heating rate and duration. Wang and Anthony (2005) recently studied the decay behaviour of CaO-derived sorbents and found that an empirical model curve describing the process was almost identical to the deactivation of catalyst due to sintering. This supports the idea that the decay of CO_2 carrying capacity is attributable to sintering of the sorbent during the carbonation and/or sorbent regeneration process.

Sintering effects are strongly dependent on temperature, and tend to cause grain size to increase, reducing pore size and surface area by causing mass transport at the atomic scale (Borgwardt *et al.*,

1986; Borgwardt, 1989a). Solid surface curvature associated with high-temperature capillary forces initiates the driving force for sintering. However, there is no consensus on how to calculate the degree of sintering for any given situation. Louisiana State University (Silaban, 1993; Silaban and Harrison, 1995) investigated the effect of the typical FBC operating temperature range of 700-900°C at atmospheric pressure on CO_2 carrying capacity of the sorbent used in the multicycle process described by reaction 3.1, and concluded that the calcination conditions ought to be as mild as possible to avoid sintering and improve carbonation capacity. Earlier studies also showed that solid impurities in sorbents and the presence of gases such as CO_2 and H_2O could enhance sorbent sintering (Dobner *et al.*, 1977; Borgwardt, 1989b). Borgwardt (1989b) found that sintering could be promoted by addition of water vapour and carbon dioxide to simulated combustion flue gases. Each gas strongly catalyzed the sintering process, while their combined effects were even more severe. Porosity reduction was also accelerated by the presence of H_2O or CO_2 in the sintering atmosphere and porosity reduction followed the Coble logarithmic law for sintering at 800-1000°C for the onset of particle shrinkage (Borgwardt, 1989b). Although multiple sintering mechanisms are possible in the presence of CO_2 and/or H_2O, the empirical model correlates isothermal surface area reduction as a function of time over the temperature range 380-1150°C and partial pressures of 39 Pa to 15 kPa for the gas associated with sintering. Dobner *et al.* (1977) studied the effects of various reaction parameters (*i.e.*, temperature, pressure, and gas composition) on the carbonation rate and found increasing temperature and partial pressure of CO_2 for calcination gave lower carbonation activities and accelerated the loss of solid reactivity with increasing cycle number. However, steam addition during the carbonation process resulted in an almost two-orders-of-magnitude increase in the carbonation rate. They summarized the effect of gas composition on sintering as: $SO_2 > CO_2 > H_2O > O_2 > Air > N_2$ (Clark, 1949).

Calcination can be achieved by burning gas, liquid or low-ash solid fuels in pure oxygen, producing a highly pure CO_2 stream (>90%) suitable for direct sequestration (Hughes *et al.*, 2005). Such CO_2 levels are much higher than used in previous studies primarily focusing on conditions appropriate to sulphation. Preliminary results from CETC's (CANMET Energy Technology Centre) pilot-scale mini-CFB system have demonstrated that limestone can be used successfully in a cyclic calcination/carbonation process under realistic conditions; however, lower CO_2 capture was observed compared to thermogravimetric analyzer (TGA) tests using the same sorbents (Salvador *et*

al., 2003; Hughes *et al.*, 2004). Here we hypothesize that CO_2 from sorbent calcination in a bubbling mode calciner will be released to the emulsion phase. Thus, sorbent particles will be surrounded by a high CO_2 stream, which could be one of the reasons for lower CO_2 capture. In particular, the high CO_2 environment during the calcination reaction enhances sintering, thereby negatively impacting sorbent reactivity.

The use of petroleum coke for heating the circulating fluidized bed calciner, which is an ideal low-ash fuel with excellent calorific value, necessarily implies the presence of high SO_2 levels. Sun *et al.* (2006) recently studied the effect of SO_2 addition on sorbent reversibility for absorbing CO_2 under pressurized and atmospheric FBC conditions, and demonstrated that SO_2 significantly lowers the sorbent reversibility and impairs cyclical CO_2 capture. However, this work was conducted using a N_2 stream for the calcination step, which does not represent a realistic calcination environment. Hence, we attempt to examine the effects of the CO_2 and SO_2 streams during the calcination process on the CO_2 carrying capacity of the sorbent using a TGA.

3.3 Experimental

3.3.1 Thermogravimetric Analyzer

The calcination/carbonation cycles using limestone sorbents were conducted in a TGA apparatus, described elsewhere (Salvador *et al.*, 2003; Hughes *et al.*, 2004). The TGA consists of an electronic balance (Cahn 1100), vertical furnace, reactor tube, carrier gas system and computerized data acquisition system. The reactor tube is made of Inconel 600 alloy and has an inner diameter of 24 mm and a height of 900 mm. It can be unscrewed from the TGA, thus uncovering the platinum sample holder (10 mm in diameter, 1.5 mm in depth). A small amount of sample (20-30 mg) was preloaded into the holder prior to the tests.

The reactor was heated externally by means of an electric furnace that can be placed around the reactor tube and then removed rapidly to cool down the reactor to the lower temperature. A thermocouple was used to measure the reactor temperature near the reaction site (*i.e.*, 10 mm below the sample holder). The furnace was heated from room temperature to the desired calcination temperature at a heating rate of 10°C/min (programmed by an electronic temperature controller).

The temperature and sample mass *vs.* time data for the sample were recorded at 5-s intervals until termination of the run, using a Keithley 2700 data acquisition system and Keithley Xlinx software.

3.3.2 Procedure

In this work a high-CO_2 (80 or 90% vol. concentration) sweep gas was used in the calcination step. A temperature in excess of 890°C was required to ensure calcination. However, preliminary runs during this study indicated that the observed calcination proceeded extremely slowly when the temperature was less than ~915°C, since the back reaction (carbonation) proceeds at a finite rate. Once the temperature was raised to 920°C, sorbent calcination occurred at an acceptable rate. This agrees with observations from CETC's mini pilot-scale FBC work, which indicated that calcination of the limestone bed (5-7 kg mass) was excessively slow at 800-850°C, when the bed was fluidized with air and electrically heated to avoid the presence of CO_2, especially during the first calcination cycle (Salvador *et al.*, 2003). Elevating the temperature strongly accelerated the calcination process; hence a sorbent regeneration temperature of 925°C was chosen for the TGA work to guarantee complete calcination in a relatively short period, *i.e.*, a few minutes. Carbonation tests were conducted at 700°C using 15% CO_2 (N_2 balance) at atmospheric pressure. Earlier work (Borgwardt, 1989b; Curran *et al.*, 1967) indicated that the carbonation process occurred in two phases: a rapid reaction phase (kinetically controlled) taking up to 4-5 minutes, depending on conditions, followed by a slower reaction that can continue for more than 10-20 h for the last 5% of the conversion. Since it is the rapid phase that is of practical importance, the carbonation process was carried out for 30 min and CO_2 capture capacity of the sample was determined by the weight gain over that period.

Limestones tested were selected from across Canada, such as Havelock from New Brunswick, Cadomin from Alberta, and Kelly Rock from Nova Scotia. Their chemical compositions are given in Table 3-1. The sorbent samples were pre-screened within a particle size range of 400-650 μm. Samples were loaded into the reactor prior to starting each run. Nitrogen was used as reference carrier gas and a digital mass flow controller (Matheson Gas Products) regulated the flow rate at 100 mL/min for the carrier stream and 60 mL/min for the purge stream. Two levels of SO_2 (5000 ppm and 1800 ppm) were used in selected tests during both calcination and carbonation reactions for comparison purposes.

Table 3-1: Limestone Sorbent Composition (wt%)

Comp.	Kelly Rock	Havelock	Cadomin
Al_2O_3	1.54	0.34	0.25
BaO	0.18	0.03	0.03
CaO	51.74	54.1	51.76
CO_2	-	-	-
Fe_2O_3	0.36	0.3	0.3
K_2O	0.36	0.06	0.12
MgO	0.58	0.29	2.18
MnO	0.16	0.07	0.01
Na_2O	0.07	0.2	0.2
NiO	-	0.01	0.01
P_2O_5	0	0.02	0.02
SiO_2	5.31	1.9	2.13
SO_3	0.98	0.46	0.32
SrO	0.04	0.02	0.03
TiO_2	0.08	0.07	0.04
V_2O_5	-	0.02	0.02
LOF	43.14	42.99	43.28
SUM	102.55	99.77	101.19

3.4 Results and Discussion

Calcination at up to 925°C did not significantly degrade sorbent reactivity associated with carbonation/calcination cycling beyond what was normally expected. It should be noted that a possible limitation of this work is that the TGA runs were conducted at the identical heating rate (10°C/min) regardless of the final temperature set point. Borgwardt *et al.* (1986; 1989a) found that heating rate, rather than final temperature, was a more critical factor in terms of sorbent sintering. In previous work, temperatures below 650°C led to carbonation reaction rates that were too low to achieve high CO_2 removal in a small pilot-scale FBC operating in the bubbling bed mode (Hughes *et al.*, 2004). For a synthetic flue gas containing 15% CO_2 at atmospheric pressure, the carbonation

temperature was limited to <780°C, and the best CO_2 capture capacity was achieved in the carbonation temperature range of 700-740°C, which is in reasonable agreement with observations by Silaban et al. (1993; 1995).

Here calcination was conducted with high concentrations of CO2 (80 or 90% in the carrying gas); the calcination temperature was set at 925°C and the carbonation occurred at 700°C. Figure 3.1 shows typical sorbent decomposition curves. Similar to the case of a typical limestone decomposition process in pure inert gas streams (such as N_2), a slight sample weight loss was seen with increasing temperature over the first 20 min (see Figure 3.1a). However, instead of sample decomposition occurring as temperatures rise above 500°C, as in the case of a pure N_2 stream (solid line), CO_2 release started at a relatively high temperature of ~900°C in the presence of 90% CO_2 in the calcination stream (dotted line).

Figure 3.1b shows the decomposition curves when hydrated lime (H-lime) was tested at a similar heating rate in the TGA. Again, rather than a rapid weight loss associated with $Ca(OH)_2$ decomposition once the temperature increased to 400°C in a pure N_2 stream (solid line), carbonation occurred in the presence of the high-concentration CO_2 stream, and sample weight increased starting at a temperature of ~350°C, until the reactor temperature exceeded 900°C, when CO_2 was released (dotted line). In this case, carbonation appeared to set in at 350°C, *i.e.*, below the temperature at which decomposition of $Ca(OH)_2$ starts when under pure N_2, indicating that it was not CaO but $Ca(OH)_2$ that reacted with CO_2.

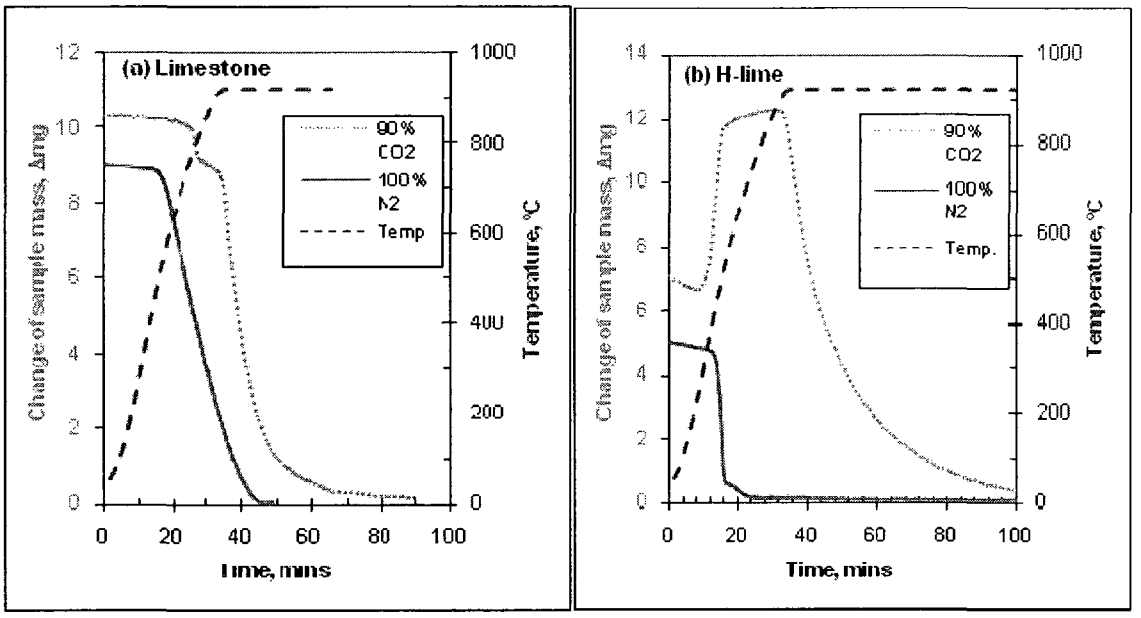

Figure 3.1: Comparison of Cadomin limestone (25 mg) calcination curves with/without a high-concentration CO_2 (90%) stream at carrier gas flowrate of 100 mL/min. a) original limestone, and b) hydrated lime.

Figure 3.2 shows the change in CO_2 capture capacity during multiple cycles of calcination and carbonation using untreated Cadomin under a high-CO_2 calcination environment. Once the calcination had been completed at high temperature (925°C), the high-CO_2 carrier gas was replaced by a pure N_2 stream until the temperature dropped and stabilized at the carbonation temperature (700°C), whereupon low-CO_2 carbonation carrier gas was introduced. After 30 min carbonation, the carrier gas was switched back to the high-CO_2 stream for calcination, while the reactor was heated to 925°C. The peak in the sample mass change increase at the beginning of each calcination period was due to the introduction of a high-CO_2 stream at low temperature (700°C). This was not observed when the calcination stream contained lower concentrations of CO_2. The curve also indicates that CO_2 is released rapidly, once the temperature is increased to the set point of 925°C, which is well in excess of the temperature required to favour calcination at atmospheric pressure.

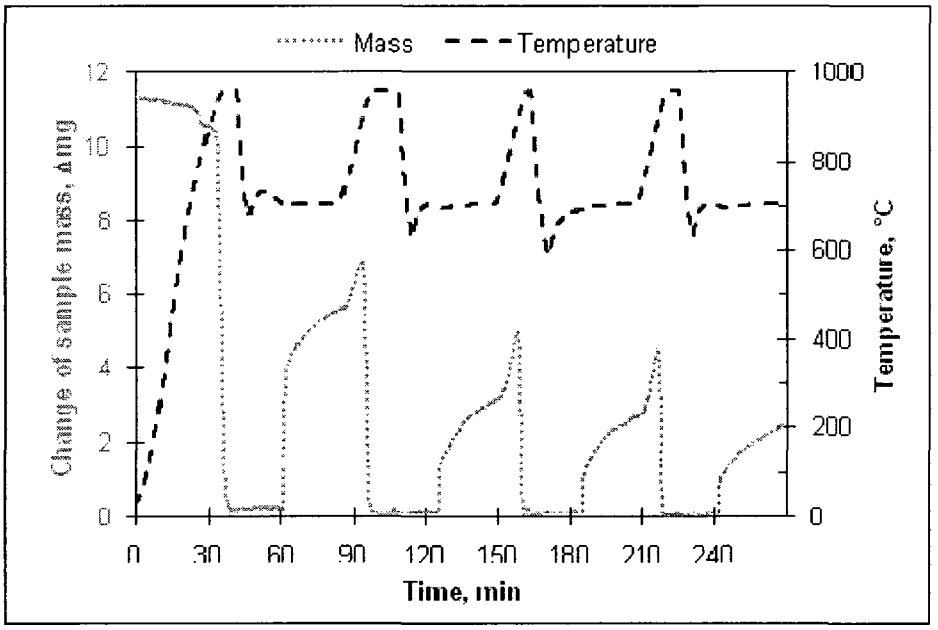

Figure 3.2: $CaO-CaCO_3$ looping cycles for Cadomin sample (25 mg) using high-CO_2 carrier gas (CO_2: 90%, and N_2: balance) in the calcination and low-CO_2 stream (CO_2: 15%, N_2: balance) in the carbonation, carrier gas flowrate = 100 mL/min.

Table 3-2 compares the CO_2 capture capacity for sorbents tested under the same carbonation conditions, with and without high-concentration CO_2 streams during regeneration. The three sorbents showed slight variations in terms of CO_2 capture capacity, particularly over the first few cycles; the differences appeared to be negligible after three cycles. With CO_2 in the calcination stream, the decay of sorbent reactivity occurred much faster than when CO_2 was absent. It can be seen in the carbonation during the first cycle that CO_2 capture capacity only reached 48-58%, which is typical of the capture level after 5-6 cycles for the same sorbent calcined in a pure N_2 atmosphere. For calcination with high-CO_2 atmospheres, the sorbent capture capacity after four cycles was depressed to around 25%, similar to the levels seen after 15-20 cycles, without CO_2 present in the calcination step.

Table 3-2: Carbonation conversions (at 700°C in 15% CO_2, N_2 balance) of various limestones with high CO_2 concentrations present during calcination

Sorbent	**Calcination**	**Conversion**				
		X_1	X_2	X_3	X_4	X_5
Cadomin	100% N_2, 700°C	0.75	0.68	0.62	0.58	0.52
Cadomin	90% CO_2 in N_2, 925°C	0.54	0.31	0.27	0.23	-
Havelock	90% CO_2 in N_2, 925°C	0.48	0.34	0.29	0.25	0.19
Kelly Rock	90% CO_2 in N_2, 925°C	0.58	0.39	0.3	0.26	-

X_n is the conversion in cycle n.

To investigate the situation where a high-sulphur feedstock such as petroleum coke is employed to provide heat for both the sorbent regenerator and combustor, SO_2 was introduced under different conditions. It was added with CO_2 to simulate a normal combustion flue gas in the carbonation process, and as well added into the regenerator with or without a high-concentration CO_2 environment. Figure 3.3 compares the typical decay of sorbent conversions without (Figure 3.3a) and with SO_2 (Figure 3.3b) present in the carbonation. The curves in Figure 3.3 indicate that the sorbent CO_2 capture capacity was dramatically reduced when SO_2 was involved in the carbonation stream, and the carbonation conversion dropped from 0.62 to 0.27 after three cycles (Table 3-2 and Table 3-3). In the test with SO_2 introduction, the base sample weight significantly increased after each cycle of sorbent regeneration, because of the accumulation of $CaSO_4$, which does not decompose at typical calcination temperatures.

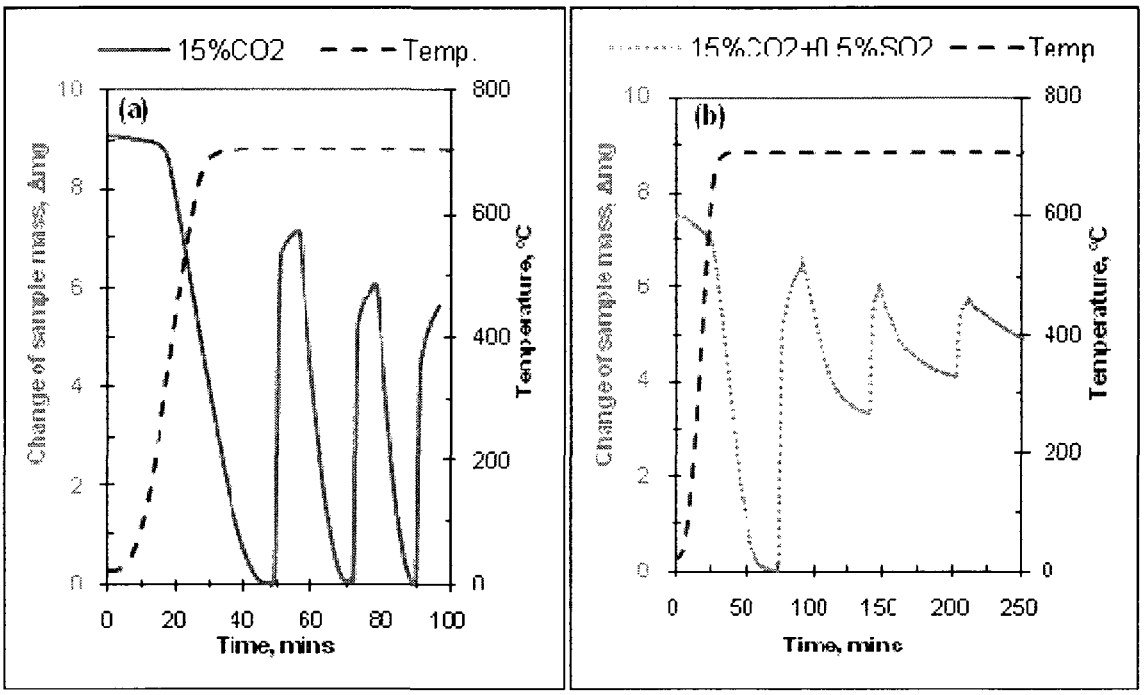

Figure 3.3: Comparison of Cadomin CaO-$CaCO_3$ looping cycles with/without added SO_2: (a) calcination in 100% N_2, 700°C, carbonation in 15% CO_2, N_2 balance, 700°C; (b) calcination in 100% N_2, 700°C, carbonation in 15% CO_2 + 0.5% SO_2, N_2 balance, 700°C

The TGA curve indicates that carbonation and sulphation reactions compete with each other (Fig. 3.3b). Table 3-3 shows the contribution of carbonation and sulphation after each cycle. Not only did the carbon conversion decrease with increasing cycle number, but the sulphur capture decreased as well. The lower sulphate conversions, compared to carbon conversion, are likely attributable to a relatively lower SO_2 concentration (0.5%) than CO_2 (15%) in the carbonation/sulphation stream.

Table 3-3: Comparison of Cadomin carbonation and sulphation conversion in cyclic process

Calcination	**Carbonation**		**Conversion**			**Ratio of Conversions**	
			X_1	X_2	X_3	$X_{1,2}$	$X_{1,3}$
N_2, 700°C	15% CO_2 & 0.5% SO_2 in N_2, 700°C	Carbonation	0.48	0.45	0.27	0.94	0.56
		Sulphation	0.25	0.17	0.07	0.68	0.28

X_n is the conversion in cycle n. $X_{n,m}$ is ratio between conversions in cycles m and n.

Figure 3.4 shows the cyclic sorbent performance when the calcination occurred in 90% CO_2 at 925°C, with 0.18% SO_2 added to 15% CO_2 in the carbonation stream at 700°C. Figure 3.5 shows the results of introducing 0.18% SO_2 into both the carbonator with 15% CO_2 and sorbent regenerator with 80% CO_2. Compared to the results shown in Figure 3.3b, sorbent regeneration is much faster at the higher temperature; however, sorbent CO_2 absorption capacity degenerates as process conditions become more severe. Table 3-4 compares results from the Cadomin TGA tests associated with and without the presence of SO_2. As expected, CO_2 conversion capacity clearly decreased with higher SO_2. These results support the importance of avoiding high SO_2 concentrations in the flue gas when using the CaO-$CaCO_3$ looping cycle with lime-based sorbents.

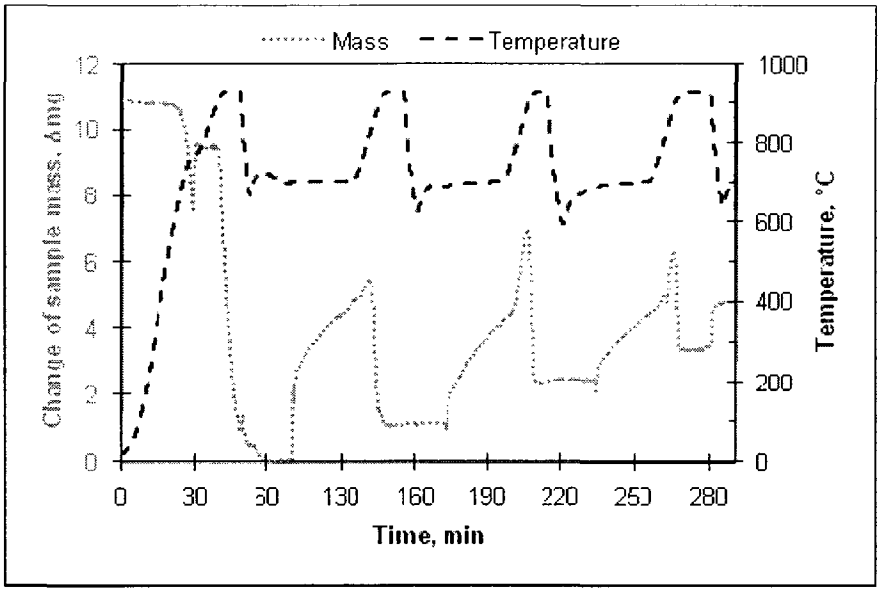

Figure 3.4: $CaO\text{-}CaCO_3$ looping cycles for Cadomin sample (25 mg) using high-CO_2 carrier gas (CO_2: 90%, and N_2: balance) in the calcination and low-CO_2 stream (CO_2: 15%, SO_2: 0.18%, and N_2: balance) in the carbonation, carrier gas flowrate = 100 mL/min.

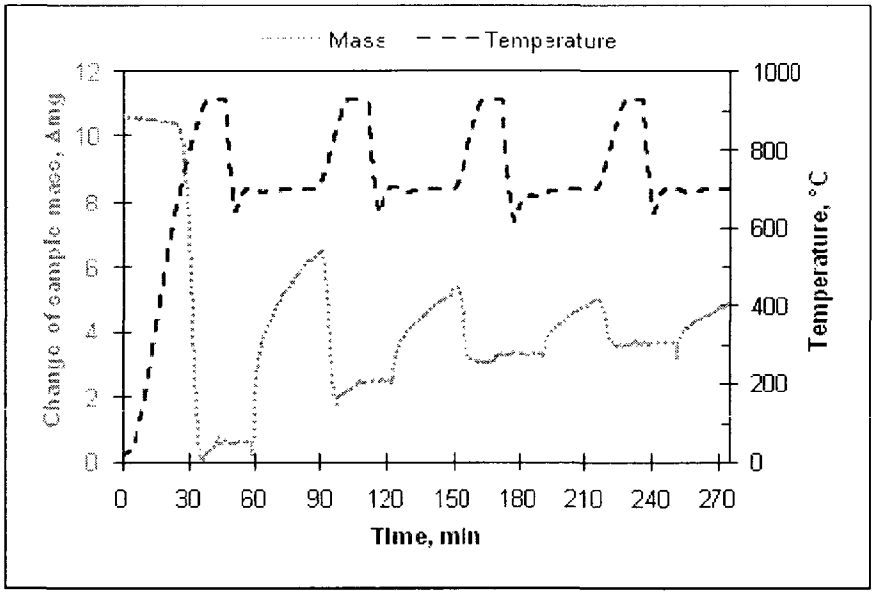

Figure 3.5: $CaO\text{-}CaCO_3$ looping cycles for Cadomin sample (25 mg) using high-CO_2 carrier gas (CO_2: 80%, SO_2: 0.18% and N_2: balance) in the calcination and low-CO_2 stream (CO_2: 15%, SO_2: 0.18%, and N_2: balance) in the carbonation, carrier gas flowrate = 100 mL/min.

Table 3-4: Carbonation conversion of Cadomin with/without SO_2 present

Calcination	Carbonation	Conversion			Ratio of Conversions	
		X1	X3	X5	X1,2	X1,3
N_2, 700°C	15% CO_2 in N_2, 700°C	0.70	0.6	0.45	0.88	0.86
N_2, 700°C	15% CO_2 and 0.5% SO_2 in N_2, 700°C	0.58	0.32	-	0.72	0.56
90% CO_2 in N_2, 925°C	15% CO_2 in N_2, 700°C	0.54	0.27	-	0.57	0.49
90% CO_2 in N_2, 925°C	15% CO_2 and 0.18% SO_2 in N_2, 700°C	0.33	0.13	-	0.54	0.41
80% CO_2 and 0.18% SO_2 in N_2, 925°C	15% CO_2 and 0.18% SO_2 in N_2, 700°C	0.44	0.13	-	0.50	0.30

Xn is the conversion in cycle n. Xn,m is ratio between conversions in cycles m and n.

It is also of interest to observe (Fig. 3.5) that the sudden increase in the sample weight in the period of transition between carbonation and calcination seemed to be eliminated when SO_2 was present in the calcination carrier gas. This can be explained by the occurrence of sulphation on the surface of the sorbent particles during the initial calcination, preventing carbonation on the sorbent surface, which is clearly represented as the sharp spike when the process switched from carbonation to calcination using the high-CO_2 stream without SO_2 at lower temperatures (Figs. 3.2 and 3.4).

Sorbent hydration, to improve performance when high-sulphur fuels are employed to achieve calcination, was also explored. The samples chosen were commercial quicklime (designated as h-lime) and hydrated limes prepared from Cadomin and Kelly Rock limestones in our laboratory. Details of the hydration procedure can be found elsewhere (Wu *et al.*, 2004; Anthony *et al.*, 2005). Some of the improvement seen previously (Hughes *et al.*, 2004) clearly occurs because previous tests avoided the severe conditions studied here; however, in general hydrated sorbent still showed much

better results in terms of carbonation conversion and maintained higher sorbent reversibility after a number of cycles, particularly in the absence of SO_2.

Table 3-5 presents results for commercial hydrated lime and hydrated lime obtained from Cadomin. The presence of high concentrations of CO_2 in the calcination cycle lowered the CO_2 capture capacity dramatically, but sorbent reactivity remained excellent for at least five cycles without elevated CO_2. However, once SO_2 was added to the carbonation stream, both the sorbent reactivity with increasing cycles and the capacity for CO_2 capture significantly decreased (see Fig. 3.6).

Table 3-5: Conversion of hydrated Cadomin and commercial hydrated lime with SO_2 present in carbonation gas

Calcination	**Carbonation**	**Conversion**			**Conversion ratio**	
		X_1	X_3	X_5	$X_{1,2}$	$X_{1,3}$
N_2, 700°C	15% CO_2 in N_2, 700°C	0.76	0.72	0.69	0.97	0.95
90% CO_2 in N_2, 925°C	15% CO_2 in N_2, 700°C	0.45	0.41	-	0.96	0.92
90% CO_2 in N_2, 925°C (*h-lime*)	15% CO_2 & 0.18% SO_2 in N_2, 700°C	0.41	0.30	-	0.73	0.73

X_n is the conversion rate (%), n is the cycle number. Xn,m is conversion ratio between cycle numbers of m and n

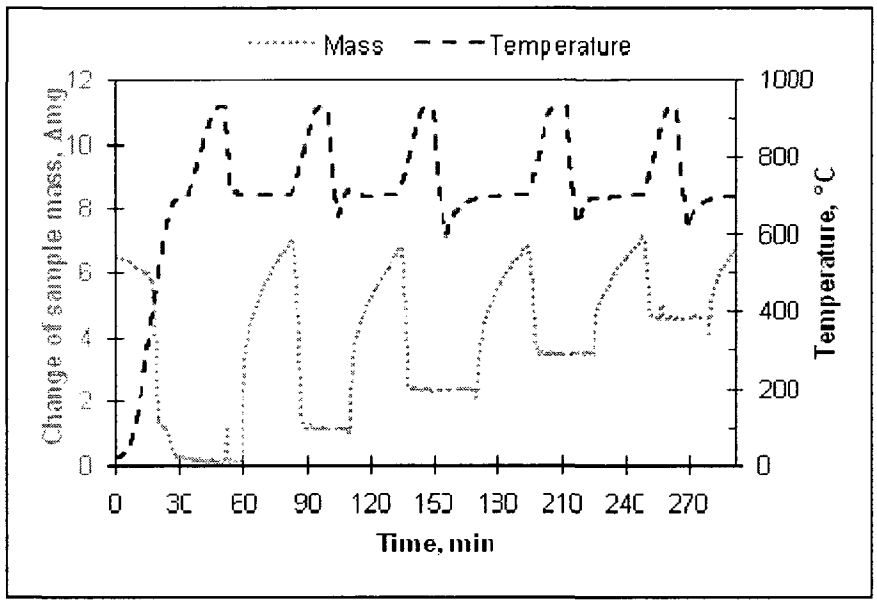

Figure 3.6: $CaO\text{-}CaCO_3$ looping cycles for hydrated Cadomin sample (25 mg) using high-CO_2 carrier gas (CO_2: 90%, and N_2: balance) in the calcination and low-CO_2 stream (CO_2: 15%, SO_2: 0.18%, and N_2: balance) in the carbonation, carrier gas flowrate = 100 mL/min

The influence of realistic conditions, as expected for $CaO\text{-}CaCO_3$ looping cycle FBC systems, was examined here, typically for 5 cycles. During this period, sorbent capture capacity fell rapidly and this tendency may be expected for longer series of cycles. This was confirmed with original and hydrated Kelly Rock samples (Figs. 3.7 and 3.8). The experiments were performed in 90% CO_2 in the calcination stage, and it can be seen that carbonation conversion in the 21st cycle was only 10.5% for the original sample. Unfortunately, the hydrated sorbent achieved only 2 percentage points higher conversion, leading to the conclusion that sorbent activated by hydration also loses activity much faster under realistic conditions than under those typically investigated. This observation is in agreement with an earlier study by Borgwardt (1989b), who found hydrated-CaO sintered faster than calcined-CaO. These results obtained for 20-cycle tests additionally confirm those for 5-cycle tests presented in this paper.

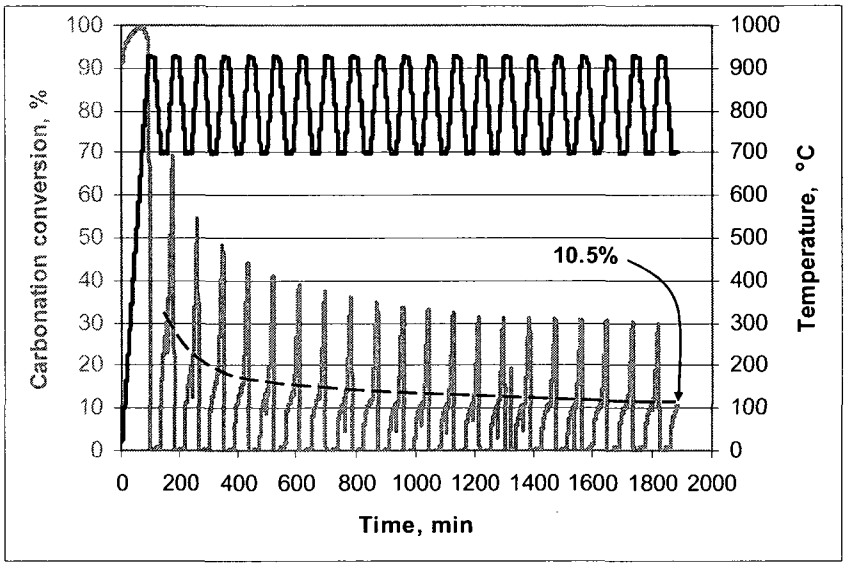

Figure 3.7: $CaO\text{-}CaCO_3$ looping cycles for Kelly Rock (25 mg) using high-CO_2 carrier gas (CO_2: 90%, and N_2: balance) in the calcination at 925°C and low-CO_2 stream (CO_2: 15%, and N_2: balance) in the carbonation at 700°C, carrier gas flowrate = 100 mL/min

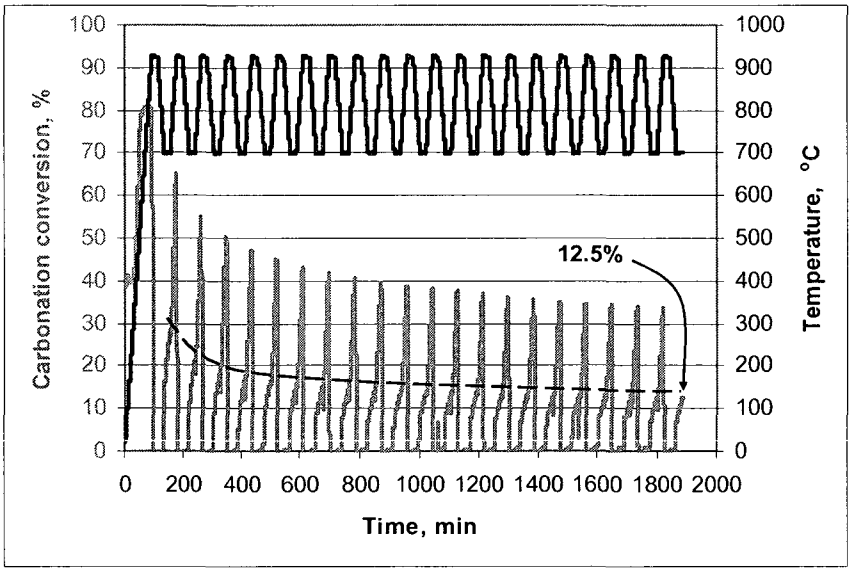

Figure 3.8: $CaO\text{-}CaCO_3$ looping cycles for hydrated Kelly Rock (25 mg) using high-CO_2 carrier gas (CO_2: 90%, and N_2: balance) in the calcination at 925°C and low-CO_2 stream (CO_2: 15%, and N_2: balance) in the carbonation at 700°C, carrier gas flowrate = 100 mL/min

It seems reasonable to suppose that the main contribution to the loss of sorbent capture capacity is carbonation that continues to occur (above dashed lines in the figures) while the temperature is being raised from that for carbonation to the level necessary for calcination under high CO_2 concentrations. During this period, formation of $CaCO_3$ (and after that it begins its decomposition) occurs at higher temperatures that enhance bulk mass transfer and sintering. Our experimental study on CO_2 capture capacity (Manovic and Anthony, 2008) showed that formation/decomposition of $CaCO_3$ is the critical step for sintering and that this is enhanced at higher temperatures. Furthermore, it may be expected that elimination of the carbonation peak at the beginning of the calcination stage may help to reduce the loss of capture capacity. For example, this can be achieved by increasing the rate of rise of sample temperature (to that needed for calcination), *i.e.*, shorter exposure to carbonation conditions at the beginning of the calcination stage. Experimentally, in TGA systems this means increasing the heating rate at the beginning of the calcination stage to the upper equipment performance limit. Practically, this is more easily achieved in FBC systems as sorbent circulates between carbonator and calciner and much more rapid heat transfer is experienced than that in a TGA. In other words, it may be expected that real FBC systems will be subjected to a slower drop in sorbent capture capacity than what was obtained in this study using TGA equipment.

3.5 Conclusions

High concentrations of CO_2 in the sorbent calcination environment lead to significant sintering of sorbent particles, and consequent lowering of sorbent reactivity for CO_2 conversion capacity and sorbent reversibility. This phenomenon is inevitable for the CaO-$CaCO_3$ looping FBC process explored, where high CO_2 concentrations (>90-95%) are produced in the sorbent regenerator. The data obtained support the contention that cycling studies done on limestones should employ realistic calcination conditions in terms of likely off-gas compositions. Also, as noted previously with different limestones, sulphate formation blocks active pores/surface area, resulting in lower CO_2 capture and causes a faster decline in sorbent reversibility, although hydration may somewhat reduce these effects, suggesting that the fuel used in the regenerator should ideally contain low sulphur concentrations. High CO_2 and SO_2 in the CaO/$CaCO_3$ formation/decomposition gas stream will lead to enhanced sorbent sintering and irreversible $CaSO_4$ formation, consequently lowering CO_2 conversion. These effects can be expected to be reduced in practice by separating sulphation and

carbonation in the two stages of the carbonator and introducing steam to avoid extremely high CO_2 atmospheres.

3.6 References

Abanades, J. C. and Alvarez, D., (2003). 'Conversion Limits in the Reaction of CO_2 with Lime', Energy Fuels 17, 308.

Abanades, J. C., Anthony, E. J., Lu, Y., Salvador, C. and Alvarez, D., (2004). 'Capture of CO_2 from Combustion Gases in a Fluidized Bed of CaO', AIChE J. 50, 1614.

Anthony, E. J., Jia, L. and Wu, Y., (2005). 'CFBC ash hydration studies', Fuel 84, 1393.

Borgwardt, R. H. (1989a). 'Sintering of nascent calcium oxide', Chem. Eng. Sci. 44, 53.

Borgwardt, R. H., (1989b). 'Calcium oxide sintering in atmospheres containing water and carbon dioxide', Ind. Eng. Chem. Res. 28, 493.

Borgwardt, R. H., Roache, N. F. and Bruce, K. R., (1986). 'Method for variation of grain size in studies of gas-solid reactions involving calcium oxide', Ind. Eng. Chem. Fundam. 25, 165.

Clark, L. L., (1949). 'The effect of gases on the sintering of lime', Recueil des travaux chimiques des Pays-Bas et de la Belgique 68, 969.

Curran, G. P., Fink, C. E. and Gorin, E., (1967). 'Carbon dioxide acceptor gasification process-studies of acceptor properties', Adv. Chem. Ser. 69, 141.

Dobner, S., Sterns, L., Graff, R. A. and Squires, A. M., (1977). 'Cyclic Calcination and Recarbonation of Calcined Dolomite', Ind. Eng. Chem. Process Des. Dev. 18(4), 479.

Fennell, P. S.; Pacciani, R. P.; Dennis, J. S.; Davidson, J. F.; Hayhurst, A. N., (2007). 'The Effects of Repeated Cycles of Calcination and Carbonation on a Variety of Different Limestones, as Measured in a Hot Fluidized Bed of Sand', Energy Fuels 21(4), 2072.

Gupta, H. and Fan, L-S., (2002). 'Carbonation-Calcination Cycle Using High Reactivity Calcium Oxide for Carbon Dioxide Separation from Flue Gas', Ind. Eng. Chem. Res. 41, 4035.

Hughes, R., Lu, D., Anthony, E. J. and Wu, Y., (2004). 'Improved Long-Term Conversion of Limestone-Derived Sorbents for In Situ Capture of CO_2 in a Fluidized Bed Combustor', Ind. Eng. Chem. Res. 43, 5529.

Hughes R., Lu D., Anthony E. J. and Macchi A., (2005). 'Design, Process Simulation and Construction of an Atmospheric Dual Fluidized Bed Combustion System for in situ CO_2 Capture using High-temperature Sorbents', Fuel Proc. Tech. 86, 1523.

Manovic, V. and Anthony, E. J., (2008). 'A parametric study on CO_2 capture capacity of CaO-based sorbents in looping cycles', Energy and Fuels 22, 1851.

Salvador, C., Lu, D., Anthony, E. J. and Abanades. J. C., (2003). 'Enhancement of CaO for CO_2 capture in an FBC environment', Chem. Eng. J. 96, 187.

Shimizu, T., Hirama, T., Hosoda, H., Kitano, K., Inagaki, M. and Tejima, K., (1999). 'A twin fluid-bed reactor for removal of CO_2 from combustion processes', Trans. IChemE 77, 62.

Silaban, A., (1993). 'High-temperature high-pressure CO_2 removal from coal gas', PhD Thesis, Louisiana State University, Department of Chemical Engineering.

Silaban, A. and Harrison, P., (1995). 'High-temperature capture of carbon dioxide: characteristics of the reversible reaction between CaO(s) and CO_2(g)', Chem. Eng. Comm. 137, 177.

Sun, P., Grace, J. R., Lim, C. J. and Anthony, E. J., (2006). 'Removal of CO_2 by calcium-based sorbents in the presence of SO_2', Energy Fuels 21, 163.

Wang, J. and Anthony, E. J., (2005). 'On the Decay Behavior of the CO_2 Absorption Capacity of CaO-Based Sorbents', Ind. Eng. Chem. Res. 44, 627.

Wu, Y., Anthony, E. J. and Jia, L., (2004). 'Steam hydration of CFBC ash and the effect of hydration conditions on reactivation', Fuel 83, 1357.

Chapter 4 Hydration and Pelletization of $CaCO_3$ Derived Sorbents for In-Situ CO_2 Capture

Published in the Proceedings of the 20th International Conference on Fluidized Bed Combustion

Lu, D.[1], **Hughes, R.W.**[1], Reid, T.[1], Anthony, E.J.[1], (2009). 'Hydration and Pelletization of $CaCO_3$ Derived Sorbents for In-Situ CO2 Capture', Proceedings of the 20th International Conference on Fluidized Bed Combustion.

[1]Natural Resources Canada, CETC-O, 1 Haanel Drive, Ottawa, Canada K1A 1M1

4.1 Abstract

Steam hydration and pelletization of limestone were investigated as methods to improve sorbent utilization for *in-situ* CO_2 capture under operating conditions typical of fluidized bed combustion. A thermogravimetric analyzer (TGA) was used to evaluate the performance of the modified sorbent. Steam hydration of CaO significantly improves the carbonation capacity but the hydrated sorbent is very fragile and its application is expected to be limited for CO_2 capture using fluidized bed combustion (FBC) technology. Similar sorbent improvements in terms of maintaining/enhancing reactivity were observed by sorbent fine grinding and pelletization, which has proven to be an excellent solution for using the hydrated sorbent in fluidized bed applications. The calcination/carbonation process conditions for CO_2 capture were optimized for the modified sorbents and compared to their original sorbent forms.

Keywords: CO_2 capture, Hydration, Pelletization, Calcination and Carbonation.

4.2 Introduction

Power generation from fossil fuel utilization is a significant contributor to atmospheric CO_2 concentration, while CO_2 separation from the flue gas has been estimated to constitute around 70% of the total cost for CO_2 management processes, including separation, compression, transportation, and sequestration(White et al., 2003; World Resources Institute, 2005; Ali et al., 2003). The capture of CO_2 imposes severe energy penalties on fossil-fuel-based power plants, reducing their net electricity output by as much as 13-37% (Rao and Rubin, 2002). The exceptional costs associated with current CO_2 separation technologies necessitate the development of economical alternatives. Adsorption processes for CO_2 separation employing physical and chemical sorbents such as limestone are thought to be technically feasible and economical. The reversible reaction between CaO and CO_2 may ultimately find application in a high-temperature process to capture CO_2 emissions from advanced power generation processes. For sorbents derived from limestone:

$$CaO\ (s) + CO_2\ (g) \Leftrightarrow CaCO_3\ (s) \qquad 4.1$$

At appropriate temperature and pressure (thermal equilibrium favourable), CO_2 from a flue gas stream can be adsorbed in the calcined limestone and form $CaCO_3$ in the carbonation reaction (the forward reaction of reaction 4.1). At higher temperature and/or lower pressure, the calcination reaction occurs to produce a gas stream having a high CO_2 concentration suitable for further application or ready for sequestration (the reverse reaction of reaction 4.1).

However, it is now well established that the carrying capacity of CaO sorbents from natural sources falls off rapidly with increasing numbers of reaction cycles, typically achieving levels of less than 10% by the time the sorbent has experienced 100 or less cycles (Anthony, 2008). This appears to be due to decay in the microporosity of the lime-based sorbents due to sintering (Borgwardt, 1989). However, superior CO_2 capture capacity can be achieved by highly porous or finely divided sorbent particles, albeit that these cannot be easily used in a practical fluidized bed combustion (FBC) system. In fact, work by Barker (1974) suggested that particles as small as 10 nm could display almost total reversibility in the carbonation reaction (for extended carbonation times and mild calcination conditions).

If sorbent utilization can be improved, not only will less fresh limestone be needed, but solids handling and disposal will be reduced as well, thereby reducing overall CO_2 emissions and total costs. Studies performed by Hughes *et al.* (2004) on crushed limestone regarding CO_2 adsorption have shown that conversion to calcium carbonate as high as 52% could be obtained consistently, if pore surface area and volume of the crushed rock were increased by steam hydration. Other studies, such as those done by Gupta *et al.* (2004) focused on the pelletization of powdered limestone. They determined that compaction of lime powder derived from calcination of mesoporous $CaCO_3$ preserves the porosity of limestone powder and allows for conversion to carbonate of 50-80% over three calcination/carbonation cycles. Gupta *et al.* used a pressure pelletization technique, and found carbonation to decrease with increasing pellet thickness (Gupta et al., 2004).

This paper presents studies for improving CO_2 capture performance using limestone-derived sorbent modification in order to moderate decay of the sorbent reactivity with increasing calcination/carbonation cycles. The sorbent modification technique used in this work is steam hydration followed by pulverization and pelletization.

4.3 Methodology

4.3.1 CaO Hydration with Steam

The hydration of calcium oxide has been extensively utilized in the limestone industries. Hydrated lime can be produced by adding water or steam to quicklime:

$$CaO + H_2O \leftrightarrow Ca(OH)_2 \qquad 4.2$$

Hydration of FBC bed ash usually results in sorbent reactivation and improved sorbent utilization (Anthony et al., 2007) and a very similar phenomenon is seen for Ca looping cycles (Hughes et al., 2004). During hydration of the spent sorbent, either water or steam permeates the particle and reacts with CaO. The product, $Ca(OH)_2$, has a larger molar volume (33 cm^3/mol) than the CaO (17 cm^3/mol) and so the particle swells, leading to cracking and regeneration of porosity lost due to sintering and/or carbonation, although it is more effective to hydrate sorbents from the calcination

step (Manovic and Anthony, 2007a; Manovic and Anthony, 2007b). Unfortunately, any small particles that have been created will have a reduced residence time in a fluidized bed and this will limit conversion for these smaller particles; recent pilot-scale tests of a Ca-based looping cycle have shown that such attrition losses can be very high indeed (Lu et al, 2008).

4.3.2 Pelletization

As noted above, small particles will be rapidly elutriated from fluidized bed reactors given sufficient fluidizing velocity. Agglomeration of the small particles into pellets can alleviate this problem. Pelletizing provides an opportunity to enhance the sorbent through the addition of additives such as salts. Pellets can be formed from powdered substances in several ways, most commonly through pressure pelletization and tumble agglomeration; the details of these techniques are described by Pietsch (1991). The pelletization method utilized in this study was tumble agglomeration with a binder to enhance the strength of the pellet. The binder and particles were rolled in a disc pelletizer to agglomerate and form semi-spherical pellets.

Pelletization *via* tumble agglomeration occurs through several different phenomena. Firstly, nucleation takes place, wherein the powder agglomerates to form seeds (very small pellets). As tumbling and binder addition continue, seeds may coalesce randomly or continue to grow by layering. The tumbling action also causes pellets to break at weak spots. Broken pieces may grow by layering or may join other growing pellets. As binder addition continues after nucleation begins, an optimal moisture level is reached in the pellet. During this stage the pellet size distribution is quite uniform. The desired pellet size should be reached in this stage, and pelletization should be stopped before moisture levels become too high and ball growth begins (when the pellets begin to coalesce and form large non-uniform masses at an uncontrollable rate). The excess moisture may also disrupt pellet pore structure, causing pores to collapse or be destroyed upon agglomeration with other pellets. It is important to add liquid binder at a slow and controlled rate to carefully control the rate of pellet growth and ensure the formation of desirable pores.

In disc pelletizers (one type of tumble agglomerator), pellet size can also be controlled by rotational speed (*i.e.*, faster rotation, smaller pellets), pan depth (*i.e.*, shallow pan, smaller pellets), and pan diameter (*i.e.*, smaller diameter, smaller pellets). Disc angle also helps to control pellet strength.

Pellets on a more inclined disc climb the disc face higher and fall farther than those on a less inclined disc. The further such pellets tumble on the disc, the more compacted they become. Weak pellets are also broken by the fall, and these broken pieces are eventually incorporated in stronger agglomerates. Increased speed of the pan carries pellets higher up the disc so that they roll farther and compact more; increased depth increases pellet residence time in the pelletizer, increasing compaction; increased diameter increases the distance available for the pellets to rise and fall in the disc, thus increasing compaction. However, if speed or angle of the disc is increased too much, pellets may not form as the force of the collision with the disc edge upon falling may prove too great and shatter the pellets.

4.3.3 Binders

Pellet moisture content is critical and highly variable from batch to batch, as well as within each batch. Optimum moisture occurs when pellets are sprayed with an extremely fine mist of liquid binder. The liquid binder forms a thin film on the particulates, so that when particles contact on another, a liquid bridge is formed. Continued misting fills interparticle spaces, and enables the binder to apply the highest tension force between the particles (Baykal and Doven, 2000). This allows pellets to grow layer by layer and form strong and elaborate pore structures. Pellets that have too little liquid binder applied are very brittle and will often disintegrate while tumbling through the disc. Too much liquid binder results in sticky pellets that may bind to the disc or to other fully formed pellets, creating oversized, less porous pellets.

Water is a common liquid binder used in many tumble agglomeration processes. Capillary and surface tension forces bind particles together as described previously. However, the water binder evaporates from the pellets in the first calcination cycle, which results in a loss of pellet cohesion.

Sodium carbonate solution has been used as a binder because of its benefits to pellet properties, as stated by Hamer (1986). Hamer's investigations found that a 5% Na_2CO_3 solution made pellets strong enough for handling and use in a fluidized bed combustor for sulphur capture. His findings also indicated that sorbent capacity (with respect to sulphation) increased nearly 30% for pellets made with sodium carbonate binder as compared to untreated, crushed limestone. Sodium carbonate, when heated with limestone above 700°C, can form eutectic melts in trace quantities. It

has been postulated that these melts increase the mobility of ions in the CaO matrix, increasing the rate of solid state diffusion and hence improving reactivity (Ripke and Kawatra, 2000). The increased mobility may also lead to increased sintering, resulting in modification of the pore size distribution both in the pellet and the particles making up the pellet. Sintering can greatly increase the strength of the pellets and particles, but can be expected to reduce the pore surface area of the particles.

Solid binders can also be used to increase pellet strength. The addition of 2 wt% bentonite to limestone prior to pelletization was shown by Hamer (1986) to increase pellet strength and sulphation capacity. Bentonite is a hydrated aluminosilicate clay primarily composed of montmorillonite: $(Na,Ca)_{0.33}(Al_{1.67},Mg_{0.33})Si_4O_{10}(OH)_2 \bullet nH_2O$. Substitution of a portion of the Al^{+3} with Mg^{+2} alters the crystal charge, which can be balanced by cations such as Na^+ and Ca^{2+}. Sufficient hydration of the interlayer cations causes the material to expand and disperse as individual platelets or fibres. These platelets or fibres can coat particles and promote agglomeration by interlayer electrostatic attraction. Bentonite binders can also result in eutectic melts with the possibility of formation of very strong pellets. Pellets formed in the iron ore industry use bentonite as a binder and are required to have compressive strengths in excess of 22 N after firing at temperatures in the area of 1300°C (Ripke and Kawatra, 2000).

Strength and porosity are the most critical pellet properties required by the dual fluidized beds (as calciner and carbonator) in the process proposed by Hughes *et al.* (2005). All factors involved in pellet making must be considered to optimize these two properties. Pellets have to be strong enough to withstand repeated transportation (pneumatic) from carbonator to calciner, and also to withstand the abrasive forces of other particles and bed walls within the fluidized beds. Pellets used for this purpose must also be porous to allow for the highest carbonation conversion rates possible. A balance must be made between strength and porosity.

4.4 Experimental Method

The work was conducted in three parts: sorbent pre-treatment (hydration), pelletization and thermogravimetric analysis.

4.4.1 Hydration of Limestone

A portion of the samples underwent pre-treatment entailing calcination of the raw limestone in an oven at atmospheric pressure in air. Each sample was weighed before and after calcination to verify that complete calcination had occurred. The sample remained in the oven at 820°C for 2 hours. Afterwards, hydration was performed within a Parr 4522M pressure reactor with saturated steam. The sample was placed on a piece of filter paper in an aluminum sample dish within the vapour space of the pressure reactor. The reactor consists of a removable top and a lower steel cylinder of 400 mm height and 100 mm ID; bolts seal the two parts together during operation. An external heater was used to raise the temperature in the bomb up to a maximum of 250°C. A small amount of sample (~2 g) was loaded into a basket, which was suspended in the middle of the bomb and immersed in the steam. The hydration temperatures were controlled at 150, 200 and 250°C and the resulting steam pressures employed were therefore 4.8, 15.6 and 39.9 bar. Pre-treatment was carried out for hydration times of 0.5, 1 and 2 hours at each temperature. At the end of the desired hydration time, the bomb was taken out of the heater and an exhaust valve was opened to release the pressure and decrease temperature in the reactor. This step significantly reduced the time (to less than 5 min) the sample was kept in the bomb after the desired hydration duration. The hydrated solids were then removed filtered under suction for 1.5-2 min and then transferred to a vacuum oven maintained at 45°C to dry for 3-4 h. The dried samples were analyzed to obtain free lime and $Ca(OH)_2$ content, or used in the CO_2 capture tests.

4.4.2 Pelletization

A disc pelletizer was used to make pellets in this experiment. The rotating disc turns around its central axis to build up spherical agglomerates by the tumbling, rolling and sliding actions of the particles and pellets. The movement of the disc pelletizer causes larger pellets to move to the top of the pellet pile resulting in a size gradient forming in the disc. Pellet size was partially controlled by disc angle. Pellets were made of binder and sorbents (< 75 micron), including original limestone, commercial hydrated lime and hydrated lime prepared in our laboratory. Binders used in combination with the sorbent were: water, 5% Na_2CO_3 solution, sodium bentonite, and calcium bentonite. Bentonite was premixed with sorbents in a ratio of 50:1 (limestone:bentonite). In this work the pelletizing disc was set to an angle of 53.4° to the horizontal. For a batch, approximately 50 g of sorbent was placed in the bottom of the pelletizing disc. The disc was turned on and water

or 5 wt% Na_2CO_3 dissolved in water was sprayed onto the disc surface at the four o'clock position. After a spray of water, the sorbent was allowed to roll in the disc. Any material not scraped off the disc by the pelletizer scraper was taken off manually with a scoopula at the six o'clock position. Water was sprayed again in the same position, and the scoopula was used to scrape the disc. The process of spraying 1-2 sprays of water onto the disc and scraping was repeated every 1-2 minute as needed to form pellets. The pellet making process required approximately 20 minutes to obtain properly made and correctly sized pellets. When the desired pellet size was reached and no sorbent powder remained in the disc, the pellets were allowed to roll in the disc for 10 minutes. The compacted pellets were removed from the disc pelletizer after a total pelletization time of approximately 30 minutes.

The pelletizing disc used for this study had fixed speed (35 rpm), depth (90 mm) and diameter (400 mm). Numerous trials were performed prior to producing pellets for friabilator (a device for determining the 'friability' of a solid) and thermogravimetric analysis to optimize the disc angle for pellet size and strength.

Freshly made pellets were placed in a vibrating wire mesh sieve for 1 min. Pellets 725-1400 μm were considered acceptable and placed in a drying oven at 105°C overnight. Pellets were stored in a vacuum oven at 55°C for the duration of the experiment. Pellet strength was tested in an Optimal Control friabilator. The friabilator has two 25.4 cm ID rotating cylinders with the circular axis in the horizontal plane. Inner baffles extend inwards from the outer perimeter of the cylinders and as the cylinder rotates pellets are repeatedly carried upwards until they slide off the baffle and impact the wall of the cylinder. Samples were weighed and sized and then rotated in the friabilator for 20 minutes at 26 rpm. Percent weight loss from the pellets was calculated after friabilator tests by resizing and reweighing pellets in the 725-1400 μm size range. The pellets were not fired at elevated temperature prior to thermogravimetric analysis.

4.4.3 Thermogravimetric Tests

Calcination/carbonation cycling of the limestone sorbents was conducted in a thermogravimetric analyzer (TGA). The TGA comprises an electronic balance (Cahn 1100), vertical furnace, reactor tube, carrier gas system and a computerized data acquisition system. The reactor tube is made of

Inconel 600 alloy and has an ID of 24 mm and a height of 900 mm. It can be unscrewed from the TGA, thus uncovering the platinum sample pan (10 mm diameter, 1.5 mm depth). Approximately 25-30 mg of sample (crushed, or powdered, or hydrated sorbent, or pellets) was loaded into the pan.

The reactor was heated externally by the electric furnace that can be placed around the reactor tube and then separated from it quickly. A thermocouple was used to measure the temperature near the reaction site (*i.e.*, just below the sample holder). The furnace was heated from room temperature to the desired calcination temperature and the heating rate employed was 10°C/min, as programmed by an electronic temperature controller, while the mass versus time (as well as the temperature) curve of the sample was recorded at 5 second intervals until termination of the run, using a Keithley 2700 data acquisition system and Keithley Xlinx software.

In this experiment of calcination/carbonation cycles, the TGA furnace temperature was set to 750°C for both carbonation and calcination. Nitrogen was used for the calcination step and a digital mass flow controller (Matheson Gas Products) regulated the flow rate at 100 mL/min for the reactant stream and 60 mL/min for the balance housing purge stream. When the sample mass stopped decreasing, the process was switched from calcination to carbonation with 15% CO_2 and 3% O_2 (N_2 balance) for 20 min. Some tests were performed with a carbonation gas composed of 0.5% SO_2, 15% CO_2 and 3% O_2 (N_2 balance). When the time for carbonation was complete, the gas stream in the reactor was switched back to the calcining gas.

Limestone powder, crushed limestone, and pellets with each binder were tested in the TGA. Each sample was run through 4 to 6 cycles (calcination/carbonation), and in the presence or absence of SO_2 in the carbonation step. Pellets run in the absence of SO_2 were allowed to carbonate for 20 minutes.

The composition of Cadomin limestone, used as sorbent, and the bentonite binders are given in Table 4-1 as analyzed by X-ray fluorescence spectroscopy (XRF). Limestone was pulverized to less than 75 μm prior to pelletization. Crushed stone was in the size range 725-1400 μm. The binder compositions provided are those typical for material as supplied by the vendor (American Colloid Company). The sodium and calcium bentonites contain small portions of feldspar, calcite, and

quartz. The sodium bentonite (SPV-200) size was specified as minimum 65% passing 200 mesh (74 μm). The calcium bentonite (Panther Creek 200) size was specified as 70% passing 200 mesh.

Table 4-1: Limestone and binder composition (wt%)

Component	Cadomin	Sodium Bentonite	Calcium Bentonite
CaO	55.12	0.65	3.14
SiO_2	1.50	63.02	60.50
Al_2O_3	<0.10	21.08	18.20
Fe_2O_3	<0.01	3.25	5.52
FeO	<0.01	0.35	<0.01
Na_2O	<0.20	2.57	0.20
K_2O	0.21	<0.02	0.14
SO_3	0.32	<0.10	<0.10
Trace	n.d.	0.72	n.d.
Loss on ignition (LOI)	n.d.	5.64	4.85
Loss on fusion (LOF)	42.77	n.d.	n.d.

4.5 Results and Discussion

4.5.1 Pelletization

Table 4-2 provides the results of the friability testing for four batches of pellets made with Cadomin limestone, each using a different binder combination. The lower loss in material from the desired size range indicates that sodium carbonate-bound pellets are much stronger and more durable than pellets made with the other binder combinations. Pellets made with Na_2CO_3 binder were quite hard and bound together well.

Table 4-2: Percent of material lost from 725-1400 μm size range during friability testing with various binders.

Binder	% weight loss
5 wt% Na_2CO_3 solution	31.3
Water	100.0
Na bentonite/H_2O	86.5
Ca bentonite/H_2O	78.2

Sodium and calcium bentonite were found to increase resistance to attrition as shown in Table 4-2, compared to water-bound pellets. In all tests sodium bentonite-bound pellets had higher mass loss than calcium-bound ones. Sodium bentonite tends to swell more than calcium bentonite upon hydration and this may result in a more open pore structure in the pellet upon dehydration. This more open pore structure will likely result in reduced strength compared to pellets made with calcium bentonite.

For comparison, crushed limestone was also run through the friabilator. Crushed limestone sprayed with water had a weight loss of 8.6%, and crushed limestone sprayed with sodium carbonate solution had a weight loss of 6.7%. These data show that the pellets are significantly weaker than the original rock. It should be noted that these pellets have not been heat treated; heat treating would likely result in much stronger pellets.

4.5.2 Thermogravimetric Tests

Figure 4.1 shows conversion across calcination /carbonation cycles for the initial cycles using crushed limestone and pellets formed with Na bentonite. It appears that reaction proceeds much more quickly in the pelletized material for both calcination and carbonation. The time required to calcine the crushed stone was 3.5 times as great as for the pellet, even though the stone and the pellet were of similar size. If this proves to be normal behaviour with such pelletized particles, it would clearly be an advantageous characteristic in a real system.

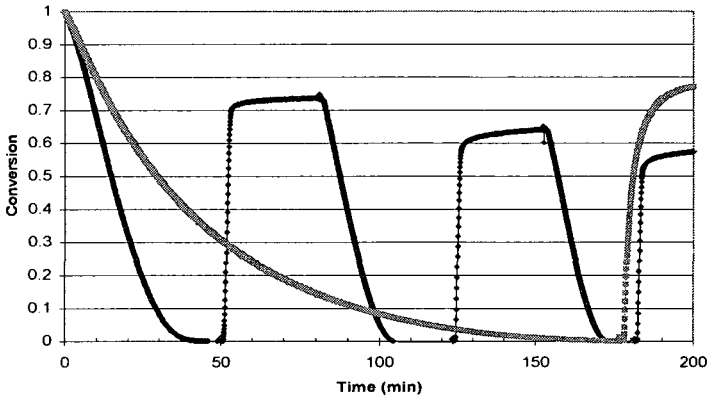

Figure 4.1: Calcination/carbonation cycles of Na bentonite-bound pellets (circle) and crushed limestone (square) at 750°C calcined with N_2 and carbonated with 15% CO_2, 3% O_2 in N_2 at 750°C .

Figure 4.2 shows carbonation conversion after 5 minutes for samples treated without SO_2 present in the carbonation step. As expected finely divided lime carbonates more fully than larger particles as there is greater surface area available for reaction adjacent to particle surfaces (Oates, 1998). The conversion of the pelletized material falls between the two extremes of pulverized and crushed limestone. Conversions of the pellets formed with bentonite are nearly identical, as are the pellets formed with water and Na_2CO_3.

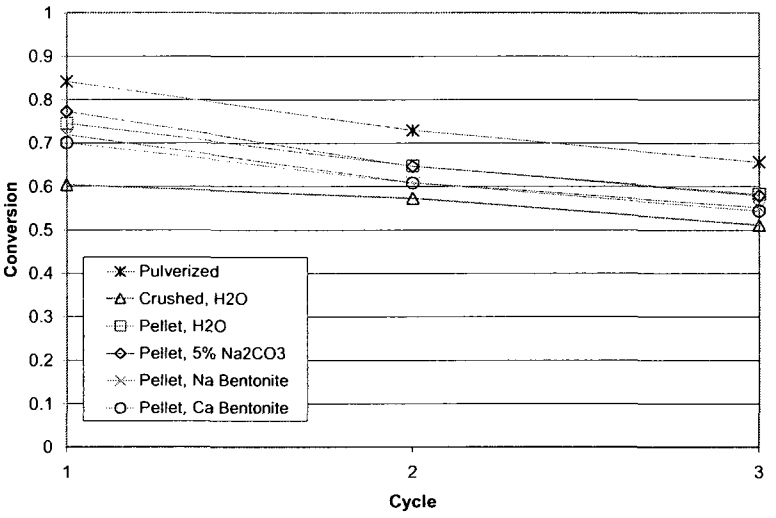

Figure 4.2: Carbonation conversion of sorbents after 5 minutes of reaction; carbonation at 750°C with 15% CO_2, 3% O_2 in N_2

Carbonation conversions in the presence of 0.5% SO_2 are shown in Figure 4.3 and the sulphation conversions for the same tests are shown in Figure 4.4. SO_2 has been shown to reduce the ability of limestone sorbents to capture CO_2 since $CaSO_4$ prevents CO_2 reacting with free CaO (Sun et al., 2007). Here, as expected, pulverized limestone has a greater ability to capture both CO_2 and SO_2 than does crushed limestone. In general, the pelletized material that has high capacity for SO_2 has a reduced capacity for CO_2, and *vice versa*. Pellets were prepared using sodium bentonite as binder. The results of TGA tests are presented in Figure 4.3 and Figure 4.4 for both pellet batches (SO_2, Pellet, Na Bentonite; and SO_2, Pellet, Na Bent REP 1). It is apparent that the two batches have significantly differing capture capacities for CO_2 and SO_2 over the limited number of samples examined here. Repeat testing from each of the batches indicates that the variation results from differences in pellet formation in each batch and not variability of pellets within a batch. One of the Na bentonite pellet batches shows a CO_2 capture capacity equivalent to that of pulverized limestone and higher capacity for SO_2, which could be important since, otherwise, one must vigorously separate the processes of sulphation and carbonation (Manovic and Anthony, 2007). In fact, all the pelletized sorbents showed improved SO_2 capacity as would be expected based on early work by Hamer (1986).

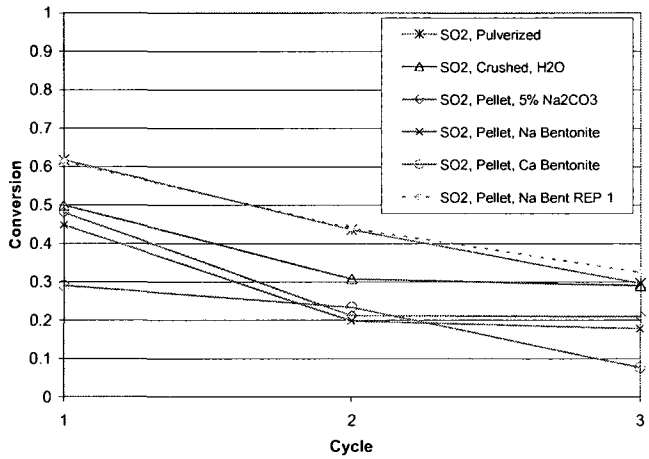

Figure 4.3: Carbonation conversion of sorbents after 5 minutes of reaction at 750°C with 0.5% SO_2, 15% CO_2, 3% O_2 in N_2.

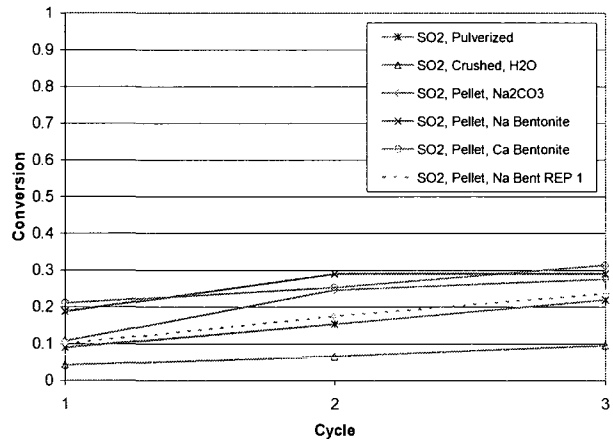

Figure 4.4: Sulphation conversion of sorbents after 5 minutes of reaction at 750°C with 0.5% SO_2, 15% CO_2, 3% O_2 in N_2.

Figure 4.5 shows carbonation conversion for a variety of finely divided $CaCO_3$-derived materials including commercial quick lime (denoted c-q-lime), pulverized limestone, commercial hydrated lime (denoted c-h-lime), and hydrated lime that was prepared in our laboratory from pulverized limestone. The commercial quick lime is prepared at high temperature and is heavily sintered, so it has a low capacity for CO_2 capture. The capacity of the quick lime increased slightly as cycles progressed and would appear to have stable conversion in the area of 20%. A similar effect was noted by Manovic and Anthony (2008), in which heavily sintered materials recover carbon capture capability after multiple carbonation/calcination cycles. The pulverized limestone follows a typical reduction in CO_2 capture capacity, as seen previously (Abanades and Alvarez, 2003). The two hydrated limes show a much greater capacity for CO_2 capture than the other materials. Unfortunately the hydrated material is also quite soft and would undergo excessive attrition from impact, thermal shock and reaction in dual fluidized bed systems. Carbonation conversions for hydrated materials in pellet form are shown in Figure 4.6.

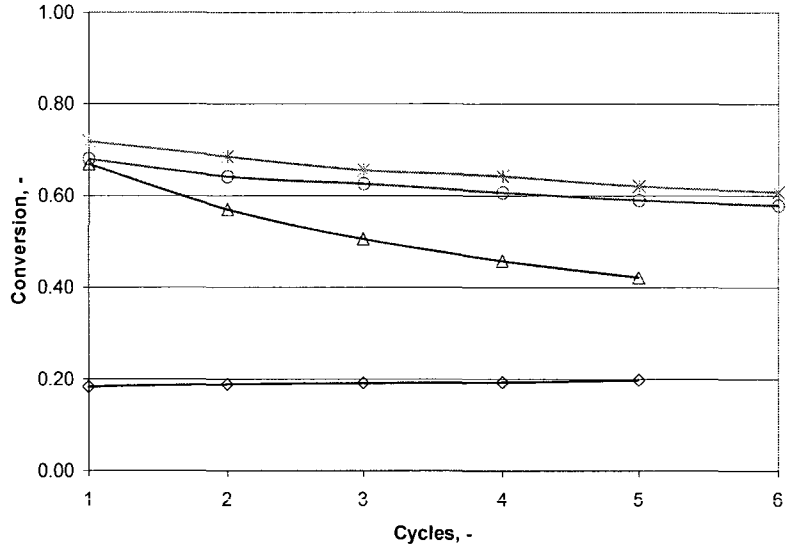

Figure 4.5: Carbonation conversion for pulverized limestone (triangle), c-q-lime, <30 μm diameter (diamond), c-h-lime, <50 μm diameter (circle), Lab-h-lime (asterisk); 750°C, 3% O_2, 15% CO_2 in N_2.

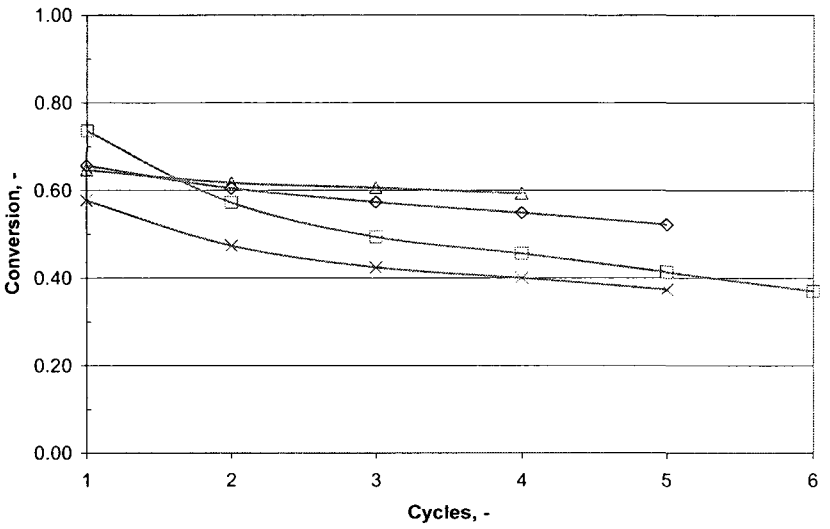

Figure 4.6: Carbonation conversion for hydrated and pelletized sorbents; Lab-h-lime pellet with water binder 1-2 mm diameter pellet (diamond), Lab-h-lime pellet with 5% Na_2CO_3 binder 1-2 mm diameter pellet (triangle), c-h-pellet 0.6-1.4 mm diameter pellet (square), c-h-pellet 3.0-4.0 mm diameter pellet (X); 750°C, 3% O_2, 15% CO_2 in N_2.

The commercial hydrated limes in pellet form both performed more poorly than their parent material, in fact, nearly as poorly as the sorbent derived from pulverized limestone. The hydrated and pelletized material performed much better. If we assume that this material deactivates in the same manner as limestone-derived sorbents do, and apply the deactivation model put forward by Abanades and Alvarez (2003):

$$X_{b,N} = f_m^N (1 - f_w) + f_w \qquad 4.3$$

then we find that, after 50 cycles the pellets formed with water as binder have a carbonation conversion of 42% while the pellets formed with 5% Na_2CO_3 have a conversion of 57%. Previous economic analysis (Abanades et al., 2004) has indicated that the CaO-CaCO3 looping process is attractive for carbon capture provided that conversion of the sorbent is in excess of 40% for at least 20 cycles. These results are thus quite promising as material that was previously considered too

fragile for use in fluidized beds (Hughes et al., 2004) has maintained excellent activity (albeit for a limited number of cycles) after having been physically strengthened using pelletization techniques.

An interesting result of this work is that, whereas Na_2CO_3 has been shown to have unfavourable effects on lime-based materials, when they were doped with Na_2CO_3 both in the TGA environment and in a FB unit, they did not do so here (Manovic et al., accepted Energy and Fuel 1998; Salvador et al., 2003).

4.6 Conclusions

Steam hydration together with pelletization of limestone was used to improve sorbent utilization for *in-situ* CO_2 capture under operating conditions typical of fluidized bed combustion. The pelletized particles in general showed good performance, comparable to or better than hydrated samples. Such pellets should allow one to use fine materials in a FBC environment, either by taking the fines actually produced in a real FB looping cycle or by using pulverized limestones and making pellets with sufficient strength to survive multiple cycles. Further work needs to be done to confirm these findings using more realistic calcination conditions (*i.e.*, higher temperatures in the presence of pure CO_2), and over a greater number of cycles. An interesting result is that the presence of Na_2CO_3 in the binders, which has been shown to have deleterious effects in a real FBC system, did not do so here, with a pulverized limestone sample.

4.7 Acknowledgment

We would like to thank Dr. Yinghai Wu for preparing the hydrated samples.

4.8 References

Abanades, J. C.; Alvarez, D., (2003). 'Conversion Limits in the Reaction of CO_2 with Lime', Energy and Fuel 17, 308-315.

Abanades, J. C.; Rubin, E. S.; Anthony, E. J., (2004). 'Sorbent Cost and Performance in CO_2 Capture Systems', Ind. Eng. Chem. Res. 43, 3462-3466.

Ali, S.; Gunwan, A.; Thomson, E., (2003). 'The Capture and Sequestration of Carbon Dioxide: CO_2 Capture Methods', Retrieved April 26, 2005, from http://www.esru.strath.ac.uk/EandE/Web_sites/02-03/carbon_sequestration/Carbon%20Sequestration-422.htm

Anthony, E. J.; Bulewicz, E. M.; Jia, L., (2007). 'Reactivation of Limestone Sorbents in FBC for SO_2 Capture', Progress in Energy and Combustion Science 33, 171-210.

Anthony, E. J., (2008). 'Solid Looping Cycles: A New Technology for Coal Conversion', Ind. Eng. Chem. Res. 47, 1747-1754.

Barker, R., (1974). 'The Reactivity of Calcium Oxide towards Carbon Dioxide and Its Use for Energy Storage', Appl. Chem. Biotechnol. 24, 221-227.

Baykal, G.; Doven, A., (2000). 'Utilization of fly ash by pelletization process; theory, application areas and research results', Resources, Conservation and Recycling 30, 59-77.

Borgwardt, R. H., (1989). 'Sintering of nascent calcium oxide', Chem. Eng. Sci. 44, 53.

Curran, G. P.; Fink, C. E.; Gorin, E., (1967). 'Carbon dioxide-acceptor gasification process: studies of acceptor properties', Adv. Chem. Serv. 69, 141-65.

Gupta, H.; Iyer, M.; Sakadjian, B. B.; Fan, L., (2004). 'Reactive separation of CO_2 using pressure pelletised limestone', Int. J. Environmental Technology and Management 4, 3-19.

Hamer, C. A., (1986). 'Evaluation of SO_2 Sorbent Utilization in Fluidized Beds', CANMET Report No. 86-9E, Energy, Mines and Resources Canada.

Hughes, R.; Lu, D.; Anthony, E. J.; Wu, Y., (2004). 'Improved Long-Term Conversion of Limestone-Derived Sorbents for In Situ Capture of CO_2 in a Fluidized Bed Combustor', Ind. Eng. Chem. Res. 43, 5529-5539.

Hughes, R. W.; Lu, D. Y.; Wang, J.; Anthony E. J., (2005). 'Design, Process Simulation and Construction of an Atmospheric Dual Fluidized Bed Combustion System for *In situ* CO_2 Capture using High-Temperature Sorbents', Fuel Process. Technol. 86, 1521-1531.

Lu., D., Hughes, R., Anthony, E.J., (2008). 'Ca-Based Sorbent Looping Combustion for CO_2 Capture in Pilot-Scale Dual Fluidized Beds', Fuel Proc. Tech. 89(12), 1386-1395.

Manovic, V.; Anthony, E. J., (2007). 'Steam Reactivation of Spent CaO-based Sorbent for Multiple CO_2 Capture Cycles', Environ. Sci. Technol. 41, 1420-1425.

Manovic, V.; Anthony, E. J., (2007). 'Sequential SO_2/CO_2 capture enhanced by steam reactivation of a CaO-based sorbent', Fuel 87, 1564-1573.

Manovic, V.; Anthony, E. J., (2007). 'SO_2 Retention by Reactivated CaO-based Sorbent from Multiple CO_2 Capture Cycles', Environ. Sci. Technol. 41, 4435-4440.

Manovic, V.; Anthony, E. J., (2008). 'Thermal Activation of CaO-based Sorbent and Self-Reactivation during CO_2 Capture Looping Cycles', Environ. Sci. Technol. 42, 4170-4174.

Manovic, V.; Anthony, E. J.; Abanades, J. C.; Grasa, G., (2008) '$CaO-CaCO_3$ looping Cycle Performance of a High-Purity Limestone after Thermal Activation/Doping', Energy & Fuels 22(5), 3258.

Oates, J. A. H., (1998). 'Lime and Limestone: Chemistry Technology, Production and Uses', New York, USA: Wiley-VCH.

Pietsch, W., (1991). 'Size Enlargement by Agglomeration', Chichester, UK: John Wiley & Sons Ltd.

Rao, A. B.; Rubin, E. S., (2002). 'A Technical Economical and Environmental Assessment of Amine-Based CO_2 Capture for Power Plant Greenhouse Gas Control', Environ. Sci. Technol. 36, 4467-75.

Ripke, S. J.; Kawatra, S. K., (2000). 'Can Fly-ash Extend Bentonite Binder for Iron Ore Agglomeration?', Int. J. Miner. Process. 60, 181-198.

Salvador, C.; Lu, D.; Anthony, E. J.; Abanades, J. C., (2003). 'Enhancement of CaO for CO_2 Capture in a FBC Environment', Chem. Eng. J. 96, 187-195.

Silaban, A.; Harrison, D., (1995) 'High-temperature capture of carbon dioxide: characteristics of the reversible reaction between CaO(s) and CO_2(g)', Chem. Eng. Comm. 137, 177-90.

Sun, P.; Grace, J. R.; Lim, C. J.; Anthony, E. J., (2007). 'Removal of CO_2 by Ca-Based Sorbents in the Presence of SO_2', Energy Fuel 21, 163-170.

White, C. M.; Strazisar, B. R.; Granite, E. J.; Hoffman, J. S.; Pennline, H. W., (2003). 'Critical Review: Separation and Capture of CO_2 from Large Stationary Sources and Sequestration in Geological Formations – Coalbeds and Deep Saline Aquifers', J. Air Waste Manage. Assoc. 53, 641-715.

World Resources Institute, (2005). 'Total GHG Emissions in 2000 (excludes land use change), CO_2', Retrieved April 26, 2005, from http://cait.wri.org/cait.php?page=yearly.

Chapter 5 Design, Process Simulation, and Construction of an Atmospheric Dual Fluidized Bed Combustion System for *In Situ* CO_2 Capture Using High-temperature Sorbents

Published in Fuel Processing Technology

Hughes, R.W.[1], Lu, D.[1], Anthony, E.J.[1], Macchi, A.[2], (2005). 'Design, Process Simulation, and Construction of an Atmospheric Dual Fluidized Bed Combustion System for In Situ CO_2 Capture Using High-Temperature Sorbents', Fuel Processing Technology 86, 1523-1531.

[1]Natural Resources Canada, CETC-O, 1 Haanel Drive, Ottawa, Canada K1A 1M1

[2]University of Ottawa, 161 Louis Pasteur, Ottawa, Canada, K1N 6N5

5.1 Abstract

An atmospheric dual fluidized bed combustion system using high-temperature sorbents for *in situ* CO_2 capture has been designed, simulated and constructed. The pilot plant is expected to burn petroleum coke and coal or biomass in a clean and efficient manner, generating a carbonator flue gas containing 2-5 mol% CO_2, while producing a relatively pure carbon dioxide stream ready for compression. The concentration of sulphur dioxide in the resulting flue gas is expected to be on the order of a few parts per million by volume. Initial investigations are to be carried out using limestone-derived sorbents enhanced using a simple single step process for pore modification developed at CETC-Ottawa. Carbonation occurs in a two-stage fluidized bed carbonator-combustor allowing for optimal temperature control for both combustion (850-950°C) and carbonation (650-750°C). Calcination occurs in a single-stage fluidized bed combustor burning petroleum coke. Pilot plant operational data will be used for on-going scale-up activities using the ASPEN Plus process simulator.

Keywords: Carbon dioxide capture; Sorbent; Fluidized bed combustion; Carbonation

5.2 Introduction

There may be a future legislative requirement to reduce CO_2 emissions along with pollutants such as SO_2 and NO_X (White et al., 2003; Gupta et al., 2003). The worldwide demand for electricity is projected to increase over the next twenty years. If both sets of requirements are to be met without excessive economic disadvantage to the world economy, then new electrical generation methods with low or zero CO_2 emissions must be developed.

The use of the carbonation reaction in a combustion system could potentially meet the needs of a modern, high-volume, CO_2 capture system. The process outlined below operates continuously; producing a carbonator product gas containing 2-5 mol% CO_2. CO_2 emissions at this level would result in a reduction in greenhouse gases of 70-85% as compared to a typical coal fired power generating station. A calciner product gas, with a CO_2 purity exceeding 95 mol% (dry basis), would be produced that could be used in enhanced oil recovery or enhanced coal bed methane operations.

The carbonation reaction can remove carbon dioxide from combustion systems at elevated temperatures (~650-750°C) and atmospheric pressure (Shimizu *et al.*, 1999; Gupta *et al.*, 2002; Abanades *et al.*, 2003 (a); Anthony and Wang, 2003) *via*:

$$CaO\ (s) + CO_2\ (g) \Leftrightarrow CaCO_3\ (s) \qquad 5.1$$

The thermal efficiency of systems using dual fluidized beds for carbonation and sorbent regeneration has been shown to be similar to current combustion systems without CO_2 segregation. Sulphur dioxide emissions will be on the order of a few parts per million since the higher calcium requirements for CO_2 removal will result in an equivalent Ca:S molar ratio on the order of 20-30. Fluidized bed combustors are intrinsically low producers of NO and are amenable to NH_3 injection if very low emissions of NO are desired (Grace *et al.*, 1997).

The dual fluidized bed carbonation process can be applied to stationary emitters of carbon dioxide including coal-fired generating stations and cement kilns. Limestone ($CaCO_3$), the main feedstock, is inexpensive and readily available throughout most of the world allowing this process to potentially have a global impact on greenhouse gases.

Information needed for scale-up to an industrial process using dual fluidized bed technology for carbon dioxide capture is not currently available in the literature. To obtain some of the required information, a mini-pilot plant has been constructed. The design and ASPEN Plus process simulation of this system are presented here.

5.3 Experimental

5.3.1 Dual Fluidized Bed Design

Figure 5.1 shows a process flow diagram for the twin fluidized bed combustion system with CO_2 capture operating at atmospheric pressure. Solid fuel combustion, with air, occurs in the first stage of the carbonator-combustor at an optimum temperature for combustion (850-950°C) while carbonation occurs in the second stage at an optimum temperature for CO_2 capture (650-750°C for reaction 5.1). Partially spent sorbent is directed to the combustion section of the carbonator to remove sulphur in order to avoid contaminating fresh sorbent. The sorbent is regenerated in the regenerator. The dual fluidized bed pilot plant is the result of a major overhaul and expansion of the existing CETC-O mini-bed that has been in operation for nearly 15 years.

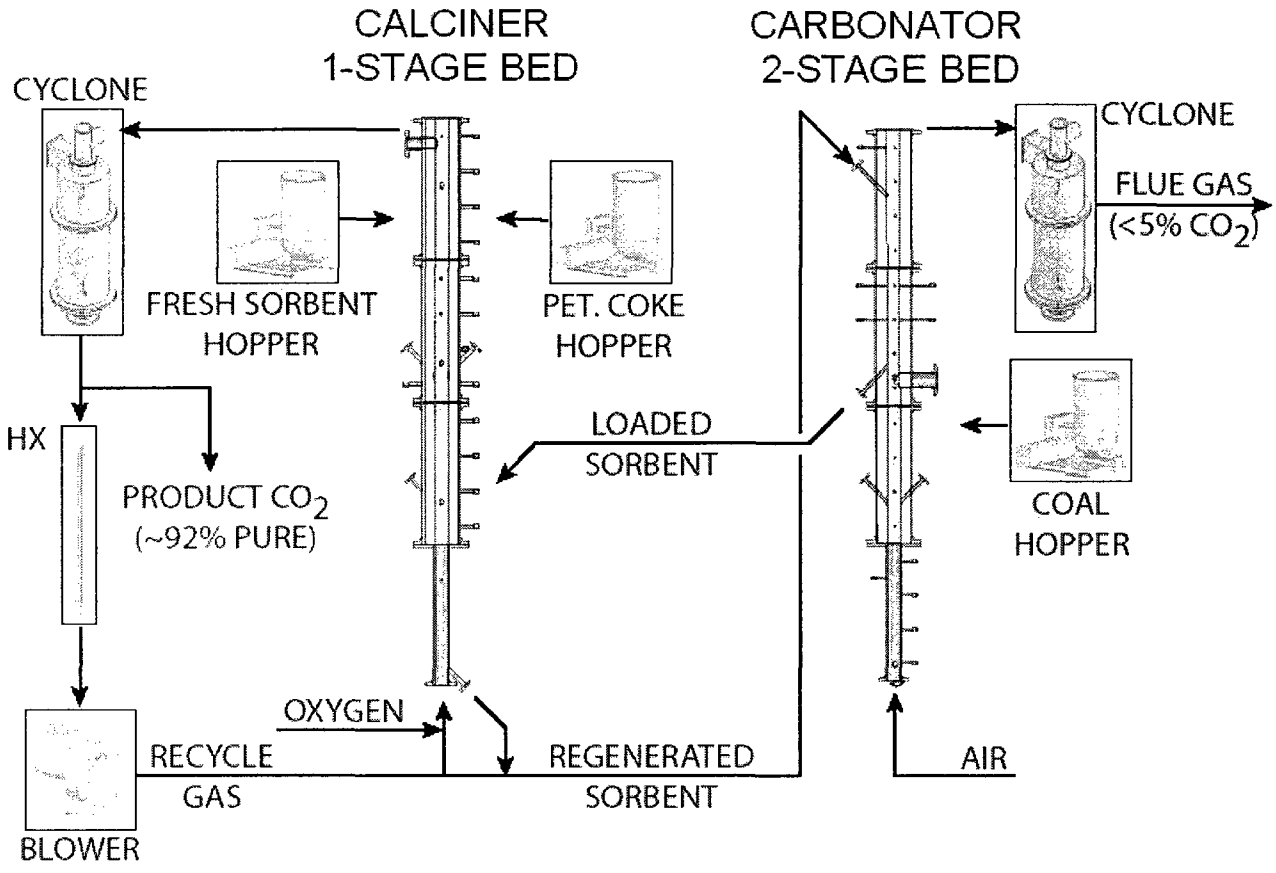

Figure 5.1. Atmospheric dual fluidized bed combustion system with CO_2 capture - regenerator operating under flue gas recycle mode.

5.3.2 Preliminary Pilot Plant Study

Practical operating issues for bubbling and circulating fluidized bed combustion have been evaluated using the existing 0.1 metre inner diameter CETC-O mini-circulating fluidized bed combustor (Abanades *et al.*, 2004). The process was previously emulated by varying the operating conditions of the single existing combustor. This was achieved by cycling the bed between calcination and carbonation conditions. Results of the dual fluidized bed pilot plant studies are used to fine-tune process simulations for both atmospheric carbonation as described here, and pressurized carbonation as described by Wang *et al.* (2003).

5.3.3 Regenerator

Limestone is fed to the regenerator where CO_2 is liberated to produce CaO. Heat is supplied in the regenerator by burning a low-ash fuel, such as petroleum coke, with oxygen to drive reaction 5.1 to the left, releasing carbon dioxide. As a result of the petroleum coke being burned within the oxygen fired regenerator, all CO_2 produced is captured by the process. The regenerator has been designed to allow operation in both high-temperature and steam-stripping modes. The regenerator operates at a suitable temperature for steam generation allowing the heat required for regeneration to be captured by the process, thus avoiding the heat penalties that are often associated with sorbent regeneration in CO_2 capture processes.

In the high-temperature mode, the regenerator is operated at a sufficiently high temperature to obtain a reasonable release rate of CO_2 for a given carbon dioxide partial pressure. In the high-temperature mode, using typical feedstocks, the partial pressure is predicted to be approximately 0.92 bar with the regenerator operating at a total pressure of 1 bar, based on ASPEN Plus simulations. For this partial pressure, the temperature in the regenerator must exceed 895°C based on the partial pressure-temperature equilibrium curve published by Barker (1962). It is expected that a reasonable rate of reaction will be achieved at around 950°C. In this case, carbon dioxide is cooled and recycled to the bottom of the bed (i.e. windbox) to act as a fluidizing medium and temperature moderator. Using pure oxygen would cause hot spots in the fluidized bed that would reduce the useful lifetime of both the sorbent and the reactor.

In the stripping mode, steam is used to reduce the partial pressure of carbon dioxide resulting in its release at a lower temperature. Operating in the steam-stripping mode may reduce the effects of

sintering during the reactivation cycles, extending sorbent life. Lower temperatures generally minimize sintering effects. Further, Dobner *et al.* (1977) have shown that the rate of sintering is lower in a water-rich environment than in a carbon dioxide-rich environment.

The regenerator can be operated as either a bubbling or circulating fluidized bed. In both cases, the overall design of the regenerator is similar to that of the carbonator except that the regenerator is a single-stage reactor.

5.3.4 Carbonator-Combustor

The combustion section will operate in the bubbling bed regime with allowance for both primary and secondary combustion air. Heat can be removed from the combustion stage of the carbonator-combustor to allow production of high quality steam. Sulphur removal is possible using partially spent sorbent through the reaction:

$$CaO + \tfrac{1}{2}O_2 + SO_2 \Leftrightarrow CaSO_4 \qquad 5.2$$

The carbonation section will operate in the bubbling bed regime. Heat removal is possible in the carbonating stage to control the reaction temperature for reaction 5.1. A gas distribution plate separates the combustion stage from the carbonating stage.

The carbonating combustor is designed such that it can also operate as a single-stage circulating fluidized bed combustor with CO_2 removal. This mode of operation is not expected to result in optimum long-term cyclic conversion of the sorbent; however, it may be of interest for commercial retrofit purposes. The sorbent is transported to the regenerator using regenerator product gas, composed primarily of CO_2, air or steam.

The reactor is made up of four sections to allow flexible operation of the system. The bottom two sections are made of stainless steel to allow direct contact heating of process gas through the reactor shell. The bottom section is heated using four 1 kW ceramic band heaters to minimize the heat loss effects in the pilot-scale unit. The top two sections are made of carbon steel where operating temperatures are reduced. The top three sections have both insulation and refractory to minimize

heat loss to the environment. The inner diameter of the reactor is 0.1 m in both the combustion and carbonating sections.

5.3.5 Modelling Procedure

Process simulation using ASPEN Plus has been used to establish the mass and energy balances of interest for equipment selection and design. A high-level view of the simulation can be seen in

Figure 5.2Figure 5.2. Combustion, carbonation, calcination and sulphation are simulated using combinations of the RYIELD (yield) and REQUIL (minimize Gibbs free energy) reactor blocks. Sorbent degradation and fluidization requirements are determined using an Excel calculation block within ASPEN Plus. This ASPEN Plus simulation is equilibrium based and therefore does not account for mass transfer and reaction rate limitations within the reactors.

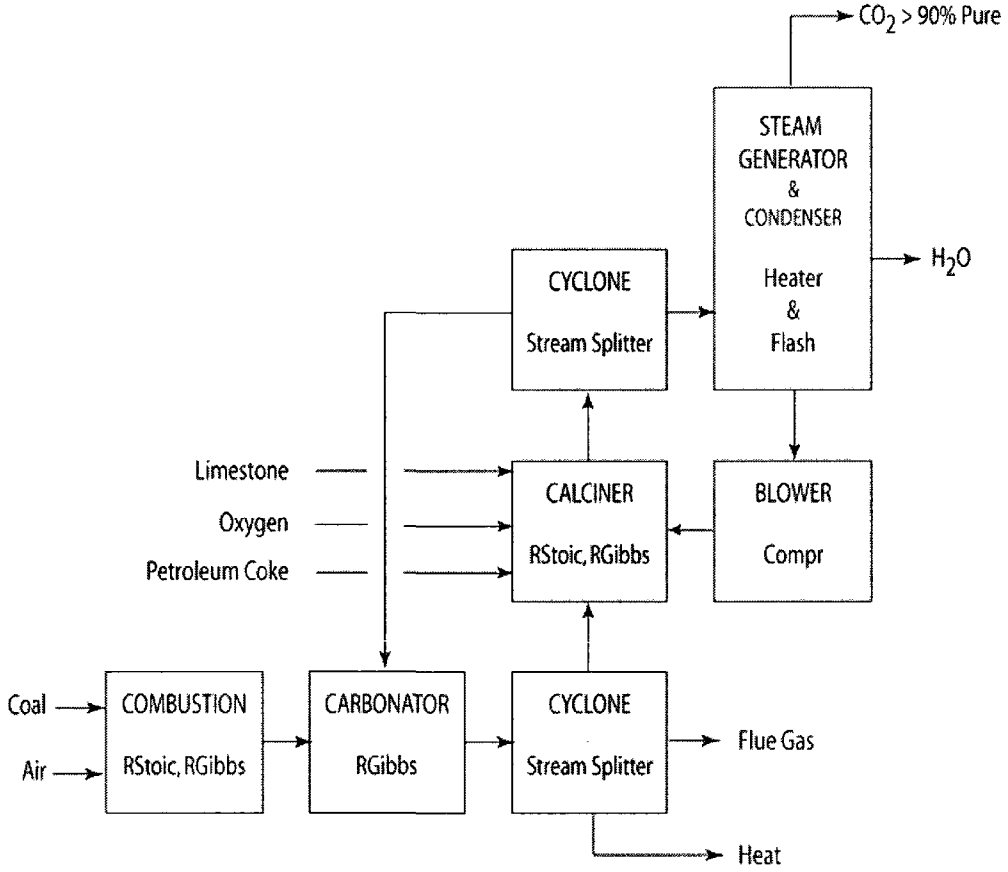

Figure 5.2. Flow Sheet for ASPEN Plus Simulation of Dual Fluidized Bed Combustion System with CO_2 Capture - Regenerator Flue Gas Recycle Mode.

5.3.6 Carbonator

In simulating combustion in the bottom stage of the carbonator, coal is first decomposed to generate its elemental components using a yield-basis reactor block. These species, with a stream representing the heat of decomposition, are then passed to a Gibbs reactor block with combustion air. The Gibbs reactor block minimizes the Gibbs free energy to arrive at the equilibrium composition of the identified combustion products at the temperature specified for reaction (typically 850°C). Heat removal from the combustion section is simulated by a heat exchanger block to meet the specified reactor temperature. The combustion air rate is automatically modified to give the desired excess oxygen in the simulation. In one simulation case, partially spent sorbent is fed to the combustion stage to remove sulphur prior to the carbonation stage in order to reduce sorbent deactivation.

The second stage of the carbonator is represented by a second Gibbs reactor block where the products of combustion and the activated sorbent are combined. The reaction temperature is specified. Heat is removed from the second stage of the carbonator using a heat exchange block in order to meet the specified reactor block temperature. The degree of conversion of calcium oxide to calcium carbonate is limited to represent the average conversion of sorbent based on thermogravimetric analyses (TGA) performed at CETC-Ottawa.

5.3.7 Regenerator

In the regenerator, petroleum coke is decomposed using a yield reactor block, as in the carbonator. Calcination of sorbent and combustion occur simultaneously in a Gibbs reactor block at a specified temperature. The temperature of the reactor is controlled by balancing the heat required for calcination with the heat of combustion. The balance is accomplished by varying the rate of petroleum coke fed to the regenerator. The desired excess oxygen concentration in the flue gas is obtained by varying the oxygen feed rate to the regenerator. The flue gas recycle rate or steam rate is varied to obtain appropriate gas velocities in the regenerator for fluidization and to obtain sufficient gas moderator concentrations to reduce the occurrence of hot spots in the combustion zone.

5.4 Results and Discussion

5.4.1 Preliminary Fluid Bed Results

Preliminary investigations using the existing CETC-Ottawa mini-fluidized bed combustor indicated that varying operating conditions and limestone sorbents can result in a range of sorbent conversions. In general, the sorbent conversion can be estimated using the model proposed by Abanades and Alvarez (2003 (b))

$$X_N = f_m^N (1 - f_W) + f_W \qquad 5.3$$

where X_N is the maximum carbonation conversion obtained after N cycles for a predetermined carbonation time (often reported at 20 minutes for TGA studies). Parameter values of f_m = 0.77 and f_W = 0.17 for this model have been shown to fit data for unmodified limestone sorbents quite well. This model indicates that conversion is reduced to ~0.17 after 20 carbonation-calcination cycles. Batch experiments in the mini-fluidized bed combustor operated in the bubbling regime give conversions similar to those reported for TGA studies under many conditions (Salvador *et al.*, 2003). Limestone type, CO_2 concentration, and operating temperature can each affect conversion.

Recent pore modification studies (Hughes *et al.*, 2004) at CETC-O indicate that conversion can be greatly increased by a simple treatment step prior to sorbent injection into the carbonator. Conversion as high as 52% after 20 cycles (20-minute carbonation) can be obtained in a TGA using Kelly Rock limestone derived sorbent. Conversions as high as 59% after 20 cycles (20-minute carbonation) are predicted through extrapolation of tests with the number of cycles limited to four using Cadomin limestone derived sorbent.

5.4.2 Simulation Results

The ASPEN Plus simulation has provided the required process parameters for construction of the dual fluidized bed combustion system to operate in both a regenerator flue gas recycle mode and a steam-stripping mode. In both modes, the carbon dioxide concentration in the calciner product gas stream was greater than 96 mol%, dry basis. The balance of gas in the CO_2 product gas stream is composed of nitrogen from the oxygen plant (assumed 97% pure oxygen) and excess oxygen required

for regenerator combustion (~3% excess O_2). The carbon dioxide concentration in the carbonator-combustor flue gas was 5 mol%.

The conversion specified for carbonation in the carbon dioxide recycle mode is 0.4. The steam-stripping option has been simulated for two levels of CaO conversion in the carbonator; 0.4 and 0.6. The conversion of 0.6 has been selected based on the best-projected conversion for a modified limestone sorbent as determined by thermogravimetric analysis (Hughes *et al.*, 2004) as mentioned above.

Key results of the simulations are given in Table 5-1. It can be seen that the purified oxygen requirement for this combustion process is in the order of 1/3 of that required for oxy-fuel combustion. The oxygen requirement for the steam-stripping mode is somewhat higher than that for the regenerator recycle mode since a portion of the process heat is lost in producing and condensing process steam. The solids transfer rate is a strong function of the conversion of calcium oxide to calcium carbonate. In the commercial case, reducing the transfer of solids will minimize attrition losses and result in reduced fresh sorbent make-up requirements.

Table 5-1. Selected Results from an ASPEN Plus Simulation of the Dual Fluidized Bed System for Carbon Dioxide Removal for Regenerator Flue Gas Recycle and Stream-stripping Modes.

Parameter	Regen. Recycle X = 0.4	Steam Stripping X = 0.4	Steam Stripping X = 0.6
Purified oxygen requirement compared to oxy-fuel combustion	0.29	0.35	0.35
Relative solids transfer rate	1	1.02	0.57
Relative heat requirements for calcination	1.00	1.33	1.39
Relative heat of combustion in carbonator *versus* regenerator	2.52	2.27	2.35

The heat requirement for calcination in the regenerator is significantly higher in the steam-stripping mode. The increased heat requirement is due to steam production needs. The steam-stripping mode

will require additional process equipment including condenser, condensate pump, and steam generator. The carbon dioxide recycle case will require a blower in place of the condensate pump.

The heat supplied by combustion in the carbonator-combustor is between 2.3 and 2.5 times the heat supplied by combustion in the regenerator. For a given operating mode, maximizing the relative heat of combustion in the carbonator will minimize operating costs by reducing fresh sorbent requirements due to sorbent deactivation by sulphation and by reducing purified oxygen requirements. With this in mind, it would appear that the regenerator flue gas recycle mode might be more cost effective than the steam-stripping mode even if conversion is greatly enhanced in the steam-stripping mode. However, practical considerations such as cost of materials for operation at higher temperatures, solids attrition due to material transfer, and a greater spread in conversions between the two modes may prove steam stripping an economic choice.

5.5 Conclusions

A flexible atmospheric dual fluidized bed combustion system using high-temperature sorbents for *in situ* CO_2 capture has been designed and constructed. The ASPEN Plus process simulations developed for the design of the mini-pilot plant (being constructed at CETC-Ottawa) will be used for scale-up studies and process verification of commercial-scale simulations based on the results of pilot plant operation. The process simulation shows that the flow rate of oxygen is one-third of that required for an oxy-fuel system with an equivalent heat rate. The pilot plant is expected to combust coal and petroleum coke in a clean and efficient manner, emitting a flue gas containing 2-5 mol% CO_2, while producing a relatively pure carbon dioxide stream ready for compression. The concentration of sulphur dioxide in the flue gas is expected to be on the order of a few parts per million by volume.

5.6 References

Anthony, E.J. and Wang, J., (2003). 'Capturing CO_2 in Coal-Fired Combustors using CaO Based Sorbents', Proceedings of the Fifth International Symposium on Coal Combustion, 20-25.

Abanades, J.C., Alvarez, D., Anthony, E.J., and Lu, D., (2003). 'In-situ Capture of CO_2 in a Fluidized Bed Combustor', Proceedings of the 17th FBC Conference, ASME, Jacksonville, Florida.

Abanades, J.C., Alvarez, D., (2003). 'The Conversion Limits in the Reaction of CO_2 with Lime', Energy and Fuels 17, 308–315.

Abanades, J.C., Anthony, E.J., Alvarez, D., Lu, D.Y. and Salvador, C., (2004). 'Capture of CO_2 in a FBC of CaO', AIChE J. 50, 1614-1622.

Baker, E.H., (1962). 'The Calcium Oxide-Carbon Dioxide System in the Pressure Range 1-300 Atmospheres', J. Chem. Soc. 70, 464–470.

Dobner, S., Sterns, L., Graff, R.A., and Squires, A.M., (1977). 'Cyclic Calcination and Recarbonation of Calcined Dolomite', Ind. Eng. Chem. Process Des. Dev. 16(4), 479-486.

Grace, J.R., Avidan, A.A., and Knowlton, T.M. (eds.), (1997). 'Circulating Fluidized Beds', Blackie Academic and Professional, London.

Gupta, H.; Iyer, M.; Sakadjian, B.; and L.S. Fan , (2002). 'CO_2 Separation from Flue Gas by the Carbonation and Calcination of Metal Oxides', Ohio Coal Research Consortium, Project Report C2.11, www.ohiocoal.org/projects/.

Gupta, M., Coyle, I., Thambimuthu, K., (2003). 'CO_2 Capture Technologies and Opportunities in Canada', 1st Canadian CC&S Technology Roadmap Workshop, Calgary, Alberta, Canada.

Harrison, R.M. (ed.), (1992). 'Understanding our Environment: An Introduction to Environmental Chemistry and Pollution', Royal Society of Chemistry.

Hughes, R.W., Lu, D., Anthony, E.J., and Wu, Y., (2004). 'Improved Long-term Capacity of a Limestone Derived Sorbent For In Situ Capture of CO_2 in a Fluidized Bed Combustor', Ind. Eng. Chem. Res. 43, 5529.

Salvador, C., Lu, D., Anthony, E.J., and Abanades, J.C., (2003). 'Enhancement of CaO for CO_2 capture in an FBC environment', Chemical Engineering Journal 96, 187.

Shimizu, T., Hirama, T., Hosoda, H., Kitano, K., Inagaki, M., and Tejima, K., (1999). 'A Twin Fluid-bed Reactor for Removal of CO_2 from Combustion Processes', Trans IChemE 77, 62.

Wang, J., Anthony, E.J., and Abanades, J.C., (2003). 'A Simulation Study for Fluidized Bed Combustion of Petroleum Coke with CO2 Capture', Proceedings of the 17th FBC Conference, ASME, Jacksonville, Florida.

White, C.M., Strazisar, B.R., Granite, E.J., Hoffman, J.S., Pennline, H.W., (2003), 'Separation and Capture of CO_2 from Large Stationary Sources and Sequestration in Geological Formations-Coalbeds and Deep Saline Aquifers', Journal of the Air & Waste Management Association 53, 645.

Chapter 6 Oxy-Fuel Combustion of Coal in a Circulating Fluidized Bed Combustor

Published in the Proceedings of the 19th International Conference on Fluidized Bed Combustion

Hughes, R.W.[1], Jia, L.[1], Tan, Y.[1], Anthony, E.J.[1], Macchi, A.[2], (2006). 'Oxy-Fuel Combustion of Coal in a Circulating Fluidized Bed Combustor', Proc. of 19th International Conference on Fluidized Bed Combustion, ASME.

[1]Natural Resources Canada, CETC-O, 1 Haanel Drive, Ottawa, Canada K1A 1M1

[2]University of Ottawa, 161 Louis Pasteur, Ottawa, Canada, K1N 6N5

6.1 Abstract

A new pilot facility for oxygen blown circulating fluidized bed combustion is described (combustor 0.1 m ID). The facility has been operated with an inert bed (silica sand) at a variety of O_2:CO_2 ratios while co-firing coal and biomass. Preliminary experimental results are reported including analyses of flue gas, temperature profiles, and general observations. The ratio of oxygen to carbon dioxide flow rate has been varied to establish the effects of this ratio on product gas composition and combustor operation. A low primary gas ratio has been used to achieve low NO_X emissions. Increasing the temperature of combustion for oxy-fuel combustion has resulted in similar CO emissions in both air blown CFBC and an oxy-fuel combustion test with 40 vol% oxygen injected at the distributor.

6.2 Introduction

Carbon dioxide can be separated from combustion flue gases and sequestered in geological formations in order to reduce the effects of fossil fuel power generation systems on global warming. A wide range of technologies are available to perform the capture, however, all existing commercial methods are expected to substantially increase the cost of electrical power production. A number of technologies are under investigation that may be able to produce a nearly pure stream of CO_2 at a lower cost; amongst these is oxy-fuel combustion.

Oxy-fuel combustion pilot scale studies have primarily focused on pulverized coal combustion (Chatel-Lepage et al., 2003; Croiset and Thambimuthu, 1999; Kimura et al., 1995; Wang et al, 1988; Weller et al., 1985; Woycenko et al., 1994; Woycenko et al., 1998). The studies have shown that there is no technical barrier prohibiting the construction of oxy-fuel pulverized coal (PC) combustors. The results of these studies as well as others have been summarized (Buhre et al., 2005) with reference given to some operational concerns including ignition and flame stability, and reduced net electrical power efficiency (~9 percentage points).

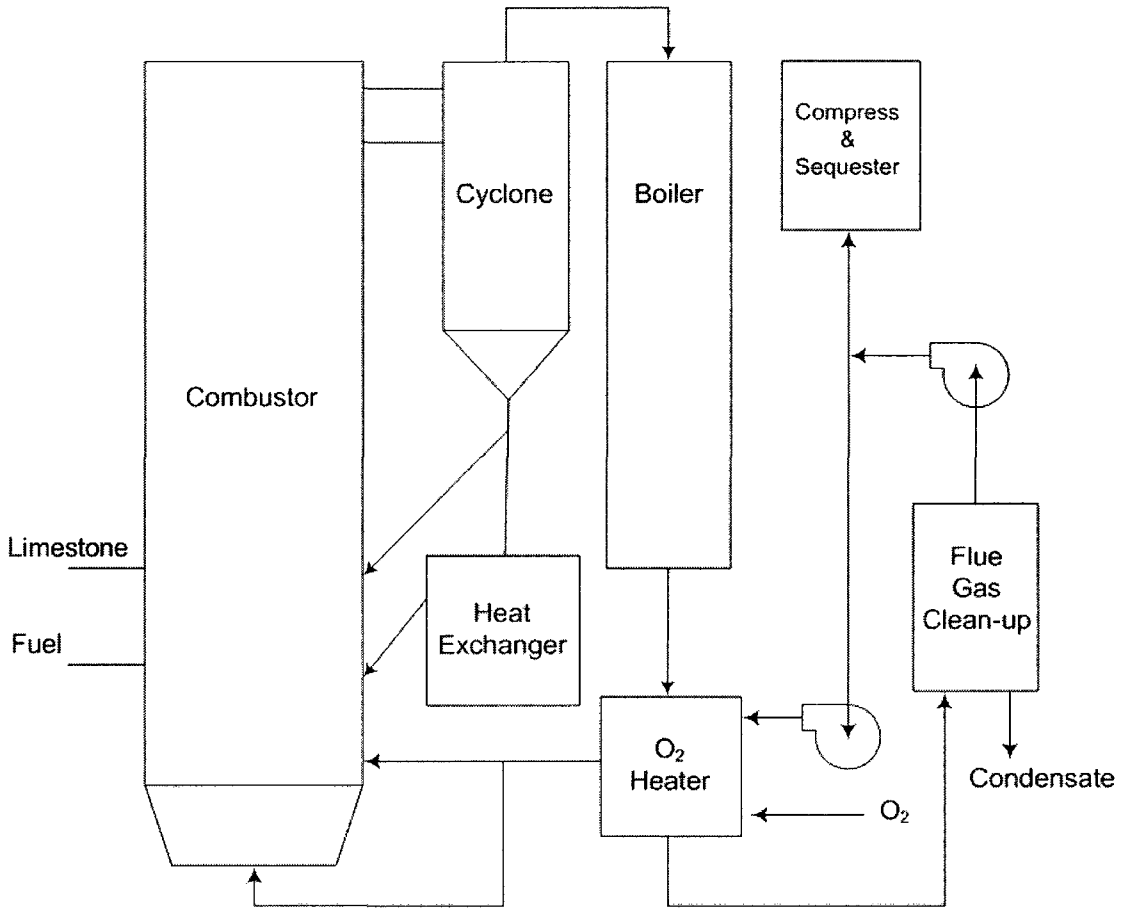

Figure 6.1. Process flow diagram of an oxy-fuel circulating fluidized bed combustor

Circulating fluidized bed combustion (CFBC) is a technology that could be used for oxy-fuel combustion (Figure 6.1). CFBC has benefits as compared to PC for oxy-fuel combustion that may make it a better choice for CO_2 capture in some cases. CFBC uses a high velocity fluidizing gas to entrain coal particles and maintain a fluidized bed of coal, ash, sulphur sorbent, and sometimes sand. The bed material acts as a heat reservoir, capturing excess heat and providing the heat needed for drying, devolatilization and ignition of the fuel. The turbulent nature of the lower combustion zone results in good solids mixing and gas-solid interaction. Heat transfer rates are high within the CFBC; the overall heat transfer coefficient in the bed is typically in the range of 200 – 500 W / m^2-K (Wu, 2004). The large area available for heat transfer (bed material surface area of 3000-45000 m^2/m^3)

allows very large quantities of heat to be exchanged (Oka, 2004). The fluidizing gas carries particles of bed material including coal, ash and sorbent through the combustion chamber and into a cyclone where the majority of the particles are separated. The particles are directed back to the combustion chamber through a return leg that may include a heat exchanger for extracting heat from the particles for steam production. The large heat capacity of return leg solids and the degree of cooling of those solids results in the ability of the CFBC to maintain a nearly constant bed temperature allowing fluidization with oxygen concentrations as high as 70 mol% (Marion et al., 2003). The high allowable oxygen concentration could enable oxy-fuel CFBC units to operate with low recycle flue gas rates. In comparison, PC oxy-fuel combustors must operate at relatively high recycle flue gas rates. The benefit of higher allowable oxygen concentrations can be quantified by comparing the ratios of the required recycle gas flow rates at various oxygen concentrations. Performing a simple mass balance for the combustor (Figure 6.2), for a constant coal flow rate, the recycle flow rate, R, for a given oxygen process configuration, *i*, can be determined given an oxygen concentration, $x_{O2,i}$, and fluidizing gas volumetric flow rate, $F_{C,i}$:

$$R_i = \left(1 - x_{O_2,i}\right) F_{C,i} \qquad 6.1$$

The oxygen volumetric flow rate, F_{O2}, entering the plant can be assumed constant and can be determined by:

$$F_{O_2,i} = x_{O_2,1} F_{C,1} = x_{O_2,2} F_{C,2} \qquad 6.2$$

where two configurations are considered. Taking the ratio of recycle gas flow rates for two processes and substituting equation 6.1 into equation 6.2:

$$\frac{R_1}{R_2} = \frac{\left(1 - x_{O_2,1}\right) x_{O_2,2}}{\left(1 - x_{O_2,2}\right) x_{O_2,1}} \qquad 6.3$$

From this relationship it can be seen that a system allowing 35% O_2 in the feed gas (CANMET oxy-fuel PC combustor (Douglas et al., 2001) will have 1.9 times greater recycle gas volumetric flow rate than a system allowing 50% O_2 in the feed gas (Alstom MTF oxy-fuel CFBC – (Nsakala et al., 2004)) and will have 4.3 times greater recycle gas volumetric flow rate than a system allowing 70% O_2 in the feed gas (suggested upper limit for oxy-fuel CFBC – (Jukkola et al., 2005). The reduced recycle gas flow rates could result in a significant reduction in capital and operating costs for the recycle gas systems for oxy-fuel CFBCs when compared to oxy-fuel PC.

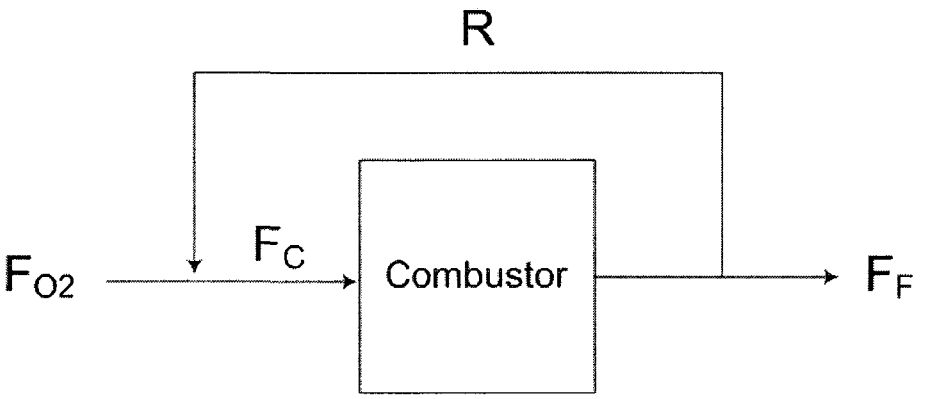

Figure 6.2. Simple mass balance around combustor with recycled flue gas

CFBCs have the benefit of being able to burn a wide variety of materials. They are able to efficiently burn biomass materials such as wood and municipal solid waste. When burning these materials and sequestering the CO_2 that is produced, oxy-fuel CFB combustors can effectively remove CO_2 from the atmosphere (net basis). CFBCs can co-fire coal and biomass to achieve improved combustion performance and economics.

6.3 Experimental Method

A pilot facility has been constructed for the demonstration and evaluation of CO_2 capture processes involving various technologies involving fluidized beds. The technologies under evaluation include oxy-fuel CFBC as well as both high (CaO-$CaCO_3$) and low (Na_2CO_3-$NaHCO_3$) temperature CaO-$CaCO_3$ looping cycles. The pilot facility includes two fluidized bed combustors where solids transfer

between the beds is possible; a circulating fluidized bed combustor and a multi-stage bubbling fluidized bed combustor.

The CFBC has been designed to allow fluidization with air, steam, O_2 and CO_2, and O_2 and recycled flue gas. It contains a 0.1 m ID stainless steel riser 5m in height (Figure 6.3) covered with 0.1m of insulation. Oxygen and additional fluidizing gas are pre-mixed prior to entering the wind box. The fluidizing gas is distributed using 18 nozzles extending 0.01 m above the distributor plate. The CFBC is equipped with external electric heaters and a natural gas burner for pre-heating. Independent feed augers can supply multiple fuel types and a sorbent. Oxygen, CO_2, and recycle flue gas flow rates are controlled by a combination of mass flow controllers and rotameters. System control and data acquisition is performed by Labview via a FieldPoint instrument interface. The recycle flue gas system includes bag house, condenser, condensate knockout, and recycle gas blower. Gas analysis includes O_2, CO (Hi - Horiba PIR-2000, Lo – Horiba VIA-510), CO_2 (Horiba VIA-510), NO_X (Thermatron 42C NO-NO2-NOx analyzer) and multi-species analysis via ABB Bomem MB series FT-IR.

Commissioning tests have been performed to evaluate the operability and performance of the CFBC with elevated oxygen concentrations in the fluidizing gas. The tests were carried out using O_2 and CO_2 from compressed gas tanks and an inert bed material (silica sand with mean Sauter diameter 454 micron).

Combustion tests were completed using an eastern bituminous coal and wood pellets with analyses given in Table 6-1 . Six of the tests were executed with a fluidizing gas stream of oxygen and carbon dioxide with oxygen concentration ranging from 17% to 40%. Two tests were operated with air as the fluidizing gas for comparison. The net oxygen concentration of gases entering the combustor, with dilution due to CO_2, at injection points including return leg and feed port, was varied between 13% and 24%. Test parameters are outlined in Table 6.2. Secondary oxidant injection occurred at the same elevation as the return leg and feed injection point at a height of 1.25m (labelled 'secondary gas' in Figure 6.3). The secondary oxidant was injected through a 4.6 mm tube terminating at the combustor wall. The return leg was cooled using a water-cooled copper tube wrapped around the return leg at the L-valve.

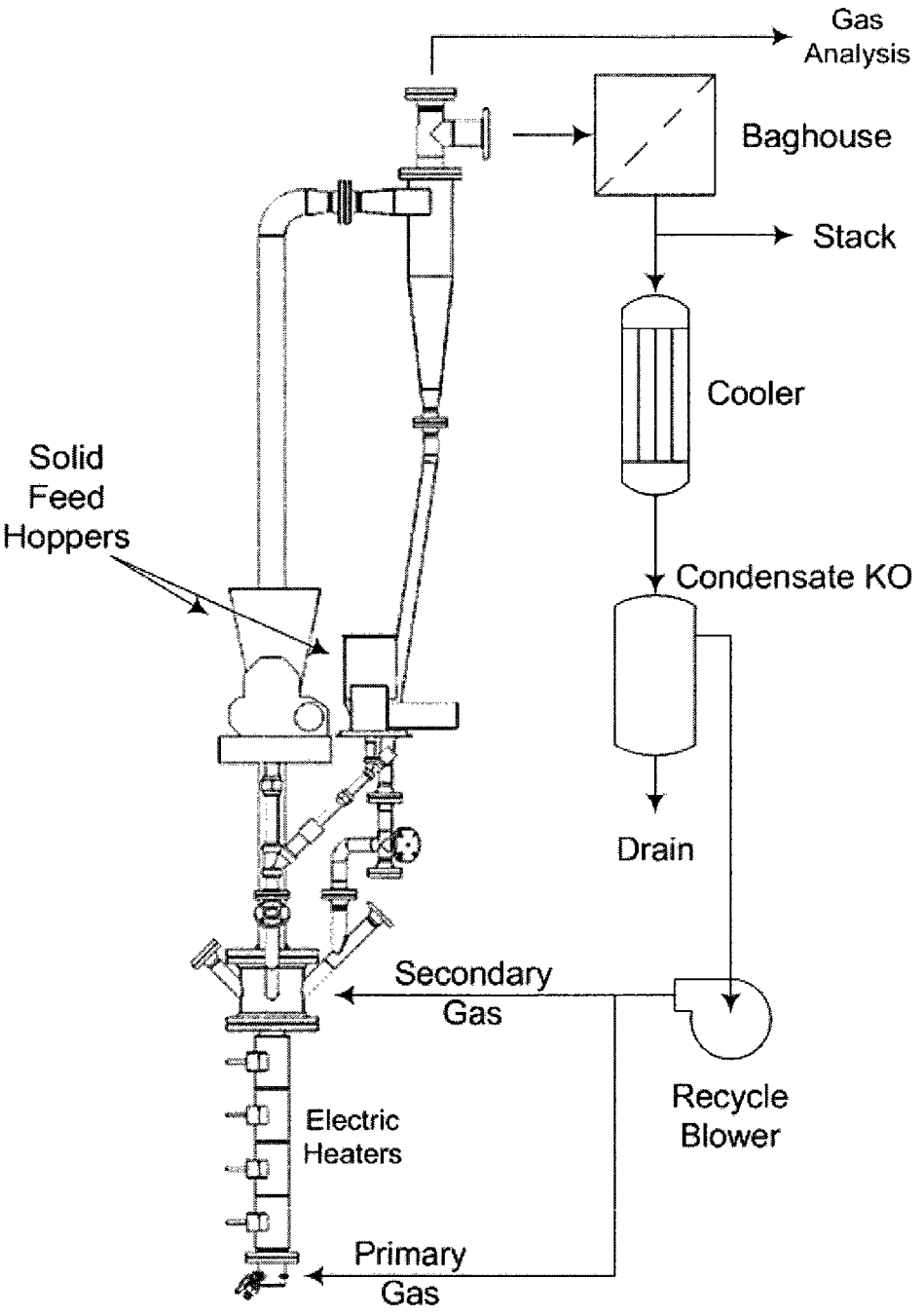

Figure 6.3. 75 kWth oxy-fuel CFBC pilot plant

Table 6-1. Eastern bituminous coal and wood pellet analyses

Proximate Analysis	EB Coal	Pellets
ASH, wt%	8.66	0.42
VOLATILES, wt%	35.78	84.67
FIXED CARBON, wt%	55.56	14.91
Ultimate Analysis		
CARBON, wt%	77.81	49.58
HYDROGEN, wt%	5.05	5.91
NITROGEN, wt%	1.49	0.14
SULFUR, wt%	0.98	<0.03
OXYGEN, wt%	6.04	43.92
HHV, MJ/kg	32.51	19.63
MOISTURE, wt%	1.08	<4%
MEAN DIAMETER, micron	842	Unknown

Table 6-2. Oxy-fuel CFBC operating parameters

	Primary Fluidizing Gas	Test ID	O_2 Conc. To Windbox	Global O_2 Conc.	Primary Gas Ratio	Velocity Dense Bed	Velocity Riser
			vol%	vol%		m/s	m/s
Fuel: EB coal							
	Air	OF-1	21%	21%	0.93	1.3	1.4
	19% O_2 / CO_2	OF-2	19%	13%	0.55	1.0	1.4
	24% O_2 / CO_2	OF-3	23%	17%	0.76	1.2	1.4
Fuel: 13% biomass by heating value (25% by mass), balance EB coal							
	Air	OF-4	21%	21%	0.62	0.8	1.3
	17% O_2 / CO_2	OF-5	17%	13%	0.64	1.6	2.1
	32% O_2 / CO_2	OF-6	32%	21%	0.81	1.1	1.6
	35% O_2 / CO_2	OF-7	35%	23%	0.81	1.0	1.6
	40% O_2 / CO_2	OF-8	40%	24%	0.81	0.9	1.4

6.4 Results and Discussion

The oxy-fuel CFBC operated smoothly for all operating conditions tested. The temperature profile in the lower bed region at the center axis remained nearly constant for all test conditions (Figure 6.4). The average bed temperature increased by ~ 60 °C (Figure 6.5) while operating with 40% oxygen injected through the distributor. It is believed that the increase in bed temperature is partially due to a reduction in dense bed superficial gas velocity as indicated in

Table 6-2Table 6.2 because of the operating philosophy for this series of tests. The fluidizing gas entering the bed was maintained at 55 ± 10 °C. There was no evidence of significant bed agglomeration i.e. no clinker was generated.

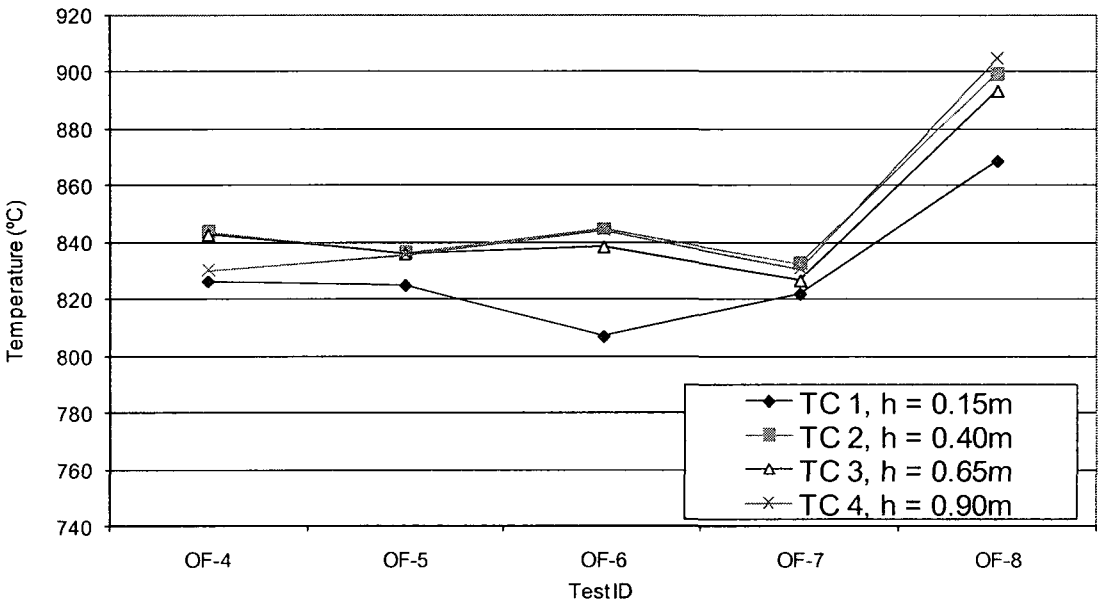

Figure 6.4. Oxy-fuel dense bed temperature profile

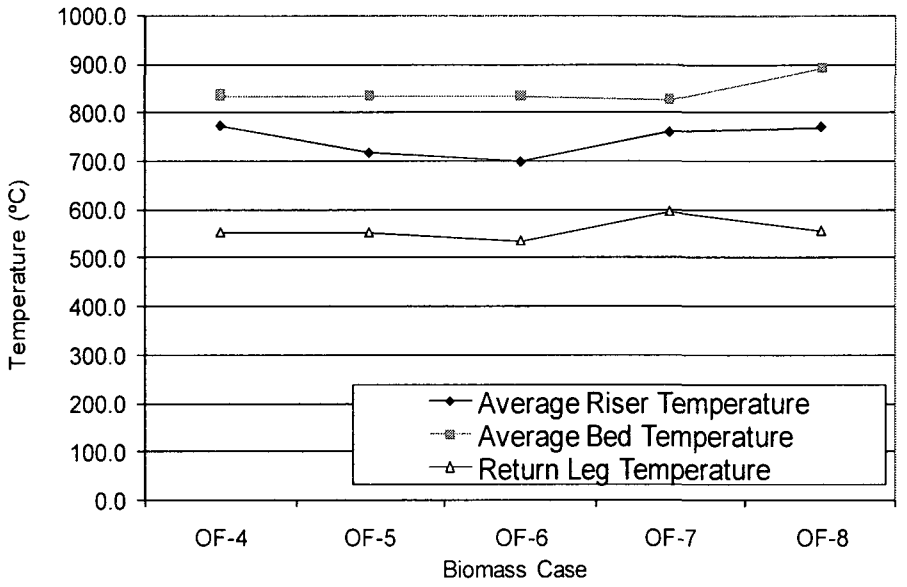

Figure 6.5. Average temperatures of dense bed, upper riser, and return leg

6.4.1 NO_X Emissions

The flue gases were analyzed for NO_X and the result has been converted to an equivalent NO_X concentration for a flue gas O_2 concentration of 3% taking into account the various oxygen sources. The NO_X concentrations can be seen in Figure 6.6 for each of the test cases. The relationship between flue gas O_2 concentration and NO_X emissions is presented in Figure 6.7. Test case OF-2 shows a very low NO_X level of 53 ppm @ 3% O_2. The low level of NO_X is a result of the low O_2 concentration in the flue gas, but also, is likely due to the reducing conditions established in the lower bed with a primary gas ratio of 0.55. A similar effect in reducing NO_X emissions has been seen by (Lyngfelt et al., 1998) while operating CFBC with low combustor air ratios. Under these conditions both NO and N_2O were reduced at the expense of increased CO emissions. To counteract the increased CO emissions it was suggested that the combustion temperature could be increased. The increased combustor temperature may result in higher SO_2 emissions. In the case of oxy-fuel CFBC the combustor may need to be operated at higher temperatures (870 – 890 °C) to allow the calcination of limestone under high CO_2 partial pressures (Nsakala et al., 2004). At the temperatures required for

calcination, subsequent SO_2 removal may be necessary and it may be beneficial to operate with a lower primary gas ratio to reduce NO_X and N_2O emissions.

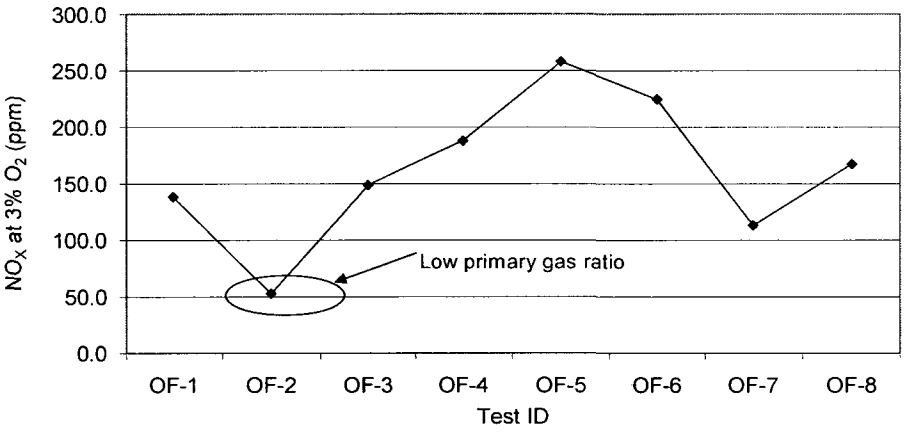

Figure 6.6. NO_X emissions for the test cases

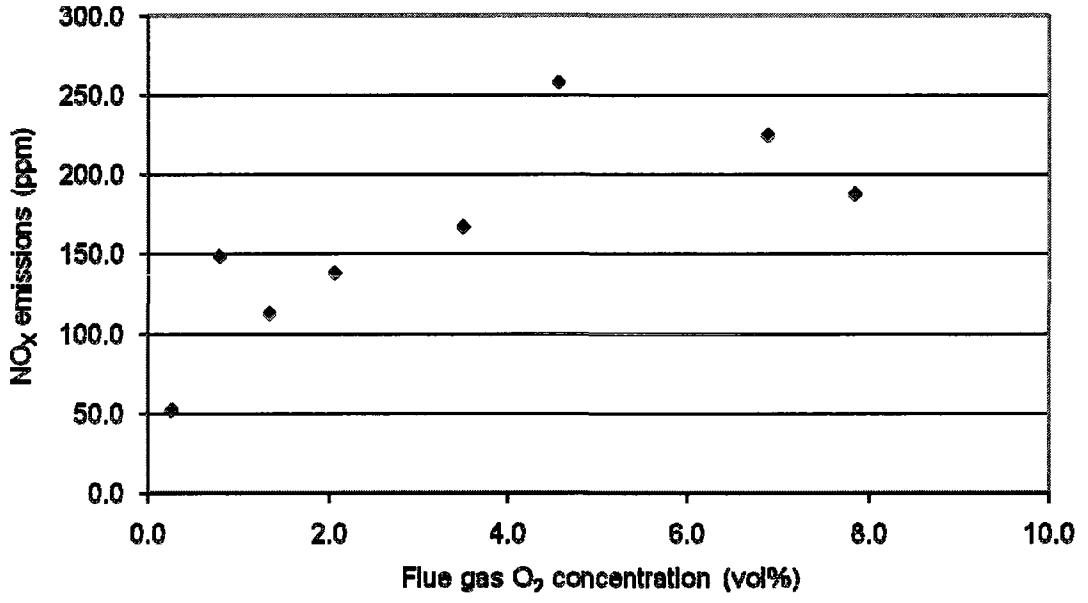

Figure 6.7. NO_X emissions for various flue gas O_2 concentrations

6.4.2 CO emissions

The CO emissions were elevated during the oxy-fuel tests as can be seen in Figure 6.8Figure 6.8. A similar effect of elevated CO emissions has been seen by various researchers in oxy-fuel combustors when CO_2 concentration is high (Douglas et al., 2001; Nsakala et al., 2004). It can be seen in Figure 6.8 that by operating the bed at 891 °C, i.e. 60 °C above the temperature for test OF-4, the CO emissions are similar to those in the air blown case for a flue gas CO_2 concentration of nearly 70 vol%.

Upon inspecting the spectral analysis from the ABB Bomem FT-IR, it was noted that there may be an overlap in the signals between the CO_2 spectra and the CO spectra when CO_2 concentrations are high as is the case in oxy-fuel CFBC. This could potentially result in recording higher CO emissions than are actually present in the flue gas when using infrared CO analyzers. It would be prudent to quantify the effects of this interference when analyzing CO emissions from CO_2 capture systems.

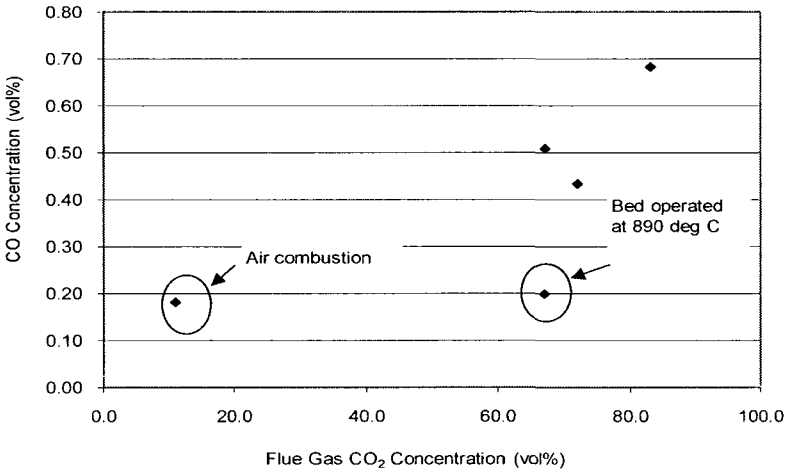

Figure 6.8. CO concentration with respect to flue gas CO_2 concentration for pellet-coal tests

6.5 Conclusions

A 0.1 m circulating fluidized bed combustor was operated with oxygen concentrations as high as 40% at the wind box while co-firing biomass and an eastern bituminous coal. The combustor operated in a stable and predictable manner with no evidence of significant bed agglomeration. The combustor achieved a low NO_X emission rate of 53 ppm while operating with a low primary gas ratio of 0.55. CO emissions were comparable for both air blown and O_2/CO_2 blown cases.

6.6 Nomenclature

R_i	Recycle gas volumetric flow rate
$x_{O2,I}$	O_2 volume fraction
$F_{C,I}$	Combustion gas volumetric flow rate
$F_{O2,I}$	Pure O_2 volumetric flow rate
h	Height above the gas distributor

6.7 Literature

Buhre B.J.P., Elliot, L.K., Sheng, C.D., Gupta, R.P., Wall, T.F., (2005). 'Oxy-fuel Combustion Technology for Coal-Fired Power Generation', Progress in Energy and Combustion Science 31, 283-307.

Chatel-Pelage F, Marin O, Perrin N, Carty R, Philo GR, Farzan H., (2003). 'A pilot-scale demonstration of oxy-combustion with flue gas recirculation in a pulverized coal-fire boiler', 28th International Conference on Coal Utilization & Fuel Systems, Clearwater, Florida.

Croiset E, Thambimuthu KV., (1999). 'Coal combustion with flue gas recirculation for CO_2 recovery', In: Riemer P, Eliasson B, Wokaun A, editors. Greenhouse gas technologies. Amsterdam, Elsevier Science, 581-586.

Douglas, M., Chui, E., Tan, Y., Lee, G., Croiset, E., Thambimuthu, K., (2001). 'Oxy-fuel combustion at the CANMET vertical combustor research facility', Proceedings of the 1st National Conference on Carbon Sequestration, NETL, DOE, May 14-17, Washington D.C.

Jukkola, G., Liljedahl, G., Nsakala, N., Morin, J.X., Andrus, H., (2005). 'An Alstom vision of future CFB technology based power plant concepts', Proceedings of the 18th International Conference on Fluidized Bed Combustion, Toronto, Canada.

Kimura K, Omata K, Kiga T, Takano S, Shikisima S., (1995). 'Characteristics of pulverized coal combustion in O_2/CO_2 mixtures for CO_2 recovery', Energy Convers. Management 36, 805-808.

Lyngfelt, A., Amand, L.E., Leckner, B., (1998). 'Reversed air staging – a method for reduction of N_2O emissions from fluidized bed combustion of coal', Fuel 77(9/10), 953-959.

Marion, J.L., Bozzuto, C.R., Andrus, H.E., Chamberland, R.P., (2003). 'Greenhouse Gas Emissions Control by Oxygen Firing in Circulating Fluidized Bed Boilers: Phase 1 – A Preliminary Systems Evaluation', PPL Report No. PPL-03-CT-09

Nsakala, N., Liljedahl, G., Turek, D., (2004). 'Greenhouse gas emissions control by oxygen firing in circulating fluidized bed boilers: Phase II – Pilot scale testing and updated performance and economics for oxygen fired CFB with CO_2 capture', PPL report No. PPL-04-CT-25.

Oka, S., (2004). 'Fluidized Bed Combustion', Marcel Dekker.

Wang CS, Berry GF, Chang KC, Wolsky AM., (1988). 'Combustion of pulverized coal using waste carbon dioxide and oxygen', Combust Flame 72, 310-310.

Weller, A.E., Rising, B.W., Boiarski, A.A., Nordstrom, R.J., Barrett, R.E., Luce, R.G., (1985). 'Experimental Evaluation of Firing Pulverised Coal in a CO_2/O_2 Atmosphere', Argonne National Laborator Report No.: ANL/CNSV-TM-168.

Woycenko. D. M., Ikeda, I. and van de Kamp W. L., (1994). 'Combustion of Pulverized Coal in a Mixture of Oxygen and Recycled flue Gas', IFRF Document No. F98/y/1.

Woycenko D.M., van de Kamp W.L., Roberts P.A., (1998). 'Combustion of pulverized coal in a mixture of oxygen and recycled flue gas', Summary of the APG research program 1995 [JOU2-CT92-0093, IFRF Doc F98/Y/4].

Wu, Z., (2004). 'Understanding Fluidised Bed Combustion', IEA Clean Coal Centre, Report CCC/76.

Chapter 7 Ca-Based Sorbent Looping Combustion for CO_2 Capture in Pilot-Scale Dual Fluidized Beds

Published in Fuel Processing Technology

Lu., D.[1], Hughes, R.[1], Anthony, E.J.[1], (2008). 'Ca-Based Sorbent Looping Combustion for CO_2 Capture in Pilot-Scale Dual Fluidized Beds', Fuel Proc. Tech. 89(12), 1386-1395.

[1]Natural Resources Canada, CETC-O, 1 Haanel Drive, Ottawa, Canada K1A 1M1

7.1 Abstract

To demonstrate process feasibility of *in situ* CO_2 capture from combustion of fossil fuels using Ca-based sorbent looping technology, a flexible atmospheric dual fluidized bed combustion system has been constructed. Both reactors have an ID of 100 mm and can be operated at up to 1000 °C at atmospheric pressure. This paper presents preliminary results for a variety of operating conditions, including sorbent looping rate, flue gas stream volume, CaO/CO_2 ratio and combustion mode for supplying heat to the sorbent regenerator, including oxy-fuel combustion of biomass and coal with flue gas recirculation to achieve high-concentration CO_2 in the off-gas. It is the authors' belief that this study is the first demonstration of this technology using a pilot-scale dual fluidized bed system, with continuous sorbent looping for *in situ* CO_2 capture, albeit at atmospheric pressure. A multicycle test was conducted and a high CO_2 capture efficiency (~90%) was achieved for the first several cycles, which decreased to a still acceptable level (~75%) even after more than 25 cycles. The cyclic sorbent was sampled on-line and showed general agreement with the features observed using a lab-scale thermogravimetric analysis (TGA) apparatus. CO_2 capture efficiency decreased with increasing number of sorbent looping cycles as expected, and sorbent attrition was found to be another significant factor to be limiting sorbent performance.

Keywords: CO_2 capture, Sorbent looping technology, Oxy-fuel combustion, Attrition, Dual fluidized beds

7.2 Introduction

Separation of CO_2 from flue gases produced from a fossil fuel fired thermal power plant is estimated to represent about 70% of the total cost for CO_2 management, including separation, compression, transportation, and sequestration (Beer, 2000; Metz et al., 2005). CO_2 capture imposes severe energy penalties on fossil fuel-based power plants, reducing net electricity output by as much as 13–37% (Rao and Rubin, 2002). These problems with current CO_2 separation technologies encourage the development of economical alternatives. Absorption processes for CO_2 separation employing chemical sorbents such as limestone are thought to be technically feasible and economically advantageous (Abanades et al., 2003; Ziock et al., 2002; Lin et al., 2002; MacKenzie et al., 2007; Abanades et al., 2007).

The reversible reaction between CaO and CO_2 may find application in a high-temperature process to control CO_2 emissions from advanced power generation. At appropriate temperatures and pressures (favourable for thermodynamic equilibrium), CO_2 from the flue gas stream is absorbed by calcined limestone, forming $CaCO_3$ (as the carbonation reaction, the forward reaction of reaction 7.1). At higher temperatures and/or lower pressures, the calcination reaction occurs, producing a gas stream having high CO_2 concentration (the reverse reaction of reaction 7.1), suitable for further use or ready for ultimate sequestration. Circulating fluidized bed (CFB) systems are particularly suitable for handling large amounts of solids (Davidson et al., 1985). Internal and external solids transport and reaction between solids and gas streams, such as absorption and desorption reactions, are greatly enhanced by excellent mixing of the reactants through the CFB's bed material circulation, which in turn maximizes mass and heat transfer and reaction rates (Shimizu et al., 1999; Wang et al., 2004; Grasa and Abanades, 2006). CFBs using limestone sorbent have another advantage: potential sulphur removal *via* the sulphation reaction (reaction 7.2) when burning sulphur-containing solid fossil fuels (Wang et al., 2004; Anthony and Granatstein, 2001), albeit that the sulphation and the carbonation reaction should, most likely, be carried out in separate reactors (Sun et al,. 2007; Hughes et al., 2005).

$$CaO(s) + CO_2(g) \Leftrightarrow CaCO_3(s) \qquad 7.1$$

$$CaO(s) + SO_2(g) + \tfrac{1}{2} O_2 \Leftrightarrow CaCO_3(s) \qquad 7.2$$

Up to now, work in this direction has focused on lab-scale thermogravimetric analysis (TGA), tube reactors or pilot-scale single beds operating in a batch mode (Salvador et al., 2003; Fennel et al., 2006; Jia et al., 2007), i.e., the processes were arranged to occur in the same reactor by adjusting the operating conditions, such as bed temperature and gas stream composition, to suit the required reaction (the forward or reverse reaction of reaction 7.1). Here, the solid sorbent remains in the same reactor instead of being transferred between two reactors, obscuring a number of interesting elements that make the concept so appealing.

This paper presents the CO_2 capture performance at the CANMET pilot-scale dual fluidized bed system using limestone as sorbent to study the decay of sorbent reactivity and particle attrition with increasing calcination/carbonation cycles. Process feasibility and system optimization were investigated at a variety of operating conditions, including sorbent looping rate, flue gas stream volume, carbonation temperature and CaO/CO_2 ratio. Besides the use of a direct external electrical heater for heating the calcination reactor, both biomass and coal were used as fuels in two different combustion modes: air-blown combustion and oxy-fuel combustion with flue gas recirculation to achieve high-concentration CO_2 in the off-gas from the calciner.

7.3 Experimental Method

7.3.1 Dual Fluidized Bed System Setup

The pilot-scale dual fluidized bed system for the calcium (limestone) looping process to capture CO_2 is illustrated in Figure 7.1. The system consists of two fluidized bed reactors: a sorbent calciner/regenerator, which is a circulating fluidized bed combustor designed for operation with oxy-fuel firing using flue gas recycle, and a combustor/carbonator, which is divided into two stages and designed for the separation of combustion/sulphation and carbonation. Alternately the combination of reactions can be conducted in the first stage. Each reactor is comprised of one 100 mm ID pipe and four refractory/insulation-lined sections of pipe also with 100 mm ID. Each section of pipe is 1 m in length. The total height of the riser is 5 m. Instrumentation ports are distributed at approximately 0.3m intervals over the height of the calciner (see Fig. 1). The bottom pipe is surrounded with four electric heaters (5 kW each) that provide supplemental heating during warm-up operation.

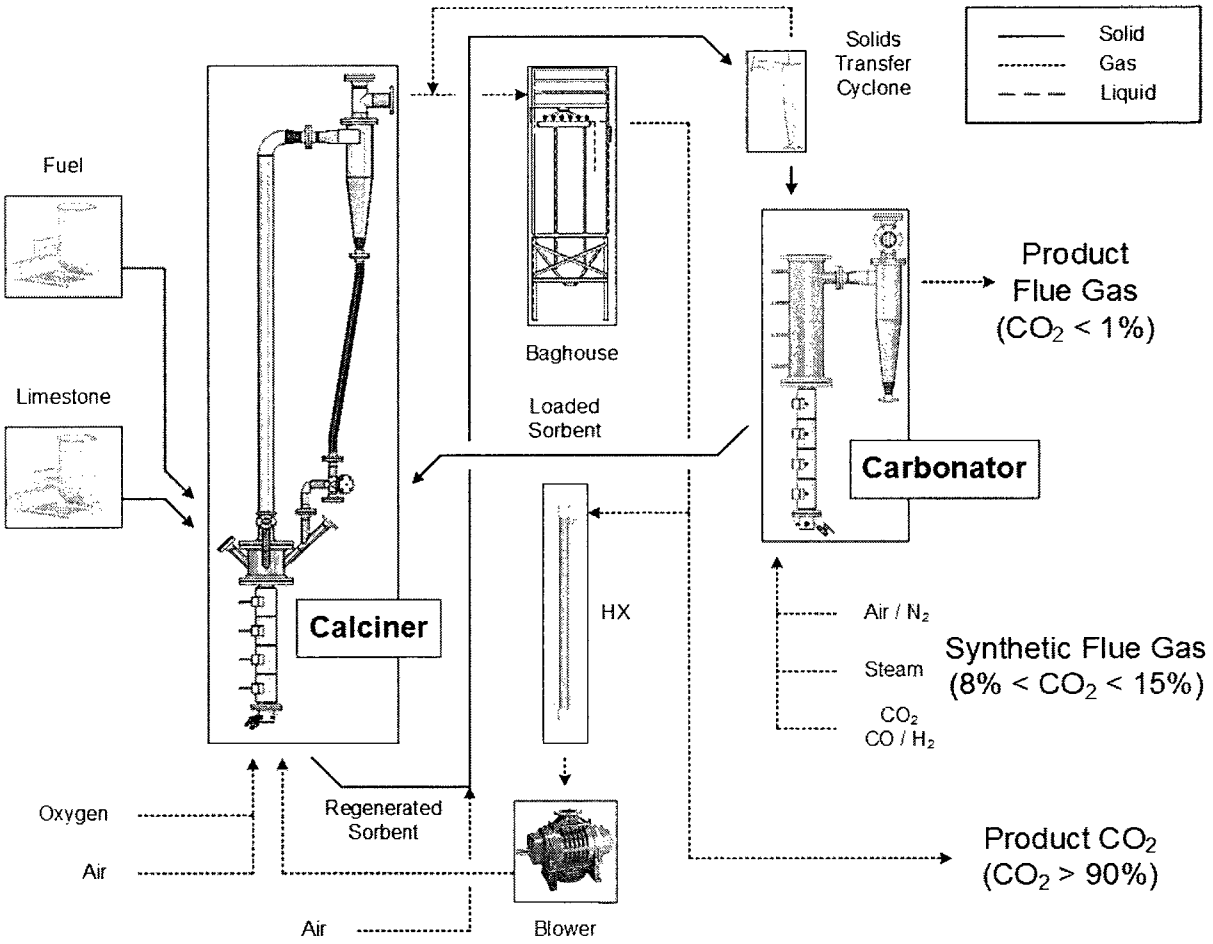

Figure 7.1: Schematic of dual-fluidized bed sorbent looping facility.

Primary gas enters the calciner through a wind box and a distributor plate that evenly distributes fluidizing gas to the bed and supports the bed materials when slumped. The fluidizing medium can be air, oxygen-enhanced air and/or recycled flue gas.

Flue gas exits tangentially at the top of the riser where it is directed to the cyclone. The cyclone is designed to recover 90% of particles, which are directed to the return leg for re-injection into the reactors. The drop pipe contains a diverter valve that allows material to be sampled when required. Material from the pipe drops into the external fluid bed heat exchanger, which can be used as a heater

or cooler. When it is used for heating, a surrounding electric heater (ceramic band type) can be controlled remotely to allow on/off and set point control. This reduces heat losses from the bed by warming up the gases and solids from the cyclone before re-injection into the calciner. In the cooling mode (to cool down the bed, as a method of temperature control), water in a cooling coil within the bed is used to cool down the bed material.

The flue gas exiting the cyclone passes through a flue gas heat exchanger (which can be fluidized with air or recycle flue gas), and then enters a bag house and/or a gas filter for fine particle removal. This heat exchanger protects the gas filter from overheating. Once the gas is cleaned, it can be exhausted through an induced draft fan or returned to the calciner (regenerator). To achieve recirculation, a second heat exchanger is required for cooling flue gas to near room temperature. This heat exchanger is necessary to cool down the flue gas to an acceptable temperature for the recycle blower.

The carbonation reactor can be fluidized with air or a mixture of air and superheated steam. A bed solid drain port, including a solenoid valve located just over the wind box, allows evacuation of all solids from the combustor-carbonator.

The solids transport system for sorbent looping is the key component in the dual-FB system. At the bottom of the calciner, a 45-degree "T" collects the solids from a pipe terminating at the upper plane of the central axis of the distributor plate, illustrated in Figure 7.2. A rapid action solenoid valve activated by computer controls the solids flow, which is lifted by conveying air to a height of 6.0 m and introduced into the carbonator using a cyclone for separating the solids from the conveying gas. Particles collected from the cyclone enter the carbonation bed through an L-valve. At the bottom of the carbonator, another 45-degree "T" line allows the solids to go from the carbonator return into the calciner/regenerator or back into the bottom stage combustor for SO_2 capture (if necessary, depending on the fuel used).

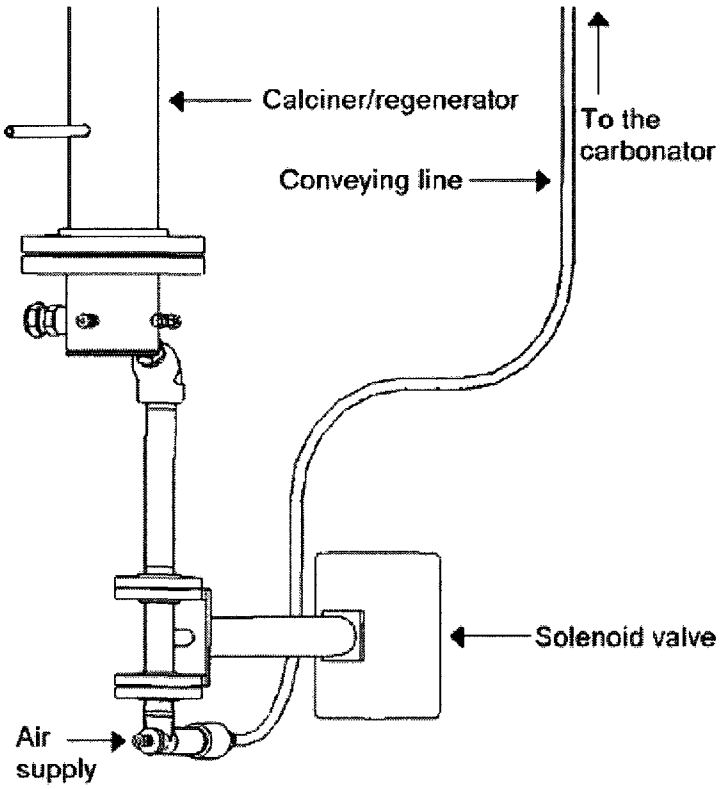

Figure 7.2: Solids transport system

Two solenoid ball valves, specified for a maximum temperature of 950 °C, control the solids path as well as the flow rate. In this study the sorbent cycle number is calculated based on the total inventory of calcined sorbent in the system and the solid conveying line. This approach was verified by solid sampling from the conveying line; however, this method is not totally precise as the solid density and size distribution change as the number of cycles increases.

7.4 Operation

In this investigation, the study was focused on demonstrating CO_2 capture in a dual fluidized bed unit. Therefore, a synthetic flue gas consisting of air and pure CO_2 was deemed appropriate rather than a 'real' combustion flue gas. Screened Havelock from eastern Canada was the only limestone used in this investigation; its properties are given in Table 7-1. The size of the sorbent particles was in the range of 0.4 to 0.8 mm and was used as received. Three operating methods for providing heat to the calciner were investigated here: using only external electric heaters; burning biomass with air; and oxy-fuel combustion with biomass and bituminous coal. The biomass used was a low ash wood pellet

material and the coal is a high-volatile, medium-sulphur eastern bituminous (EB) coal. The wood pellets were 5–10 mm in size. Table 7-2 shows the fuel properties (ultimate and proximate analyses).

Table 7-1: Sorbent composition (Havelock limestone, analysis by X-ray fluorescence)

Component	Wt%
Al_2O_3	0.34
BaO	0.03
CaO	54.1
Fe_2O_3	0.3
K_2O	0.06
MgO	0.29
MnO	0.07
Na_2O	0.2
NiO	0.01
P_2O_5	0.02
SiO_2	1.9
SO_3	0.46
SrO	0.02
TiO_2	0.07
V_2O_5	0.02
LOF	42.99
Sum	100.88

Table 7-2: Analyses of the solid fuels

	Low Ash Wood Pellet	Bituminous Coal
Moisture, wt% (as analyzed)	2.83	1.08
Proximate, wt% (dry basis)		
Ash	0.72	8.66
Volatile matter	83.56	35.78
Fixed carbon	15.72	55.56
Ultimate, wt% (dry basis)		
Carbon	52.04	77.81
Hydrogen	5.97	5.05
Nitrogen	0.1	1.49
Sulphur	0.01	0.95
Ash	0.72	8.66
Oxygen (by difference)	41.16	6.04
Heating value, MJ/kg	19.53	32.51

Prior to starting heating, the combustor was preloaded with a 100% sorbent bed. The external electric heaters were used to heat the dense bed region of the combustor, but an internal natural gas burner was also sometimes used to accelerate the warm-up period. It was noted that the calcination reaction for the limestone bed began at a temperature of ~700 °C; however, the reaction was relatively slow until the bed temperature reached ~875 °C and the calcination process was quickly completed when the bed temperature exceeded 900 °C. Once calcination was completed, the sorbent was ready to be transferred to the carbonator; subsequently the solids were continuously looped between the two reactors. The solids conveying rate was controlled by the valves located at the inlet of both transfer lines and the bed depths were monitored by pressure transmitters across the beds.

The carbonator was fluidized by compressed air, which was preheated to 250 °C prior to entering the reactor. External electric heaters surrounding the bed region were used to bring the carbonator to the desired carbonation temperature, and no other heat sources were applied to the carbonator. CO_2 from

a high pressure cylinder was introduced into the carbonator's fluidizing medium, at a volume concentration of 15–16% of the total stream to the carbonator. The continuous looping operation was usually straightforward to control and the electric heaters on the carbonator were the only components needing adjustment during the test runs.

The dual fluidized beds are equipped with several access ports for measurement of process variables such as temperature, pressure and gas concentration. Data acquisition and control are performed with Labview software. Gas analysis samples are taken from lines at the top of the cyclones from both the calciner and the carbonator. Valves allow switching of gas samples between the two sampling lines. After passing through a gas sample-conditioner, including solid filtration and water removal, the gas sample is then directed to the gas analysis rack. Flue gases are continuously analyzed for CO, CO_2, SO_2, NO_x and O_2 concentrations.

Figure 7.3 shows the operation record for 10 h of continuous operation, without fuel addition. CO_2 data were recorded mostly from the carbonator and occasionally switched to the calciner to check the performance of sorbent regeneration. More than 50 hours in total run time has been accumulated.

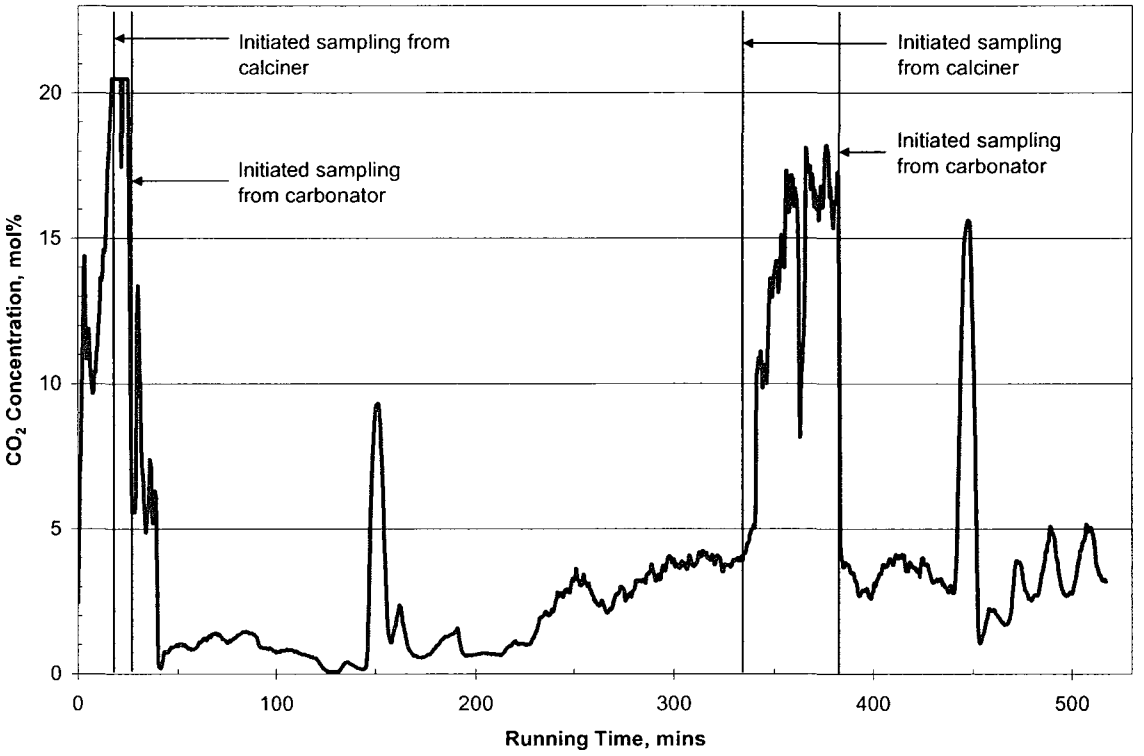

Figure 7.3: CO_2 emissions from calciner and carbonator during Ca looping tests.

In oxy-fuel firing with biomass or coal, part of the flue gas exiting the calciner was directed through a bag filter and a tube-in-shell condenser for moisture removal before entering the recycle blower, then mixed with pure oxygen (as primary fluidizing stream). A portion of the recycled flue gas was directed through the secondary gas ports, through the fuel injector, and through the particle return leg under the cyclone. The transition from air-blown to oxy-fuel combustion went smoothly with the current configuration in the dual fluidized bed system (see Figure 7.4). CO_2 concentration in the flue gas depends on the extent of the reactor vacuum, which causes some ingress of air from the surroundings, diluting the CO_2 stream. Unfortunately, this situation is a necessary limitation of the current setup of the fuel feeder. Table 7-3 gives the ranges of operating parameters in this investigation.

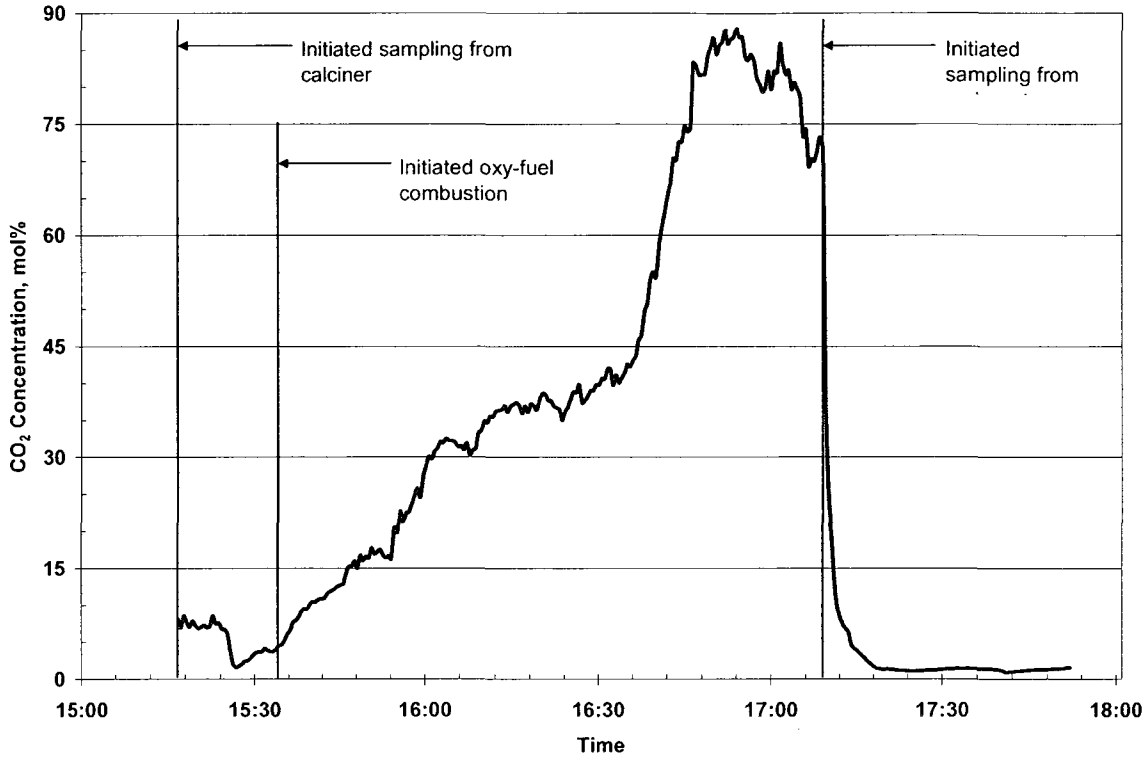

Figure 7.4: CO_2 emissions from calciner and carbonator during Ca looping tests with oxy-fuel firing with EB coal.

Table 7-3 Operating parameters

	Minimum	Maximum
At calciner / regenerator		
Bed temperature, °C	850	950
Initial sorbent load, kg	4.5	5.0
Batch of sorbent added, kg	0.3	0.5
Biomass feed rate, kg/h	4.0	7.6
Coal feed rate, kg/h	2.6	5.8
O_2 flow in oxy-fuel, slpm	60	90
Air flow in air combustion, kg/h	8.0	14.4
At carbonator		
Bed temperature, °C	580	720
Air flow rate, slpm	40	100
CO_2 flow rate, slpm	7.5	19.0
CO_2 concentration at inlet, vol%	15	16.5
Air flow for solids conveying, slpm	35	55

7.4.1 Scanning Electron Microscopy

An Hitachi S-3400N scanning electron microscope (SEM) was used to take images of the solid samples collected from the carbonator and calciner in various combustion modes. Samples were taken during continuous operation tests and identified by a calculated sorbent cycle number. When images were taken, samples were mounted onto carbon templates. All samples were coated in Au/Pd (~20 nm) to reduce charging. An accelerating voltage of 20 kV, and a 10 mm working distance were used in all cases.

7.5 Results and Discussion

7.5.1 CO_2 Capture

Figure 7.5 shows the CO_2 capture at different volume flow rates for the gas stream entering into the carbonator. The gas residence time is inversely proportional to the flow rate, and so flow rate gives a

measure of the residence time of the gas stream in the carbonator. Initially, the CO_2 capture efficiency increased with decreasing gas flow rate (i.e., longer residence time). This is expected as the carbonation reaction is kinetically controlled; longer reaction time is beneficial to the completion of the reaction. Greater than 97% CO_2 removal could be achieved, with the highest captures seen over the first few hours of operation, i.e., the sorbent looping during the first several cycles. These results indicate that the Ca looping process using dual fluidized beds has potential as a practical, high-CO_2 capture, technology for separating CO_2 for sequestration from air-blown combustion flue gas.

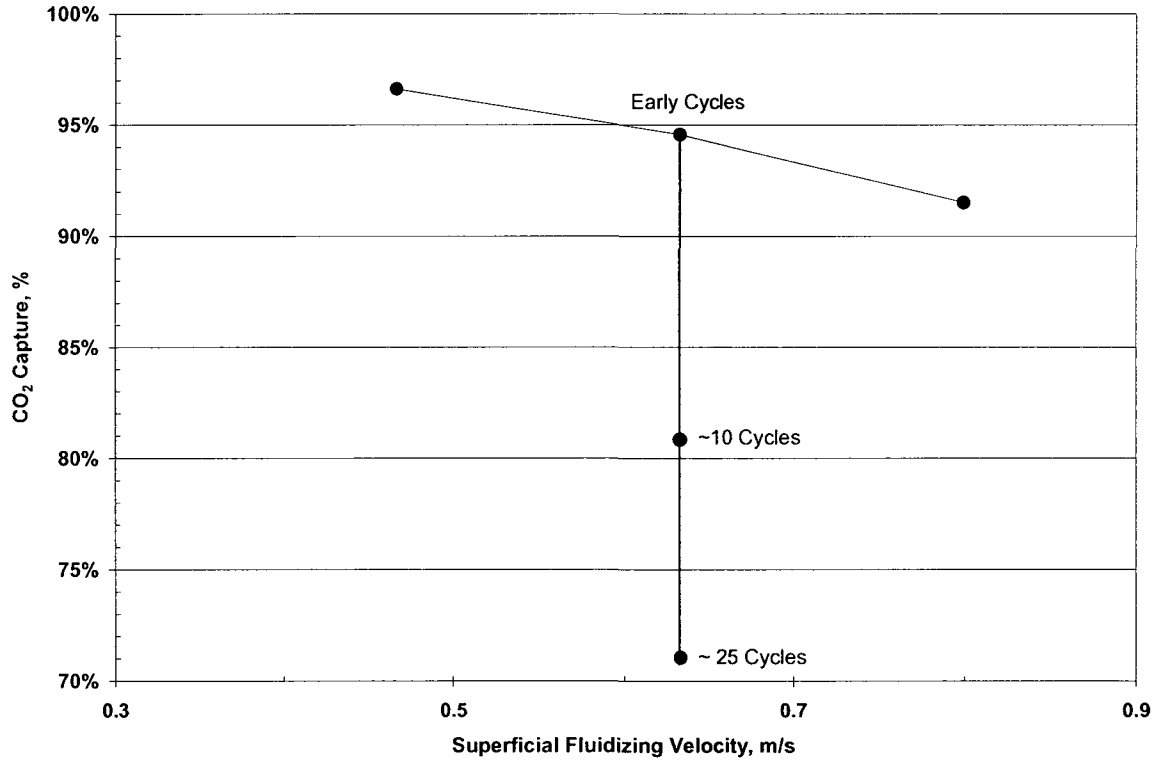

Figure 7.5: CO_2 capture vs. carbonator fluidizing velocity from Ca looping tests.

CO_2 capture rate fell slightly with time, i.e., with the number of sorbent looping cycles. This decay in sorbent reactivity or reversibility, as a function of reaction cycles, has been observed in work with bench-scale TGA and pilot-scale batch operation in single units. Here, after ~10 cycles the capture efficiency dropped below 90% and stayed between 75 and 85% until sorbent looping increased to 20 cycles (see Figure 7.5). Subsequently, the capture rate decreased further, to ~72%, once the solids looping reached 25 cycles. In addition to loss of activity *via* decay in the reversibility of sorbent,

particle attrition was found to be a significant problem as about 50% of the original sorbent particles, in the range 0.4–0.8 mm, eventually became smaller than 0.1 mm. Most of these solids can be collected by cyclones, but were not recycled back into the reactors in the current system configuration. This resulted in a significant drop in the quantity of sorbent in the carbonator after more than 20 cycles without sorbent makeup. In consequence, some of the decrease in CO_2 capture with increasing looping cycles must be attributed to the loss of fine sorbent produced by particle attrition.

7.5.2 Attrition

Fines captured by the cyclones were typically <0.1 mm (compared to the original sorbent size range of 0.4–0.8 mm), and were assumed to result from particle attrition during operation. Fine particles captured by the cyclones, at the outlets of both calciner and carbonator, were collected and weighed after several hours of operation (interpreted here as the number of sorbent looping cycles), and then reloaded into the calciner bed. Figure 7.6 shows the amount of fines collected by the cyclones vs. the number of sorbent cycles. It can be seen that ~30% of the total material was captured by the cyclones after just 3 cycles. This amount is large, but not surprising, as it is similar to the results found in batch tests using a single fluidized bed unit (Jia et al., 2007) (the same reactor used as the calciner in this work). Furthermore, this result is in agreement with the results seen elsewhere (Fennell et al., 2006). However, unlike previous work, where the most significant attrition was observed in the first few cycles, here attrition appeared to continue at a relatively high level with increasing cycle numbers. Thus, about 60% of the original material was found in the cyclones after 25 cycles, resulting in a considerable drop in CO_2 capture rate.

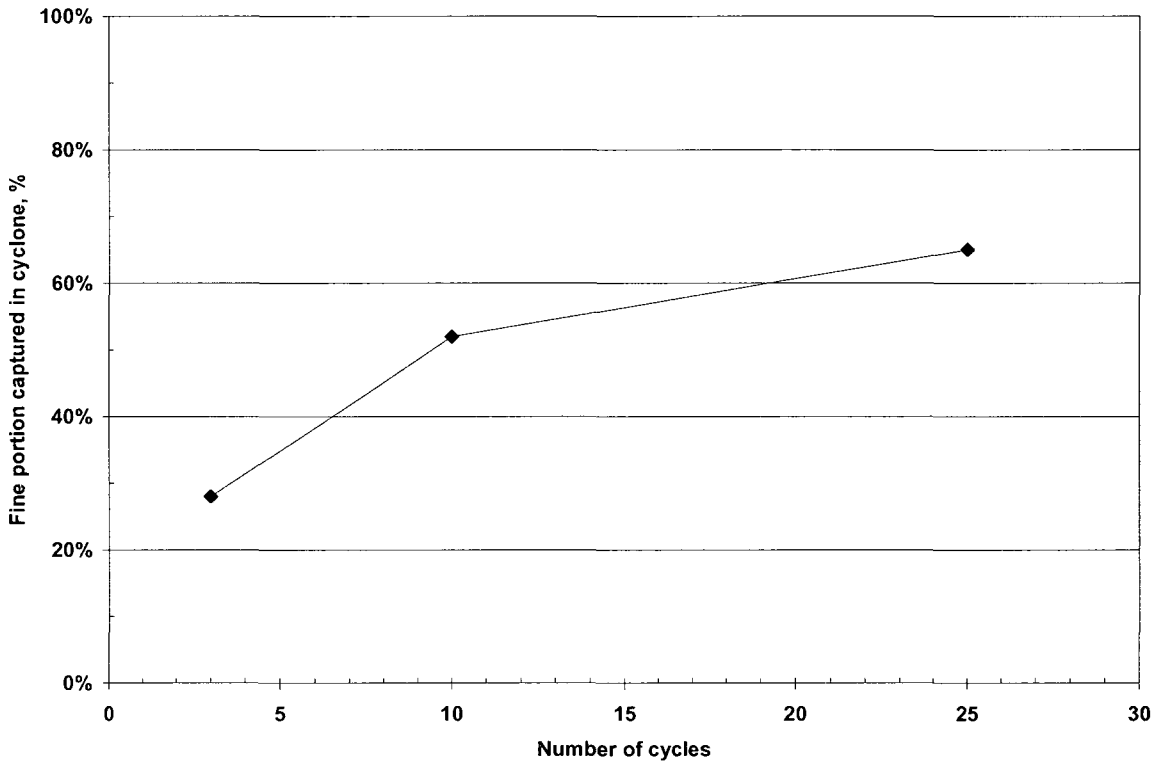

Figure 7.6: Sorbent particle attrition after number of sorbent cycles.

It was also noted that most fines were collected from the cyclone located at the exit of calciner. This is because a number of problems are associated with the complex calcination process, such as sintering, diffusion of impurities to grain boundaries and the release of CO_2, hence the particles will become lighter and more fragile, while carbonation makes sorbent particles denser and more durable. Additionally, the calciner is operated in a turbulent/slugging mode while the carbonator has been operated as a moving bed in this study. The degree of attrition due to pneumatic solid conveying was determined to be insignificant compared to attrition occurring within the reactors.

7.5.3 Effect of Temperature in Carbonator

Figure 7.7 illustrates the sorbent performance for CO_2 removal versus carbonator temperature when the bed temperature in the calciner was fixed at ~900 °C. The carbonator temperature was first set at 650–700 °C, which was selected as an optimized temperature window based on previous bench-scale TGA cycle studies using a number of limestones (Hughes et al., 2004). Under this initial temperature condition about 90% CO_2 capture was achieved, which is higher than that predicted from

thermodynamic equilibrium calculations. However, this can be explained by the carbonator bed temperature profile, which indicated a higher temperature at the bottom of the bed and a lower temperature at the top. As a consequence of lower temperature CO_2 capture is improved. Decreasing bed temperature further below 600 °C, the high CO_2 removal continued, until the temperature dropped below 500 °C, which appeared to be too low to drive the carbonation reaction in a kinetic control mode (see the sharp CO_2 peak in Figure 7.7). The best CO_2 removal (~98%) was achieved in the temperature window of 580–600 °C. It was also interesting to note that the optimized temperature window associated with CO_2 capture in the carbonator became higher with the number of sorbent cycles. Better CO_2 capture was obtained at carbonator temperatures of ~700 °C after more than 20 cycles, compared to 600 °C for the initial cycles with fresh sorbent. This supports the hypothesis that particle sintering and pore plugging experienced after a number of cycles hinder the ability of the CO_2 stream to penetrate into the deep pores available inside the particles. More investigation on sorbent characteristics and particle structures produced after many cycles is clearly needed.

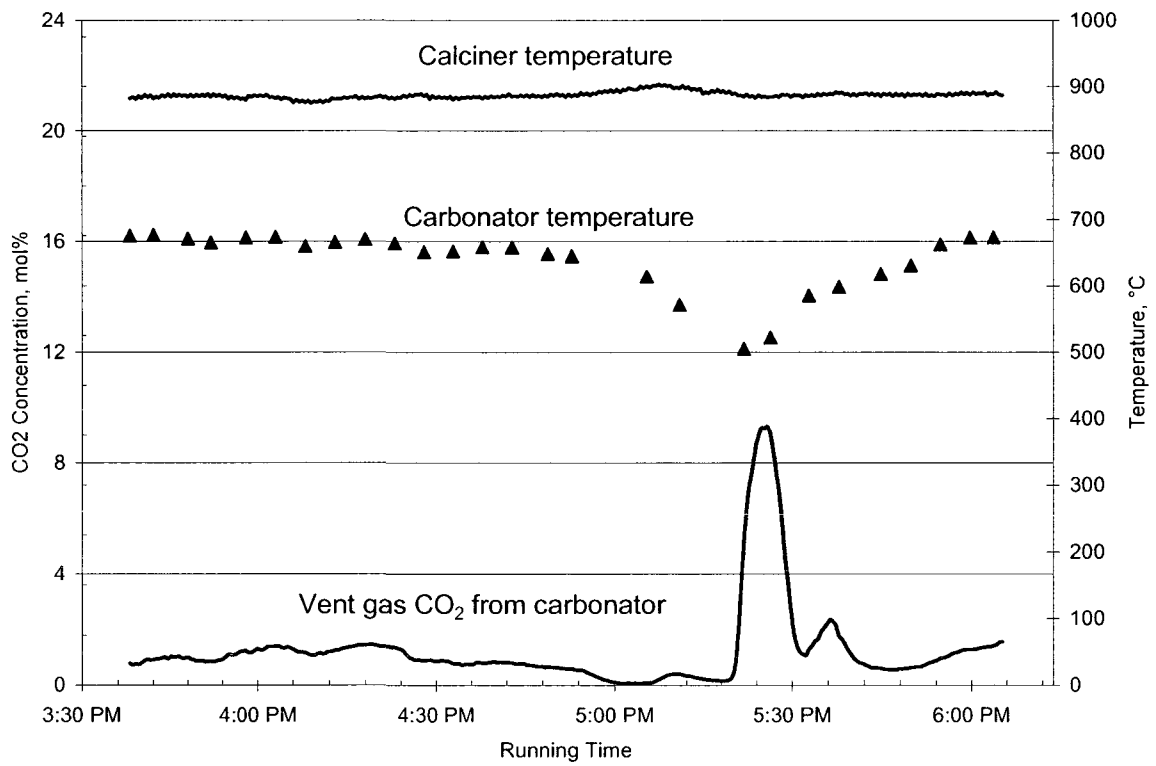

Figure 7.7: CO_2 capture vs. carbonator temperature from Ca looping cycle tests.

7.5.4 Oxy-fuel Combustion

Initially, we used external electric heaters with the calciner. However, this does not represent a practical situation, and hence, in later experiments oxy-combustion of solid fuel was employed to provide a heat source for sorbent regeneration. The results obtained with oxy-combustion confirm the general applicability of this approach for the sorbent regeneration. In our experiments, a high-concentration CO_2 off-gas stream was achieved from the calciner, once the air-blown combustion was shifted to pure oxygen blown (mixed with recycled flue gas). O_2 concentration in the primary gas was ~40–50% by volume and bed temperature was well controlled by solid recirculation *via* the cyclone and return leg. Flue gas recycle was in the range of 50–60% to provide both primary gas mixture and fuel injection. In these tests CO_2 concentration from the calciner off-gas of ~85 vol% (dry basis) was achieved. Figure 7.4 shows the CO_2 concentration from the calciner during the transition period from air-blown to oxy-fuel combustion.

It was noted that the Ca looping performed well for CO_2 capture regardless of the heat source. However, biomass pellets were found to be too fragile, shredding into smaller pieces after they passed through the fuel feeder screws. The smaller wood pieces were eventually burnt in the riser instead of the dense bed, resulting in a decrease in bed temperature. Here, this could only be overcome by keeping the electric heaters on. By contrast, in oxy-coal combustion, having coal ash mixed with the sorbent and transferred between the two reactors, has an inherent energy penalty associated with solid conveying and heat loss. In addition coal sulphur results in sulphation of the CaO-based sorbent, consuming sorbent and accelerating the decay of sorbent activity. Calcium sulphate is preferentially formed primarily on the surface of the sorbent particles and is not removed during sorbent regeneration (Sun et al., 2007).

As expected, no SO_2 was detected during oxy-fuel firing with EB coal in a 3-h continuous run, indicating that all SO_2 in the flue gas was indeed trapped by the sorbent. Interestingly, no significant drop in CO_2 capture was observed and the sorbent appears to be effective for removal of both CO_2 and SO_2 from combustion flue gas, providing the stoichiometry is sufficient for the removal of both S and C. This result is somewhat different from results from previous bench-scale TGA experiments (Sun et al., 2007). However, longer-term operation is required to confirm these observations and determine the full impact of sulphation on sorbent reactivity and attrition.

7.5.5 SEM Analysis

The porosity characteristics of the sorbent are crucial to sorbent conversion capability. To provide an illustration of the textural changes of the sorbent as a function of reaction cycles, SEM analysis was performed for both the calcined and carbonated material. Figure 7.8, Figure 7.9 and Figure 7.10 show the fracture surface of sorbent samples taken from the carbonator and the calciner as a function of the calculated number of reaction cycles.

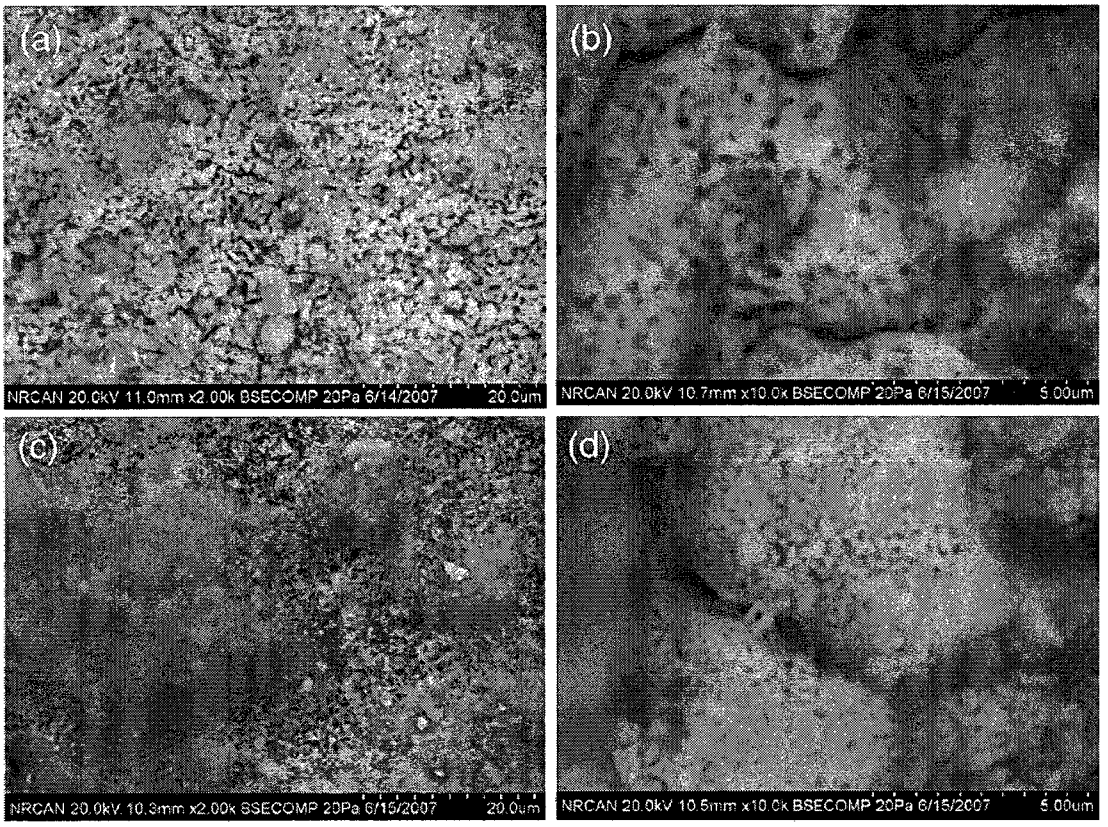

Figure 7.8: SEM of surface area of samples from carbonator. (a,b) after 3 cycles, (c,d) after 25 cycles.

Figure 7.8a shows the carbonated sorbent sample after 3 cycles and reveals a similar structure to the parent limestone, with crystalline domains by some small pores connecting the grains to the interior, producing an overall mosaic pattern. At higher magnification within one of these fragmented mosaic textures (Figure 7.8b), it can be seen that the carbonates are arranged in small (~0.1 μm breadth,

variable length) rods, forming a quasi-cylindrical pore network. Fractures appear to propagate along the grain boundaries, but the interior of some of the grains is visible.

It was noted that the microstructure grain pattern was not affected by the number of reaction cycles, as the parent crystalline domains can still be readily recognized after as many as 25 calcination/carbonation cycles. Alvarez and Abanades observed a similar behaviour in a number of limestones they investigated (Alvarez and Abanades, 2005). However, an apparent burnish (which is interpreted here as "a smooth glossy finish or appearance") is visible on the SEM of the particle surface (Figure 7.8c) after 25 cycles. This phenomenon could be associated with swelling at the particle surface, due to carbonation of active CaO sites, given that the molar volume of $CaCO_3$ is significantly greater than that of CaO (36.9 vs. 16.9 cm^3/g, respectively). The regenerated outer layer could also cause subsequent plugging of the surface pores and inhibit diffusion of CO_2 into the inner structure of the particles, thus explaining in part the lower CO_2 capture efficiency observed with increasing carbonation/calcination cycles.

At a higher magnification of ×1000 (Figure 7.8d), a grain texture is still present; however, the holes between the grain rods are much smaller compared to those from the sample seen during the initial cycles (Fig. 7.8b). This suggests that the decay in sorbent reversibility occurs due to filling/sealing of pores with a suitable porosity as the $CaCO_3$ layer grows.

When coal is introduced into the calciner in the oxy-fuel combustion mode, the sealing and filling of the sorbent grains are more pronounced through both sulphation and the formation of coal-derived ash. Figure 7.9a shows the particle surface observed after the initial cycles from the calciner. Here, the sorbent retains the network pattern seen without burning coal, but its surface is contaminated with different grains associated with sulphates and fine ash. The larger grains are probably due to the formation of sulphate, which has an even larger molar volume (45.6 cm^3/g) than the carbonate, and cannot be eliminated in the sorbent regeneration process, resulting in permanent blockage of the CaO pores. The fine grains, either in lighter or darker colour (Figure 7.9a) than the limestone-based textures, are believed to be related to coal ash, which is expected to accelerate decay of the sorbent reactivity with CO_2.

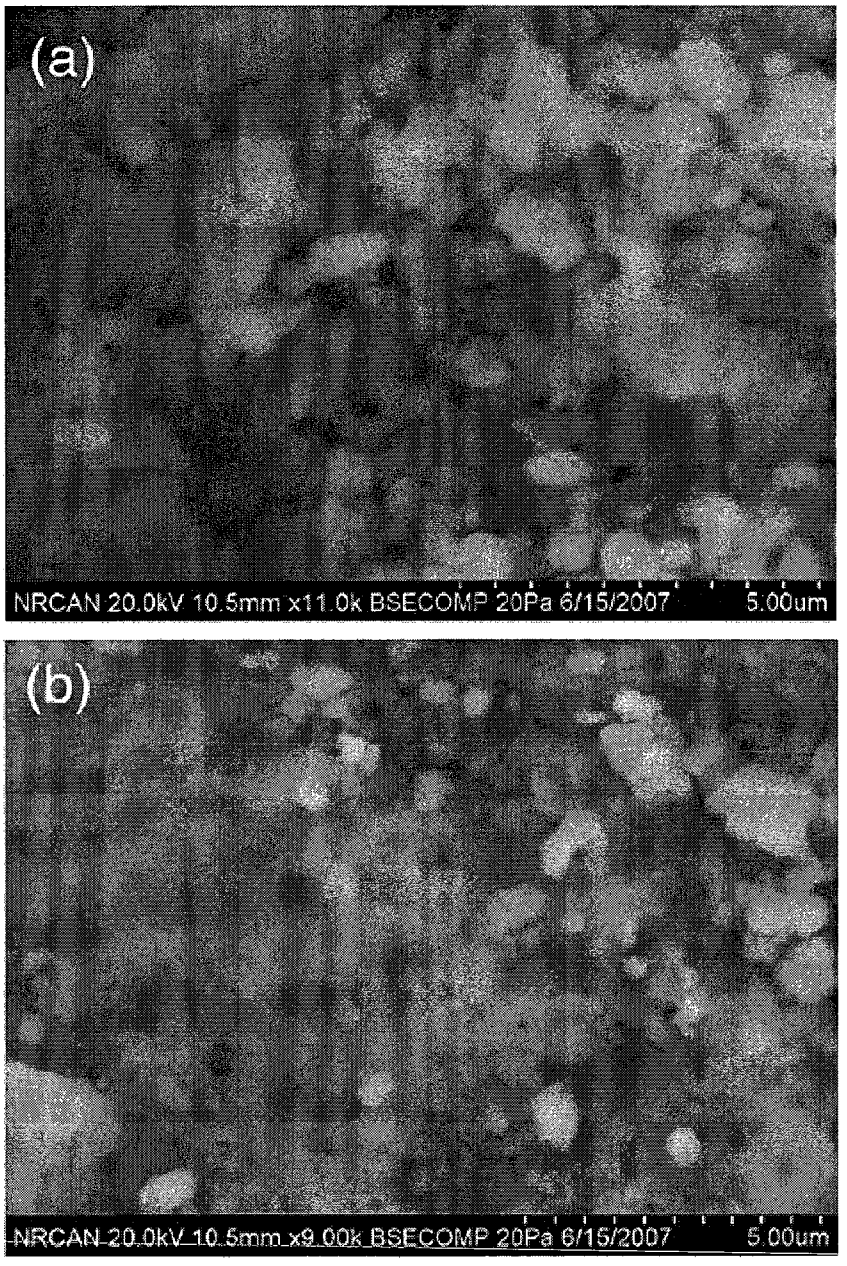

Figure 7.9: SEM of surface of samples from calciner in oxy-coal combustion. (a) after 3 cycles, (b) after 10 cycles.

Figure 7.9b reveals almost complete disappearance of a visible CaO mosaic pattern after 10 cycles. This indicates a significant change of the sorbent structure texture compared to the samples seen from the calciner without burning coal (Figure 7.10). Further work is needed to ascertain the effect of these contaminants when oxy-coal combustion is used for sorbent.

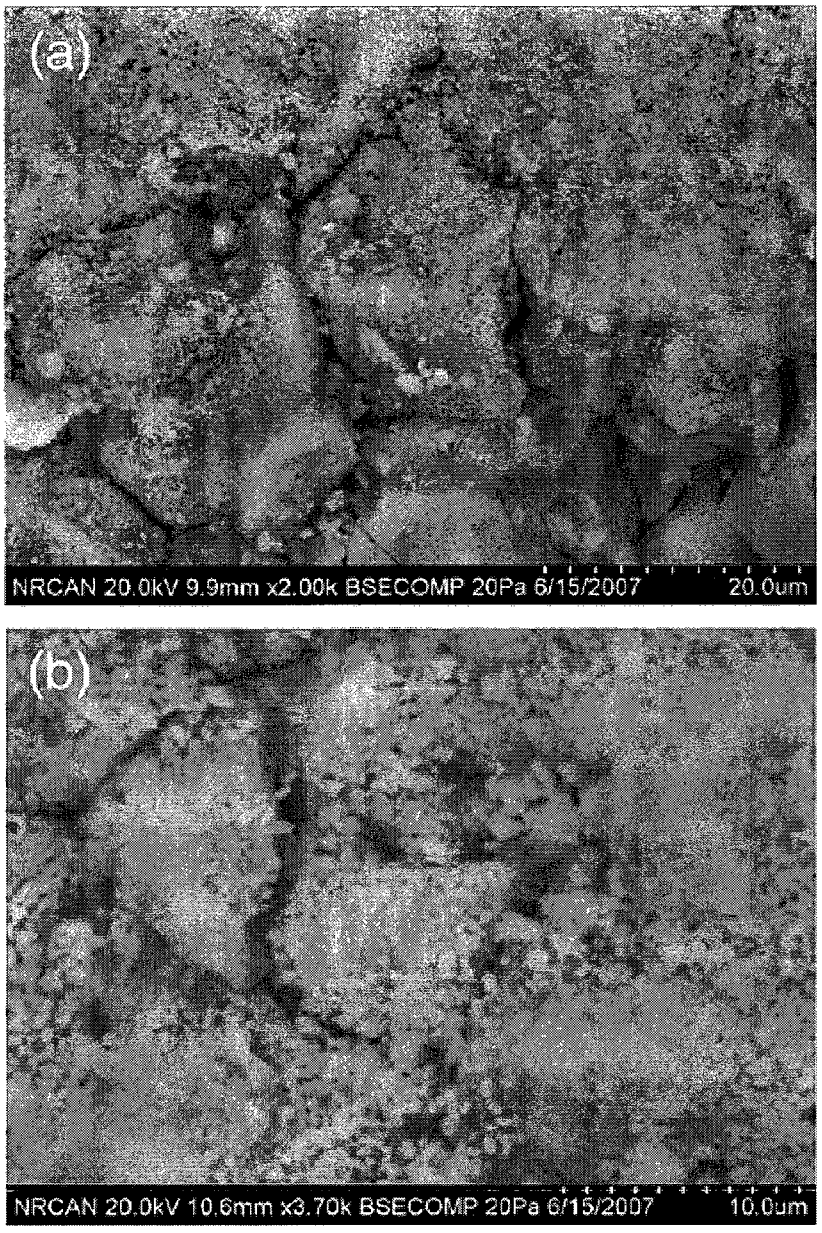

Figure 7.10: SEM of surface of samples from calciner with air-combustion of wood pellets. (a) after 3 cycles, (b) after 25 cycles.

Sorbent/coal ash interactions might have important effects in terms of enhancing or inhibiting carbonation, and influencing attrition behaviour. Compared to the carbonated samples, the initial calcined particle surface displays two network pattern textures clearly (Figure 7.10a). One is a grain

structure network with well-organized small pores, which has been seen in other surface SEM images in Figure 7.8 and Figure 7.9. The other network links the small pore grains and consists of some very large pores of 2–4 μm in diameter (Figure 7.10a). The deep inner structure of the large pores can be seen, and must contribute significantly to enhancing carbonation in the initial cycles. However, these large pores appeared to be eliminated, through pluggage or sintering, after a number of cycles (see Figure 7.10b for the sample after 25 cycles).

The SEM image of the sample from the calciner after 25 cycles (Figure 7.10b) also reveals that the 'burnished' material is visible on the microstructure pore surface, similar to results from samples obtained from the carbonator (Figure 7.8c). Fennell et al. (2007) also made similar observations from their work using natural sorbents in a fluidized bed, and found that the burnish seen on sorbent samples appeared to increase with increasing cycle number. Evidently, if the carbonate, once formed at the surface, cannot migrate back to the original surface, swelling must result in dislocating the CaO moiety, and the appearance of material above the surface will increase with cycle number. The influence of this migration of CaO from the particle surface needs to be investigated in much more detail in future.

Figure 7.11 shows the pore size distributions for the calcined sorbent after calcination/carbonation cycles of 3 (diamond), 10 (square) and 15 (triangle), respectively. The data (diamond) illustrates a pore size distribution similar to the first calcination, which is typically in the range of a few nanometres to several hundred nanometres with two prominent peaks around 5–7 nm and 100 nm. With increasing cycle numbers, both peaks shrink dramatically, in particular for the larger pores. After 10 cycles (squares), most of the large pores have disappeared, and pores sizes <10 nm are dominant, although the total number of small pores is still less than seen after the initial cycles.

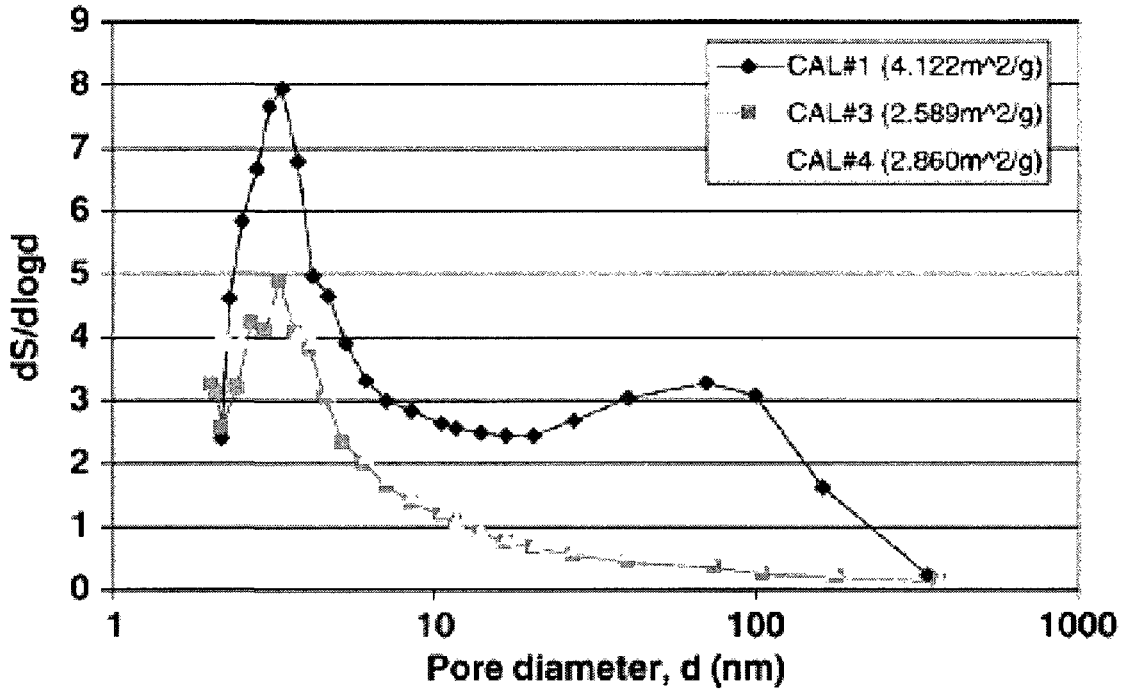

Figure 7.11: Pore diameter distributions in spent sorbent samples from calciner after 3 (diamond), 10 (square), and 15 (triangle) cycles.

The microporosity network (pore sizes <10 nm) remained unchanged after about 10 cycles. This behaviour could explain why the sorbent conversion remains at an almost constant level after a given number of cycles (Salvador et al., 2003; Fennell et al., 2006), assuming that the bulk of the recarbonation occurs at the microstructure grain level (Bhatia and Perlmutter, 1983).

7.6 Conclusions

The calcium-based sorbent looping cycle process has been demonstrated using the CANMET 75 kW_{th} pilot-scale dual fluidized bed facility and more than 50 hrs operating experience in total has been accumulated. Havelock limestone from eastern Canada was used as the CO_2 sorbent, while a synthesis gas mixture of air and CO_2 (15%) was employed to simulate combustion flue gas. A high CO_2 capture efficiency (>95%) was achieved for the first several cycles, which decreased to a lower level (>72%) after more than 25 cycles. Oxy-fuel combustion of biomass and coal was employed in the sorbent regeneration step, in which pure O_2 was mixed with recycled off-gas and this, along with the excellent heat transfer characteristics of CFBs, allowed the use of an O_2 concentration of 40 vol% in the

combustion gas. The final off-gas had CO_2 levels of 83%, and even higher levels are expected as the unit design is improved to minimize reactor leakage. Examination of the sorbent surface characteristics suggests that a number of complicated processes are occurring on the particle surface as a consequence of the number of reaction cycles. The issues of sorbent loss through attrition, impact of sulphation and optimization of the process need further investigation.

7.7 Acknowledgements

The authors would like to thank Dr. Ashleigh Cousins from Natural Resources Canada, CETC-O for operating the scanning electron microscope and providing the SEM images presented here.

7.8 References

Abanades. J.C., Anthony. E.J., Alvarez. D., Lu. D., (2003). 'In-situ capture of CO_2 in a fluidized bed combustor', 17th International Conference on Fluidized Bed Combustion, ASME.

Abanades, J.C., Grasa, G., Alonso, M., Rodriguez, N., Anthony, E.J., Romeo, L.M., (2007). 'Cost structure of a postcombustion CO_2 capture system using CaO', Environ. Sci. Technol. ASAP Web Release Date: 20-Jun-2007.

Alvarez, D., Abanades, J.C., (2005). 'Pore-size and shape effects on the recarbonation performance of calcium oxide submitted to repeated calcination/recarbonation cycles', Energy & Fuels 19, 270–278.

Anthony, E.J., Granatstein, D.L., (2001). 'Sulfation phenomena in fluidized bed combustion systems', Prog. Energy Combust. Sci. 27, 215–236.

Beér, J.M., (2000). 'Combustion technology developments in power generation in response to environmental challenges', Prog. Ener. Comb. Sci. 26, 301–327.

Bhatia, S., Perlmutter, D., (1983). 'Effect of the product layer on the kinetics of the CO_2–lime reaction', AIChE J. 29, 79–86.

Davidson, J.F., Clift, R., Harrison, D. (Eds.), (1985). 'Fluidization', 2nd edition, Academic Press.

Fennell, P.S., Pacciani, R., Davidson, J.F., Dennis, J.S., Hayhurst, A.N., (2006). 'The use of limestone particles for the capture of CO_2: its initial reactivity and loss of reactivity after repeated cycles of calcination and carbonation', 19th International Conference on Fluidized Bed Combustion, Vienna , 311–320.

Fennell, P.S., Dennis, J.S., (2007). 'A comparison of natural sorbents for cyclical removal of CO_2', 3rd International Workshop on *In-Situ* CO_2 Removal (ISCR_2007), Ottawa, Canada.

Grasa, G.S., Abanades, J.C., (2006). 'CO_2 capture capacity of CaO in long series of carbonation/calcination cycles', Ind. Eng. Chem. Res. 45, 8846–8851.

Hughes, R., Lu, D., Anthony, E.J., Wu, Y., (2004). 'Improved long-term conversion of limestone-derived sorbents for *in situ* capture of CO_2 in a fluidized bed combustor', Ind. Eng. Chem. Res. 43, 5529–5539.

Hughes, R., Lu, D., Anthony, E.J., Macchi, A., (2005). 'Design, process simulation and construction of an atmospheric dual fluidized bed combustion system for *in situ* CO_2 capture using high-temperature sorbents', Fuel Process. Technol. 86, 1523–1531.

Jia, L., Hughes, R., Lu, D., Anthony, E.J., Lau, I., (2007). 'Attrition of calcining limestones in circulating fluidized bed systems', Ind. Eng. Chem. Res. 46 (15), 5199–5209.

Lin, S.Y., Suzuki, Y., Hatano, H., Harada, M., (2002). 'Developing an innovative method, HyPr-RING, to produce hydrogen from hydrocarbons', Energy Convers. Manag. 43 (9–12), 1283–1290.

MacKenzie, A., Granatstein, D.L., Anthony, E.J., Abanades, J.C., (2007). 'Economics of CO_2 capture using the calcium cycle with a pressurized fluidized bed combustor', Energy & Fuels 21 (2), 920–926.

Metz, B., Davidson, O., de Coninck, H., Loos, M., Meyer, L. (Eds.), (2005). 'Special report on carbon dioxide capture and storage', in: Intergovernmental Panel on Climate Change, Cambridge Univ. Press.

Rao, A.B., Rubin, E.S., (2002). 'A technical economical and environmental assessment of amine-based CO_2 capture for power plant greenhouse gas control., Environ. Sci. Technol. 36, 4467–4475.

Salvador, C., Lu, D., Anthony, E.J., Abanades, J.C., (2003). 'Enhancement of CaO for CO_2 capture in an FBC environment', Chem. Eng. J. 96, 187–195.

Shimizu, T., Hirama, T., Hosoda, H., Kitani, K.,M. Inagaki, Tejima, K., (1999). 'A twin fluid-bed reactor for removal of CO_2 from combustion processes', Trans. IChemE 77 (Part A), 62–68.

Sun, P., Grace, J.R., Lim, C.J., Anthony, E.J., (2007). 'Sequential capture of CO_2 and SO_2 in a pressurized TGA simulating FBC conditions', Environ. Sci. Technol. 41 (8), 2943–2949.

Wang, J., Anthony, E.J., Abanades, J.C., (2004). 'Clean and efficient use of petroleum coke for combustion and power generation', Fuel 83, 1341–1348.

Ziock, H.J., Anthony, E.J., Brosha, E.L., Garzon, F.H., Guthrie, G.D., Johnson, A.A., et al., (2002). 'Technical progress in the development of zero emission coal technologies', 19th Annual Pittsburgh Coal Conference, Pittsburgh, PA.

Chapter 8 Attrition of Calcining Limestones in Circulating Fluidized-Bed Systems

Published in Industrial and Engineering Chemistry Research

Jia, L. [1], Hughes, R.[1], Lu., D.[1], Anthony, E.J.[1], (2007). 'Attrition of Calcinning Limestones in Circulating Fluidized-Bed Systems', Ind. Eng. Chem. Res. 46, 5199-5209.

[1]Natural Resources Canada, CETC-O, 1 Haanel Drive, Ottawa, Canada K1A 1M1

8.1 Abstract

Limestone attrition in circulating fluidized bed combustors (CFBCs) has received limited attention. Although there are a number of early studies on attrition in bubbling bed systems, most current studies focus on simultaneous calcination and sulphation. However, this subject is increasing in importance as CaO-$CaCO_3$ looping cycles are proposed. CaO-$CaCO_3$ looping cycles involve repeatedly calcining the $CaCO_3$ component of the limestone to drive off a pure stream of CO_2 for storage or sequestration. Here we have looked at five limestones from across Canada, the United States and Mexico to determine the extent of their attrition under calcining conditions in fluidized bed systems. This work shows that attrition varies very significantly from limestone to limestone, and even among different batches. It is clear, therefore, that each limestone will have to be carefully categorized to determine its potential for use in such cycles. Also, since limestones crush differently, even those limestones that are double-sieved may have very different initial size distributions. This will affect the results seen in tests carried out under realistic conditions. This work shows that most of the material loss in multiple calcination/carbonation cycles is in the first few cycles, and that even a very low level of sulphation can be a very effective means of reducing that material loss.

Keywords: Limestone, attrition, CFBC and looping cycles.

8.2 Introduction

There are a number of early studies on limestone attrition (Merrick and Highley, 1974; Franceschi et al., 1980; Vaux, 1978; Forsythe and Hertwig, 1949; Fuertes et al., 1991; Vaux and Keairns, 1980; Vaux and Fellers, 1981; Vaux and Shruben, 1983; Ray et al., 1987; Lee at al., 1993; Cook et al., 1996; Chandran and Duqum, 1989), with subsequent studies focusing primarily on the interplay of calcination and sulphation, mostly using small bubbling bed reactors (Couturier et al., 1993; Scala et al., 1997; Benedetto and Scala, 1998; Scala and Salatino, 2000). The general conclusion of such work is that size reduction is most dramatic during the initial calcination process or during a simultaneous calcination-sulphation process and least significant after particles are fully sulphated. If CaO-$CaCO_3$ looping cycles are to be used (Abanades et al., 2003; Abanades et al., 2004; Hughes et al., 2004;

Abanades et al., 2005), large quantities of limestone will need to be repeatedly calcined. This might be expected to lead to higher material losses. Here we have looked at particle size reduction in batch experiments in the absence of sand or any other "inert material", under conditions more closely reminiscent of "real" CaO-$CaCO_3$ looping cycle circulating fluidized bed combustor (CFBC) operation" (*i.e.*, higher fluidizing velocities, and temperatures that are also more typical of fluidized bed conditions for which we have carried out tests on CaO-$CaCO_3$ looping cycles (Abanades et al., 2004; Hughes et al., 2004)).

8.2.1 Attrition Criteria

According to Vaux (1978) two parameters can be used to describe attrition:

(1) attrition rate, R

$$R = -\frac{1}{M}\frac{dM}{dt} \qquad 8.1$$

and (2) extent of attrition, A (%)

$$A = -100\int_0^t R\,dt = -100\ln\left(\frac{M_0}{M}\right) \qquad 8.2$$

where M and M_0 are the mass of particles in the bed at time t and at time zero, respectively. It is implicit in these equations that the amount of material elutriated is used as a measure of the attrition (which would not be the case for pilot- or full-scale equipment operating on a continuous basis).

Forsythe and Hertwig (1949) proposed an attrition rate based on the production of material finer than 45 μm (325 mesh). Their definition is:

$$\frac{(\%\ of\ -45\mu m\ at\ start) - (\%\ of\ -45\mu m\ after\ 1 hour)}{\%\ of\ +45\mu m\ at\ start} \times 100\% / hour \qquad 8.3$$

The choice of 45 μm (325 mesh) as the limiting value was arbitrary and they also produced similar definitions based on 40 and 20 μm.

In CFBC operations most elutriated materials will be captured and returned to the riser, and only the very fine particles are lost. For such a system, the larger particles in the attrited fines are accumulated in the bed. An appropriate method of combining these two approaches might be to define the attrition rate R as:

$$R = -\frac{1}{M_{+75}} \frac{dM_{+75}}{dt} \qquad 8.4$$

and the extent of attrition A as

$$A = -100 \int_0^t R dt = -100 \ln(\frac{M_{+75,0}}{M_{+75}}) \qquad 8.5$$

where M_{+75} and $M_{+75,0}$ are the mass of the particles in the bed at time t and at time zero, respectively, with size greater than 75 μm. The choice of 75 μm as the upper limit for the attrited particle size is based on the findings of Fuertes *et al.* (1991). Since particles smaller than 75 μm will tend to report to the overhead ash stream in a CFBC, this approach will be used here.

8.3 Experimental

Five limestones were studied in these tests, from Mexico, Canada and the United States. Table 8-1 lists the compositional characteristics. For multiple calcination/carbonation tests a new batch of Cadomin was used, and this material was analyzed to confirm that its properties had not changed. Two facilities were used in tests evaluating attrition behaviour under varying conditions: one was a laboratory-scale CFB unit (0.05 m ID); and the other was a pilot-scale CFBC (0.1 m ID) plant.

Table 8-1: Limestone compositional characteristics, wt%

Composition	TP1	TP2	Tamuin	NISCO	Cadomin	Havelock	New Cadomin
CaO	47.8	35.47	53.99	55.4	55.12	55.24	50.64
SiO_2	9.05	23.61	<1.07	0.16	1.5	0.65	1.3
Al_2O_3	1.61	5.13	<0.23	0.08	<0.38	0.24	0.4
Fe_2O_3	1.47	2.34	<0.30	0.09	<0.55	<0.01	0.11
TiO_2	0.13	0.34	0.05	0.011	<0.04	<0.03	0.04
P_2O_5	0	0	0.05	0.02	<0.02	<0.03	<0.03
MgO	2.3	1.77	0.22	0.52	2.25	0.21	3.28
SO_3	0.59	1.51	<0.46	-	0.32	<0.10	<0.1
Na_2O	0.07	0.2	<0.02	<0.01	<0.17	<0.2	<0.2
K_2O	0.65	1.44	<0.06	<0.01	0.21	0.043	0.14
BaO	0	0	<0.03	<0.02	<0.02	0	0
SrO	0.01	0	0.05	0.08	<0.02	0	0
V_2O_5	0	0.01	<0.02	<0.02	<0.02	0	0
NiO	0	0	<0.007	<0.01	<0.01	0	0
LOI	38.52	29.97	43.62	43.4	42.77	42.35	43.99
Sum	101.48	101.77	98.00	100.1	102.19	99.95	99.92
Geological classification/age	--	--	Cretaceous, Campanian [21]	--	Devonian [22]	Carbonifierous, Mississipian [23]	Devonian [22]

8.3.1 Laboratory CFB

The laboratory-scale apparatus is made of quartz glass (Figure 8.1). An external electrical heater surrounds the dense bed zone, and its temperature is controlled by means of a thermocouple attached to the outer heated wall. The fluidizing air supplied to the CFB is pre-heated in a fixed bed pre-heater to 900°C, before entering the porous ceramic distributor at the base of the fluidized bed. A cyclone on top of the riser separates the entrained solid particles from the gas. The trapped solids are returned to the bed through a central downcomer. A small draft tube located in the lower bed section is also used to promote solid circulation and prevent slugging.

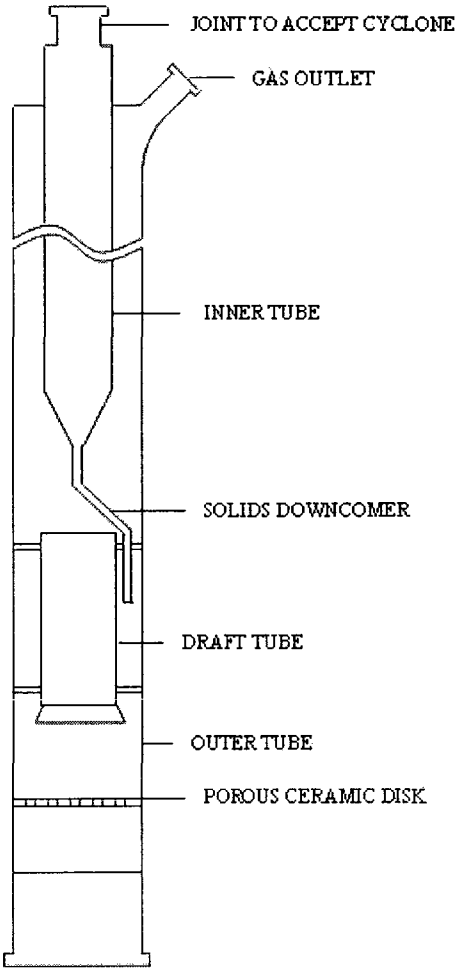

Figure 8.1: Quartz CFB Attrition Test Apparatus

For each run a 250 g limestone sample was fed into the CFB through its gas exit opening. The particles were fluidized with air, and the air pre-heater and the heater around the fluidized bed were switched on. It took about 90 to 120 minutes for the bed to reach the desired temperature of 850°C. During the heating period the air flow rate was continuously adjusted to maintain a superficial gas velocity of 3.5 m/s in the riser. On reaching the desired bed temperature, the operation was continued for 3 hours. The bed was then cooled and the sample removed and weighed to estimate the loss of fines due to attrition. The particle size distribution (PSD) of the samples was then determined using a sonic sifter. The extent of attrition due to calcination was estimated by comparing the PSD of materials remaining in the bed before and after the hot CFB experiment. It was assumed that the effect of attrition on the PSD is negligible, since fines generated by attrition were mostly elutriated. Even though the conditions in the laboratory-scale unit were not identical to an industrial unit, the test results enable one to compare attrition properties of different limestones under the same conditions.

It should be noted that, when the reactor was heated over a period of 90-120 min, calcination would start gradually. The particles would not suffer thermal shock, as they normally do in a CFBC combustor, which is likely to aid attrition.

It is arguable whether constant gas velocity or constant fluidization number, U/U_{mf} is more important (where U is the superficial gas velocity and U_{mf} the minimum fluidizing velocity). However, many variables affect the U_{mf}. The volumetric gas flow is also influenced by the CO_2 evolved during calcination, although the effect will be small since the heating rate was quite low. U_{mf} depends on the temperature and properties of the fluidizing gas. In addition, the properties of the solids, both density and size, vary as a function of time and temperature. All of these factors made keeping U/U_{mf} constant during the heating period impractical. Therefore, constant fluidizing gas velocity was maintained throughout the duration of the attrition test.

Two limestone samples from Alberta (TP1 and TP2) were first pre-sieved into size fractions of a, b and c with particle size ranges of 850-1000 μm, 600-850 μm, and 75-600 μm, respectively. As

agglomeration of particles occurred in some tests, it was decided to perform all subsequent tests in a pilot-scale CFBC.

8.3.2 Pilot-scale CFBC

The pilot-scale-CFBC has an internal diameter of 0.1 m and an internal height of 5 m (Figure 8.2). The bottom 0.95 m section of the riser is surrounded with four electrical heaters. There is a natural gas burner located 1.05 m above the distributor plate. During the attrition test, the pilot-scale-CFBC was heated with electrical heaters and natural gas combustion. Since the sulphur content of natural gas used was very low, virtually no sulphation of the material occurred. Two series of experiments were carried out first on the pilot-scale CFBC unit: rate of attrition testing; and experiments where the bed material was alternately calcined and carbonated. A final set of experiments was then carried out in which a known amount of SO_2 was added with the calcining gases to determine how sulphation affected attrition.

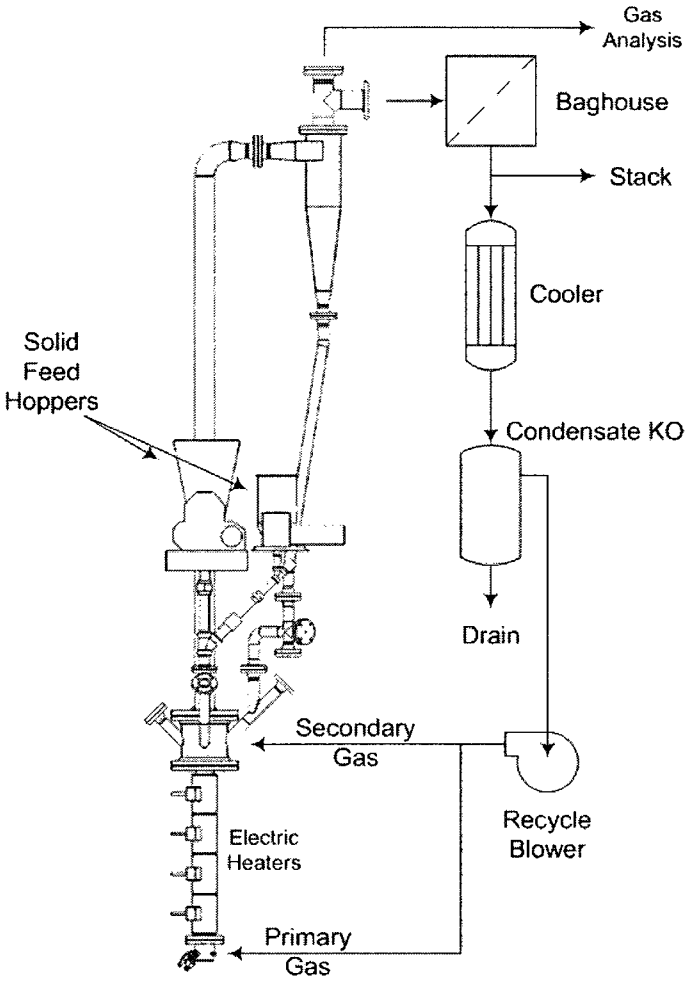

Figure 8.2: Pilot-scale CFBC – scaled 3D solid model. Riser is 4" pipe.

The longer duration testing lasted for 5.5 h for Tamuin (Mexican) limestone and 4.5 h for NISCO (US) and Cadomin (Canadian) limestones. The fluidized bed temperature (lower 1 m section of the riser) was 810 ± 20°C, and the average temperature of the riser was 550 ± 40°C. Superficial gas velocity in the riser was 1.4 ± 0.1 m/s. It is assumed that all materials recovered from the duct linking the cyclone and the bag house, and from the bag house itself, are fully calcined. This assumption was made to avoid exaggerating the contribution of the fines elutriated to the final particle size distribution. Even if very fine particles were carried out of the system in their first pass and were not fully calcined, their size should not change much, and in large industrial FBC systems they will be fully calcined.

Experiments with alternating calcination and carbonation cycles were conducted in the pilot-scale-CFBC at a superficial gas velocity of 0.35 m/s at 850°C for the calcination period, and 1 m/s at 700°C during the carbonation period. Gas velocity at the L-valve was 2.2 m/s as it returned to the riser. For the carbonation process a synthetic flue gas was used consisting of 15% CO_2, with the balance air; for calcination air was the fluidizing gas.

8.3.3 Materials

The limestone samples were calcined at 850°C in a box furnace to measure their weight loss on heating. Limestone samples were weighed, loaded into crucibles and placed in the furnace. The samples were retrieved after 2 h, cooled in a desiccator and weighed again. The particle size distribution of the limestone for these tests was determined by sieve analysis. The size distribution of materials recovered from the pilot-scale CFBC after the attrition test was also determined by the same method.

Cadomin limestone was received in large chunks and was pulverized in a disc pulverizer to the required size range.

The Havelock material was available at the appropriate size for the tests. Double-sieved bed material (125 μm to 1400 μm) was added at the beginning of the run with air injected through the distributor. Mass flow rate of air was held constant throughout the warm-up period. External electric heaters were used to heat the fluid bed to 850°C. The superficial gas velocity was 0.35 m/s at 850°C. The bed material was calcined at 850°C until CFBC flue gas contained less than 0.2% CO_2. At the completion of the calcining period the bed material was removed and weighed. The extent of attrition, A, was calculated with appropriate correction for the reduction in particle mass after calcination. A 100 g sample was retained to determine PSD and sphericity. The bed material was then returned to the CFB and heated to 700°C in air. The material was carbonated using a pre-mixed stream of air and CO_2 for a period of 20 min at a superficial gas velocity of 1 m/s. On completion of the carbonation period the bed was reheated to 850°C and calcination repeated. The calcination step was completed five times for Havelock limestone and only three times for Cadomin limestone (due to excessive material loss).

Sphericity was determined using a CCD-equipped microscope and Buehler Omnimet image analysis software. Limestone particles were identified by setting image threshold limits within the software. The particles analyzed were limited to those in the range between 50 μm and 1400 μm. Perimeters and areas required for the calculations were determined by software through pixel counting algorithms. Particle sphericity, S, was calculated according to:

$$S = \frac{4\pi Ap}{P^2} \qquad 8.6$$

where Ap is the apparent area of a particle, and P is the perimeter of a particle. The mean sphericity was determined for multiple fields of view for the fresh limestones and for each of the samples removed from the fluid bed. The sphericity was determined for 26 to 45 particles for each calcination cycle.

8.4 Results and Discussion

8.4.1 Laboratory CFB

The quartz test rig was used to look at how different size fractions would respond, to obtain a general idea of how attrition might vary between different particle size fractions under more realistic conditions. Table 8.2 gives the mean sizes of the particles before and after testing and appears to show that the finest particle size is most resistant to attrition, but for the larger particle size ranges there is a clear change in particle size.

Table 8-3Table 8.3 gives the attrition characteristics of two limestones in terms of the parameters R and A. These results show significant differences between the two limestones, which both come from Fort McMurray, Alberta. Unfortunately, on more detailed analysis it became clear that the numbers generated in this test series have to be treated with caution as both limestones showed clear agglomeration behaviour in this test apparatus. For particles in the c size range (*i.e.*, those with an initial size range of 75-600 μm), there was evidence of 1-3% by mass of particles being formed with size ranges above 600 μm, *i.e.*, larger than the initial size range. No evidence of agglomeration was found with particles in the larger size range; however, we speculate that the test rig may be too small and thus allows sticking of particles on walls. As the possibility of agglomeration necessarily compromises the test results, in consequence it was decided to work directly with the pilot-scale CFBC plant for all remaining work.

Table 8-2: Mean particle size before and after quartz CFB attrition run

Limestone	Initial d_p, μm	Final d_p, μm
TP1a	845 (850-1000)	799
TP1b	673 (600-850)	442
TP1c	166 (75-600)	165
TP2a	833(850-1000)	572
TP2b	627(600-850)	381
TP2c	192 (75-600)	197

Table 8-3: Comparison of attrition between two limestones (TP1 and TP2) in quartz CFB

Sample	R (1/h)	*A* %
TP1a (850-1000μm)	0.0045	2.04
TP1b (600-850 μm)	0.00284	1.29
TP1b*(600-850μm)	0.00427	1.94
TP1c (75-600 μm)	0.0022	0.994
TP2a (850-1000μm)	0.00869	3.99
TP2b (600-850 μm)	0.00511	2.33
TP2c (75-600 μm)	0.00868	3.99

* Repeated result

8.4.2 Pilot-scale CFBC

Rate of Attrition.

Tamuin limestone was used first in the pilot-scale CFBC attrition test. The box furnace test showed that, upon calcination, the limestone sample lost 43.18% of its weight (average of two determinations).

The initial charge of limestone into the CFBC was 8.05 kg. After 4 h of continuous operation, the amount of material collected from the riser and the back leg was 2.866 kg. Since the limestone will lose 43.18% of its original weight upon calcination, the amount of material that escaped from the cyclone should be

$8.05 \times (1-0.4318)-2.866 = 1.708$ kg

Based on these data and the sieve analysis, the particle size distribution of this limestone before and after the attrition test is shown in Fig. 8.3. Particle size distribution for materials recovered from the bag house and the ductwork is shown in Table 8-4. Results in Table 8-4 show that material that

escaped the cyclone was extremely fine, with 87.4% smaller than 75 μm and only 1.33% in the size range > 250 μm.

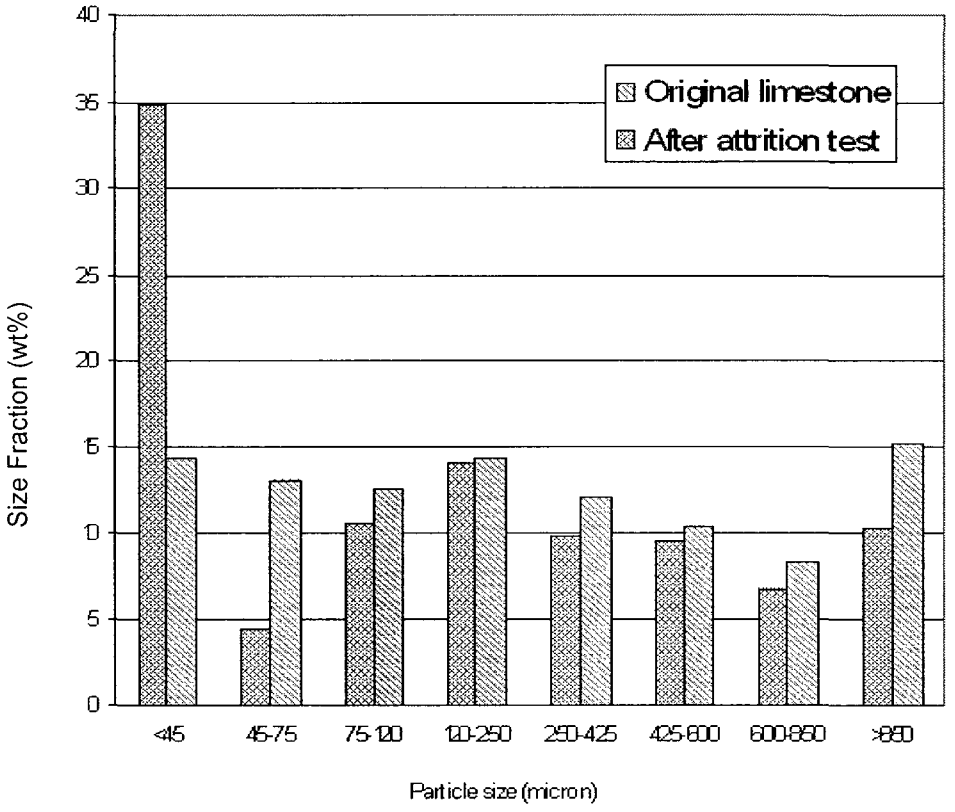

Figure 8.3: Variation of particle size distribution of Tamuin limestone. Test conducted in pilot-scale CFBC. The temperature of the fluidized bed (lower 1 m section of the riser) was 810 ± 20°C, and the average temperature of the riser was 550 ± 40°C. Superficial gas velocity in the riser was 1.4 ± 0.1 m/s. Test duration was 5.5 h.

Table 8-4: Particle size distribution for materials recovered from bag house and the duct after Tamuin limestone attrition test

Size, μm	Weight percent
>250	1.33
150-250	2.28
106-150	2.66
75-106	6.32
45-75	4.47
38-45	12.48
0-38	70.47

Particles in the very fine size fraction (0-45 μm) more than doubled their share in the mixture. Average attrition rate, R, and extent of attrition, A (corrected to 4.5 h to be comparable with previous data, assuming during these long tests, attrition is linear with time), based on equations 8.4 and 8.5, are calculated with corrections for limestone calcination loss determined in the box furnace test. The results are shown in Table 8-5.

Table 8-5: Attrition rates for CFB limestone tests

Limestone	Average R, 1/h	A, %
Tamuin	0.0324	14.60
TP1	0.00284-0.00450	1.29-2.04
TP2	0.00511-0.00869	2.33-3.99
NISCO	0.0877	39.47
Cadomin	0.0130	5.86

Table 8-5 also contains attrition test results for the two Alberta limestone samples. As noted, these results were obtained after 4.5 h of operation at a bed temperature of 850°C. The superficial gas velocity was 3.5 m/s. It can be seen that the Tamuin limestone is much more susceptible to attrition than are the two Alberta limestones. However, caution must be taken as the two sets of data were obtained in different scales of experimental apparatus and the initial particle size distributions of the two Alberta limestones were coarser than the Tamuin test sample (with 10.2 wt% <75 μm for TP1 and only 5.9 wt% <75 μm for TP2 compared to 26.83 wt% <75 μm for the Tamuin sample).

NISCO and Cadomin limestones were tested under the same conditions in the same CFBC. The particle size of the NISCO limestone provided to CETC-Ottawa was 1.5-2.5". It was crushed using laboratory-scale crushers. Particle size distributions for NISCO and Cadomin limestones before and after attrition tests are given in

Figure 8.5 and

Figure 8.5, respectively. The NISCO limestone contains a large amount of particles in the size range of 75-150 μm. This is the result of the laboratory crusher. The NISCO sample also showed a large increase in fines after the attrition test. The average attrition rate and the extent of attrition for NISCO and Cadomin limestones are also given in Table 8-5.

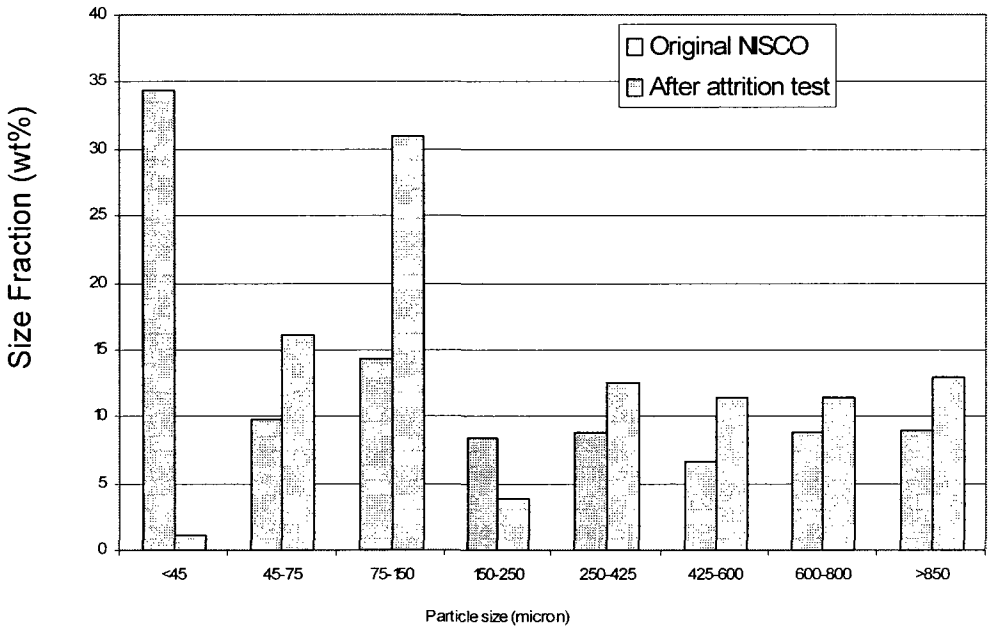

Figure 8.4: Particle Size Distribution for NISCO Limestone. Test conducted in pilot-scale CFBC. The temperature of the fluidized bed (lower 1 m section of the riser) was 810 ± 20°C, and the average temperature of the riser was 550 ± 40°C. Superficial gas velocity in the riser was 1.4 ± 0.1 m/s. Test duration was 4.5 h.

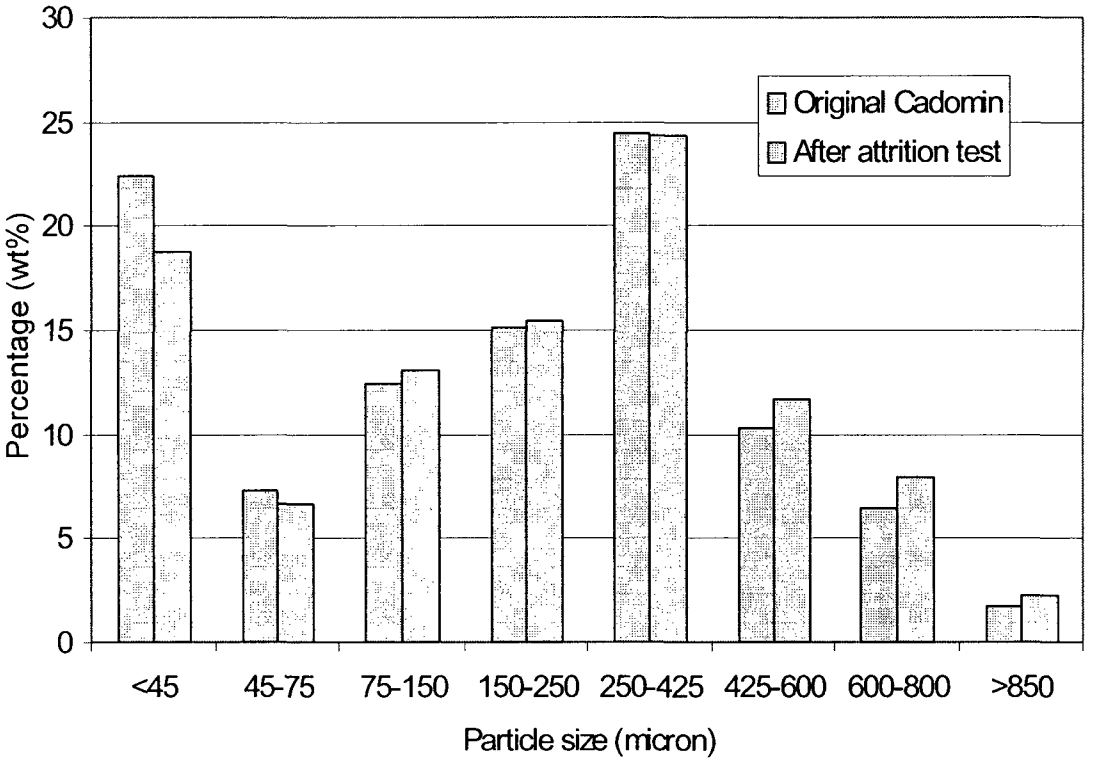

Figure 8.5: Particle Size Distribution for Cadomin Limestone. Test conducted in pilot-scale CFBC. The temperature of the fluidized bed (lower 1 m section of the riser) was 810 ± 20°C, and the average temperature of the riser was 550 ± 40°C. Superficial gas velocity in the riser was 1.4 ± 0.1 m/s. Test duration was 4.5 h.

Alternating Calcination and Carbonation.

Images of fresh and calcined Havelock and Cadomin limestone were taken (not shown here). The Havelock samples contain very few 'fines', while the Cadomin samples contain more. The fines in the Cadomin sample were small enough that electrostatic forces caused them to agglomerate on the microscope slide to a certain extent as the sample was being prepared. For both Havelock and Cadomin samples, the fresh limestones have a more jagged appearance than the calcined samples.

The Cadomin limestone showed a greater degree of elutriation and subsequent loss of material through the cyclone than did Havelock limestone during the first calcination cycle. Figure 8.6 shows the total mass of material in the CFBC at the completion of each calcination cycle. The data points indicated by 'Lime eq' (lime equivalent) indicate the mass of the initially loaded bed material assuming calcination had been completed with no loss of material from the CFBC. Both limestones had a rapid initial loss in bed mass during the first calcination, and a reduced rate of bed mass loss during subsequent calcination periods. Only three cycles were completed on Cadomin limestone.

Figure 8.7 shows the extent of attrition for both Havelock and Cadomin limestones over multiple cycles. It is apparent that the Cadomin limestone has undergone a great deal more attrition than has the Havelock limestone. The Havelock sample experiences the greatest attrition during the first calcination cycle, with relatively little attrition in subsequent calcination cycles. Cadomin limestone experiences a great deal of attrition during the first calcination period and then substantial attrition in the second calcination cycle. Attrition of the Cadomin limestone appears to be reduced in subsequent cycles.

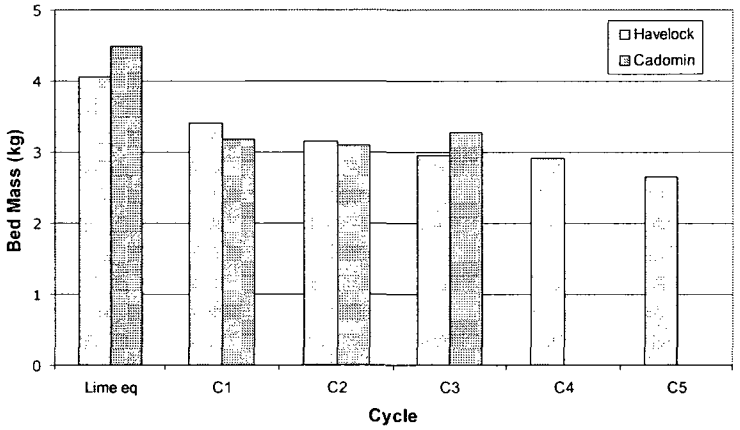

Figure 8.6: Bed mass over multiple calcination cycles. Test conducted in pilot-scale CFBC. Calcination was at 850°C and 0.35 m/s superficial gas velocity.

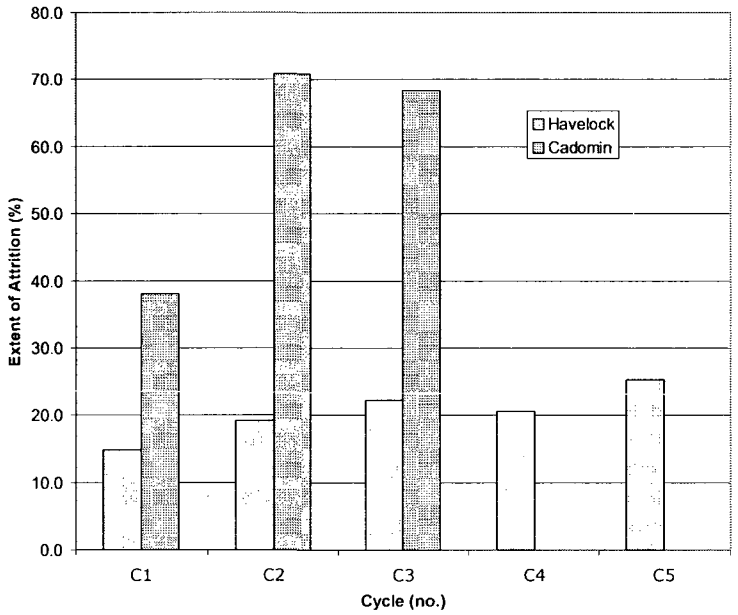

Figure 8.7: Extent of attrition over multiple calcination cycles. Test conducted in pilot-scale CFBC. Calcination was at 850°C and 0.35 m/s superficial gas velocity.

The particle size distributions of the Havelock and Cadomin limestones, Figure 8.8 and, Figure 8.9 respectively, give some information on how this attrition is proceeding. The Havelock PSD indicates that there is a shift in mass distribution from the larger size ranges to both the 425-600 micron range and the 75-125 micron range during the first calcination cycle. This may be indicative of the jagged peaks, seen in the fresh limestone, cleaving off. The process is probably not unlike that which produces beach pebbles, only much faster, since the sorbents are relatively soft. All rough corners are knocked off, so that the particles tend to become rounded. The Cadomin limestone shows a more rapid reduction of particle size from the larger size ranges to the 75-125 micron and 125-425 micron size ranges, indicating that the particles are initially fragmenting, cleaving off large pieces of stone. The Cadomin particles have a plate-like structure as a result of size reduction produced in a disc pulverizer rather than a crusher (which does not rule out some influence from the Cadomin limestone properties). It would appear that the initial size reduction of the Cadomin particles is more akin to a plate shattering than to the peak shaving that is expected from a more spherical particle. The significant attrition by this mechanism has resulted in an extent of attrition far greater than that seen in the rate of attrition test discussed earlier. Particles in the size fractions of 425-600 and 600-850 μm appear to have increased. It seems unlikely that this was the result of agglomeration; instead the increase was probably due to the result of particle size distribution shift due to the loss of fines coupled with experimental uncertainty.

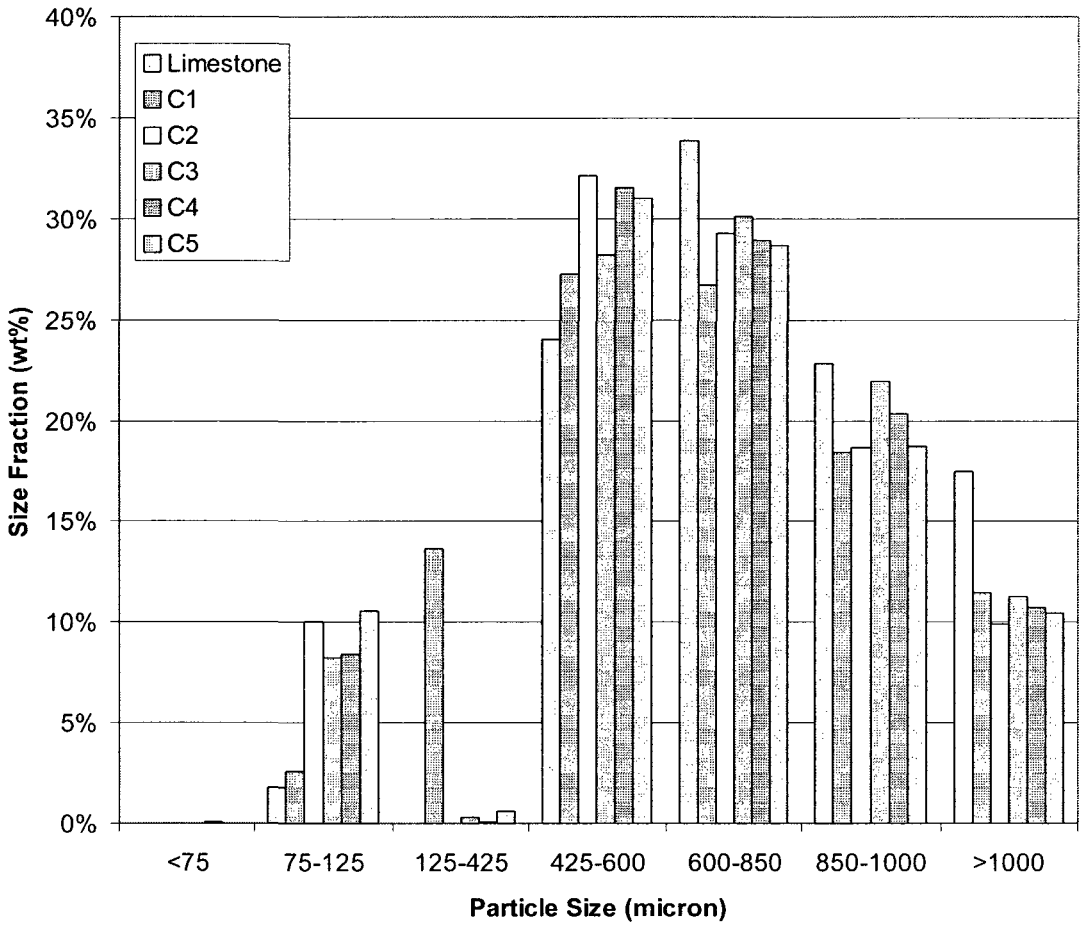

Figure 8.8: Particle size distribution of Havelock limestone through multiple calcination cycles. Test conducted in pilot-scale CFBC. Calcination was at 850°C and 0.35 m/s superficial gas velocity.

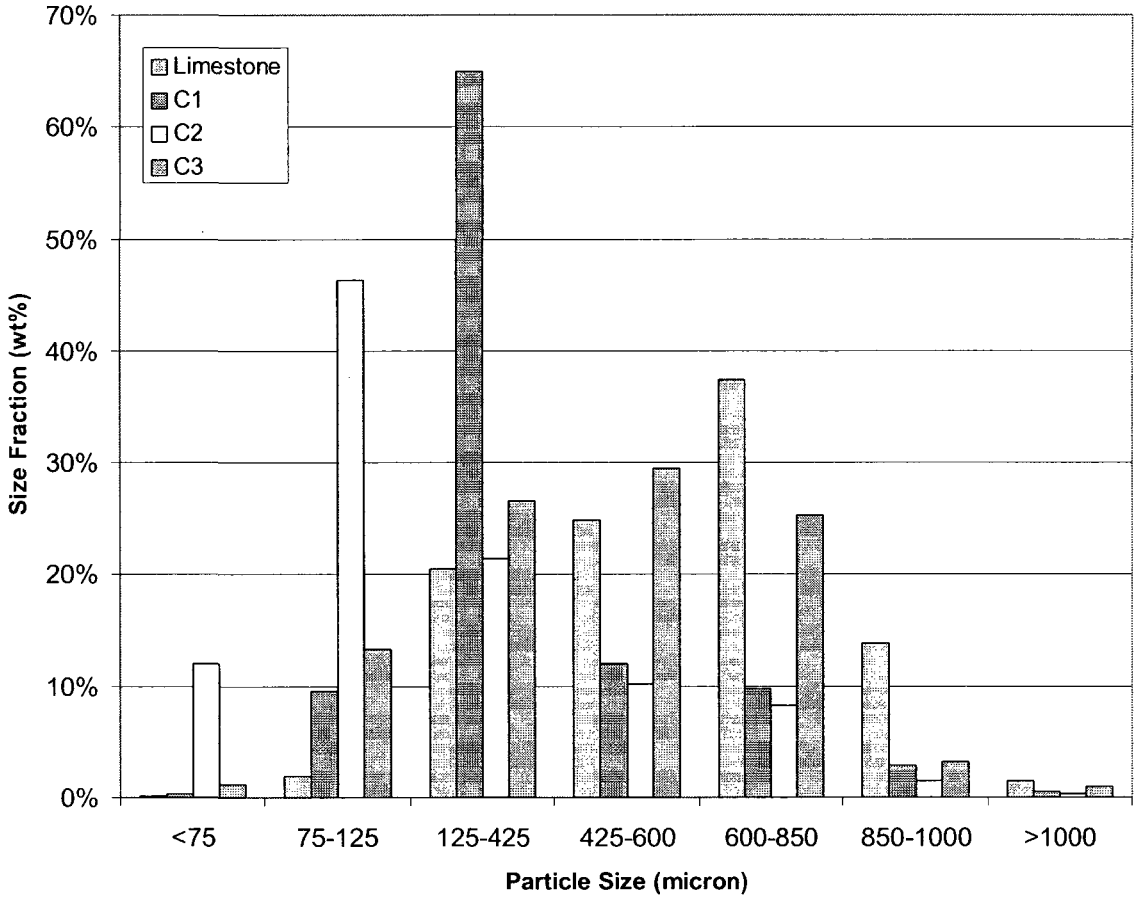

Figure 8.9: Particle size distribution of Cadomin limestone through multiple calcination cycles. Test conducted in pilot-scale CFBC. Calcination was at 850°C and 0.35 m/s superficial gas velocity.

The sphericity of the Cadomin and Havelock limestones over multiple calcination cycles is shown in Figure 8.10 The Havelock limestone displayed increased sphericity upon completion of its initial calcination. For Cadomin limestone sphericity at first falls slightly, but then increases. The Cadomin stone has a lower sphericity than the Havelock. However, sphericity may not be the most appropriate shape factor for gaining an understanding of attrition phenomena when size reduction results in plate-like particles.

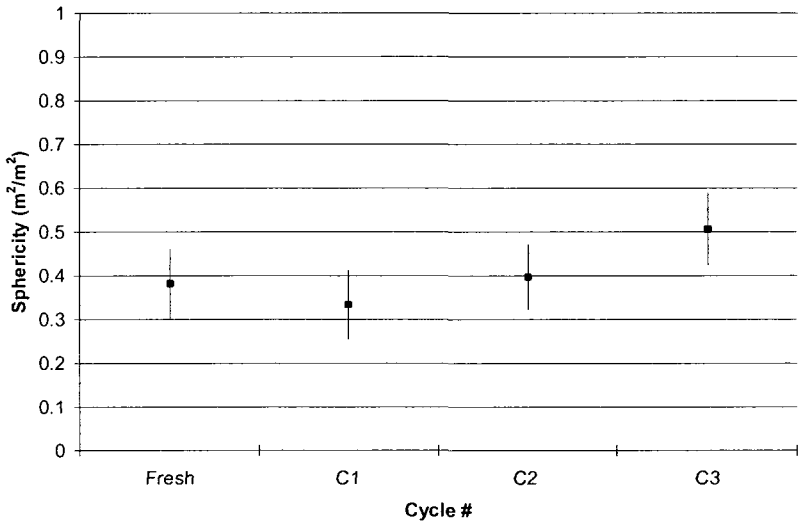

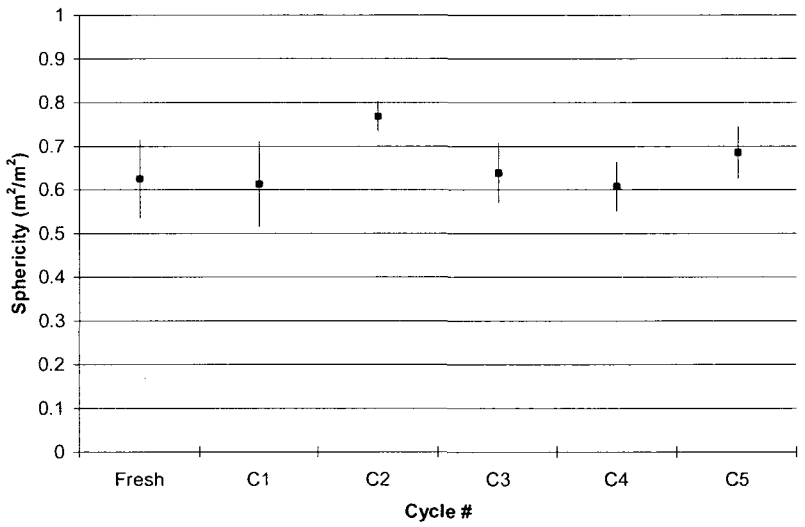

Figure 8.10: Sphericity of Havelock (top) and Cadomin (bottom) limestones over multiple calcination cycles. Test conducted in pilot-scale CFBC. Calcination was at 850°C and 0.35 m/s superficial gas velocity. 95% confidence interval.

Fuertes *et al.* (1991) studied attrition of limestone at room temperature for particles with an initial size range of 0.5-1.0 mm and fluidization velocity of 0.7 m/s. They found that during the initial period, the attrition rate decreased with time. Over 4.5 h the extent of attrition was about 0.6%. Clearly the calcined limestone samples are more fragile than uncalcined limestones used by Fuertes *et al.*

However, the high velocity (1.4 ± 0.1 m/s *vs.* 0.7 m/s) and very much higher temperature (810 ± 20°C, which allows calcination, *vs.* room temperature) and much finer initial particle size distribution (greater specific area) may also explain at least in part the higher attrition rate observed for the Tamuin limestone. It is also interesting to note that there was no evidence of agglomeration phenomena and we conclude that these results give a reasonably reliable measure of both the extent and rate of attrition that will occur in real systems. These results also show that there is considerable variation between limestones in terms of the extent of attrition since even for the five limestones examined here, attrition is shown to vary by more than an order of magnitude under CFBC conditions.

Cadomin limestone was used in both the rate of attrition testing and in the alternating calcination and carbonation experiments. The limestone showed remarkably different extents of attrition between the two types of tests. Although the limestone was from the same source, the material was crushed with a jaw crusher in the first case and pulverized with a disc mill in the second case. The disc pulverizer tended to form more plate-like particles in the course of size reduction. This form of particle should be subject to more attrition than the more spherical particles formed with the jaw crusher.

In order to investigate the effect of sulphation on the attrition of sorbents used to capture CO_2 in looping cycles, runs were carried out with both Havelock and Cadomin limestones with SO_2 added to the fluidizing gas. These experiments were done for two reasons: to assess whether a small amount of sulphation could make a significant improvement in reducing material loss in multiple carbonation/calcination cycles; and to assess how drastically the carbonation behaviour of the sorbent had been reduced by the final cycle with very "light" sulphation, since it appears that SO_2 limits the CO_2 carrying capacity or reversibility in multiple cycles (Sun et al., 2005).

For the Havelock test, 1800 ppm of SO_2 was added to the air for 30 min during the calcination period at a temperature of about 880-900°C. The carbonation process was carried out without SO_2 addition at 700°C. Here a SO_2 analyzer was used to measure the SO_2 in the flue gases. However, this was effectively zero as expected in this situation where limestone is in such large excess. Calculations indicated that the sulphation levels of the sorbent increased by approximately 0.13% in each calcination cycle, reaching about 0.4% by the end of the third cycle. For Cadomin limestone the sulphation levels were around 1.3% by the second cycle.

The calcined bed material was removed through the bottom discharge nozzle. The recovered material was weighed and a 100 g sample was collected and sieved in order to obtain the size distribution of the particles after the first calcination. The same process was repeated after each carbonation/calcination cycle. As with previous experiments without SO_2 addition, the 100 g samples were further analyzed with a CCD-equipped microscope. Buehler Omnimet image analysis software was used to calculate the sphericity and roughness of these samples.

For Cadomin limestone, SO_2 was added only during the first two cycles. The effect of SO_2 addition on the mass loss for Cadomin was quite remarkable (Figure 8.11), and in the first cycle only 10% of mass was lost (allowing for sulphur capture), and even by the fourth cycle, cumulative weight loss was only 28%. This is compared with nearly 40% material loss for the first cycle and nearly 70% by the third cycle, at which point the previous experiments without SO_2 addition were terminated due to material loss in Cadomin runs. However, the carrying capacity of the sorbent also appeared to fall considerably based on the weight gain (equivalent to 17% CO_2), whereas a figure of around 40% would be expected by the fourth cycle, based on modeling (Wang and Anthony, 2005). Again analysis of the material from the fourth carbonation cycle was carried out. This indicates a $CaSO_4$ content of 0.75%, while the CO_2 content of this material was only 11.7%, which is even lower than the 17% calculated. TGA data for this single cycle, here equivalent to a fifth cycle, gave the conversion rate for Cadomin as 27% and 35% at 30 min and 60 min of carbonation again supportive of considerable fall-off in activity.

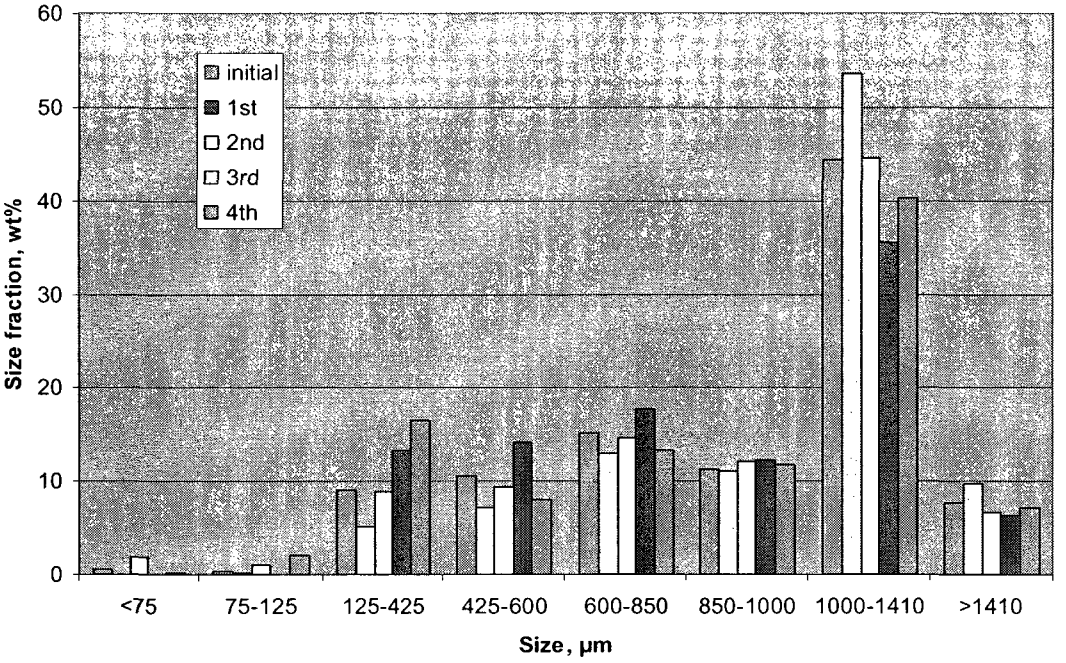

Figure 8.11: Particle size distribution of Cadomin limestone through multiple calcination cycles, with 1800 ppm SO_2 addition during calcination. Test conducted in pilot-scale CFBC. Calcination was at 880-890°C and 0.35 m/s superficial gas velocity for 30 min

For Havelock limestone (Figure 8.12), the weight loss was about 13% in the first cycle, and then it remained almost constant over the next two cycles, compared with a 25% loss by the third cycle in tests without SO_2 addition. The CO_2 carrying capacity has been calculated based on weight gain during the carbonation cycle at about 36%, which does not suggest much change from what one might expect on the basis of reversibility without sulphation (Wang and Anthony, 2005). Direct chemical analysis of the carbonated material in the third carbonation cycle gave values for CO_2 content of 26.4% which is again somewhat lower than the value calculated on the basis of weight gain.

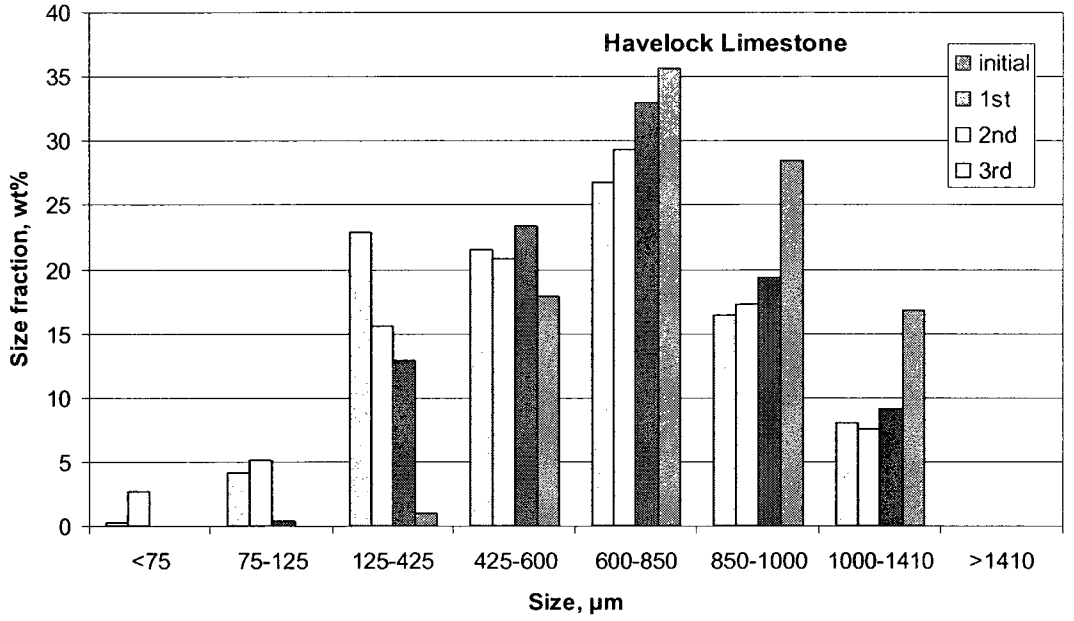

Figure 8.12: Particle size distribution of Havelock limestone through multiple calcination cycles, with 1800 ppm SO_2 addition during calcination. Test conducted in pilot-scale CFBC. Calcination was at 880-890°C and 0.35 m/s superficial gas velocity for 30 min.

For comparison the $CaSO_4$ content of this sample was 0.96%. As a cross check, some of the sample from the third carbonation cycle were first calcined in N_2 to 900°C (at 30°C/min heating rate) and then carbonated for what amounts to a fourth cycle in 15% CO_2 (N_2 balance) at 700°C for 60 minutes in a Perkin Elmer TGA 7HT. The CO_2 capture was surprisingly high, *i.e.*, 50% and 54% at 30 min and 60 min of carbonation, respectively. The carbonation results in the FBC are in line with previous FBC results that showed that Havelock achieved much higher levels of carbonation in the pilot-scale FBC than did Cadomin (Salvador et al., 2003). Another interesting observation was that the sulphate content in the non-elutriated material appears to be preferentially retained, as has been reported previously (Scala et al., 1997).

For both sorbents the measured sphericities are around 0.7 rising to about 0.75 by the third cycle. The reason for the discrepancies between earlier runs with Havelock and Cadomin without SO_2 addition is not clear, but results suggest that there may be small variations in sphericity between batches of samples, in which case sphericity measurements must be used with caution.

It is clear that if any loss of activity can be reversed by a reactivation technique, then it may be worthwhile to allow some sorbents to become partially sulphated before use in a $CaO\text{-}CaCO_3$ looping cycle, since there is a clear and very dramatic reduction in material loss for sorbent treated in this manner. This could be done in two ways: either by regenerating the sorbent in the calcination cycle with a sulphur-containing fuel, as has been suggested by the authors previously (Wang et al,. 2004); or by taking materials that have first been used in a CFBC, then reactivating for CO_2 capture (Sun et al., 2005; Salvador et al., 2003). However, either scenario still envisages separating the SO_2 and CO_2 capture processes, which fortunately still appears to be economically promising compared with amine scrubbing (MacKenzie et al,. 2006), a process that has often been suggested for CO_2 capture from coal-fired electricity generation plants.

8.5 Conclusions

Attrition tests have been conducted in a quartz reactor and a small pilot-scale CFBC using limestone beds. Results indicate that, even for the limited number of limestones tested, the degree of attrition varied considerably. Tests in a small-scale reactor indicated some degree of agglomeration (possibly due to wall effects) and also suggest that agglomeration is greater than reported from earlier bubbling bed studies. Subsequent tests were conducted in a pilot-scale CFBC, which showed no signs of this phenomenon. Tests using Cadomin limestone, where both disc pulverizers and jaw crushers were used for size reduction, indicated that the method of size reduction may have a significant effect on the rate of attrition.

This work suggests that multiple carbonation/calcination cycles result in severe attrition during the first one or two calcination periods. Afterwards, the particles attrite at rates similar to what would be expected from a bed of particles continuously subjected to similar forces over an extended period of time. In limestones where material loss is a problem, however, it is clear that partial sulphation can dramatically reduce this loss, albeit with the risk of reduction of CO_2 carrying capacity or $CaO\text{-}CaCO_3$ looping cycle reversibility. A surprising finding is the relatively large effect of even slight sulphation on material loss. This suggests that partial sulphation may be useful in reducing material loss for susceptible limestones if a way can be found to either retain reversibility, or more likely to recover

reversibility by means of a reactivation technique, or if the loss of activity can be minimized by keeping sulphation levels low.

8.6 References

Abanades, J.C., Anthony, E.J., Alvarez, D., Lu, D.Y. and Salvador, C., (2004). 'Capture of CO_2 from Combustion Gases in a Fluidized Bed of Lime', AIChE Journal 50(7), 1614.

Abanades, J.C., Alvarez, D., Anthony, E.J. and Lu, D., (2003). 'In situ Capture of CO_2 in a Fluidized Bed Combustor', Paper No. 10, Proceedings of the 17th International (ASME) Conference on Fluidized Bed Combustion.

Abanades, J.C., Anthony, E.J., Wang, J. and Oakey, J., (2005). 'Fluidized Bed Combustion Systems Integrating CO_2 Capture with CaO', Environmental Science and Technology 39, 2861.

Aguayo, J.E., (1977). 'Sedimentary Environments and Diagenesis of a Cretaceous Reef Complex, Eastern Mexico, Instituto Mexicano del Petroleo.

Benedetto, A., and Salatino, P., (1998). 'Modelling Attrition of Limestone During Calcination and Sulfation in a Fluidized Bed Reactor', Powder Technology 95, 119.

Broster, B.E., Allaby, G.M., Pronk, A.G., 'Lithology and Geochemical Dispersal in Till: Petitcodiac Area, New Brunswick', Atlantic Geology 40(2), 169.

Chandran, R.R. and Duqum, J.N., in J.R. Grace, L.W. Shemilt and A.A. Bergougnou (Eds.), (1989). 'Attrition Characteristics Relevant for Fluidized Bed Combustion', Fluidization VI. Engineering Foundation, New York, 571.

Cook, J.L., Khang, S.J., Lee, S.K. and Keener, T.C., (1996). 'Attrition and Changes in Sized Distribution of Lime Sorbents in a Circulating Fluidized Bed Absorber', Powder Technology, 89(1) 1-8.

Couturier, M.F., Karidio, I. and Steward, F.R., in A.A. Avidan (Ed.), (1993). 'Study on the Rate of Breakage of Various Canadian Limestones in a Circulating Transport Reactor', Circulating Fluidized Bed Technology IV, Am. Inst. Chem Eng., New York, 672.

Forsythe, W.L. and Hertwig, W.R., (1949). 'Attrition Characteristics of Fluid Cracking Catalysts', Industrial and Engineering Chemistry 41(6), 1200.

Franceschi, J., Kolar, A., Miller, G., Zakkay, V., Ho, C., Skelley, S., and Hakim, S., (1980). 'Natural Sorbent Attrition Studies Related to Fluidized Bed Coal Combustion', Proceedings of the 6th International Conference on Fluidized Bed Combustion, 1028.

Fuertes, A.B., Pis, J.J., Garcia, J.C., Rubiera, F., and Artos, V., (1991). 'Prediction of Attrition in a Continuous Fluid-Bed System', Powder Technology, 67, 291.

Holter, M.E., (1975). 'Economic Geology Report 4 - Limestone Resources of Alberta', Alberta Geological Survey.

Hughes, R., Lu, D., Anthony, E.J., Wu, Y., (2004). 'Improved long-term conversion of limestone-derived sorbents for *in situ* capture of CO_2 in a fluidized bed combustor', Ind. Eng. Chem. Res. 43, 5529–5539.

Lee, S., Jiang, X., Keener, T.C. and Khang, S.J., (1993). 'Attrition of Lime Sorbents During Fluidization in a Circulating Fluidized Bed Absorber', Ind. Eng. Chem Res., 32(11), 2758.

MacKenzie, A., Granatstein, D.L. and Anthony, E.J., (2006). 'Economics of CO_2 Capture using the Calcium Cycle with a Pressurized Fluidized Bed Combustor', Paper No. 19, Proceedings of the 19th International Conference on Fluidized Bed Combustion.

Merrick, D. and Highley, J., (1974). 'Particle Size Reduction and Elutriation in a Fluidized Bed Process', AIChE Symp. Ser. 137, 366.

Ray, Y., Jiang, T.S. and Wen, C.J., (1987). 'Particle Attrition Phenomena in a Fluidized Bed', Powder Technology 49, 193.

Salvador, C., Lu, D., Anthony, E.J., Abanades, J.C., (2003). 'Enhancement of CaO for CO_2 capture in an FBC environment', Chem. Eng. J. 96, 187–195.

Scala, F., Cammarota, A., Chirone, R. and Salatino, P., (1997). 'Communition of Limestone During Batch Fluidized-Bed Calcination and Sulfation', AIChE Journal 43, 363.

Scala, F., Salatino, P., Boerefijn, R. and Ghadiri, M., (2000)., 'Attrition of Sorbents During Fluidized Bed Calcination and Sulfation', Powder Technology, 107, 153.

Sun, P., Grace, J.R., Lim, C.J. and Anthony, E.J., (2005). 'Simultaneous CO_2 and SO_2 Capture at Fluidized Bed Combustion Temperatures', Proceedings of the 18th (ASME) International Conference on Fluidized Bed Combustion, paper 78125.

Vaux, W.G., (1978). 'Attrition of Particles in the Bubbling Zone of a Fluidized Bed', Am. Power Conf. 40(1978), 793.

Vaux, W.G. and Keairns, D.L., (1980). 'Particle Attrition', in J.R. Grace and J.M. Matsen (Eds.), Fluidization Conf., Plenum, New York, 437.

Vaux, W.G. and Fellers, A.W., (1981). 'Measurement of Attrition Tendency in Fluidization', AIChE Symp. Ser. 205, 107.

Vaux, W.G. and Shruben, J.S., (1983). 'Kinetics of Attrition in the Bubbling Zone of a Fluidized Bed', AIChE Symp. Ser. 222, 97.

Wang, J., Anthony, E.J. and Abanades, J.C., (2004). 'Clean and Efficient Use of Petroleum Coke for Combustion and Power Generation', Fuel 83(10), 1341-1348.

Wang, J. and Anthony E.J., (2005). 'On the Decay Behavior of the CO_2 Absorption Capacity of CaO-Based Sorbents', Industrial and Engineering Chemistry Research 44(3), 627-629.

Chapter 9 Changes in Limestone Sorbent Morphology During CaO-$CaCO_3$ Looping at Pilot Scale

Published in Chemical Engineering and Technology

Hughes, R.W.[1], Macchi, A.[2], Lu, D.Y.[1], Anthony, E.J.[1], (2009). 'Changes in Limestone Sorbent Morphology during CaO-$CaCO_3$ Looping at Pilot Scale', Chem. Eng. & Tech 32(3), 425-434.

[1]Natural Resources Canada, CETC-O, 1 Haanel Drive, Ottawa, Canada K1A 1M1

[2]University of Ottawa, 161 Louis Pasteur, Ottawa, Canada, K1N 6N5

9.1 Abstract

A pilot-scale dual fluidized bed combustion system has been used for CO_2 capture using limestone sorbent with CaO-$CaCO_3$ looping. The sorbent was regenerated at high temperature using an air- or oxygen-fired fluidized bed calciner with flue gas recycle firing hardwood pellets.

Two limestones have been evaluated for CaO-$CaCO_3$ looping. Changes in the sorbent morphology during the tests have been identified by scanning electron microscopy (SEM) with energy dispersive X-ray spectroscopy (EDX). Changes in pore size distribution and sorbent surface area that occurred during reaction have been determined by N_2 porosimetry. Thermogravimetric analysis (TGA) has been used to determine the activity of the sorbent after processing in the dual fluidized bed combustion system.

It has been found that oxygen-fired calcination with high CO_2 partial pressure reduced the effectiveness of the two limestone sorbents for CO_2 capture when compared to material calcined under oxygen-enhanced air combustion. A shell 1-2 μm thick, with reduced porosity, has been formed around the sorbent particle and is believed to be responsible for reduced conversion of CaO to $CaCO_3$. It is believed that ash deposition is contributing to the formation of the shell.

9.2 Introduction

CaO-based CaO-$CaCO_3$ looping combustion is expected to be an energy efficient and cost effective carbon dioxide capture process that can be retrofitted to existing combustion systems or operate in new, more tightly integrated systems. To date the majority of research on the topic has been carried out using thermogravimetric analysis (TGA) with the $CaCO_3$ calcined under a N_2 atmosphere. Untreated limestones typically have reduced capacity for recarbonation after each reaction cycle with an initial rapid decrease in capacity eventually levelling off at a molar conversion of around 8-15% (Sun et al., 2008). In a commercial process the rate of decay in sorbent activity will increase as a result of a number of effects such as increased temperatures, increased CO_2 concentration, and ash impurities.

The reduction in capacity of the sorbent is due to sintering, resulting in reduced surface area and reduced suitable porosity for rapid gas diffusion into the sorbent interior. Three physical changes take

place during calcination: (1) formation of calcium oxide having a pseudo-lattice of calcium carbonate (rhombohedral), (2) recrystallization of the pseudo-lattice to a more stable calcium oxide lattice (face-centred cubic), and (3) sintering of the recrystallized CaO (Glasson, 1958). Sintering begins before recrystallization is complete, thus curves of specific surface area *versus* temperature of calcination show maxima at or near the temperature of calcination for which decomposition is just complete.

The presence of both CO_2 and water can increase the rate of sintering of CaO-based sorbents. Enhanced sintering in the presence of carbon dioxide may depend on the formation of carbonates at the surface of CaO by chemisorbed carbon dioxide (Glasson, 1961). H_2O vapour enhances the rate of crystal growth of CaO at temperatures as low as 300-400°C. Water may increase the mobility of ions by briefly forming surface hydroxyl groups (Anderson et al., 1965).

Ions with a different valence from Ca^{2+} such as K^+, Na^+, Mo^{3+}, when incorporated in a CaO lattice, result in defects that increase the rate of solid-state diffusion. Ions such as these have been shown to increase the rate of sintering of CaO (Borgwardt, 1989).

In this work we have operated a pilot-scale CaO-$CaCO_3$ looping system (Hughes et al., 2005) to determine the morphological changes that occur in the sorbent as a result of elevated CO_2 concentrations, high bulk temperatures required for calcination, even higher localized temperatures resulting from the combustion of the fuel required to provide the heat of calcination with high oxygen concentrations, and ash effects.

9.3 Experimental

9.3.1 Pilot Operations

The pilot operations for these tests were designed to investigate the changes in morphology of limestone with the reversible CaO-$CaCO_3$ reaction while minimizing side reactions such as direct or indirect sulphation that would obscure the effects of the primary reaction of interest. The operating conditions of the facility were intended to result in temperatures, partial pressures of CO_2, O_2, and H_2O, and particle mechanical stresses that would be expected in commercially operating equipment. Matching these conditions in the pilot facility with those of an operating facility should provide similar sintering rates and, hence, changes in sorbent morphology and sorbent activity at the two equipment scales. The changes in sorbent morphology will provide the basis for selecting appropriate particle

reaction models for calciner and carbonator reactor modelling in the future and may provide insights that will allow improved sorbent performance.

The CANMET Energy Technology Centre-Ottawa (CETC-O) dual fluidized bed combustion (FBC) system for CaO-$CaCO_3$ looping studies (Hughes et al., 2005) was used to calcine and carbonate limestone sorbent in a sequential manner. The test conditions are summarized in Table 9-1. First the sorbent was fully calcined in the calciner and then the entire batch of sorbent was conveyed with air to the carbonator. After a carbonation period of 70 min the sorbent was discharged from the carbonator through a transport line where the sorbent fell freely into the calciner. This cycle was repeated two or three times for each material and test condition, as time permitted. The heating rate of the sorbent was controlled to some extent in one of two ways. In the slow heating method the sorbent was heated gradually with electrical heaters in the fluidized bed to 600-650°C. Above this temperature combustion was initiated and the sorbent bed continued to heat gradually until calcination began. In the rapid heating method the sorbent was injected into the fluidized bed, which was operating at a temperature sufficient for calcination. Tests were completed for all test conditions with the slow heating rate method. In addition, the fast heating rate method was used for runs 1o-p, 1a-c, 1o-c, 1a-c-h, and 1o-c-h (see Table 9-1).

Table 9-1: Test conditions for pilot-scale operations

Sorbent	Calciner Fluidizing Gas	Fuel	Carbonator Fluidizing Gas (balance air)	Run ID
Katowice	Air	Low Ash	8% CO_2	1a-p
		Low Ash	8% CO_2, 17% H_2O(g)	2a-p
	Oxyfuel	Low Ash	8% CO_2	1o-p
		Low Ash	8% CO_2, 17% H_2O(g)	2o-p
Cadomin	Air	Low Ash	8% CO_2	1a-c
		Low Ash	8% CO_2, 17% H_2O(g)	2a-c
	Oxyfuel	Low Ash	8% CO_2	1o-c
	Air	High Ash	8% CO_2	1a-c-h
	Oxyfuel	High Ash	8% CO_2	1o-c-h

The calciner was operated as a bubbling fluidized bed combustor firing one of two types of wood pellets—low-ash or high-ash. The ash fusion, ultimate, proximate, and major oxides analyses for the fuels and two limestone sorbents tested, where appropriate, are provided in Table 9-2. The calciner was fluidized with oxygen-enhanced air or by oxygen with recycled flue gas.

In the oxygen-enhanced air firing mode the fluidizing gas composition was around 46 vol% N_2 and 54 vol% O_2. The flue gas exiting the calciner typically had a dry basis composition of 43 vol% CO_2, 2.5-7 vol% O_2, and balance mainly N_2. The fuel feed rate was maintained at 1.5 kg/h. Air and oxygen were mixed prior to entering the calciner windbox..

In the oxygen-fired mode the flue gas exiting the calciner passed through a baghouse that removed particulates. The gas was then cooled to approximately 15°C in a tube-in-shell heat exchanger arranged in such a fashion that the condensate that was formed could be removed from the system using a peristaltic pump. The flue gas was pressurized using a rotary lobe blower which resulted in a

flue gas temperature of approximately 30°C prior to mixing with the oxygen. Recycled flue gas and oxygen were mixed prior to entering the calciner windbox. Oxygen firing in these tests resulted in fluidizing gas composition of around 36 vol% CO_2, 60 vol% O_2, and balance mainly N_2. The flue gas exiting the calciner typically had a dry basis composition of 84-92 vol% CO_2, 2.5-7 vol% O_2, and balance mainly N_2. The fuel feed rate in oxygen-enhanced air firing mode was maintained at 1.7 kg/h.

The carbonator was fluidized with either 8 vol% CO_2 with balance air or 8 vol% CO_2, 17 vol% $H_2O_{(g)}$ with balance air, as indicated in Table 9-1. Water has been shown to have an effect on the rate of carbonation (Symonds, 2008) even at temperatures in excess of those where stable calcium hydrate is expected. The two fluidizing streams provided conditions in the carbonator that corresponded to wet and dry flue gases. Moisture content of the flue gas entering the carbonator may have an effect on how both retrofit and greenfield power plants are heat integrated with the CaO-$CaCO_3$ looping CO_2 capture system. The effect on heat integration may have a small, but noticeable, effect on the net efficiency of the system.

9.3.2 Sample Conversion

Loss in sample weight during heating to 850°C in an air atmosphere was used to determine the carbonate content of the sorbent from different locations in the pilot facility. The carbonate content was calculated *via* loss in mass assuming all changes in mass were due to the release of CO_2.

9.3.3 Scanning Electron Microscopy (SEM) with Energy Dispersive X-ray Spectroscopy (EDX)

Pilot plant samples were mounted on carbon stickers and analyzed by SEM with EDX with scale ranges between 10 and 60 μm. Magnification at this scale is suitable for seeing changes in the grain structure of the sorbent and surface structures of the particle. The EDX results provide semi-quantitative compositions for various surface and interior regions. The sum of component weight fractions for the analyses performed in this work range from about 0.2 to 0.55, so a significant portion of the sample is not accounted for. Where EDX compositions are provided, caution should be exercised in interpreting the results. The thermogravimetric analysis can increase the certainty in the EDX results by providing the degree of carbonation for the bulk of the particle.

Table 9-2: Ash fusion, proximate, ultimate, and major oxides analyses for fuels and sorbents

Analysis	High-ash Wood Pellet	Low-ash Wood Pellet	Katowice Limestone	Cadomin Limestone
Initial Softening, Oxidizing ASTM D1857, °C	1129	1215		
Fluid, Oxidizing ASTM D1857, °C	1235	1349		
Proximate, wt%				
Moisture	8.08	7.81		
Ash	4.69	0.68		
Volatiles	68.32	75.54		
Fixed Carbon	18.91	15.97		
Ultimate, wt%				
C	45.13	45.80		
H	5.07	5.52		
N	0.22	<0.10		
S	<0.05	<0.05		
O	36.76	40.04		
Major Oxides, wt%				
CaO	21.25	16.64	54.10	50.64
MgO	2.13	3.86	0.89	3.28
SiO_2	41.10	33.06	0.85	1.30
Al_2O_3	10.06	11.11	0.24	0.40
Fe_2O_3	3.78	3.16	0.09	0.11
TiO_2	0.45	0.262	<0.03	0.04
P_2O_3	1.10	2.00	<0.03	<0.03
SO_3	0.65	1.78	<0.100	<0.100
Na_2O	1.53	2.13	<0.20	<0.20
K_2O	4.15	13.02	0.06	0.14
Loss on fusion	12.48	10.91	43.64	43.99

9.3.4 N_2 Porosimetry

A porosimeter has been used with N_2 to determine the pore volume and pore surface area distributions of the sorbent samples.

9.4 Results

9.4.1 SEM with EDX

An SEM image of a particle from a sample taken at the end of the 2nd cycle of oxygen-enhanced calcination can be seen in Figure 9.1. This particle was calcined by burning low-ash wood pellets at 860°C with oxygen-enhanced air as fluidizing gas. The fluidizing gas was 53% oxygen with balance nitrogen. The particle has been broken in order to see both the surface and the interior. 'Spectrum 2' in Figure 9.1 shows the surface of the particle to be heavily sintered when compared to the interior of the particle in the area identified as 'Spectrum 1'. The surface layer appears to be thin, 1-2 μm thick, with greatly reduced porosity. This surface layer could pose significant resistance to mass transfer into and out of the particle resulting in increased time required for calcination and reduced carbonation conversion in the 'fast' reaction phase. The EDX results shown in Table 9-3 indicate that the interior of the particle is composed mainly of CaO, with other major oxides consistent with those in the parent limestone. The TGA results are in agreement with the EDX results for the particle interior indicating that there is almost no $CaCO_3$ present.

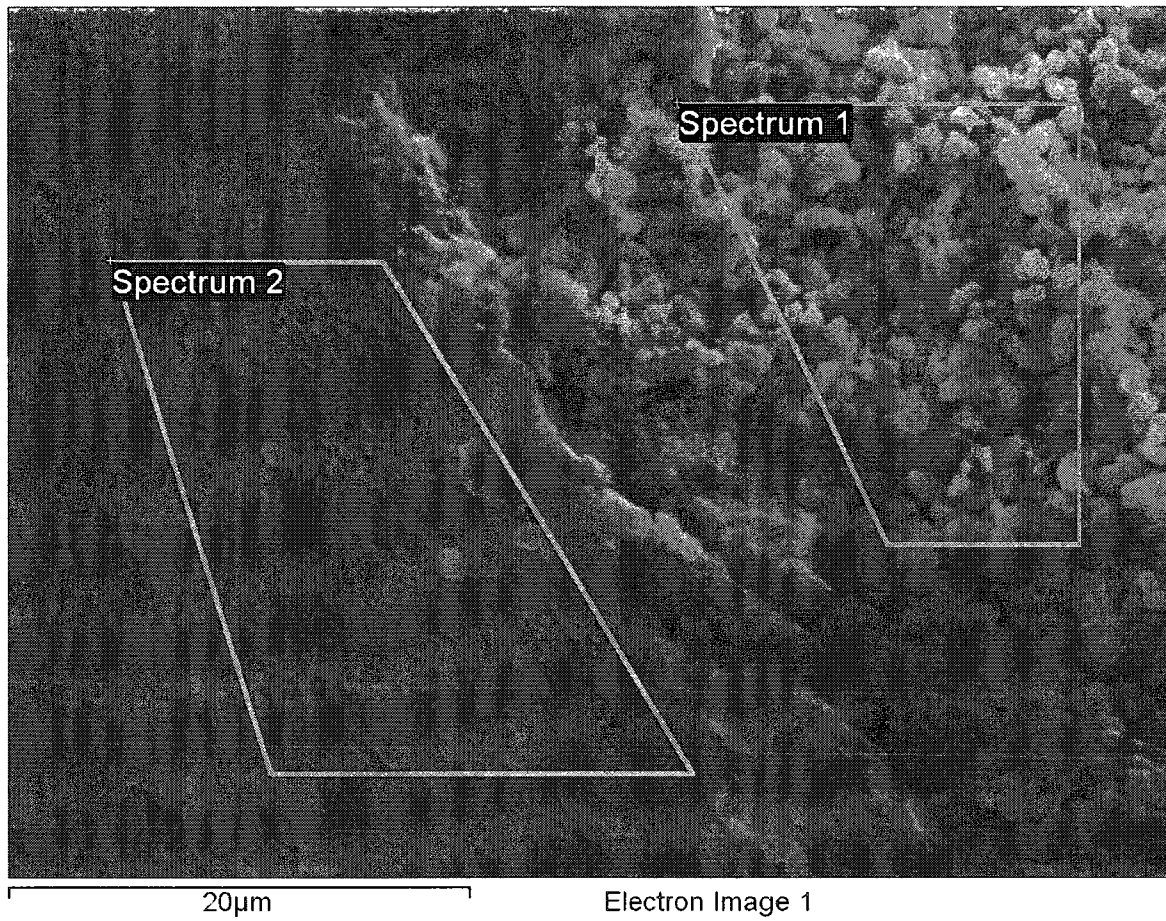

Figure 9.1 SEM image of a Katowice limestone particle calcined with a fluidizing gas of oxygen-enhanced air (53% O_2, balance N_2) burning low-ash wood pellets (860°C). 'Spectrum 1'- particle interior with partially carbonated CaO; 'Spectrum 2'- particle surface with major oxide composition similar to parent limestone.

Table 9-3: EDX results (wt%) for sorbent particles taken from calciner or carbonator with spectrums corresponding to those seen in Figures 9.1 to 9.5.

Spectrum	1-1	1-2	2-1	2-2	3-1	3-2	4-1	4-2	4-3	4-4	5-1	5-2
Run ID	1a-p	1a-p	1a-p	1a-p	1a-p	1a-p	1o-c	1o-c	1o-c	1o-c	1o-c	1o-c
C	1.84	0.15	16.22	2.81	1.36	5.36	4.23	20.2	24.12	4.33	1.07	2.81
O	23.24	5.5	10.7	15.91	10.35	26.79	21.71	10.54	11.83	21.87	5.69	17.03
Mg	0.19	0.18	0.28	0.41	0.06	0.75	0.69	0.27	0.21	0.43	0.11	0.09
Al	0	0	0	0.08	0	0.07	0.78	0.39	0.27	0.68	0.18	0
Si	0	0.2	0.13	0.22	0	0.19	1.47	0.7	0.52	1.42	0.39	0
Ca	26.95	15.04	12.51	20.96	20.21	21.4	22.06	11.46	9.76	22.51	16.33	23.46
Mn	0	0	0	0	0	0	0.22	0.11	0.08	0.19	0.09	0
Na	0	0.02	0.27	0	0	0	0	0.11	0.23	0	0	0
K	0	0.04	0.21	0	0	0	0	0.14	0.27	0	0	0
Fe	0	0.07	0	0.07	0	0.07	0.4	0.4	0.11	0.24	0.16	0
Sum	52.22	21.2	40.32	40.46	31.98	54.63	51.56	44.32	47.4	51.67	24.02	43.39

An SEM image of a particle that was calcined under the same conditions as the previously described particle and then carbonated at 600°C with a fluidizing gas of 8% CO_2 with balance dry air is shown in Figure 9.2. This particle has also been broken to see both the surface ('Spectrum 1') and the interior ('Spectrum 2'). The region identified as 'Spectrum 1' appears to be completely non-porous and would prevent gas phase diffusion of CO_2 into and out of the particle. The EDX results indicate elevated levels of Na_2O and K_2O in this area compared to the parent limestone, indicating that some fuel ash may have deposited on the surface. There is no evidence of these materials in the region identified as 'Spectrum 2'. The level of carbonation calculated for both regions (41-52%) are in excess of those determined for the bulk of the particle (16%), so it would appear that carbonation occurs at or near the surface of the particle more so than deep within the particle. This can be seen more clearly in Figure 9.3, which was drawn from the same sample as that shown in Figure 9.2. The particle in this figure does not appear to have any ash deposition on it, as evidenced by both EDX and the absence

of the non-porous layer seen in Figure 9.2. It is believed that this is a particle that fragmented after transport from the calciner to the carbonator. The surface ('Spectrum 2') is fully carbonated according to the EDX results, while the particle interior has approximately the same degree of carbonation as determined by loss-in-weight for the whole particle; 14% *vs.* 16%, respectively.

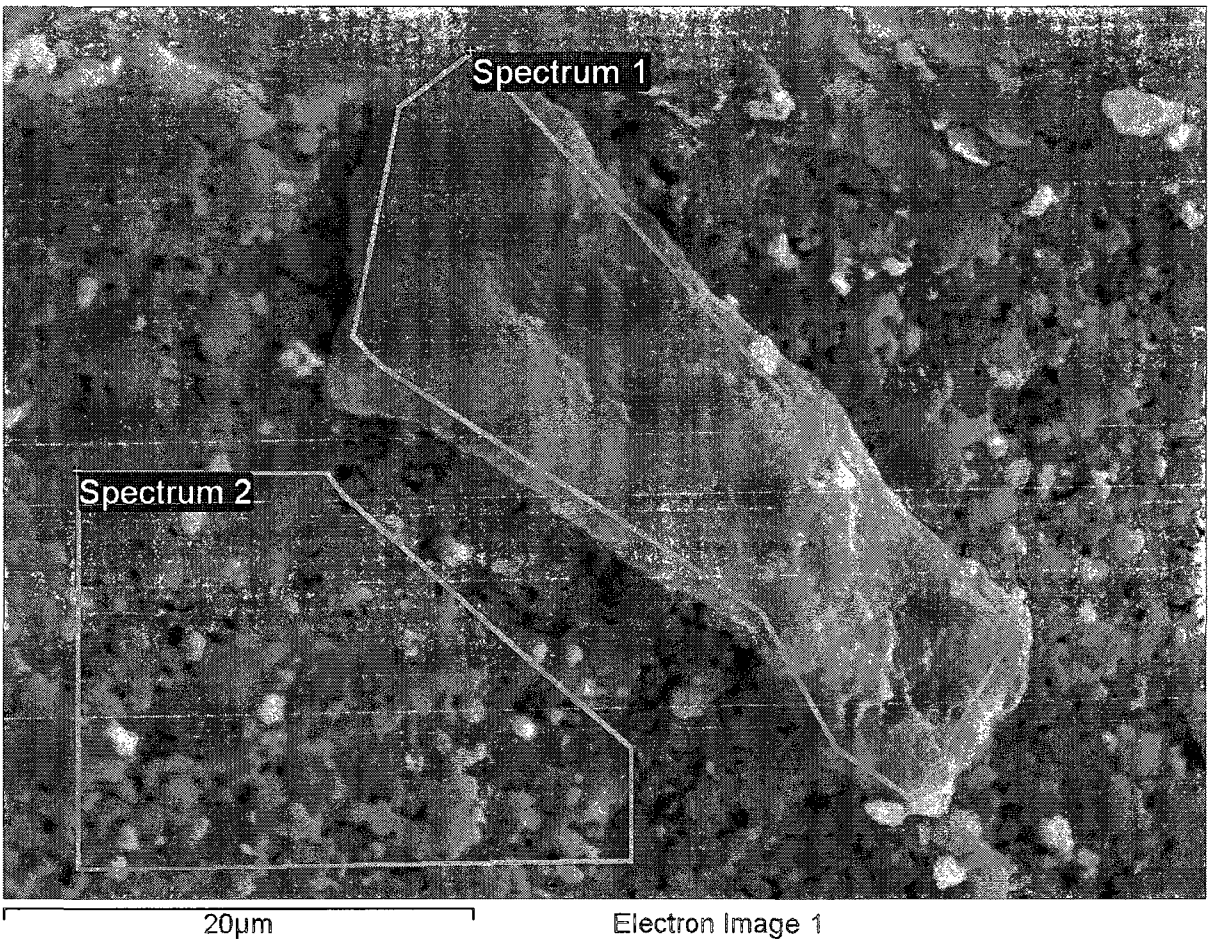

Figure 9.2: SEM image of a Katowice limestone particle carbonated (600°C) with a fluidizing gas of 8% CO_2, balance air, after having been calcined with a fluidizing gas of oxygen-enhanced air (53% O_2, balance N_2) burning low-ash wood pellets (860°C). 'Spectrum 1'- particle surface with high C content; 'Spectrum 2'- particle interior partially carbonated.

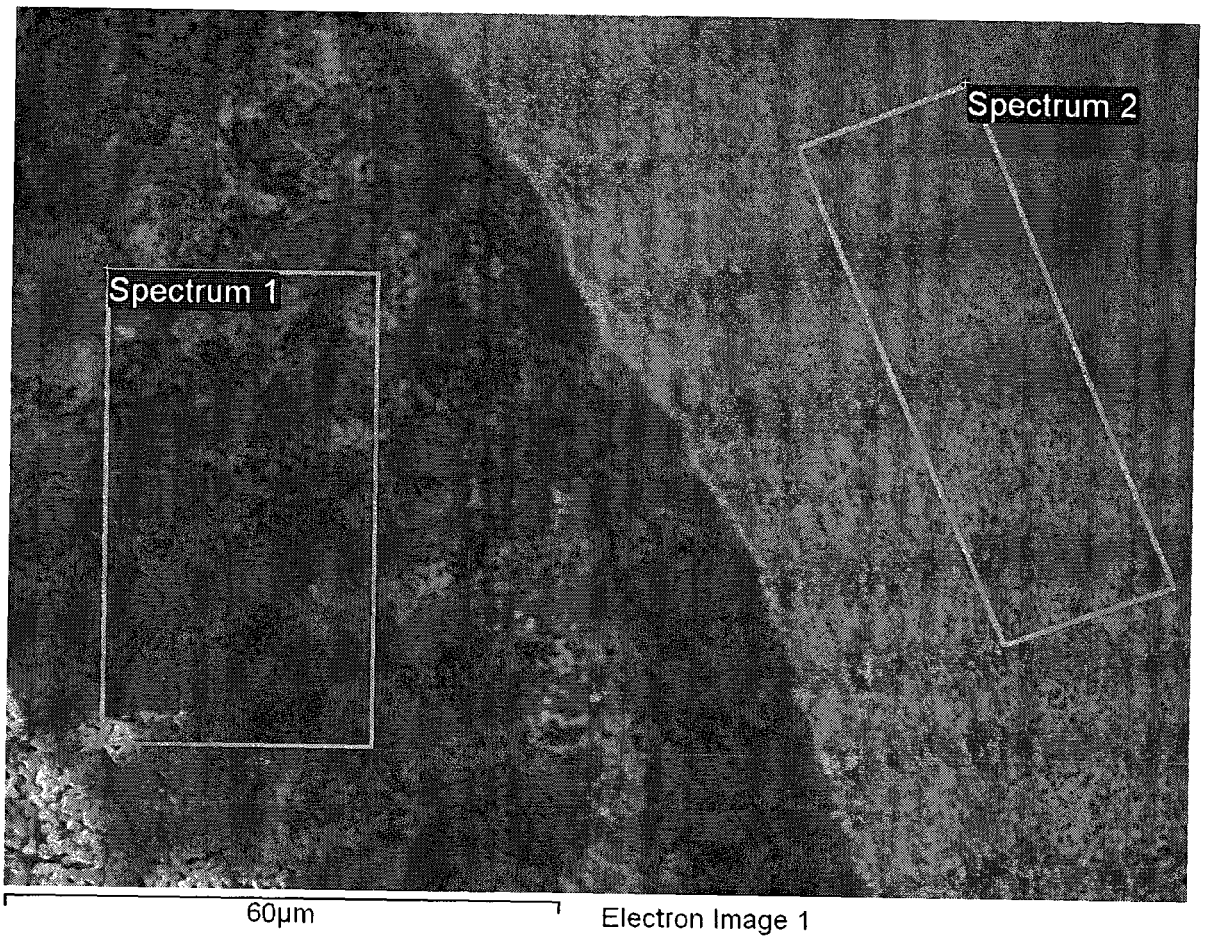

Figure 9.3: SEM image of a Katowice limestone particle carbonated (600°C) with a fluidizing gas of 8% CO_2, balance air, after having been calcined with a fluidizing gas of oxygen-enhanced air (53% O_2, balance N_2) burning low-ash wood pellets (860°C). 'Spectrum 1'- particle interior with light carbonation; 'Spectrum 2'- particle surface with more heavily carbonated grains.

Figure 9.4 provides an image of a Cadomin limestone particle calcined with a fluidizing gas of oxygen mixed with recycled flue gas (60% O_2, 36% CO_2, balance mainly N_2) burning high-ash wood pellets (910°C). Here again we see a low-porosity surface layer, but it would appear that this is at least partially due to the surface being carbonated to various extents. The concentrations of Na and K are elevated in the regions identified as 'Spectrum 2' and 'Spectrum 3', so some ash deposition may have occurred here. Loss-in-weight analysis shows that material drawn with this particle is only 3.7% carbonated. It would appear that the material near the surface is carbonated, while deep within the

interior of the particle it is nearly completed calcined. The variation in degree of carbonation is clear in Figure 9.5, which shows an image of a Cadomin limestone particle carbonated (600°C) with a fluidizing gas of 8% CO_2, balance air after having been calcined in the same manner as the particle in Figure 9.4. The outer surface appears to be heavily sintered and carbonated while the interior is somewhat less so. The degree of carbonation in the area identified as 'Spectrum 1' is 40% while loss-in-weight analysis provides a total particle carbonation of 30%.

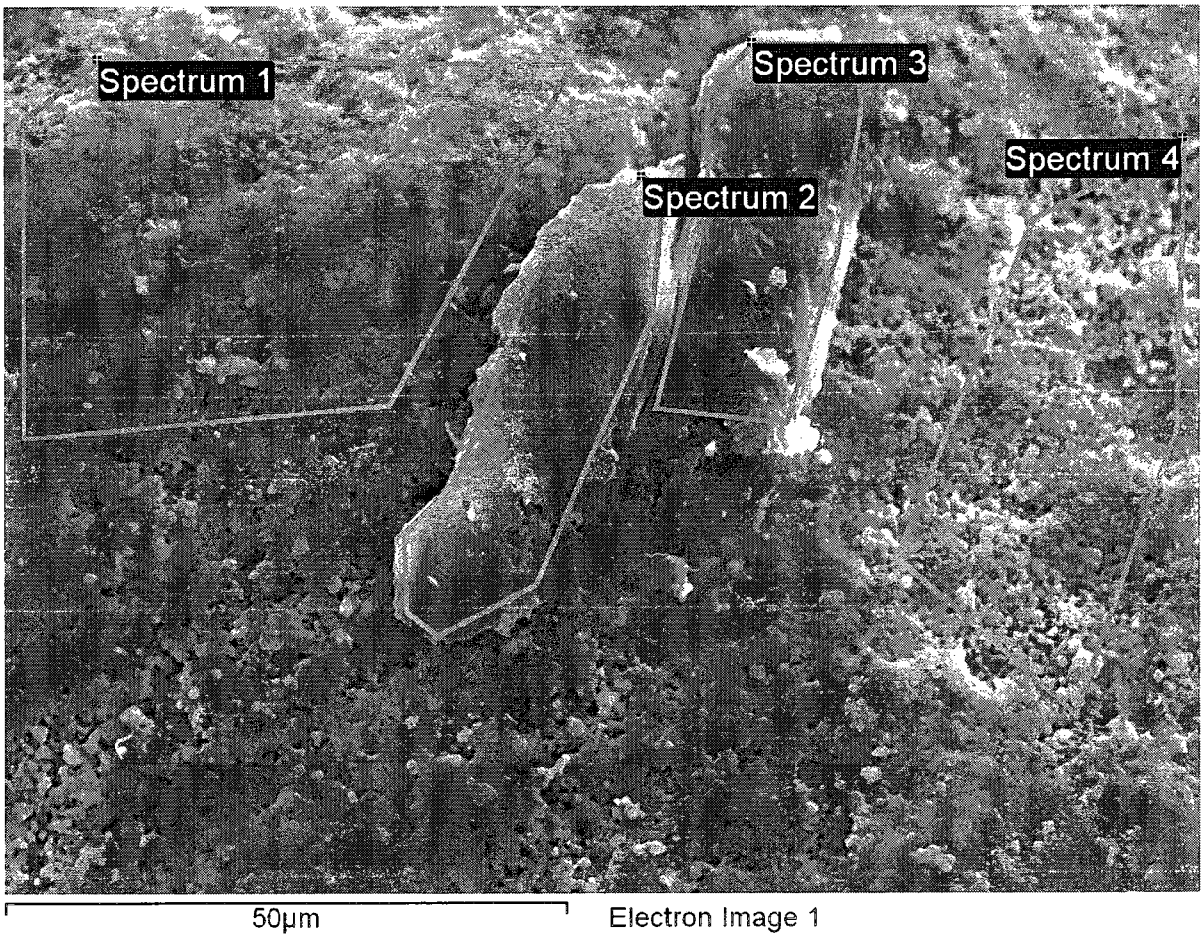

Figure 9.4 SEM image of a Cadomin limestone particle calcined with a fluidizing gas of oxygen mixed with recycled flue gas (60% O_2, 36% CO_2, balance mainly N_2) burning high-ash wood pellets (910°C). 'Spectrum 1'- particle surface; 'Spectrum 2' and 'Spectrum 3'- sorbent surface coated with a blend of sorbent and ash constituents (elevated Na and K) with high C; 'Spectrum 4'- highly sintered sorbent grains at particle surface.

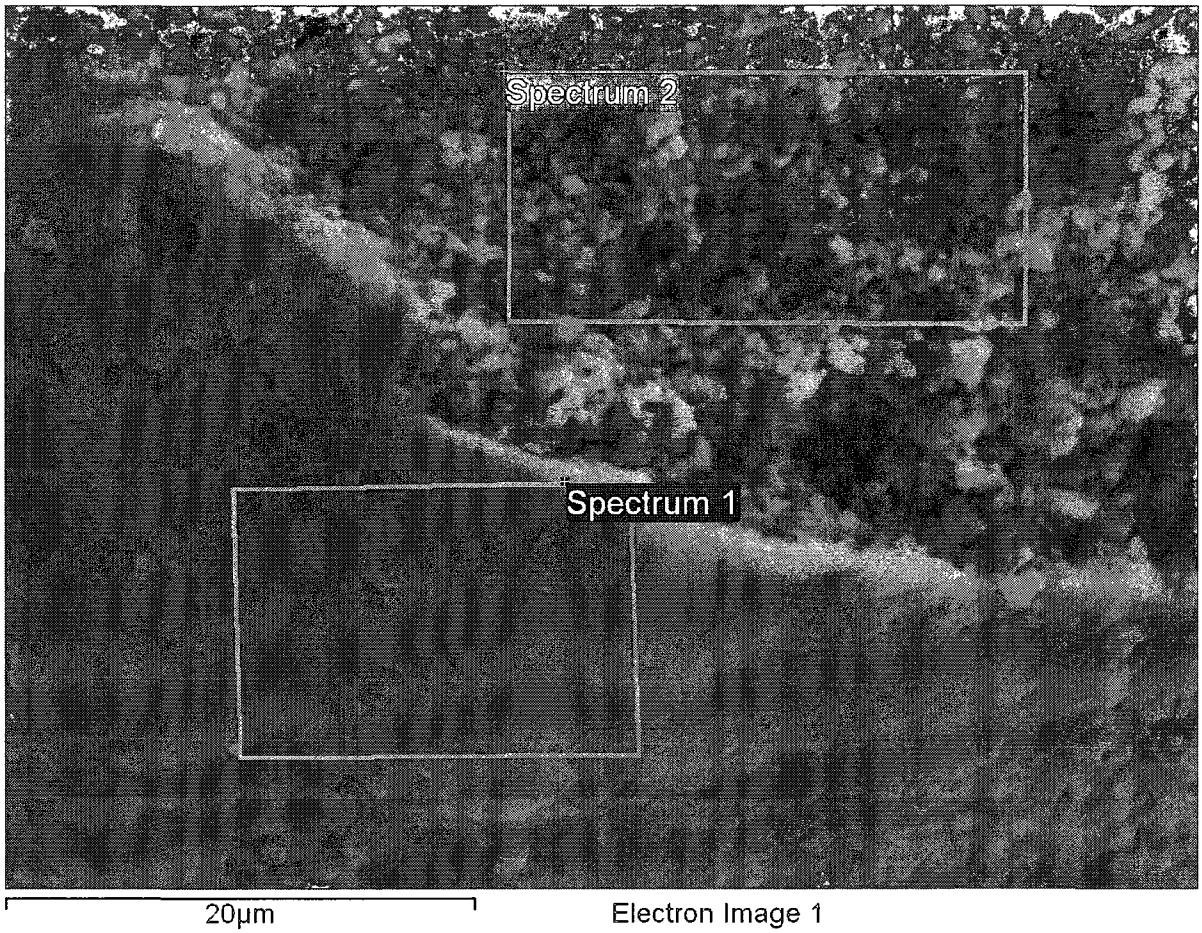

Figure 9.5: SEM image of a Cadomin limestone particle carbonated (600°C) with a fluidizing gas of 8% CO_2, balance air, after having been calcined with a fluidizing gas of oxygen mixed with recycled flue gas (60% O_2, 36% CO_2, balance mainly N_2) burning high-ash wood pellets (910°C). 'Spectrum 1'- particle surface; 'Spectrum 2'- particle interior.

9.4.2 Porosimetry

Changes in surface area (dS) after calcination for Katowice and Cadomin limestones are shown in Figure 9.6 and Figure 9.7, respectively. It is apparent that the material calcined with oxy-fuel with recycled flue gas has a substantially lower surface area for both limestones than does the oxygen-enhanced case. The changes in the heating rate of the oxy-fuel with recycled flue gas cases have resulted in similar surface areas (1.3-1.4 m^2/g), whereas the surface area (1.9 m^2/g) for the slowly heated oxygen-enhanced Cadomin calcine is lower than for the one that was heated rapidly (3.0 m^2/g).

For comparison, we have previously reported surface areas for this material, calcined in a TGA in a N_2 atmosphere, of 2.2 m^2/g (915°C) to 3.2 m^2/g (750°C) (Hughes et al., 2004).

Changes in pore volume (dV) after calcination of the two limestones are provided in Figure 9.8 and Figure 9.9. Here we see greater variation between each of the samples analyzed. There are differences in the way the two limestones have behaved, differences between heating rates, and differences between the calcination atmospheres.

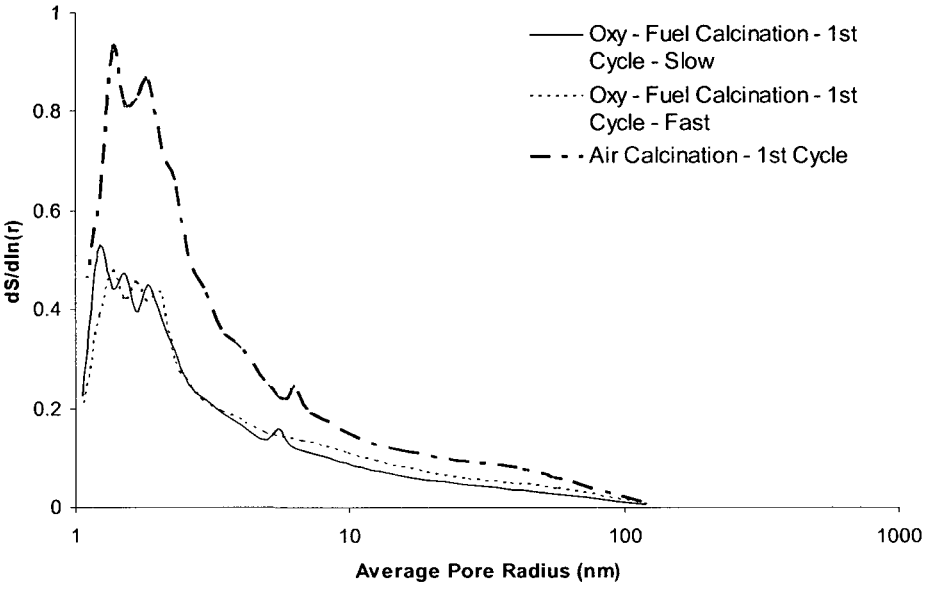

Figure 9.6: dS/d ln (r) vs. average pore radius for Katowice limestone calcined with low-ash wood pellets by (a) oxyfuel combustion with recycled flue gas using the slow heating method, (b) oxyfuel combustion with recycled flue gas using the fast heating method, and (c) oxygen-enhanced air combustion.

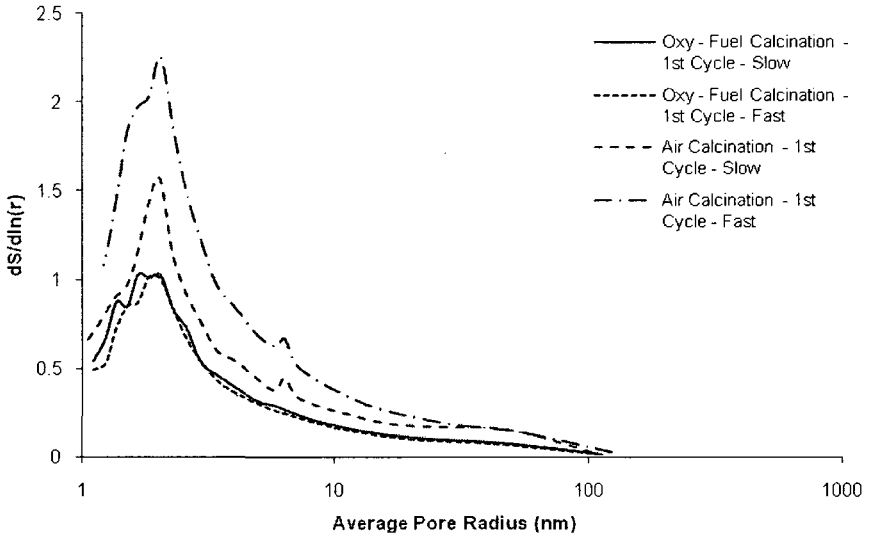

Figure 9.7: dS/d ln (r) vs. average pore radius for Cadomin limestone calcined with high-ash wood pellets by (a) oxyfuel combustion with recycled flue gas using the slow-heating method, (b) oxyfuel combustion with recycled flue gas using the fast-heating method, (c) oxygen-enhanced air combustion using slow-heating method, and (d) oxygen-enhanced air combustion using fast-heating method.

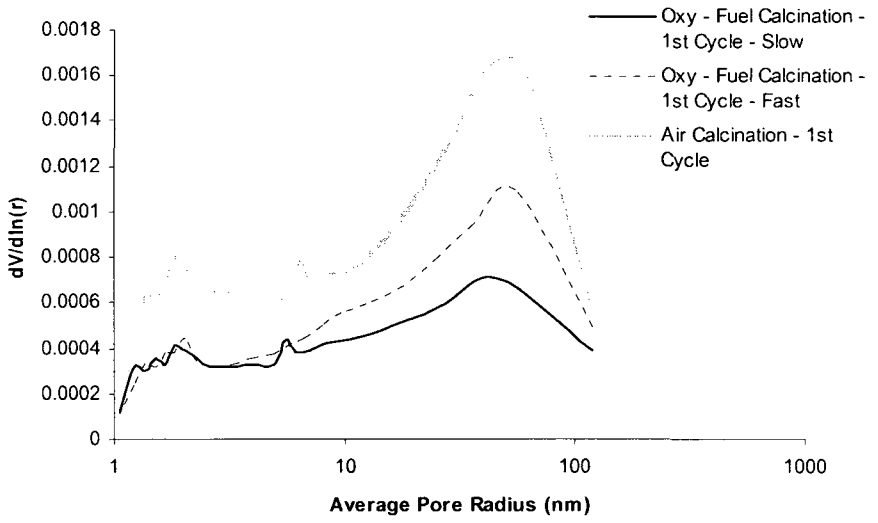

Figure 9.8: dV/d ln (r) vs. average pore radius for Katowice limestone calcined with high-ash wood pellets by (a) oxyfuel combustion with recycled flue gas using the slow-heating method, (b) oxyfuel combustion with recycled flue gas using the fast-heating method, and (c) oxygen-enhanced air combustion using slow-heating method.

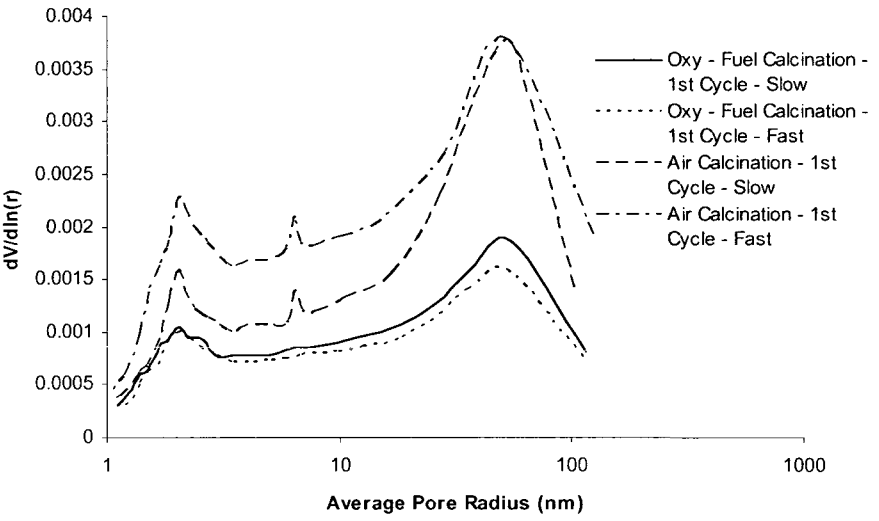

Figure 9.9: dV/d ln (r) vs. average pore radius for Cadomin limestone calcined with high-ash wood pellets by (a) oxyfuel combustion with recycled flue gas using the slow-heating method, (b) oxyfuel combustion with recycled flue gas using the fast-heating method, (c) oxygen-

enhanced air combustion using slow-heating method, and (d) oxygen-enhanced air combustion using fast-heating method.

The pore volume is greatest for the Katowice limestone (Figure 9.8) that has been calcined using oxygen-enhanced combustion, followed by oxy-fuel with recycled flue gas using the fast heating method. The greatest loss in pore volume as we proceed to lower total pore volumes is for pores of radii of 30 to 40 nm. Note that the surface areas of the calcines from oxy-fuel with recycled flue gas have similar surface areas, but the sample that has been heated rapidly has greater pore volume—especially in the 10-50 nm range. This should allow the rapidly-heated material to achieve greater conversion as pore pluggage will occur only at a higher level of carbonation.

In the case of Cadomin limestone (Figure 9.9) the pore volume is greatest for the samples that were calcined using oxygen-enhanced air combustion (cumulative totals: fast 0.0085 mL/g, slow 0.0070 mL/g). The sample heated using the fast method has similar pore volume in the 30-50 nm pore radius range as does that heated by the slower method, but significantly more pore volume at lower pore sizes. The samples treated in oxy-fuel with recycled flue gas both have similar pore volume distributions (cumulative totals: fast 0.0039 mL/g, slow 0.0044 mL/g).

9.4.3 CO_2 Capture

Initial fluidized bed carbonation resulted in carbonator flue gas outlet CO_2 concentrations near equilibrium levels, based on the equilibrium vapour pressures reported by Baker (1962) for the first 10 to 20 minutes of reaction. After this period the CO_2 concentration in the carbonator outlet rose rapidly to a value 1 to 4 percentage points below the CO_2 inlet concentration. Figure 9.10 shows the carbonator outlet flue gas concentration for Katowice limestone carbonated (600°C) with a fluidizing gas of 8% CO_2, balance air, after having been calcined with a fluidizing gas of oxygen-enhanced air (53% O_2, balance N_2) burning low ash wood pellets (860°C) for three cycles of calcination and carbonation. Fluctuations in CO_2 concentration in the first four minutes of reaction are due to variations in carbonator temperature as the reactor was being brought to steady state operation. The introduction of CO_2 to the carbonator results in heat release due to the exothermic carbonation reaction. This heat release requires that most of the power to the electric heaters surrounding the fluid bed be shut-off to maintain bed temperature. The pilot facility operators gained experience in

predicting the change in power requirements, so this variation is less evident in the later tests. The lowest values of CO_2 concentration shown here are approaching the minimum detection limits of the CO_2 analyzer, so the minimum outlet concentration of CO_2 should not be considered to be less than equilibrium. Taking the difference between inlet concentration and outlet concentration and then integrating over the period of carbonation indicates that the amount of CO_2 captured is the same as would be expected for the extent of carbonation measured from the thermogravimetric analysis. The carbonation conversion for the three cycles was nearly the same at about 16%.

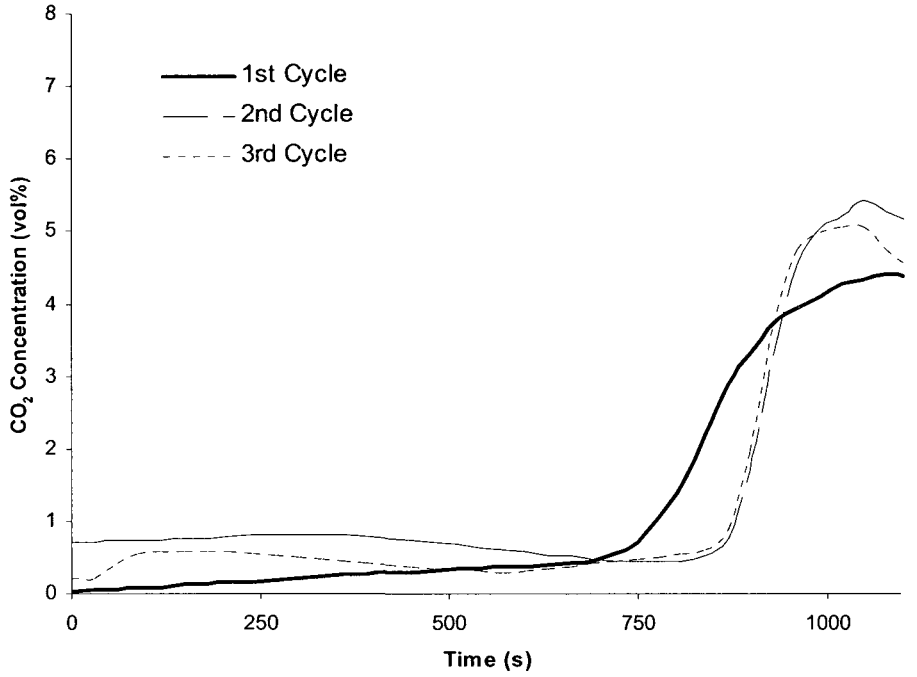

Figure 9.10: Carbonator outlet flue gas concentration for Katowice limestone carbonated (~600°C) with a fluidizing gas of 8% CO_2, balance air, after having been calcined with a fluidizing gas of oxygen-enhanced air (53% O_2, balance N_2) burning low-ash wood pellets (860°C).

Carbonator outlet flue gas concentration for Katowice limestone carbonated (~600°C) with a fluidizing gas of 8% CO_2, balance air, after having been calcined with a fluidizing gas of oxygen mixed with recycled flue gas (60% O_2, 36% CO_2, balance mainly N_2) burning high ash wood pellets (910°C)

can be seen in Figure 9.11 for three cycles of calcination and carbonation. This sorbent also captured enough CO_2 to achieve near-equilibrium levels; however, it did so for a shorter period. The carbonation conversion for the three cycles was similar at about 12%.

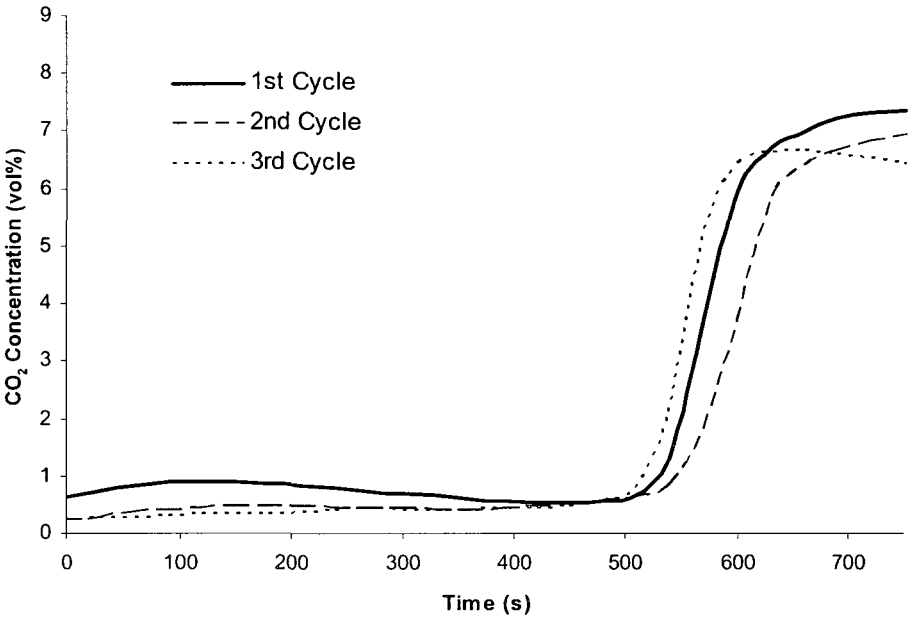

Figure 9.11: Carbonator outlet flue gas concentration for Katowice limestone carbonated (~600°C) with a fluidizing gas of 8% CO_2, balance air, after having been calcined with a fluidizing gas of oxygen mixed with recycled flue gas (60% O_2, 36% CO_2, balance mainly N_2) burning high-ash wood pellets (910°C).

9.5 Discussion

A very thin shell with low porosity was formed on the surface of the sorbent. There are a number of phenomena that may lead to this surface feature including char and ash deposition, ash sintering, cyclic carbonation and calcination, and carbonate formation during sample extraction. Increased CaO sintering due to the high CO_2 concentration is not believed to be the direct cause of this phenomenon, as the interior of the sorbent, where CO_2 partial pressure is expected to be highest during calcination, has similar surface and grain structure to sorbent prepared in high-CO_2 partial pressure calcination TGA experiments. Since the interior of the sorbent has similar morphology to the surface and interior of sorbents prepared *via* TGA, it would seem reasonable to look to exterior

influences on the particle that are related to fluidized bed combustion, for the cause of the shell formation.

Char in fluid bed combustors may be at temperatures far exceeding the bulk bed temperature (Scala et al., 2003). Chirone et al. (2000) have concluded that, in combination with char fines and high particle temperatures caused by combustion, ash-layered bed material will be formed. In a CaO-based CaO-$CaCO_3$ looping system, ash could build up on the surface of the sorbent in the calciner if the ash composition was appropriate.

Joutsenoja *et al.* (1999) showed that for a series of coals and a coal char, the average particle temperature was on average 87-191°C above the average bed temperature. Peak particle temperatures ranged from 275-592°C above the nominal bed temperature. In fluidized beds blown with high-oxygen-concentration fluidizing gas, peak particle temperatures can be expected to be still higher, since the rate of reaction and hence heat release are proportional to the concentration of oxygen. It is reasonable to expect that average fuel char temperatures in an oxygen-blown calciner operating at 900°C may be in the area of 1000 to 1150°C.

Fuel ashes do not melt at an exact single temperature; instead they melt over a temperature range in which both solid and liquid phases are present. It has been found that in certain types of FBC boilers, ashes containing 10-20 wt% liquid will be sticky and tend to adhere to surfaces within the combustor. FACTSage (Facility for Advanced Chemical Thermodynamics) software has been used to predict the portion of the fuel ash that is liquid for both the high-ash and low-ash wood pellets used for the tests described in this paper. Carbon and CaO mixed with the fuel ash stream have been varied to represent fuel char in various states of burnout and contact with the sorbent respectively. Figure 9.12 shows the weight percent of ash that is liquid *vs.* the CaO content for the high-ash wood pellets for the temperature of the calciner operating with recycled flue gas (910°C) and at two possible fuel char temperatures (1000°C and 1150°C). It is apparent that even at the bulk bed temperature the fuel ash contains more than 15% liquid, which, depending on the viscosity of the eutectic, may or may not stick to the sorbent. The fuel ash at 1150°C is more than half liquid and has a significantly greater chance of depositing on the surface of the sorbent. The high-ash wood pellet ash has a lower initial deformation temperature (1129°C) than the low-ash wood pellet ash (1216°C). The initial

deformation temperatures indicate that the FACTSage simulation is providing reasonable values for the temperature at which a substantial portion of the ash is liquid.

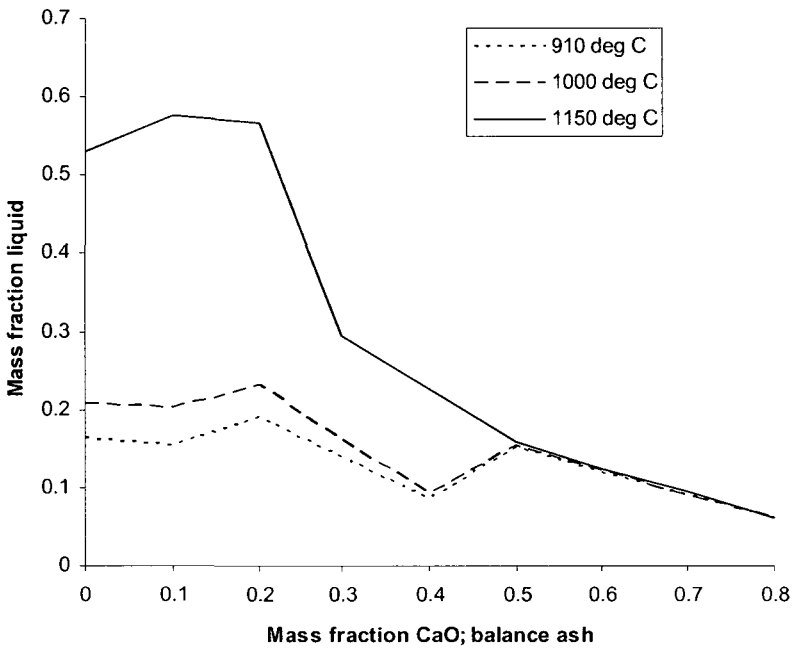

Figure 9.12: Mass fraction of liquid phase vs. CaO added to ash from the high-ash wood pellets, from FACTSage analysis.

Skrifvars *et al.* (1998) characterized the sintering tendency of biomass ashes with compression-strength-based sintering analysis. The ash pellets were heated to various temperatures, cooled and then their compressive strengths determined. If the compressive strength increased significantly, the ash was considered to have been heavily sintered. The compressive strength typically increased rapidly over a fairly narrow temperature range at a liquid weight fraction of about 15% for 7 out of the 10 samples. If the ashes examined here behave in a similar manner to those tested by Skrifvars *et al.* (1998) then we can expect them to sinter heavily in areas when the ash content is greater than about 30 wt%. Severe sintering can result in low-porosity structures as we see on the sorbent surface.

There have been a number of approaches that have been used to reduce ash agglomeration that may be of use in improving sorbent performance if the shell formation is due to ash deposition. Increasing flue gas recirculation will reduce the oxygen concentration and, hence, will reduce char particle temperatures (Obernberger, 1998) and the portion of the ash that is liquid, and should reduce ash deposition. However, increasing flue gas recirculation will increase parasitic energy losses for recycle blower operation and increase the size of the calciner and ancillaries. Fuels or blends of fuels, such as biomass with coals or petroleum coke, that do not form high-liquid-fraction eutectics at temperatures expected in the calciner, should be used (Werther, 2000). Such fuels include most coals and petroleum coke. Finally, the calciner should be operated at lower temperatures by using a stripping gas such as steam to reduce the partial pressure of CO_2 and thereby allowing a reduced operating temperature. For some fuels, operating with a wet recycled flue gas may sufficiently reduce the required operating temperature of the calciner.

9.6 Conclusions

The sorbents in these tests were able to capture CO_2 from a synthetic flue gas to achieve near equilibrium levels down to CO_2 concentration of around 0.4 vol%.

Sorbent capacity was significantly lower than expected based on previous thermogravimetric analyses. This is believed to be at least partially due to the formation of a thin, low-porosity shell being formed around the sorbent, enhanced by the deposition of ash from the solid fuel under oxygen fired conditions. There are a number of methods that could be used to reduce or eliminate the shell formation and these will be explored in the near future at our laboratory.

9.7 References

Anderson, P., Horlock, R., Avery, R., (1965). 'Some Effects of Water Vapour During the Preparation and Calcination of Oxide Powers', Proc. Brit. Ceram. Soc. 3, 33.

Baker, E., (1962). 'The Calcium Oxide-Carbon Dioxide System in the Pressure Range 1-300 Atmospheres', J. Chem. Soc *70,* 464.

Borgwardt, R.H., (1989). 'Sintering of Nascent Calcium Oxide', Chem. Eng. Sci. 44(1), 53.

Chirone, R., Salatino, P., Scala, F., (2000). 'The Relevance of Attrition to the Fate of Ashes During Fluidized Bed Combustion of Biomass', Proc. Combust. Inst. 28, 2279.

Glasson, D., (1958). 'Reactivity of Lime and Related Oxides. I. Production of Calcium Oxide', J. Appl. Chem. 8, 793.

Glasson, D., (1961). 'Reactivity of Lime and Related Oxides. VII. Crystal Size Variation in Calcium Oxide Produced From Limestone', J. Appl. Chem. 11(6), 201.

Hughes, R.W., Lu, D., Anthony, E.J., Wu, Y., (2004). 'Improved Long-Term Conversion of Limestone-Derived Sorbents for In Situ Capture of CO_2 in a Fluidized Bed Combustor', Ind. Eng. Chem. Res. 43, 5529.

Hughes, R.W., Lu, D.Y., Anthony, E.J., Macchi, A., (2005). 'Design, Process Simulation and Construction of an Atmospheric Dual Fluidized Bed Combustion System for in situ CO_2 Capture using High-temperature Sorbents', Fuel Proc. Tech. 86(14-15), 1523.

Joutsenoja, T., Heino, P., Hernberg, R., Bonn, B., (1999). 'Pyrometric Temperature and Size Measurements of Burning Coal Particles in a Fluidized Bed Combustion Reactor',Combustion and Flame 118, 707.

Obernberger, I., (1998). 'Decentralized Biomass Combustion: State of the Art and Future Development', Biomass and Bioenergy 14(1), 33.

Scala, F., Chirone, R., Salatino, P., (2003). 'The Influence of Fine Char Particles Burnout on Bed Agglomeration During the Fluidized Bed Combustion of a Biomass Fuel', Fuel Proc. Tech. 84, 229.

Skrifvars, B., Backman, R., Hupa, M., (1998). 'Ash Behaviour in a CFB Boiler During Combustion of Coal, Peat or Wood', Fuel Proc. Tech. 56, 55.

Sun, P., Lim, C.J., Grace, J.R., (2008). 'Cyclic CO_2 Capture by Limestone-Derived Sorbent During Prolonged Calcination / Carbonation Cycling', AIChE Journal 54, 1668.

Symonds, R., (2008). 'CO_2 Capture from Gasification Syngas via Cyclic Carbonation/Calcination', Master's Thesis, University of Ottawa, Ottawa, ON, Canada.

Werther, J., Saenger, M., Hartge, E.U., Ogada, T., Siagi, Z., (2000). 'Combustion of Agricultural Residues', Prog. Energy Combust. Sci. 26, 1.

Chapter 10 Conclusions and Future Research

The conclusions are presented and sub-divided according to the primary research objectives; sorbent development, process simulation, design and construct a pilot plant for proof of technology, and evaluate sorbent characterisitics and performance at pilot scale. As this is a paper - based thesis written over many years the conclusions within some of the papers are somewhat dated. Commentary is provided on these conclusions based on the current state-of-the-art. The recommendations for future research are provided with the state-of-the-art in mind. Blamey et al. (2010) provide a thorough review of calcium looping cycles for CO_2 capture with over 90 references to published work in the area of CaO-$CaCO_3$ looping cycles since this thesis was initiated.

10.1 Sorbent Development

The bench scale studies have shown that high CO_2 concentration in the calciner is highly detrimental to the performance of the sorbent. Hydration of the sorbent can greatly improve the capacity of the sorbent when relatively low CO_2 concentrations are present, however, when CO_2 concentration is high there is little difference between untreated and hydrated sorbent capacity after 20 cycles.

A variety of authors have performed work in the area of hydration of the CaO sorbent for improving performance. Perhaps the most important of this work has been performed by Fennel et al. (2007), who have shown that the use of humidified air in place of steam can provide substantial benefits to improving conversion. Performing the hydration at such mild conditions will greatly reduce the costs associated with this processing step. This work also includes testing in which intermittent hydration steps are used to reactivate the sorbent.

Hydration of spent sorbent may prove to be an economically attractive option for extending the useful life of the material. Additional optimization studies of hydrated sorbents should be performed to determine optimal hydration conditions for providing suitable sorbent pore structure. If hydrated materials are to be used then they may need to be pelletized in order to provide a sorbent of a suitable size for fluidized bed operations.

The results of Chapter 4 show that pelletization would appear to be a useful means of re-introducing attrited sorbent to the CaO-$CaCO_3$ looping cycle. In addition, pelletization provides a means of dispersing additivies within a sorbent particle.

As a result of contining work from Chapter 4, in characterizing binders for pelletization, Manovic and Anthony (2009) have obtained interesting results on the effects of various additives to the rate of deactivation of the sorbent. They have shown that binders containing Na and Si are not suitable for maintaing activity over extended cycles. However, the use of calcium aluminate cements as binder shows great promise with respect to both sorbent activity and particle strength. A better understanding of the effects of impurities in CaO sintering may prove fruitful in reducing the extent of sintering and increasing the sorbent capacity over many cycles.

With the understanding that CO_2 causes such a great deal of sintering it seems necessary to reduce its partial pressure in at least part of the calciner. Steam is an obvious contender for use as a stripping gas in the calciner, but steam production at the required flow rates would be costly and entail a substantial energy penalty. In addition, water vapour is well known to enhance sorbent sintering, though to a lesser degree than carbon dioxide.

An option that would result in lower CO_2 concentration involves operating a substantial portion of the calciner under deeply reducing conditions. Under reducing conditions CO and H_2 would be prevalent in place of CO_2 and H_2O which may reduce the required operating temperature as a result of lower CO_2 partial pressure and reduce sintering as CO and H_2 are believed to have a lesser sintering effect on CaO. Secondary oxidant injection ports could complete combustion in an upper portion of the fluid bed supplying the heat required for calcination. Solids circulation would then carry the heat into the lower portions of the bed. This method would need to be explored with caution as eutectic melts typically form at lower temperatures under reducing conditions, especially when Fe is present in substantial concentration.

Bench scale studies to determine sorbent capacity over multiple cycles involving calcination with various stripping gases including H_2O, O_2, H_2, H_2S, and CO should be performed.

10.2 Process Simulation

The process simulations developed as part of this thesis have been quite effective in determining equipment sizing and selection for the majority of the facility as would be expected since most of the process is composed of conventional operations at moderate conditions with gaseous and liquid substances with very well defined thermodynamic properties.

However, the $CaO\text{-}CaCO_3$ looping pilot scale tests have shown that the sorbent decay models that have been used to develop previous process and economic studies do not accurately predict sorbent performance under realistic conditions i.e. high CO_2 concentration, high fuel particle temperatures, ash contamination, and sorbents under kinetic and thermal stresses. Further development of process simulations and economic analyses is required once more realistic sorbent decay models are available in order to adequately evaluate and optimize the technology.

Process modelling results have been published by a number of groups in recent years to determine performance and feasibility of $CaO\text{-}CaCO_3$ technology. The performance driven models have included both determination of heat requirements in the calciner (Rodriquez et al., 2008) and optimizing limestone make-up flows (Romeo 2009). These papers make it clear that low sorbent purge rates are attractive due to energy requirements for both sensible heating and calcining fresh limestone. Strohle (2009) has completed a feasibility study which includes power production and basic equipment sizing for a large commercial power plant involving $CaO\text{-}CaCO_3$ looping technology for CO_2 capture.

In 2007 Abanades et al. published a cost analysis for the technologies studied in this thesis. Provided in the study were comparative costs for a base case without CO_2 capture, an oxygen fired case, and a $CaO\text{-}CaCO_3$ looping technology case. Selected results from this analysis are given in Table 10.1. Also provided in the table are results for CO_2 capture through amine scrubbing provided by Zahra (2007).

Table 10-1: Summary of economic results from studies by Abanades (2007); base case, oxy-fuel CFBC, CO_2 capture via calcium looping and Abu-Zahra (2007) for CO_2 capture via amine scrubbing.

Case	Item	Units	Low	**Estimate**	High
Base	Efficiency	% net, LHV	45	**43**	40
	Cost of Electricity	US$/kWe	0.025	**0.039**	0.066
	Emission	kg CO_2/kWhe	760	**795**	855
Oxy-fuel CFB	Efficiency	% net, LHV	35	**32**	28
	Cost of Electricity	US$/kWe	0.037	**0.057**	0.097
	Avoided CO_2 Cost	US$/ton	16.4	**23.8**	44.2
Calcium Looping	Efficiency	% net, LHV	39	**36**	32
	Cost of Electricity	US$/kWe	0.031	**0.049**	0.089
	Avoided CO_2 Cost	US$/ton	8.3	**15.5**	36.6
Amine	Avoided CO_2 Cost	US$/ton	45	**54**	82

Process and economic modelling in recent years has continued to show that oxy-fuel CFBC and CaO-$CaCO_3$ looping are attractive options for power generation with near zero emissions. It should be noted that the economics of CaO-$CaCO_3$ looping technology will be greatly improved if the spent sorbent is used as a source for lime in the manufacture of cement – which of course will also displace CO_2 emissions from that industry.

10.3 Design and Construct a Pilot Plant for Proof of Technology

10.3.1 Oxy-fuel combustion

The oxy-fuel CFBC has operated reliably at the small pilot scale giving our research team the confidence and knw-how to scale up the technology to 1 MW_{th}. The first commissioning run for the 1 MW_{th} facility operating with oxygen was completed in 2009 in collaboration with Foster Wheeler (Hotta 2009). Foster Wheeler is supporting additional oxy CFB pilot and demonstration facilities in Spain (CIUDEN, 30 MWth) and the USA. Feasibility studies have been completed for full commercial scale facilties (ENDESA & CIUDEN 300 MWe; Vattenfall 500 MWe combined heat and power; PVO 500 MWe multifuel with biomass co-firing).

Additional work is required to determine sorbent capacity for sulphur capture and determine optimal operating conditions for various fuels, changes in hydrodynamics, behaviour of materials, emissions prediction, and further development of design tools.

10.3.2 CaO-$CaCO_3$ looping combustion

The CaO-$CaCO_3$ pilot facility was able to capture nearly all of the carbon dioxide in the synthetic flue gas that was fed to it (>95% capture). This demonstrates that the technology is feasible and could be competitive with the conventionally considered carbon capture technologies. However, the technology still has some technical hurdles that need to be dealt with before it can be commercialized.

One of these hurdles is the propensity for the sorbent to attrite. With careful and knowledgeable consideration for the characteristics of the parent limestone and the preparation of the stone sorbents it should be possible to obtain sorbents with acceptable attrition rates.

The carbonation capacity has been shown to be lower than expected at the pilot scale with dry synthetic flue gas, however, there is evidence that the presence of water vapour in the carbonator can greatly increase carbonation from both combustion flue gases and gasification syngas. Further studies should be performed at both bench scale and pilot scale with varying water contents in the flue gas.

10.4 Evaluate Sorbent Characteristics and Performance at Pilot Scale

The pilot scale studies have made it clear that thermogravimetric analysis has not revealed all of the sintering mechanisms that are present in an oxy-fired calciner. Further studies at the pilot scale will be required to determine realistic sorbent decay models. Any apparent breakthroughs discovered at the bench scale will need to be vetted at the pilot scale before a substantiated claim of success is made. The pilot scale studies have also made it clear that it is necessary to achieve similar concentrations of CO_2 and SO_2 as would be found in commercially operating equipment in order to quantify the capacity of the sorbent for capturing CO_2. Great efforts should be made in preventing air in-leakage to facilities when evaluating CO_2 and SO_2 capture performance of CaO derived sorbents.

A thin, non-porous shell was formed around the sorbent particles under some of the test conditions at the pilot scale. The causes for the formation of this shell must be verified prior to investing substantially in this technology as the shell may greatly reduce the capacity of the sorbent. The fact that the shell was not formed in all tests provides hope that a suitable set of conditions can be found for operation where the shell does not hinder sorbent performance. Possible causes for shell formation that have been previously discussed include high particle temperatures and ash deposition. Additional possible causes include melting of $CaCO_3$ (melting point ~825 C) prior to CaO crystal nucleation and 'instantaneous' recarbonation of the sorbent as the particle passes through low temperature regions in the calciner such as around metal walls, gas injection ports and fuel ports.

10.5 Process Evaluation

Table 10-2 summarizes the strengths, weaknesses, opportunities and threats that I have identified for the two processes considered. Here oxy-fuel circulating fluidized bed combustion is considered as a stand-alone process for power generation with CO_2 capture, and as an integral part of CaO-$CaCO_3$ looping with oxy-fuel sorbent regeneration.

Table 10-2: Strengths, weaknesses, opportunities and threats of fluidized bed combustion systems with integrated CO_2 capture

	Oxy-fuel Circulating Fluidized Bed Combustion	$CaO-CaCO_3$ Looping Cycle with Oxy-Fuel Sorbent Regeneration
Strengths	• Low complexity • High heat transfer rates in circulating fluidized beds result in minimal temperature gradients • Small plant foot print as compared to conventional combustion systems without CO_2 capture due to low N_2 concentrations in flue gas • Sulphur removal possible within combustor via CaO sorbent reducing corrosion issues in downstream processes • Suitable for a wide variety of fuels	• Low oxygen demand • Sulphur removal to low parts per million level inherent to process • Low efficiency penalty for CO2 capture compared to conventional combustion systems without CO2 capture if sorbent conversion objectives are achieved • Fluidized bed combustion results in low NO production and is amenable to NH4 injection for very low NO emissions • Sorbent costs are very low on a per unit mass basis
Weaknesses	• High oxygen demand • High efficiency penalty for CO2 capture compared to conventional combustion systems without CO2 capture • Need for oxygen safe materials in fluidizing gas	• Higher complexity than oxy-fuel technologies • Sorbent is deactivated with each carbonation-calcination cycle • Sorbent is deactivated through reaction with sulphur dioxide

	supply • Sulphur species are concentrated in flue gas resulting in acidic condensate if sulphur is not removed within combustor	• Need for oxygen safe materials in fluidizing gas supply
Opportunities	• High impurity concentrations in flue gas increase driving forces for impurity removal • Reduced recycle gas rates as compared to PC oxy-fuel combustion possible due to higher heat transfer rates in circulating fluidized beds	• Calcination temperature can be reduced by the addition of steam potentially increasing sorbent lifetime • Sorbent lifetime can be extended through hydration and other treatments • Attrited sorbent can be pelletized for re-injection into the system • Partially spent sorbent can be injected prior to the carbonator to capture sulphur extending sorbent lifetime in the CaO-CaCO3 loop • Technology can be applied in gasification systems for hydrogen production • Spent sorbent could be pulverized, hydrated, pelletized and re-used provided that sulphur content is sufficiently low. • The dense bed region of the calciner can be operated under reducing conditions resulting in potentially reduced sintering

Threats	• Jetting region may experience high O2 concentrations resulting in hot spots	• Spent sorbent may need to be land-filled if there is not sufficient demand for it as a product

10.6 Conclusion

The most innovative portion of this work is the study of oxy-fuel fluidized bed combustion with regeneration of CaO sorbent at pilot scale. It is believed that demonstration of oxy-fuel fluidized bed combustion with recycled flue gas was first performed as part of this thesis work. It is also believed, that continuous CaO-$CaCO_3$ looping with oxy-fuel sorbent regeneration was first performed as part of this thesis work.

The technology being developed within this thesis has the potential to greatly reduce greenhouse gas emissions. The technology can be applied to large stationary emitters of carbon dioxide including gasifiers, coal power generating stations, and cement kilns. Coal, petroleum coke, biomass, limestone and water, the main feedstocks to the processes, are inexpensive and readily available in Canada and throughout most of the world. This will allow the processes to have a global impact on greenhouse gas emissions.

The research carried out in this thesis brings two important carbon dioxide capture technologies from concept through to bench scale testing, simulation, and demonstration at pilot scale.

10.7 References

Abanades, J.C., Grasa, G., Alonso, M., Rodriguez, N., Anthony, E.J., Romeo, L.M. (2007). 'Cost Structure of a Postcombustion CO_2 Capture System Using CaO', Environ. Sci. Technol. 41, 5523.

Abu-Zahra, M., Niederer, J., Feron, P., Versteeg, G. (2007). 'CO_2 Captrue from Power Plants: Part II. A Parametric Study of the Economical Performance Based on Mono-ethanolamine', International Journal of Greenhouse Gas Control 1(2), 135.

Blamey, J., Anthony, E.J., Wang, J., Fennell, P.S. (2010). 'The Calcium Looping Cycle for Large-Scale CO_2 Capture', Prog. Energy Comb. Sci. 36, 260.

Fennell, P., Davidson, J.F., Dennis, J.S., Hayhurst, A.N. (2007). 'Regeneration of Sintered Limestone Sorbents for the Sequestration of CO_2 from Combustion and Other Systems', J. Energy Institute 80(2) 116.

Hotta, A. (2009). 'Development and Demonstration of Oxy CFB for Power Plants with CO_2 Capture', 1st International Oxyfuel Combustion Conference, Cottbus, Germany.

Manovic, V., Anthony, E.J. (2009). 'Screening of Binders for Pelletization of CaO-Based Sorbents for CO_2 Capture', Energy & Fuels 23(10) 4797

Rodriguez, N., Alonso, M., Grasa, G., Abanades, J.C. (2008). 'Heat Requirements in a Calciner of $CaCO_3$ integrated in a CO_2 Capture System Using CaO', Chem. Eng. J. 138, 148.

Romeo, L.M., Lara, Y., Lisbona, P., Escosa, J.M. (2009). 'Optimizing make-up flow in a CO_2 Capture System using CaO', Chem. Eng. J. 147, 252.

Appendix 1 – Determination of Surface Area

Developed from course notes from CHG8132 – Adsorption Separation Processes at the University of Ottawa

Appendix 1 – Determination of Surface Area

BET Method for Surface Area Determination

Adsorbed Gas	N_2		
R	cm^3-atm/gmol-K	82.06	
T_{STD}	K	273.15	
P_{STD}	atm	1	
P^{SAT}	atm	1	Normal boiling point of N2 is 77 K

To determine amount of N2 adsorbed on molar basis use ideal gas law at STP; 273.1K, 1atm

$$n = \frac{PV}{RT}$$

From the linear trendline given on the BET plot the values of the slope and the intercept can be seen to be:

$I = 1/(A_M c)$	m^{-3}	2.1959	**(1)**
$S = (c-1)/A_M c$	m^{-3}	1070	**(2)** am=(c-1)/Sc

Sub (1) into (2)

S=(c-1)I
c=S/I+1 and Am=1/(Ic)

c	Dimensionless	488.272
Am	g N2 Ads/ g cat	9.33E-04

$$SA_{BET} = \frac{A_M N_{AV} A_{N2}}{MW}$$

A_{N2}	nm^2/molecule N2	0.162
	m^2/molecule N2	1.62.E-19
N_{AV}	molecules N2/g-mole n2	6.E+23
MW	g-mole N2/MW g N2	28
SA_{BET}	m^2	3.25

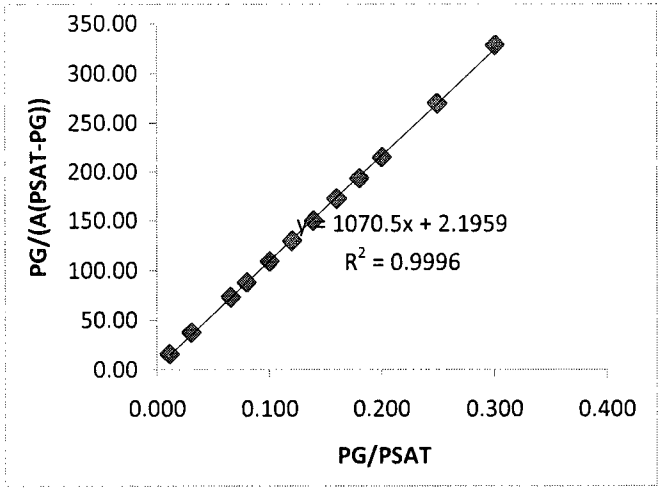

Appendix 1 – Determination of Surface Area

T-Curve Method

amt adsorbed at Pg/Psat = 0.05

	g N_2/g cat	0.0007
$eta_{0.05}$		1.037751856

amt adsorbed at Pg/Psat = 0.3

	g N_2/g cat	0.0013
$eta_{0.3}$		1.608655999

Am t-curve	g N_2/g cat	0.001041961	
$S_{t-curve} = \frac{A_M N_{AV} A_{N2}}{MW}$			
$S_{t\text{-}curve}$	m^2/g	3.6	convert nm2 to m2 by *10-18

If this sorbent had a lower $SA_{t\text{-}curve}$ then SA_{BET} then the micropore volume could be estimated by:

$$V_{Micropore} = \left(A_{M,BET} - A_{M,t-curve}\right) \times \rho_{L,N_2}$$

Appendix 1 – Determination of Surface Area

Adsorption - Desorption Isotherm

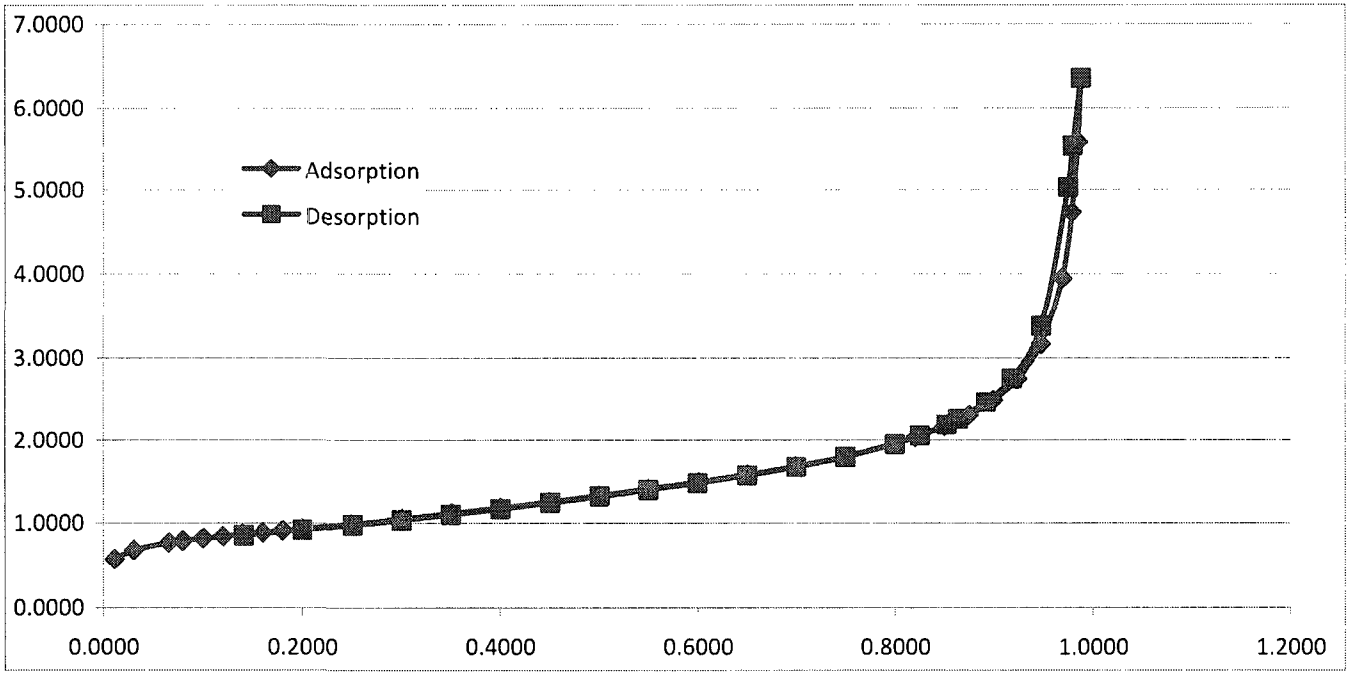

Isotherm Type 2
Hysteresis Low

Appendix 1 – Determination of Surface Area

	Relative Pressure	Adsorbed		BET Plot		eta
	P_G / P^{SAT}	mL N_2 (STP) / g cat	g N_2/g cat	$P_G/(A(P^{SAT}-P_G))$	P_G/P^{SAT}	
Adsorption	0.0114	0.5728	0.0007	16.12	0.011	1.038
	0.0308	0.6784	0.0008	37.55	0.031	1.129
	0.0659	0.7698	0.0010	73.38	0.066	1.225
	0.0801	0.7923	0.0010	88.03	0.080	1.256
	0.1004	0.8196	0.0010	109.07	0.100	1.296
	0.1204	0.8438	0.0011	129.81	0.120	1.332
	0.1399	0.8668	0.0011	150.16	0.140	1.365
	0.1605	0.8887	0.0011	172.20	0.160	1.398
	0.1805	0.9111	0.0011	193.47	0.180	1.429
	0.2005	0.9337	0.0012	215.00	0.200	1.460
	0.2496	0.9873	0.0012	269.70	0.250	1.533
	0.3009	1.0490	0.0013	328.41	0.301	1.609
	0.3513	1.1145	0.0014			1.684
	0.4003	1.1811	0.0015			1.761
	0.4502	1.2523	0.0016			1.843
	0.5001	1.3282	0.0017			1.932
	0.5502	1.4082	0.0018			2.030
	0.6001	1.4910	0.0019			2.139
	0.6500	1.5780	0.0020			2.264
	0.6996	1.6805	0.0021			2.410
	0.7501	1.7999	0.0022			2.590
	0.7991	1.9541	0.0024			2.815
	0.8208	2.0347	0.0025			2.936
	0.8496	2.1655	0.0027			3.131
	0.8748	2.3064	0.0029			3.344
	0.8993	2.4886	0.0031			3.612
	0.9238	2.7509	0.0034			3.981
	0.9476	3.1697	0.0040			4.530
	0.9690	3.9480	0.0049			5.415
	0.9788	4.7265	0.0059			6.153
	0.9851	5.5854	0.0070			6.938
	0.9885	6.3616	0.0079			7.557

Appendix 1 – Determination of Surface Area

	Relative Pressure	Adsorbed		BET Plot		eta
	P_G / P^{SAT}	mL N_2 (STP) / g cat	g N_2/g cat	$P_G/(A(P^{SAT}-P_G))$	P_G/P^{SAT}	
Desorption	0.9799	5.5361	0.0069			6.264
	0.9752	5.0301	0.0063			5.838
	0.9481	3.3845	0.0042			4.542
	0.9182	2.7540	0.0034			3.884
	0.8920	2.4647	0.0031			3.523
	0.8638	2.2577	0.0028			3.244
	0.8521	2.1894	0.0027			3.150
	0.8251	2.0554	0.0026			2.963
	0.7997	1.9525	0.0024			2.818
	0.7497	1.7943	0.0022			2.589
	0.7000	1.6721	0.0021			2.411
	0.6503	1.5696	0.0020			2.265
	0.6000	1.4799	0.0018			2.139
	0.5500	1.3969	0.0017			2.030
	0.5007	1.3192	0.0016			1.933
	0.4507	1.2420	0.0016			1.844
	0.4002	1.1689	0.0015			1.761
	0.3504	1.1009	0.0014			1.683
	0.3005	1.0362	0.0013			1.608
	0.2510	0.9773	0.0012			1.535
	0.2006	0.9201	0.0011			1.460
	0.1410	0.8533	0.0011			1.367

Appendix 2 – Determination of Pore Size Distribution

Developed from method in Thomas, J.M., Thomas, W.J. (1997). 'Principles and Practice of Heterogeneous Catalysis', VCH, p. 268.

Appendix 2 – Determination of Pore Size Distribution

Column	Equation	Description
A	Data	Relative pressure
B	Data	Amount adsorbed
C	$\mathbf{A}_i$-$\mathbf{A}_{i+1}$	Change in quantity of gas adsorbed on surface
D	0.9516/LN(1/**A**)	Kelvin radius
E	($\mathbf{D}_i$-$\mathbf{D}_{i+1}$)/2	Average Kelvin radius between adsorption increments
F	(5/LN(1/**A**))^(1/3)*0.43	Thickness of adsorbed layer
G	**D+F**	Pore radius as a function of Kelvin radius and adsorbed layer thickness
H	($\mathbf{G}_i$-$\mathbf{G}_{i+1}$)/2	Average pore radius between adsorption increments
I	$\mathbf{F}_i$-$\mathbf{F}_{i+1}$	Change in the thickness of the adsorbed gas film between adsorption increments
J	**P*I**/10^9*10^6*0.808/28.02*22.4	Change in the volume of the adsorbed gas film between adsorption increments on a liquid basis
K	0.6459***J**	Change in the volume of the adsorbed gas film between adsorption increments on a gas basis
L	**C-K**	Change in Kelvin volume mL gas
M	0.001548***L**	Change in Kelvin volume mL liquid
N	**M***(**H**^2/**E**^2)	Change in liquid pore volume mL liquid
O	2*1000***N**/**H**	Change in SA m2
P	**O+P**	Cumulative surface area in pores larger than rp m2
Q	$\mathbf{G}_i$-$\mathbf{G}_{i+1}$	del rp = rp, prev - rp,next
R	LN($\mathbf{G}_i$)-LN($\mathbf{G}_{i+1}$)	del ln(rp) = ln(rp)prev - ln(rp)next
S	**N**/**Q**	del PV/del rp
T	**N**/**R**	del PV / del ln rp
U	**O**/**Q**	del SA/del rp
V	**O**/**R**	del SA/del ln rp
W	LN($\mathbf{G}_i$)-LN($\mathbf{G}_{i+1}$))/2	avg ln rp = ln rp,prev - ln rp,next

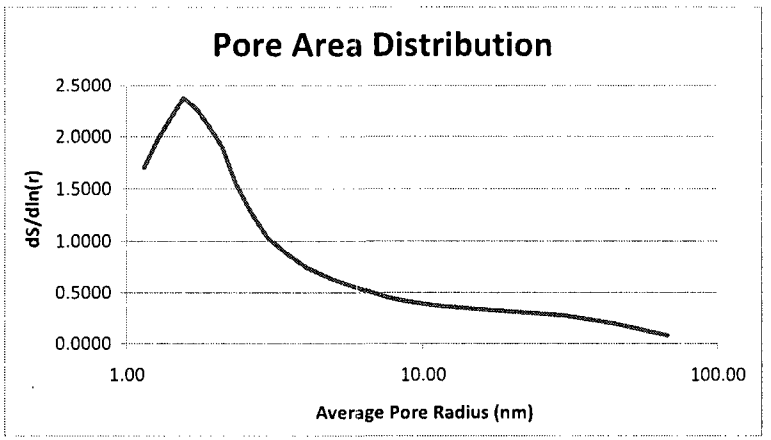

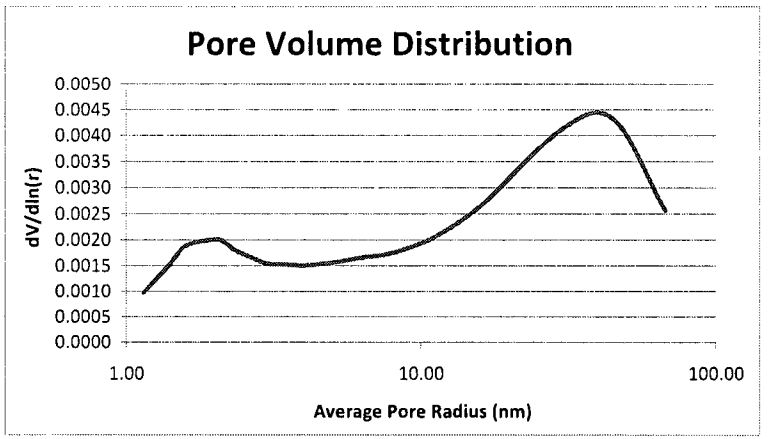

Appendix 2 – Determination of Pore Size Distribution

1	2	3	4	5	6	7	8	9	10	11	12	13
Pg/Psat	Volume Desorbed vol MLN2/g cat	Increment Desorbed Volume mL N2 / g cat	Kelvin radius nm	Average Kelvin Radius	Multilayer Thickness nm	Pore radius rK + t nm	Average Pore Radius nm	Change in multilayer film thickness nm	Change in multilayer film volume mL liquid	Change in multilayer film volume mL gas	Change in Kelvin volume mL gas	Change in Kelvin volume mL liquid
0.9885	6.362	0.83	82.14	64.46	3.25	85.39	67.43	0.556	0.000	0.000	0.826	1.3E-03
0.9799	5.536	0.51	46.78	42.33	2.69	49.48	44.93	0.183	0.005	0.003	0.503	7.8E-04
0.9752	5.030	1.65	37.88	27.86	2.51	40.39	30.09	0.557	0.029	0.019	1.627	2.5E-03
0.9481	3.385	0.63	17.84	14.49	1.95	19.79	16.31	0.283	0.050	0.033	0.598	9.3E-04
0.9182	2.754	0.29	11.15	9.74	1.67	12.82	11.33	0.155	0.042	0.027	0.262	4.1E-04
0.8920	2.465	0.21	8.32	7.41	1.52	9.84	8.87	0.120	0.040	0.026	0.181	2.8E-04
0.8638	2.258	0.07	6.50	6.22	1.39	7.89	7.60	0.041	0.016	0.010	0.058	9.0E-05
0.8521	2.189	0.13	5.95	5.45	1.35	7.30	6.76	0.080	0.033	0.022	0.112	1.7E-04
0.8251	2.055	0.10	4.95	4.60	1.27	6.22	5.85	0.062	0.029	0.019	0.084	1.3E-04
0.7997	1.953	0.16	4.26	3.78	1.21	5.47	4.94	0.098	0.050	0.033	0.126	1.9E-04
0.7497	1.794	0.12	3.30	2.99	1.11	4.42	4.06	0.077	0.046	0.030	0.093	1.4E-04
0.7000	1.672	0.10	2.67	2.44	1.04	3.71	3.45	0.063	0.043	0.028	0.075	1.2E-04
0.6503	1.570	0.09	2.21	2.04	0.97	3.19	2.98	0.054	0.042	0.027	0.063	9.7E-05
0.6000	1.480	0.08	1.86	1.73	0.92	2.78	2.62	0.047	0.040	0.026	0.057	8.8E-05
0.5500	1.397	0.08	1.59	1.48	0.87	2.46	2.34	0.041	0.040	0.026	0.052	8.0E-05
0.5007	1.319	0.08	1.38	1.28	0.83	2.21	2.10	0.038	0.041	0.026	0.051	7.9E-05
0.4507	1.242	0.07	1.19	1.12	0.79	1.99	1.89	0.036	0.043	0.028	0.045	7.0E-05
0.4002	1.169	0.07	1.04	0.97	0.76	1.80	1.71	0.033	0.045	0.029	0.039	6.1E-05
0.3504	1.101	0.06	0.91	0.85	0.72	1.63	1.56	0.032	0.048	0.031	0.034	5.2E-05
0.3005	1.036	0.06	0.79	0.74	0.69	1.48	1.42	0.031	0.051	0.033	0.026	4.0E-05
0.2510	0.977	0.06	0.69	0.64	0.66	1.35	1.28	0.032	0.057	0.037	0.021	3.2E-05
0.2006	0.920	0.07	0.59	0.54	0.63	1.22	1.15	0.0401	0.0758	0.0489	0.0179	2.8E-05
0.1410	0.853		0.5		0.59	1.1						

Appendix 2 – Determination of Pore Size Distribution

1	13	14	15	16	17	18	19	20	21	22	23
Pg/Psat	Change in Kelvin volume mL liquid	Change in liquid pore volume mL liquid	Change in SA m2	Cumulative surface area in pores larger than rp m2	del rp = rp, prev - rp,next	del ln(rp) = ln(rp)prev - ln(rp)next	del PV/del rp	del PV / del ln rp	del SA/del rp	del SA/del ln rp	avg ln rp = ln rp,prev - ln rp,next
0.9885	1.3E-03	0.0014	0.041	0.0415	35.9181	0.5458	0.0000	0.0026	0.0012	0.0760	4.1744
0.9799	7.8E-04	0.0009	0.039	0.0805	9.0896	0.2030	0.0001	0.0043	0.0043	0.1923	3.8000
0.9752	2.5E-03	0.0029	0.195	0.2758	20.5932	0.7132	0.0001	0.0041	0.0095	0.2738	3.3419
0.9481	9.3E-04	0.0012	0.144	0.4195	6.9746	0.4344	0.0002	0.0027	0.0206	0.3307	2.7681
0.9182	4.1E-04	0.0005	0.097	0.5165	2.9791	0.2645	0.0002	0.0021	0.0326	0.3668	2.4186
0.8920	2.8E-04	0.0004	0.091	0.6070	1.9459	0.2204	0.0002	0.0018	0.0465	0.4108	2.1762
0.8638	9.0E-05	0.0001	0.035	0.6422	0.5924	0.0780	0.0002	0.0017	0.0595	0.4516	2.0270
0.8521	1.7E-04	0.0003	0.079	0.7216	1.0780	0.1598	0.0002	0.0017	0.0736	0.4965	1.9081
0.8251	1.3E-04	0.0002	0.072	0.7934	0.7536	0.1291	0.0003	0.0016	0.0954	0.5567	1.7637
0.7997	1.9E-04	0.0003	0.135	0.9280	1.0521	0.2136	0.0003	0.0016	0.1279	0.6299	1.5923
0.7497	1.4E-04	0.0003	0.131	1.0585	0.7118	0.1757	0.0004	0.0015	0.1834	0.7429	1.3976
0.7000	1.2E-04	0.0002	0.134	1.1924	0.5202	0.1513	0.0004	0.0015	0.2572	0.8846	1.2341
0.6503	9.7E-05	0.0002	0.140	1.3322	0.4026	0.1351	0.0005	0.0015	0.3472	1.0344	1.0909
0.6000	8.8E-05	0.0002	0.155	1.4871	0.3178	0.1213	0.0006	0.0017	0.4875	1.2774	0.9627
0.5500	8.0E-05	0.0002	0.171	1.6578	0.2578	0.1105	0.0008	0.0018	0.6623	1.5455	0.8468
0.5007	7.9E-05	0.0002	0.199	1.8573	0.2197	0.1049	0.0010	0.0020	0.9077	1.9018	0.7392
0.4507	7.0E-05	0.0002	0.213	2.0699	0.1909	0.1010	0.0011	0.0020	1.1140	2.1055	0.6362
0.4002	6.1E-05	0.0002	0.219	2.2891	0.1651	0.0964	0.0011	0.0019	1.3275	2.2733	0.5375
0.3504	5.2E-05	0.0002	0.226	2.5154	0.1483	0.0953	0.0012	0.0018	1.5258	2.3739	0.4416
0.3005	4.0E-05	0.0001	0.208	2.7231	0.1344	0.0950	0.0011	0.0015	1.5449	2.1854	0.3465
0.2510	3.2E-05	0.0001	0.199	2.9223	0.1284	0.1000	0.0010	0.0013	1.5520	1.9915	0.2489
0.2006	2.8E-05	0.0001	0.218	3.1406	0.1466	0.1280	0.0009	0.0010	1.4892	1.7054	0.1349
0.1410											

Appendix 3 – Determination of Conversion

Appendix 3 – Determination of Conversion

Determination of Conversion of CaO Sorbent

Constants

MW_{CaO}		56.08 Molecular weight of CaO
MW_{CO2}		44.00 Molecular weight of CO_2
MW_{SO2}		64.06 Molecular weight of SO2

Data

m_0	mg	**24** Initial sample mass - weighted on scale
m_{CO2}	mg	**10.56** Change in sample mass during 1st calcination (if hydrates are present this is the mass after hydrates have decomposed - should be complete by 514 C)
$m_{CO2,i+1}$	mg	**4** Decrease in sample mass during carbonation cycle i+1
x_{CaO}	mole/mole	**0.54** Mole fraction of CaO from major oxides analysis
x_{oxides}	mole/mole	**0.57** Sum of oxidemole fractions from major oxides analysis
$m_{SO2,i}$	mg	**2** Cycle i - Cycle i+1 calcine mass

$$M_{CaO} = \frac{x_{CaO}(m_0 - m_{CO2}))}{x_{oxides} MW_{CaO}}$$

$$M_{CO2} = \frac{m_{CO2,i}}{MW_{CO2}}$$

$$X_{CaO+CO2 \rightarrow CaCO3} = \frac{M_{CO2}}{M_{CaO}}$$

$$M_{SO2} = \frac{m_{SO2,i}}{MW_{SO2}}$$

$$X_{CaO+SO2+1/2O2 \rightarrow CaCO3} = \frac{M_{SO2}}{M_{CaO}}$$

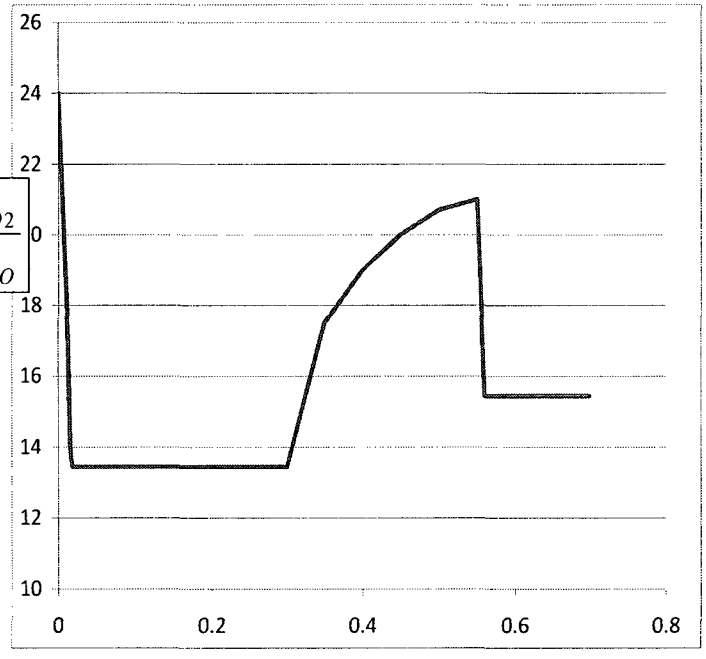

Conversion of: $CaO + CO_2 \rightarrow CaCO_3$

Calculations

M_{CaO}	mole	0.227 Mole of CaO
M_{CO2}	mole	0.091 Mole of CO_2
$X_{CaO+CO2 \text{ to } CaCO3}$		0.400 Conversion of CaO to CaCO3

Conversion of: $CaO + SO_2 + 1/2O_2 \rightarrow CaSO_4$

Calculations

$M_{SO2,i}$	mole	0.031 Mole CaSO4 formed
$X_{CaO+SO2+1/2SO2 \text{ to } CaCO3}$		0.138 Conversion of CaO to CaSO4

Appendix 4 – Facility Layout Drawings

Views of solid model of dual fluidized bed facility 'as-built' prior to initial commissioning. Various pieces of equipment and piping hidden for clarity.

Appendix 4 – Facility Layout Drawings

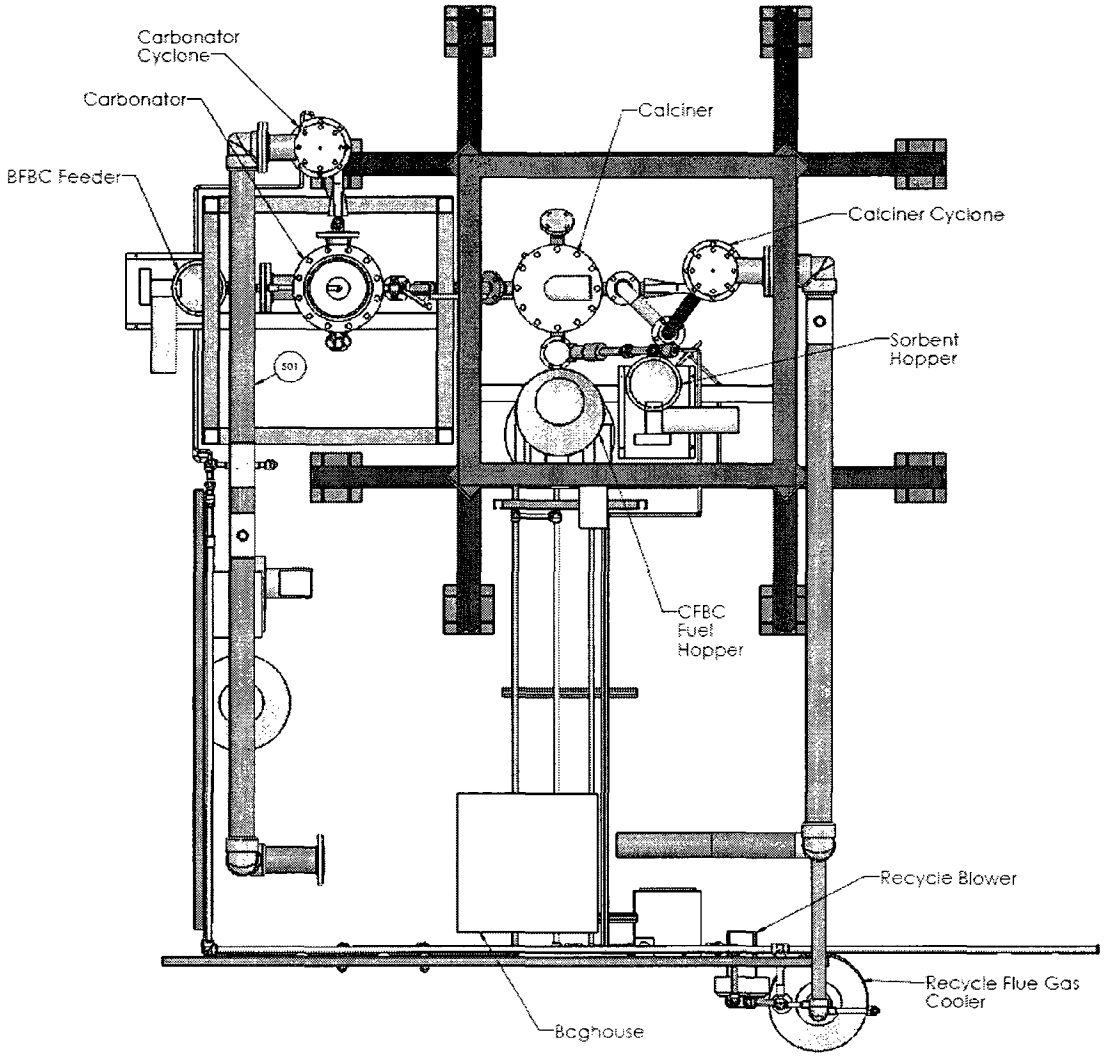

Plan view of dual fluidized bed facility.

Appendix 4 – Facility Layout Drawings

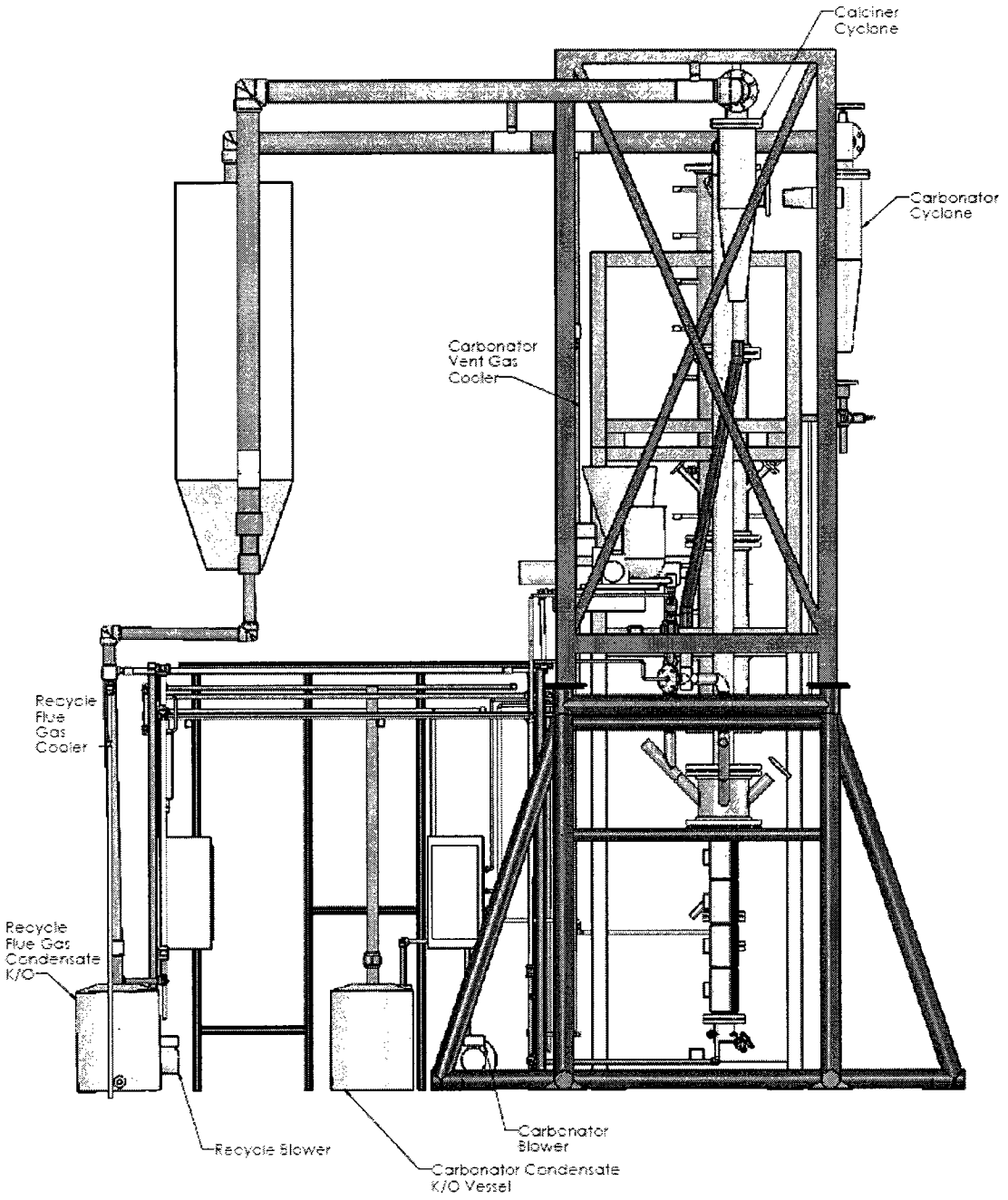

Right view of dual fluidized bed facility.

Appendix 4 – Facility Layout Drawings

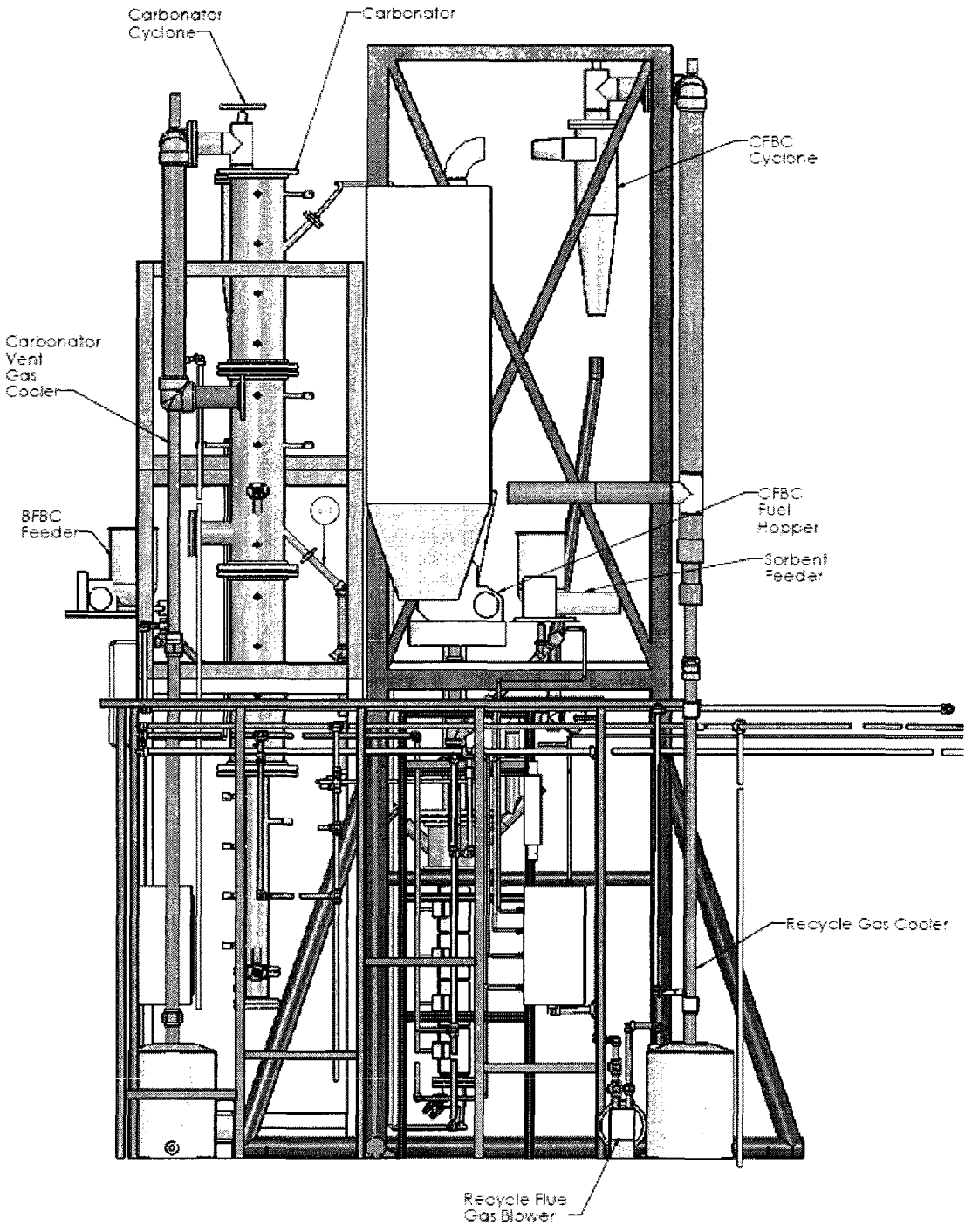

Front view of dual fluidized bed facility.

Appendix 5 – Selected Process & Instrumentation Diagrams

'As-built' P&IDs of the dual fluidized bed facility prior to initial commissioning.

Appendix 5 – Selected Process & Instrumentation Diagrams

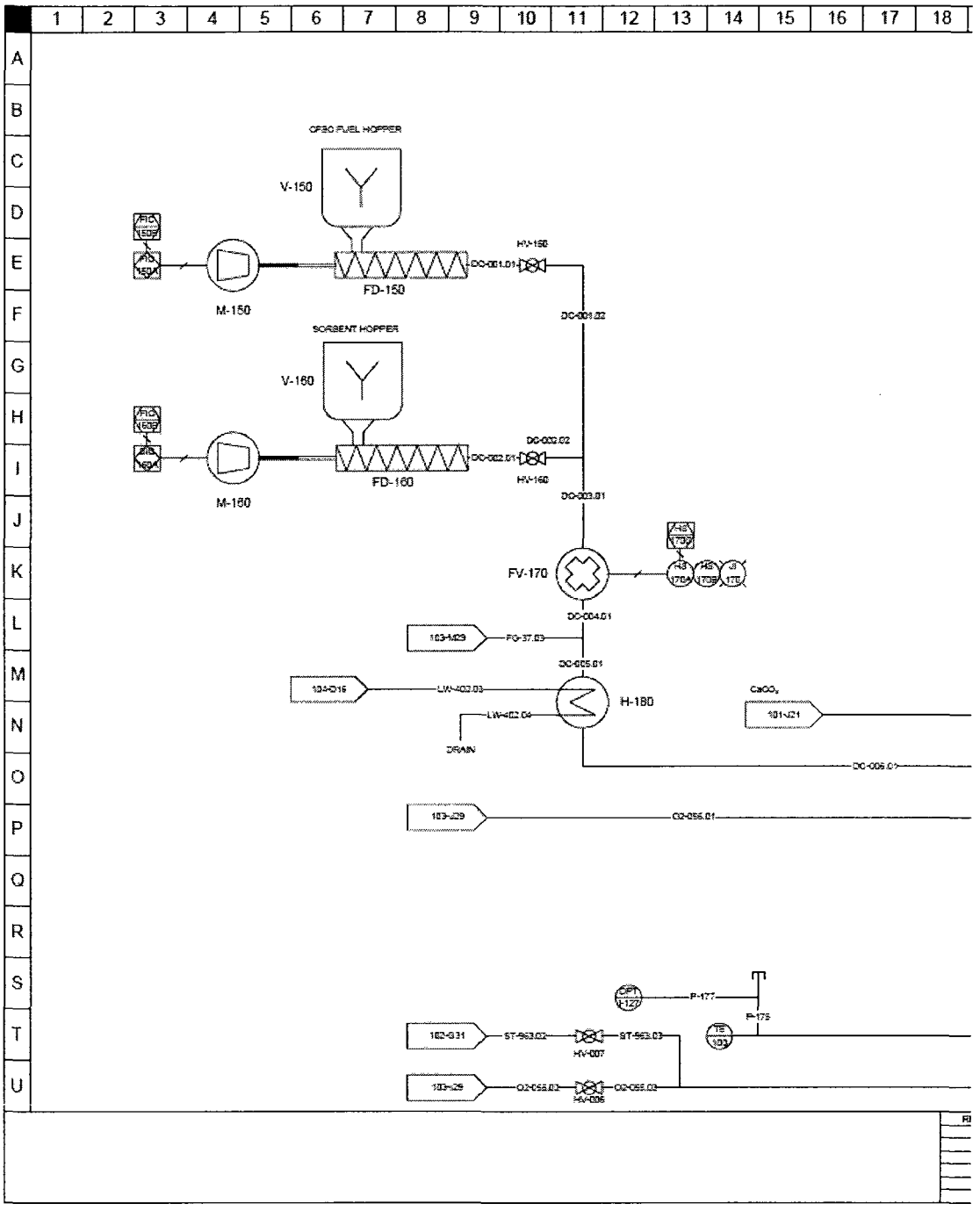

Appendix 5 – Selected Process & Instrumentation Diagrams

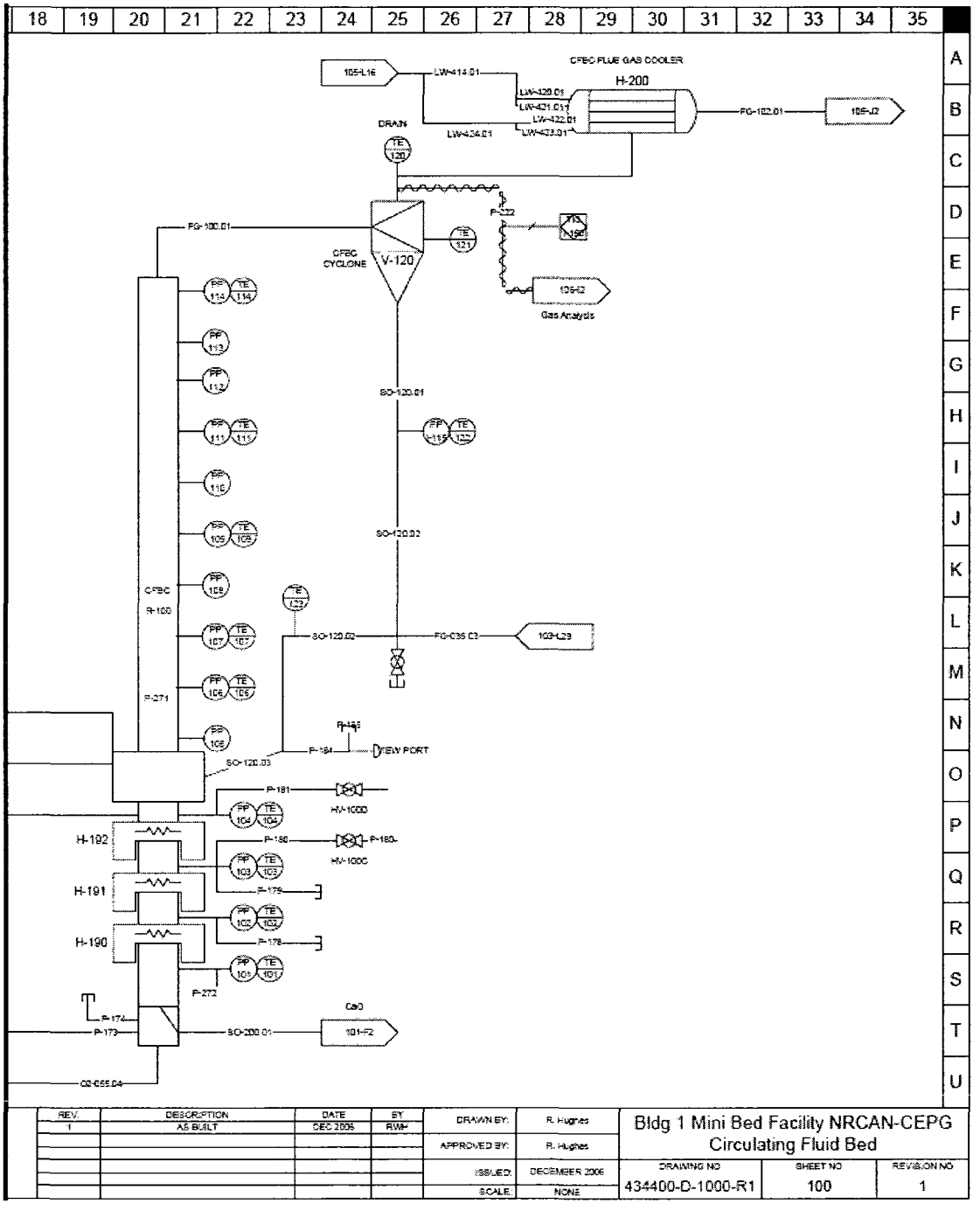

Appendix 5 – Selected Process & Instrumentation Diagrams

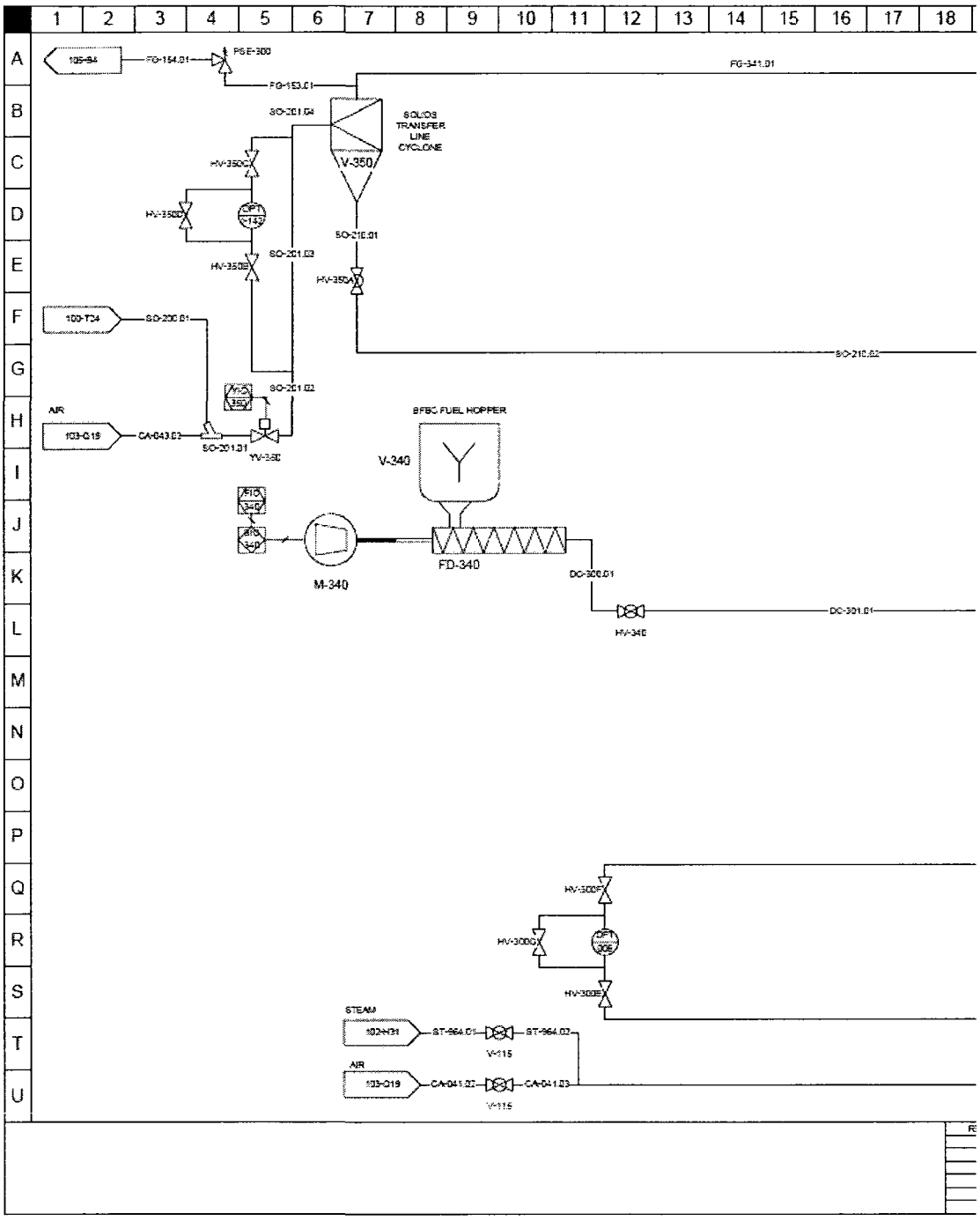

Appendix 5 – Selected Process & Instrumentation Diagrams

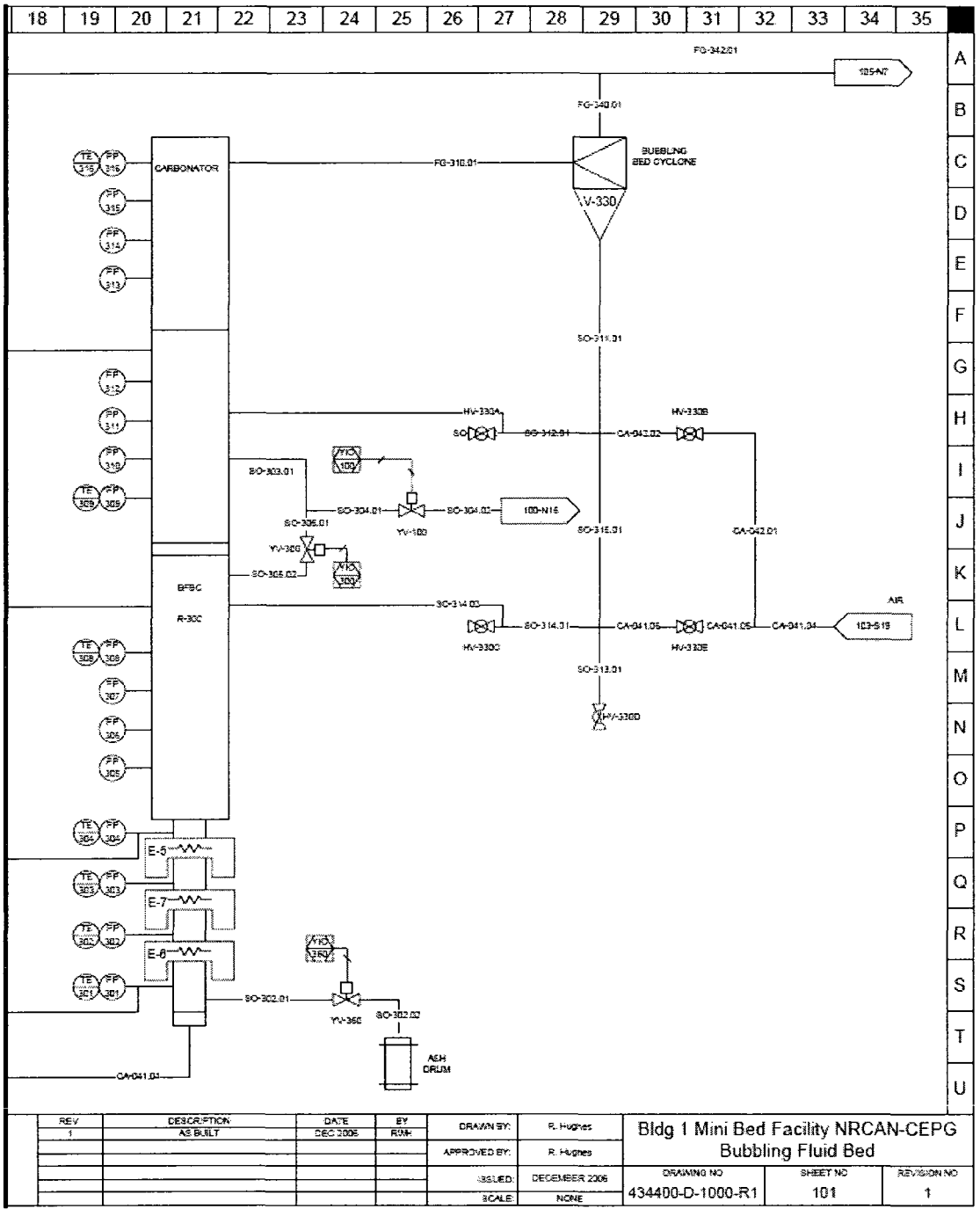

REV	DESCRIPTION	DATE	BY
1	AS BUILT	DEC 2006	RWH

DRAWN BY:	R. Hughes
APPROVED BY:	R. Hughes
ISSUED:	DECEMBER 2006
SCALE:	NONE

Bldg 1 Mini Bed Facility NRCAN-CEPG
Bubbling Fluid Bed

DRAWING NO	SHEET NO	REVISION NO
434400-D-1000-R1	101	1

Appendix 5 – Selected Process & Instrumentation Diagrams

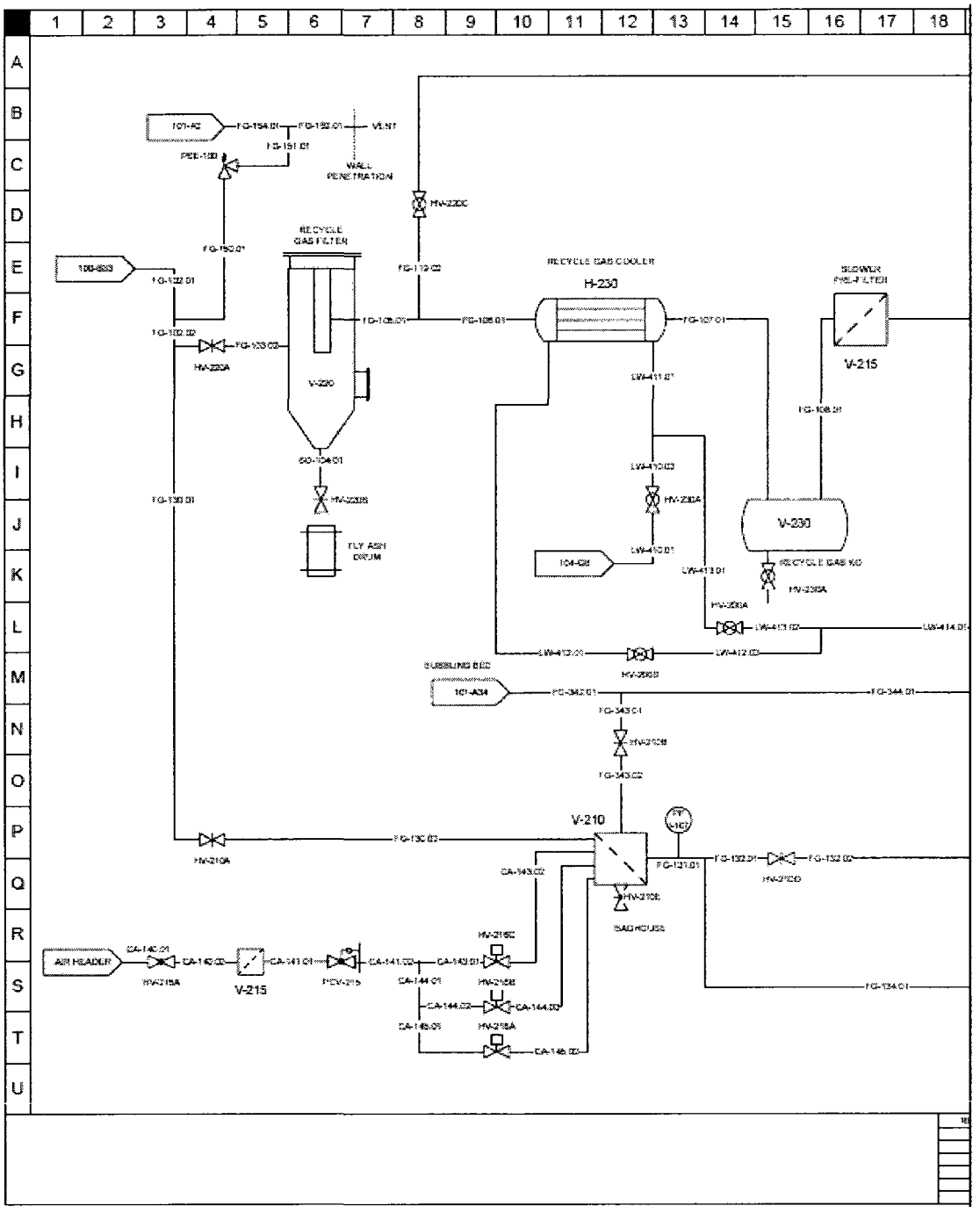

Appendix 5 – Selected Process & Instrumentation Diagrams